UNIVERSITÀ DEGLI STUDI DI NAPOLI FEDERICO II

ÉCOLE CENTRALE LYON

Joint-Doctorate with
Ecole Centrale de Lyon, France
LTDS - Laboratory of Tribology and Systems Dynamics

Department of Industrial Engineering - Aerospace Section
Doctorate School in Industrial Engineering
PhD Course in Industrial Engineering
XXXII cycle

Stochastic Analysis of Periodic Structures with Uncertainties

Candidate :
Ravi Pratap Singh

Chairman of PhD school :
Michele Grassi, Professor, UNINA, Italy

Research advisor :

Sergio De Rosa	Professor, UNINA, Italy	Advisor
Mohamed Ichchou	Professor, LTDS, ECL, France	Advisor
Francesco Franco	Associate Professor, UNINA, Italy	Co-advisor
Olivier Bareille	Associate Professor, HDR, LTDS, ECL, France	Co-advisor
Giuseppe Petrone	Assistant Professor, UNINA, Italy	Co-advisor

Public defence on 20/02/2020

Acknowledgements

I would like to acknowledge and to extend my sincere appreciation to the many individuals with whom I had the pleasure to collaborate in the course of my research work on probabilistic and non-probabilistic Wave Finite Element Methods (WFEM).

I wish to express my foremost appreciation and sincere gratitude to my advisors for their continuous support, encouragement, and guidance. Without their comments, suggestions, and help, it would not have been possible for me to complete this work.

First, I wish to thank Professor Sergio De Rosa and Professor Francesco Franco for their invaluable guidance, assistance and encouragement throughout my years at University of Naples "Federico II" (UNINA); Professors Mohamed Ichchou and Professor Olivier Bareille for guiding my incursions into the Wave Finite Element Method and Stochastic Methods and encouragement throughout my years at Ecole Centrale de Lyon (ECL); and Dr Christoph Droz (ECL) and Dr Giuseppe Petrone (UNINA), for discussions on various topics. Special mentioned to Prof. Bruno Toaldo, department of mathematics at UNINA for the discussion on uncertainty theories.

I would like to mention my special thanks to Professor Francesco Marulo for interesting and thought-provoking conversation, Professor Michele Grassi for doctoral school related communications, Dr Paola Muratto for administrative help and to all those people mentioned below.

Dr. Mauro Fontana at Powerflex S.R.L, Italy, for introducing me to the experimental test facilities, particularly the qualification, environmental, and mechanical tests.

Mr. Maurizio Maggioni and Mr. Federico Carrara Castelli at Lamiflex, Italy, for introducing the manufacturing process of periodic composites and discussions on the aspects of uncertainty in various applications.

I am also indebted to my other colleagues inside and outside the VIPER project:

Mr. Regis Boukadia at ECL for sharing his insights into the mysteries of the WFEM, first-hand assistance with programming deterministic WFEM, and many discussions on stochastic modelling.

Mr. Marc-Antoine at the University of Bristol for the introduction to the inverse form of deterministic WFEM and programming.

Mr. Safiullah Timorian, at UNINA, for the sharing thoughts and discussion on a day-to-day basis.

Mr. Dario Magliacano at the University of Franche-Comté, France (UFC), for discussion regarding data processing in COMSOL Multiphysics® software.

Mr. Fabrizion Enricco at ECL for the discussions on the WFEM.

Mr. Taoufik Bourgana and Ms. Sepide Ahsani at KU Leuven, Ms. Rita Palumbo and Mr. Simone del Broccolo at the University of Bristol, and Mr. Giovanni Tufano and Mr. Nassardin Guenfoud at ECL for fruitful discussions during half-yearly meetings about different scientific topics.

I would like to thank all my friends and co-workers from my time at UNINA, especially, Dr. Vittorio Memmolo, Dr. Leandro Maio, Dr. Francesco Rea, and Lessandro Casaburo.

I would also like to thank all my friends and co-workers from my time at ECL, especially, Guang Zhu, Weizhen you, Adrien Pyskir, and Dr. Yifan Yang.

I would like to express my deepest gratitude to my family, for their firm belief in education, and for teaching me to always strive towards a higher goal. I am also deeply grateful to my many good friends and colleagues who have contributed their friendship, support, and encouragement throughout my academic and professional career both in the EU and abroad.

Finally, many thanks to the VIPER project and to the Marie Sklodowska-Curie Actions grants for their financial support over the duration of the project.

Abstract

Structures having periodic properties or repeating patterns exhibit a peculiar feature known as band gaps. Band gaps are defined as frequency intervals for which both sound and vibration cannot propagate in the material. This feature of periodic structures offers a unique dynamic effect that can be exploited for a range of engineering applications. The design of periodic media is generally based on deterministic models without considering the effect of inherent uncertainties existing in these structures. In general, the design is aimed at controlling the mechanical waves as much as possible; however, inherent uncertainties may affect their characteristics. The uncertainties, in terms of material properties and geometrical parameters, are mostly caused by in manufacturing and assembly processes.

The uncertainties play an important role in altering the wave states. To address this unavoidable actuality, the effects of uncertainties need to be considered when analyzing frequency band structures (pass and stop bands) and frequency response function. With this in mind, the presented work is intended as a contribution to the probabilistic and non-probabilistic approaches, with reduced computation time, in conjunction with the wave finite element method.

The contributions of this study consist of considering uncertainties in the system to evaluate the deviation of the parameters (spectral and dynamics) and their influence on the global response (band gaps and frequency response function) of 1D and 2D periodic structures. The research contribution can be partitioned into two main parts. The first part involves the probabilistic development of a direct and explicit spectral formulation employing the first-order perturbation theory to predict the dispersion of different parameters. The second part involves non-probabilistic development, using the fuzzy set theory for the assessment of the effects of data uncertainties on the dynamics of 1D and 2D periodic structures.

List of abbreviations

1D	One Dimension
2D	Two Dimension
COV	Coefficient of Variation
DOF	Degree of Freedom
FE	Finite Element
FEM	Finite Element Method
FRF	Frequency Response Function
FWFEM	Fuzzy Wave Finite Element Method
IBZ	Irreducible Brillouin Zone
LR	Locally Resonance
MCS	Monte Carlo Simulation
PCE	Polynomial Chaos Expansion
PDF	Probability Density Function
Pn(Cs)	Phononic Crystals
SDOF	Single Degree of Freedom
SWFEM	Stochastic Wave Finite Element Method
SWFEM QEV	Stochastic Wave Finite Element Method Quadratic EigenValue
SWFEM TM	Stochastic Wave Finite Element Method Transfer Matrix
TM	Transfer Matrix
UQ	Uncertainty Quantification
WFEM	Wave Finite Element Method
WFEM MCS	Wave Finite Element Method Monte Carlo Simulation
WKB	Wentzel Kramers Brillouin

Contents

List of Tables

List of Figures

Chapter 1

Introduction

1.1 Introduction

Periodic structures can be defined as heterogeneous domains with a characteristic pattern obtained through the translation in space of a repetitive element called an elementary unit cell. The two material truss shown in Fig. 1.1 is an example of this type of periodic assembly. The levels of structural complexity are linked to the composition of the medium and shape. Other examples of periodic structures in engineering design, are honeycomb panels Fig. 1.2, and trusses and frames of beams, which are used in the majority of large constructions, as shown in Fig. 1.3. Periodic media are exploited in engineering for advanced material and structure design, owing to their superior performance. They are widely used in the aerospace industry, where the weight of the structure is the fundamental design criterion. Such structures also offer interesting vibration filtering behavior and can be utilized in vibration absorption devices. Periodic media can be manufactured in a wide variety of materials, such as steel, aluminum, rubber, ceramics, or plastics.

1.2 Band gap phenomenon

Structures having periodic properties or repeating patterns exhibit a peculiar feature known as band gaps. Band gaps or 'stop bands' are defined as frequency intervals for which both sound and vibration cannot propagate in the material. Thus, in periodic structures

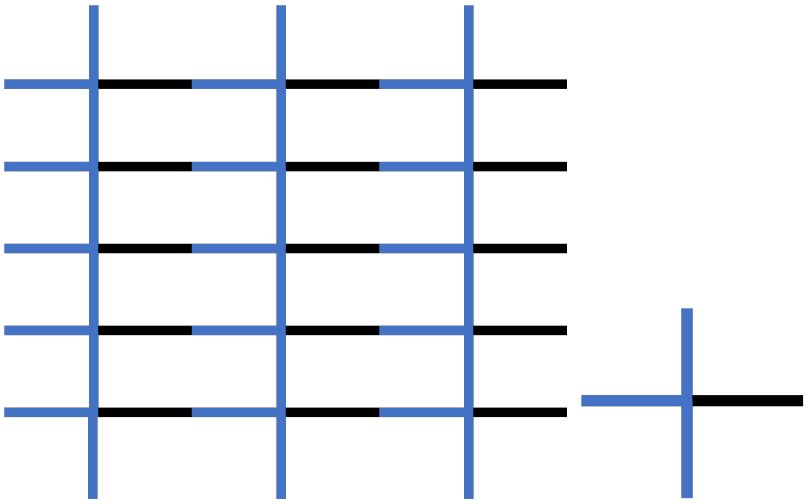

(a) Periodic media (b) Unit cell

Figure 1.1: Periodic media

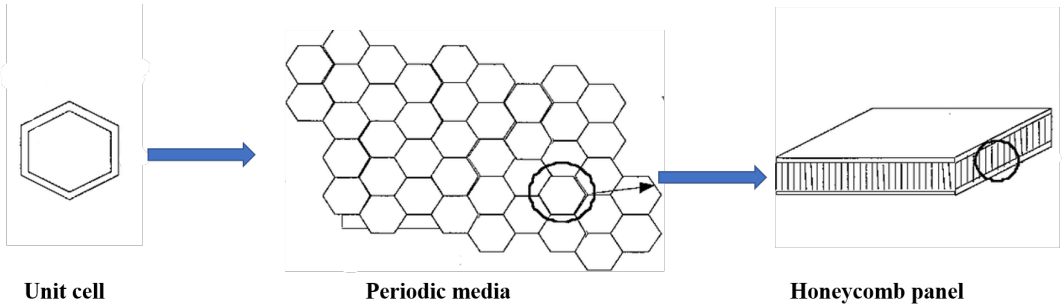

Figure 1.2: Honeycomb panel

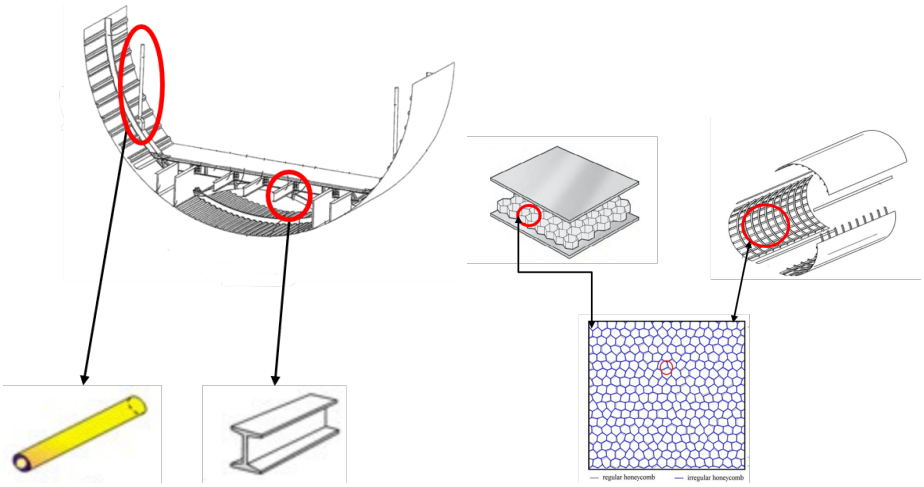

(a) 1D (b) 2D

Figure 1.3: 1D and 2D periodic media

wave propagation only occurs over specific frequency bands, known as 'pass bands'. The location and width of these bands are dependent upon the topology and geometry of the

unit cell. This feature of periodic assemblies offers a unique dynamic effect that can be exploited for a range of engineering applications. The phenomenon of band gaps in periodic structures has been widely investigated by various researchers [Faulkner and Hong, 1985], [Sigalas and Economou, 1992],[Jensen and Sigmund, 2003], [Hussein et al., 2003], [Ruzzene and Tsopelas, 2003], [Tian et al., 2011], [Droz et al., 2016], [Sun et al., 2017], [Zhou et al., 2018].

It is essential that the vibroacoustic performance and dynamics of a structure should meet design criteria in aeronautics, transport, energy and space application. Application of the periodic structure concept can be used for vibration reduction, acoustic blocking acoustic channeling, and acoustic cloaking [Cheng et al., 2018]. Periodic models are also used for vibration attenuation and control in dynamic system [Syed and Bishay, 2018], [Yu et al., 2008] and acoustic reduction in railway tracks [Wang et al., 2017].

1.3 Periodic media and uncertainties

The design of periodic media is generally based on deterministic models without considering the effect of inherent uncertainties existing in these media. In general, the design effort is aimed at controlling the mechanical waves as much as possible; however, inherent uncertainties may affect their characteristics. The uncertainties, in terms of material properties and geometrical parameters, are mostly caused by in both manufacturing and assembly processes. To address this unavoidable actuality, the effects of uncertainties need to be considered when analyzing frequency band structures (pass and stop bands) [Singh et al., 2018] and frequency response [Singh et al., 2019].

In this thesis, the term ‘uncertainty’ is used to describe those terms that are unknown or not known precisely. The response uncertainty of a system can arise from data uncertainty and model uncertainty [Roy and Oberkampf, 2011]. In data uncertainty, the input of a particular problem of interest is uncertain, for example, the mechanical properties and geometrical parameters of an engineering structure, and loading condition. Model uncertainty can arise from modelling simplifications, such as using the Euler-Bernoulli model instead of the Timoshenko model for describing the behavior of beam, which involves use of a linear model to describe a non-linear phenomenon. This means that the predicted

output data will not be representative of the real system behavior. In this thesis, the focus is on data uncertainty.

Data uncertainty can be classified as aleatory (or stochastic) uncertainty or epistemic uncertainty [Abdo et al., 2017],[Li et al., 2016]. The aleatory uncertainty is irreducible uncertainty that is a property of the system associated with fluctuations or variability [Kiureghian and Ditlevsen, 2009]. Aleatory uncertainty can be interpreted as stochastic uncertainty that results from underlying randomness or natural variability. Thus, if the parameter has one value at some time and another value at another time, then it has aleatory uncertainty. Epistemic uncertainty is due to imperfect knowledge. Thus, if the exact parameter value is unknown due to lack of information, then it has epistemic uncertainty [Kiureghian and Ditlevsen, 2009]. Fig. 1.4 gives a summary of different types of parameter uncertainty discussed in this thesis, together with practical examples of aleatory and epistemic uncertainties. In the example of epistemic uncertainty in Fig. 1.4, we suppose that the expert initially has no empirical data about the material properties of the plate.

The stochastic characteristics of periodic media can be determined by studying the design parameter uncertainties that are often modelled by random variables with consideration for spatial variability of the material and geometrical properties. Probabilistic models to account for these uncertainties and employ probabilistic methods that require a wealth of data on probabilistic parameters. Furthermore, even small inaccuracies in the data can lead to large errors in the computed characteristics of response [Sarkar and Ghanem, 2002]. When designers and scientists adopt a probabilistic representation, the parameters of the adopted probability density functions are corrected with reference to personal judgments and/or expert opinions. In fact, statements as “the mean is approximately equal to...” and “the variance lies in the range...” are typical when handling real mechanical data and – by virtue of their subjective nature – they deal with fuzzy uncertainties [Quaranta, 2011]. The exact sources of uncertainty are rarely identified, because their identification is difficult. When faced with incomplete information about the uncertainties, the adoption of the probabilistic approach can result in very challenging evaluations. In this scenario, the fuzzy set theory offers a method of approximating the uncertainty distribution in the form of the confidence interval through fuzzy membership functions. These are equiv-

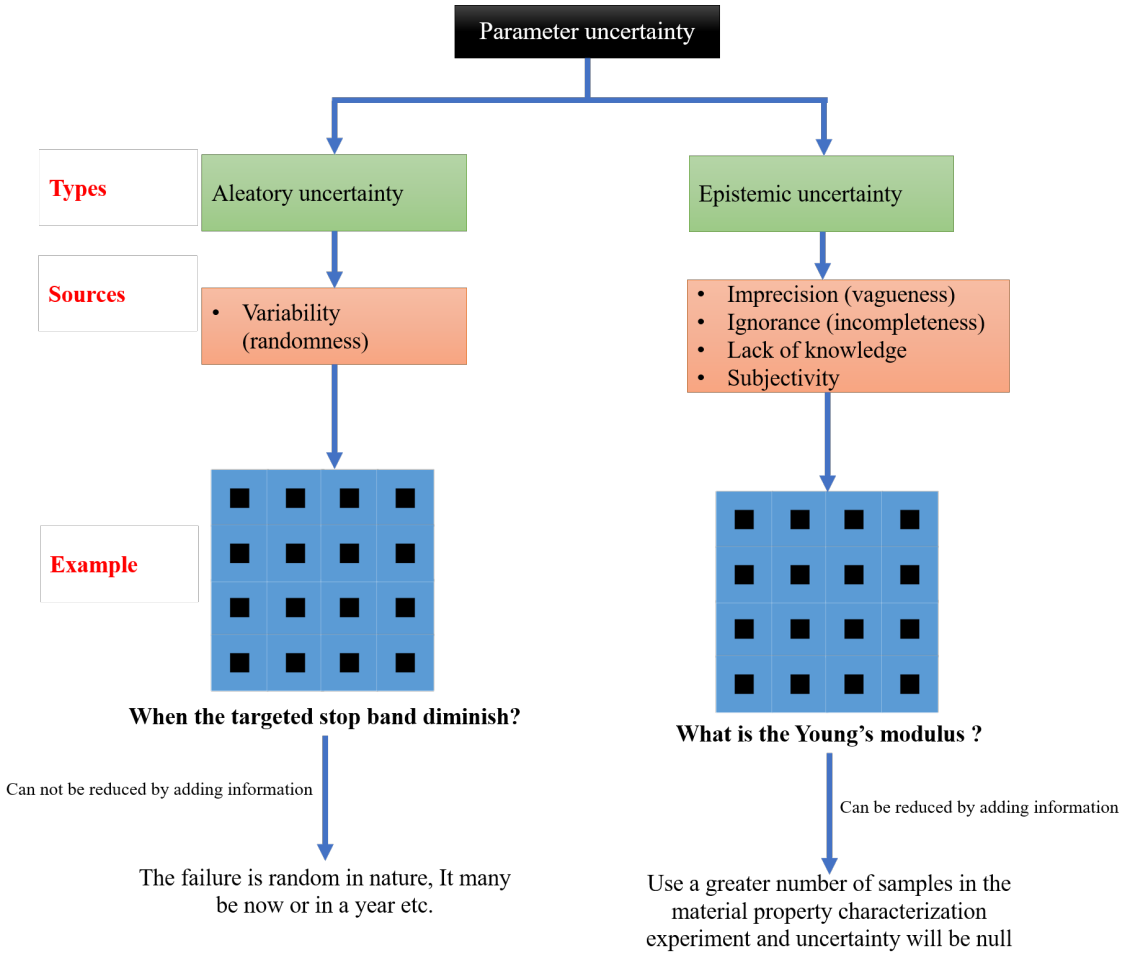

Figure 1.4: Classification of parametric uncertainty used in this thesis

alent representations for the characterization of the linguistic, vague, and missing data uncertainties.

Considering the advances in the performance and capabilities of computing machines, it is becoming easier to obtain more realistic results from the processing of complex systems with random variables, such as periodic media. The uncertainties in the material properties scatter the wave in comparison with the deterministic prediction. A better knowledge of the structural response of periodic structures can be achieved through the classification of possible uncertainty, to be included in the predictive models. Modelling uncertainties in a numerical simulation introduces higher complexity and increased computation cost in the model formulation. Nowadays, the wave finite element approach is used for the simulation of periodic structures to reduce the computational cost [Hussein,2014][Zhou,2018]. I this thesis we ask the following questions:

- How to predict the resulting uncertainty for the periodic media in 1D unbound and bounded cases?
- How to exploit commercial finite element packages and FE routines for amassing capabilities during modelling real structures for response uncertainty prediction?
- How to describe the parametric uncertainties given available information is limited, as it may be imprecise and in linguistic form?
- How to effectively propagate imprecise description of the uncertainty in periodic media for the 1D and 2D cases?

The research questions addressed in the present thesis led to investigation of the dynamic behavior of periodic media through the application of uncertainty modelling using probabilistic and non-probabilistic methods in conjunction with WFEM in the following ways:

- The SWFEM based on a transfer matrix [Ichchou et al., 2011] is extended to 1D periodic media to obtain the band gap and FRF, for the weak level (small level) of uncertainties.
- The development of a spectral formulation based on a quadratic eigenvalue problem for the stochastic modelling of 1D and 2D periodic media for the weak level of uncertainties at reduced computation cost.
- The development of new non-probabilistic uncertainty quantification method, which is effective when very little information about the uncertain parameter is available, or the available information is imprecise.
- The development of the FWFEM for 1D periodic media to obtain the band gap and FRF, and in 2D periodic media to obtain the dispersion curve through both direct and inverse formulation.

1.4 Numerical models in the thesis

The main purpose of this work is development of new methods for uncertainty modelling in conjunction with WFEM and to describe how uncertainties affect the dispersion and

FRF performance in 1D and 2D periodic media. The schematic idea is represented in Fig. 1.5. We considered the 1D and 2D periodic media in the continuous form. The continuous system discretized using FE steps is considered because it provides all the generality necessary to analyze the periodic structure. In this procedure, FE issues are also considered. The numerical validations presented in the thesis are focused on 1D and 2D periodic media. The following models (shown in Fig. 1.6) have been validated with MCS results in 1D and 2D periodic media.

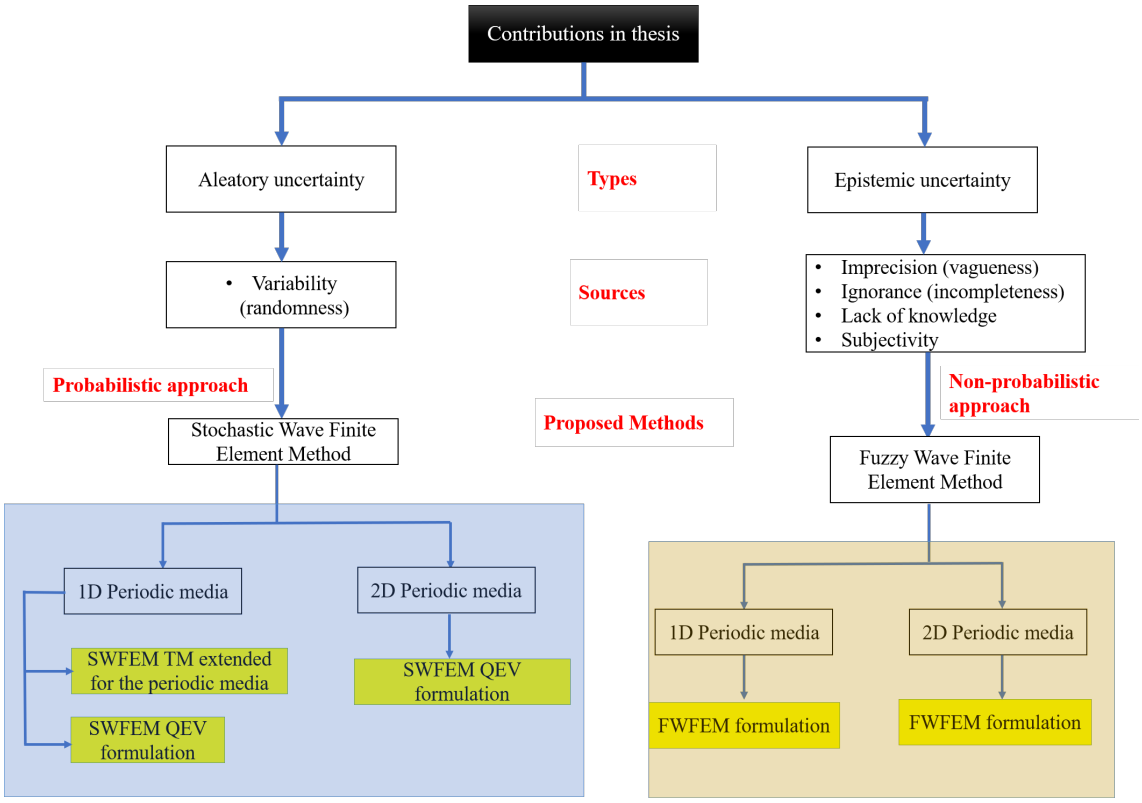

Figure 1.5: Proposed probabilistic and non-probabilistic methods in this thesis

1.5 Thesis outlines

The thesis is divided into 6 chapters.

- The current chapter presented the overview and motivation of the present work. The objectives and scope of the thesis are summarized, and the remaining contents of the thesis are organized in the following order.
- Chapter 2 describes the background of the work presented in the thesis by providing

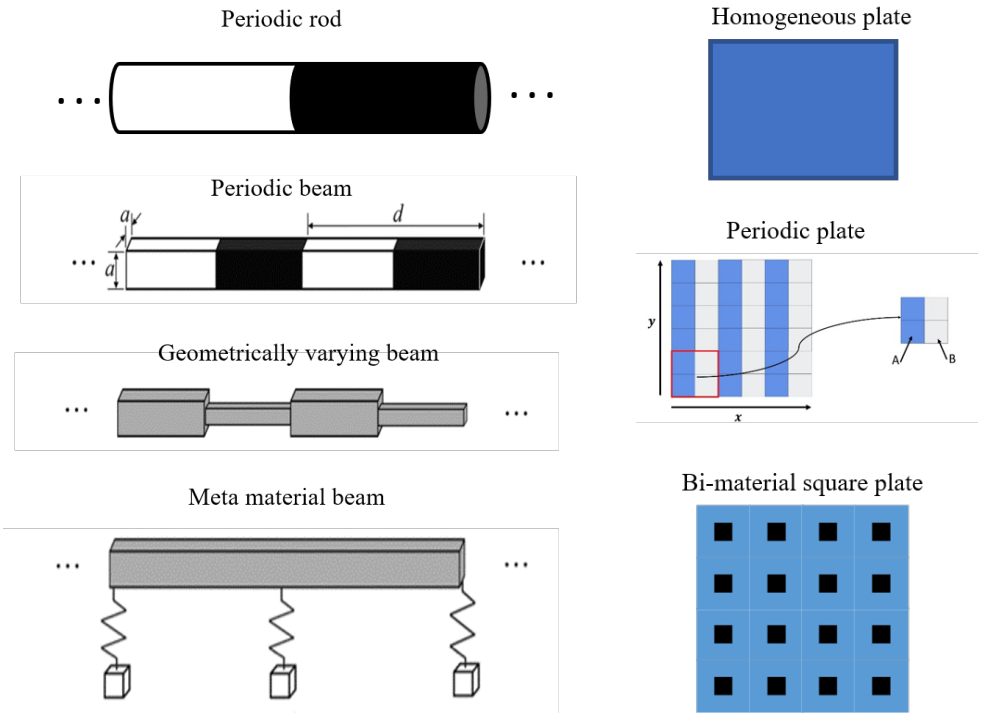

(a) 1D cases (b) 2D cases

Figure 1.6: Numerical models in this thesis

various studies related to the scope of the current area of interest. Initially a review of existing uncertainty quantification methods is furnished. Subsequently, literature available on free wave propagation and forced response have been reviewed for both deterministic and stochastic environments.

- Chapter 3 presents a stochastic WFEM formulation based on the transfer matrix approach. The formulation is based on the first-order perturbation technique. The methodology of deriving the standard deviation of the dynamic stiffness matrix, eigenvalues and eigenvector are described in detail. The extension of the SWFEM for the periodic media and metamaterial system for the bounded and unbounded cases is presented by deriving the standard deviation of the condensed dynamic stiffness matrix. The formulation is followed by a numerical validation for the free and forced cases. The numerical examples include a periodic bar, periodic beam, metamaterial rod, metamaterial beam, and geometrically varying beam cases validated with MCS for the band gap and FRF computation.

- Chapter 4 presents a stochastic formulation for the Bloch analysis of periodic structures, based on the quadratic 1D and 2D forms of the WFEM to analyze the bandgap.

In the 1D case, numerical examples of periodic rod and metamaterial rod systems are considered; for the 2D case, homogeneous and periodic plates considered. The obtained results are compared with the analytical solution (in 1D cases) and WFEM MCS results, to describe the accuracy and efficiency of the proposed formulation.

- Chapter 5 presents a fuzzy spectral formulation for the Bloch analysis of 1D and 2D periodic structures. The state space formulation is used for 1D case, analysing free wave propagation and FRF. The spectral formulation is used for 2D case and presented in both direct and inverse forms. Numerical experiments with the models of periodic bar, periodic beam, homogeneous and periodic plates and bi-material square plate are performed using proposed method. The effect of uncertainties on wavenumber variation and FRF are studied. The accuracy and performance of the developed formulations are compared with MCS results.

- Finally, in Chapter 6, the conclusions of the study are presented, together with suggestions for future research.

Chapter 2

Literature review

2.1 Introduction

A better knowledge of the structural response of periodic structures can be achieved through the classification of possible uncertainties to be included in the predictive models. The aim of the present chapter is to review models of uncertainty for the periodic structure analysis, and periodic media analysis methodologies. The chapter is organized in the following way: In the first part, the UQ process is explained, then the classification of uncertainty is presented, followed by the classification of the UQ methods. In the second part, a brief review of various approaches for the periodic structure (1D and 2D) is summarized.

2.2 Uncertainty modeling

In engineering, the available information is frequently not specific or precise, and may possess a data-based, expert-specified, objective, or subjective background. The basis of the available information usually consists of observations, plans, drawings, expert knowledge, measurements, experiences, codes and standards, influences from human mistakes and errors during manufacturing, from the use and maintenance of the constructions, and on-going changes in the boundary and environmental conditions. These phenomena may be summarized by the collective term 'uncertainty' [Möller and Beer, 2008]. In this the-

sis, the term 'uncertainty' is used to describe the terms that are unknown or not known precisely. Design of a system or a component involves selection of a design configuration, which is intended to result in the most desirable outcome (e.g., safety, performance, reliability) during the life cycle of the product. However, the variabilities in the modelling, manufacturing, and installation leads to some room for uncertainties. In general, the goal of product design can be summarized as per Fig. 2.1.

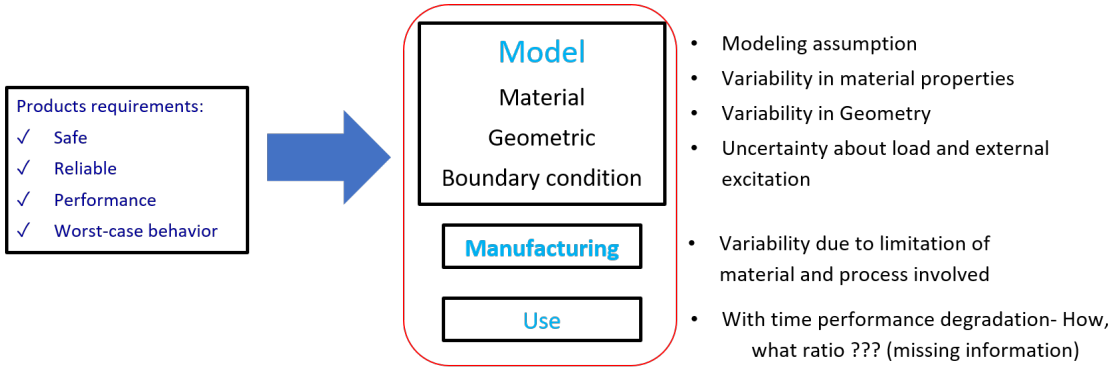

Figure 2.1: Goal of uncertainty quantification

In this scenario where uncertainty is inevitable, design with maximum probability or possibility to achieve the performance is targeted. To achieve it, uncertainty should be managed effectively, which requires process and tools to quantify uncertainty. In general term, the UQ involves the four steps [Singh et al., 2017] described in Fig. 2.2:

1. Identification: Finding the source and location of uncertainties in the system. In reality, many sources of uncertainty exist, such as uncertainties due to variabilities in the design parameter values, environmental conditions, initial conditions, boundary conditions, imprecise and simplified physics, missing physics, model implementation, numerical errors, and most importantly lack of sufficient data.

2. Characterization: Finding the form in which they are available. Generally, the parametric uncertainty is characterized and defined in the form of probability distributions and intervals bounds. Furthermore, non-parametric uncertainty, or so-called model uncertainties, also contribute uncertainties.

3. Propagation: Understanding how uncertainties are transmitting and spreading in the model, and finding a relation between parameter uncertainties and the response of the model.

4. Analysis and reduction: Establishing the relation between the uncertainty and its influence on the system response, and the underlying reasons for the relationship. Once this is done, the corrective measures that can be taken to improve the reliability of the original system should be determined.

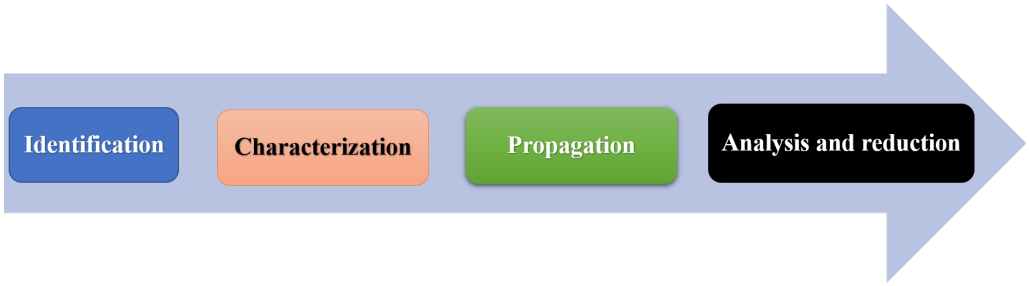

Figure 2.2: Steps in uncertainty quantification process

2.3 Classification of uncertainty quantification methods

Periodic structures exhibit a considerable amount of scattering in material properties such as Young's modulus, Poisson's ratio, and density, owing to tailoring of the media to meet specifications such as the manufacturer process, mechanical properties, and geometrical parameters. As these uncertainties involve in various stages of the manufacturing process, the exact value of these properties and parameters are impossible to achieve, and therefore become random. If randomness is present in the material properties, the stiffness and mass matrices become stochastic, which contributes to randomness in the band gap and FRF.

To capture the response with uncertainty in models and parameters, various approaches have been used for modeling the uncertainty. The basic techniques available for uncertainty modeling in structural dynamics are summarized in Fig. 2.3 [Chen and Rao, 1997], [Soize, 2003], [Soize, 2005], [Stefanou, 2009], [Zhang et al., 2010], [Moens, 2012], [Daouk et al., 2015], [Nannapaneni and Mahadevan, 2016], [Tomar et al., 2018], [Faes and Moens, 2019]. The uncertainty in structural response such as frequency response function, natural frequency, and mode shape are the result of propagation of uncertainty, which may be parametrical or non-parametric. The aim of a parametric approach is to propagate the uncertainty model through the dynamic equations to convert the description of the uncertain input variables into a description of the uncertain

response variables.

In this thesis, a parametric approach is implemented for the uncertainty propagation. The aleatory uncertainty propagation is implemented using the perturbation and MCS method, and epistemic uncertainty propagation is implemented with the fuzzy approach. A detailed description of the implemented method is given in the following sections.

2.4 Probabilistic models

In uncertainty quantification, the validity of the result of a numerical method is always limited by the validity of the input data of the model. The probabilistic methods generally require a significant amount of information about the input quantities. When information about uncertainties is sufficient, as per the law of large numbers, then the subjective probabilistic analysis result will prove to be of value; however, this is at the cost of tremendous computational resources. In this context, the perturbation method, MCS method, and PCE approach are the most popular for the uncertainty analysis of numerical models. The description of the perturbation method, MCS, and PCE are detailed below.

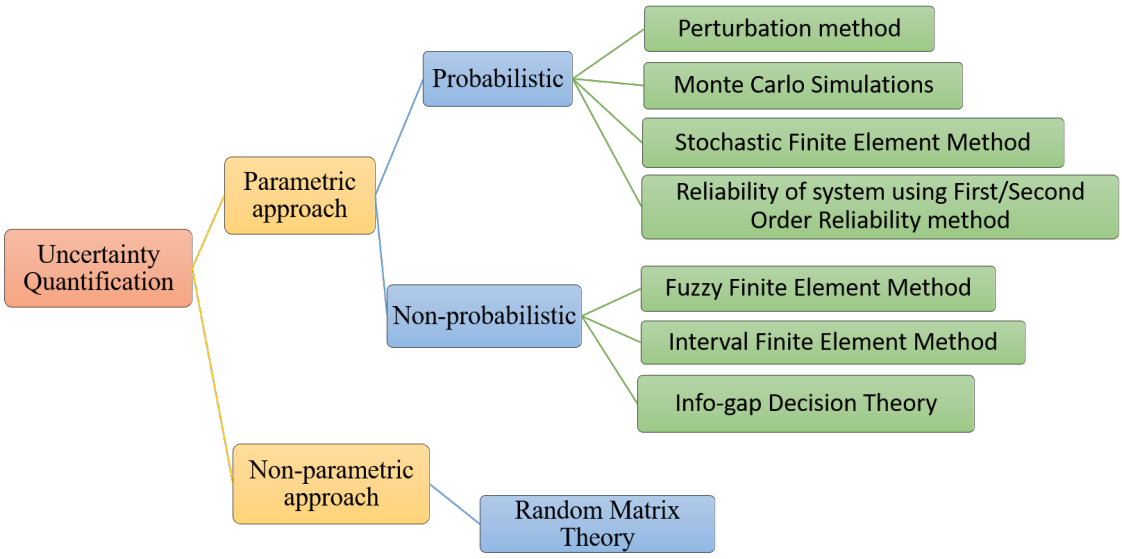

Figure 2.3: Classification of uncertainty quantification methods

2.4.1 Perturbation

To obtain a realistic response, it is essential to quantify the uncertainties arising due to randomness in material parameters. The perturbation method relates the characteristics between the random structural parameter and random response [Kleiber and Hien, 1992]. To model the uncertainties in material parameters, a first-order perturbation method has been used in this thesis for the weak level of uncertainties, as explained in the following. First, the random field variables are assumed as:

$$\Re(x,y) = \{\Re_1(x,y), \Re_2(x,y), \Re_3(x,y), \ldots., \Re_r(x,y)\} \tag{2.1}$$

where $\Re_i$ is the random parameter.

Then by application of the FE approximation, the random field variable is represented as nodal random variable. To better explain this method, we will present a simple case of the application of this theory. The equation of a discrete system is:

$$[M]\{\ddot{q}\} + [K]\{q\} + [K_G]\{q\} = \{F\} \tag{2.2}$$

If system contains uncertainties in the parameters, that leads to stochastic nature of the mass and stiffness matrices. For a structure with random parameters $\Re(x,y)$, every term in Eq. (2.2) becomes random in nature and is assumed as:

$$\begin{aligned}
[M_{ij}] &= [M_{ij}](\Re_\alpha) \\
[K_{ij}] &= [K_{ij}](\Re_\alpha) \\
\left[K_{G_{ij}}\right] &= \left[K_{G_{ij}}\right](\Re_\alpha) \\
\{q_i\} &= \{q_i\}(\Re_\alpha) \\
\{F_i\} &= \{F_i\}(\Re_\alpha)
\end{aligned} \tag{2.3}$$

The first-order perturbation is appropriate for a problem with a weak level of variation in the system properties with reference to their mean values. Then, for the expansion of the random variable with a given small parameter ζ, the first order is obtained as per

[Kleiber and Hien, 1992]:

$$\begin{aligned}
[M_{ij}] &= \left[M_{ij}^0\right] + \zeta \left[M_{ij}^r\right] \Delta\Re_r \\
[K_{ij}] &= \left[K_{ij}^0\right] + \zeta \left[K_{ij}^r\right] \Delta\Re_r \\
\left[K_{G_{ij}}\right] &= \left[K_{G_{ij}}^0\right] + \zeta \left[K_{Gij}^r\right] \Delta\Re_r \\
\{q_i\} &= \left\{q_i^0\right\} + \zeta \left\{q_i^r\right\} \Delta\Re_r \\
\{F_i\} &= \left\{F_i^0\right\} + \zeta \left\{F_i^r\right\} \Delta\Re_r
\end{aligned} \tag{2.4}$$

where $\zeta\Delta\Re_r(x,y) = \{q\}\Re_r(x,y) = \zeta\left[\Re_r(x,y) - \Re_r^0(x,y)\right]$ is first order variation of $\Re_r(x,y)$ around $\Re_r^0(x,y)$. The symbol $()^0$ denotes the value of the function obtained at $\Re_r^0(x,y)$. In addition, $()^r$ is the first-order partial derivative with respect to the random variable $\Re_r(x,y)$, obtained at their mean value $\Re_r^0(x,y)$. Now, substituting Eq. (2.4) into Eq.(2.2) and equating the power of the small parameter ζ, the zeroth and first-order equations are obtained. The zeroth order equation is obtained as:

$$\left[M_{ij}^0\right]\left\{\dot{q}_j^0\right\} + \left[K_{ij}^0\right]\left\{q_j^0\right\} + \left[K_{G_{ij}}^0\right]\left\{q_j^0\right\} = \left\{F_j^0\right\} \tag{2.5}$$

The first order equation is obtained as:

$$\left[M_v^0\right]\left\{\tilde{q}_j^r\right\} + \left[M_v^0\right]\left\{\tilde{q}_j^0\right\} + \left(\left[K_v^0\right] + \left[K_{G_v}^0\right]\right)\left\{q_j^r\right\} + \left(\left[K_i^r\right] + \left[K_{G_v}^r\right]\right), \left\{q_j^0\right\} = \left\{F_j^r\right\} \tag{2.6}$$

The above equations are used to solve the stochastic problem, which gives the mean responce of system parameter and variance of the responce. The Eq. (2.5) and Eq. (2.6) are used to obtain the zeroth and first-order expansion of the dynamic equation Eq. (2.7) and discussed in subsequent chapters in details.

$$(K - \omega^2 M)U = F \tag{2.7}$$

where K is the stiffness matrix, M is the mass matrix, U is the displacements vector, F is the force vector, and ω is the circular frequency.

2.4.2 Monte Carlo simulation

The MCS is used in a situation where the problem in question is complex, and thus an analytical resolution is considered. It provides successful resolution of classical deterministic systems, by considering uncertainty in the modelled parameters by adopting them as random variables [Ibrahim, 1987], [Mester and Benaroya, 1995]. Random sampling is performed of all parameters based on the correction and probability distribution. Then for every new sample, a new parameter is obtained, and the deterministic numerical model calculation is performed. It is applicable for any size and complexity of problem and predicts statistically accurate results. Although it has some uncertainty, this can be decreased by increasing the number of samples. However, to obtain reasonable accuracy, a large number of samples is required, which makes MCS prohibitive in term of computation cost.In this work, MCS is used as reference method to check the accuracy and efficiency of the SWFEM implementation.

Implementation of MCS

The classical MCS function is given in the form Z=N(Y), where Y represent the vector of uncertainty parameters modelled using a random vector, N is the deterministic model, and Z represents the estimated output arranged in the form of a random vector. The algorithm for the implementation of MCS in summarized in Fig. 2.4.

2.4.3 Polynomial chaos expansion

The basic idea of the polynomial chaos method is that the random process of interest can be approximated by sums of orthogonal polynomial chaos functions of random independent variables. In this context, the uncertain parameters are considered as second-order random processes (finite variance processes). The basis functions are selected depending on the type of random variable functions. For uniformly distributed random variables the basis functions are Legendre polynomials, for beta distributed random variables the basis functions are Jacobi polynomials, for gaussian random variables the basis functions are Hermite polynomials, and for gamma-distributed random variables the basis functions

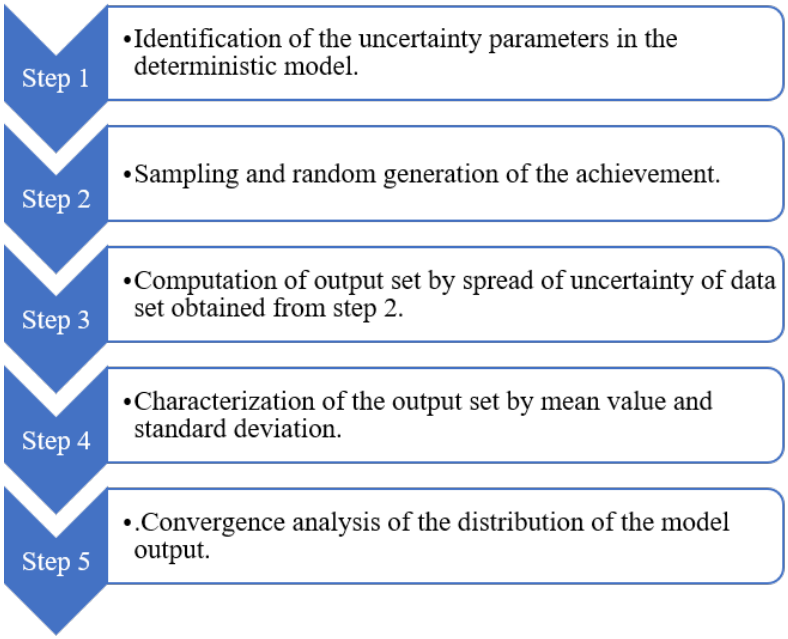

Figure 2.4: MCS workflow

are Lagrange polynomials. Ghanem et al. [Ghanem and Spanos, 1990] proposed stochastic spectral elements in the framework of elastic linear mechanics. This merger of the parametric stochastic approach with the finite element method allowed development of all the random variables of inputs of chaos polynomials so as to express the output solutions using the same basis function. Then, it is possible to study the stochastic dynamics of mechanical systems by post-processing of the coefficients of the output parameters. The calculation of the modal coefficients of the response is performed by two approaches: intrusive and non-intrusive.

In the intrusive approach, Galerkin's projection is used to progress from an uncertain system projected on the basis function of the chaos into a system of deterministic equations. The challenge in this approach that it requires modification of the algorithm for every problem to be studied. Whereas the non-intrusive approach does not require any change in the stochastic model, and only the modal coefficient needs to be calculated. Here, different methods are available to compute the coefficient numerical such as projection methods and regression methods. Xiu and Karniadakis proposed the generalized polynomial chaos for any type of random process [Xiu and Em Karniadakis, 2002], [Xiu, 2009]. The general procedure for the PCE is shown in Fig. 2.5.

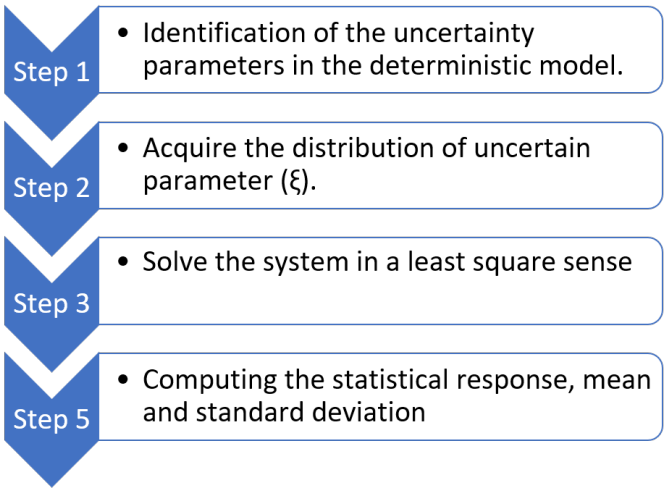

Figure 2.5: Polynomial chaos workflow for non-intrusive method

2.5 Non-probabilistic models

When objective information about uncertainties is limited, then the subjective probabilistic analysis result proves to be of very little value and does not justify its high computational cost. Consequently, alternative non-probabilistic models have been introduced for uncertainty modelling. In this context, interval and fuzzy approaches are the most popular for the uncertainty analysis of numerical models. The description of the interval and fuzzy approaches is detailed below.

2.5.1 Interval model

In the interval approach, the uncertain parameter/variables can vary within intervals between two possibilistic (extreme) values. In this model, no assumption is made about the probability distribution of the uncertain parameter/variable. The uncertain variable $\widetilde{X}$, is represented as an interval and definition of the interval scaler is defined as

$$\widetilde{X} \in [\underline{x}, \overline{x}] = [x \in \Re | [\underline{x} \leq x \leq \overline{x}]] \tag{2.8}$$

where $\underline{()}$ is the lower bound and $\overline{()}$ is the upper bound. The upper and lower bounds belong to the set, hence the interval is called 'close'. The radius and midpoint are expressed as

r_x and m_x respectively and defined as:

$$m_x = \frac{\underline{x} + \overline{x}}{2} \tag{2.9}$$

$$r_x = \frac{\overline{x} - \underline{x}}{2} \tag{2.10}$$

From Eq. (2.8) the interval vectors and matrices can be extended. Both interval vector $\left\{\tilde{X}_i\right\} \in \Re^p$ and matrices $[\tilde{x}_{ij}] \in \Re^{pXq}$ belong to the interval scaler in $\Re$ and can be expressed as [Moens and Hanss, 2011], [Faes and Moens, 2019].

$$\left\{\tilde{X}_i\right\} \in \left([\underline{x}_1, \overline{x}_1] \cup \ldots \cup \left[\underline{x}_p, \overline{x}_p\right]\right) \quad i = 1, \ldots, p \tag{2.11}$$

$$\left[\tilde{X}_{ij}\right] \in \left([\underline{x}_{11}, \overline{x}_{11}] \cup \ldots \cup \left[\underline{x}_{pq}, \overline{x}_{pq}\right]\right) \quad i = 1, \ldots, p \quad j = 1, \ldots, q \tag{2.12}$$

From Eq. (2.11) and Eq. (2.12) the components of the uncertain vector and uncertain matrices are independent. Thereby, the interval vector consists of a hypercube containing a set of vector elements. The set of vectors contains all possible combination of the vector elements. Thus, an n-dimensional interval vector describes a hypercube in n-dimensional space. The upper and lower bounds of the vector's element are used to find the vertices of this hypercube. When the interval vector or interval matrices cannot be independent, the convex modelling approach can be considered [Zhu and Elis, 1993]. In engineering applications, the parameters are statistically independent in most cases. Therefore, the description of these variables by a hypercube is generally more practical. In practical terms, the interval approach requires only a range of possible values, which allow that conversion from a probabilistic description to an interval description is always possible. In this conversion, the range of PDF forms the interval, and the likelihood of each value that lies within the range is lost. However, the interval concept does not require information on the likelihood, and thus is perfectly suited to model this kind of non-determinism. Thereby, an interval can be interpreted as a collective description of all possible probability density functions over the considered interval range. In the situation where uncertainty is used to describe the property of the model, even after finishing the design, the exact value inside

the interval can remain unknown.

2.5.2 Fuzzy sets

The concept of the fuzzy set was first introduced by Zadeh [Zadeh, 1965] as a tool to express vague linguistic information. Later Dubois and Prade [DuBois and Prade, 1980] applied the concept of fuzzy sets in numerical analysis. A fuzzy set is considered as an extension of a crisp set. A crisp set distinguishes between members and non-members of the set, whereas the fuzzy set introduces a soft gradual transition from members and non-members with the help of the membership level. The membership function $\mu_{\tilde{x}}(x)$ describes the membership level of each element x in the domain X to the fuzzy set:

$$\tilde{x} = \{(x, \mu_{\tilde{x}}(x)) \,|x \in X \wedge \mu_{\tilde{x}}(x) \in [0, 1]\} \tag{2.13}$$

if $\mu_{\tilde{x}}(x) = 1$, x is a member of fuzzy set $\tilde{x}$. and if $\mu_{\tilde{x}}(x) = 0$, x is definitely not a member of fuzzy set $\tilde{x}$. if $0 < \mu_{\tilde{x}}(x) < 1$, then the membership is uncertain. The most frequently applied membership function are triangular and gaussian shape functions [Moens and Hanss, 2011]. Zadeh's extension principle provides a general definition to calculate the fuzzy output $\tilde{x}$ of a crisp function $f(x_1, x_2, \ldots, x_n)$. It is applied to n fuzzy input $\tilde{x}_1, \tilde{x}_2, \ldots, \tilde{x}_n$. This approach is difficult and computationally expensive. The alternate approach consists of searching the output domain for the sets that have an equal membership level. It is realized by analyzing the input domain at a specific membership level α. The α-cut of the input quantities at membership level α is defined as:

$$x_{i,\alpha}^{\mathrm{I}} = \{x_i \in X_i | \mu_{\tilde{x}_i}(x_i) \geq \alpha\} \tag{2.14}$$

It can be inferred that the α-cut is the interval resulting from intersecting the membership function at $\mu_{\tilde{x}_i}(x_i) = \alpha$. Once the input quantities are identified, and at a specific membership level, the α-cuts are derived, then an interval analysis is performed on these intervals. In practice, a fuzzy numerical analysis can be replaced by a sequence of interval numerical analyses, because the output membership functions can be obtained by repeating the α-cut procedure at a number of membership levels. The α-cut procedure for the

fuzzy analysis is illustrated in Fig. 2.6.

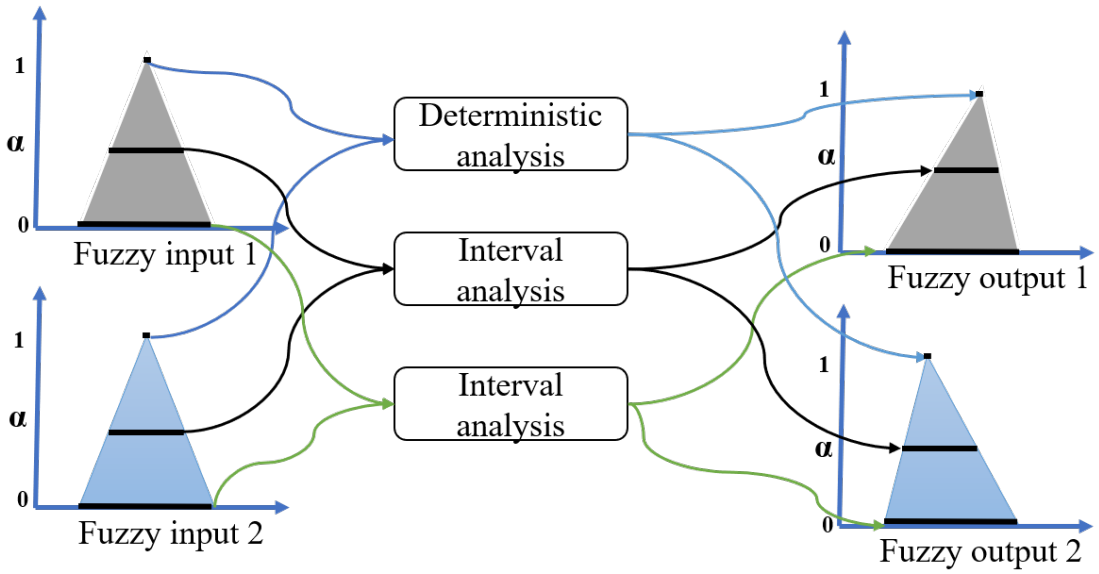

Figure 2.6: α-cut procedure with two input and three membership levels

2.6 Methods for modeling periodic media (deterministic case)

Several different methods have been previously developed for modelling periodic structures, such as plane wave expansion [Kushwaha et al., 1994], finite difference time domain [Tanaka et al., 2000], multiple scattering [Psarobas et al., 2000], TM[Yu et al., 2008], WFEM [Mencik and Ichchou, 2005],[Mace et al., 2005a], differential quadrature [Xiang and Shi, 2009], and shift cell operator method [Collet et al., 2011].

Among them, the WFEM is gaining interest in the analysis of periodic structures. The WFEM allows investigation of only a single cell of the structure, and can be modelled using FEM. Once the matrices (mass, stiffness, and damping matrices) of the cell are estimated, the application of the periodic boundary condition leads to the formulation of an eigenvalue problem. The solution of the eigenvalue problem constitutes the propagation constants of the waves travelling through the structure. The free wave propagation problem can be solved by different approaches; the two typically used are the direct and inverse approaches [Boukadia et al., 2018]. In the direct approach, $\omega(\mu)$, imposes real ω

(circular frequency), allowing description of the spatial wave attenuation; whereas the inverse approach, $\omega(\mu)$ impose the real μ (propagation constant), that does not allow the wave attenuation, and can be applied to an undamped unit cell model. In what follows, the direct and inverse approaches that have been used in this work for the undamped dispersion curve calculations, are further elaborated.

2.6.1 Wave finite element method in 1D periodic media

In a 1D periodic structure, the nodes on the boundaries of the periodic structure are denoted as on the left boundary (L), right boundary (R) and the remaining/internal nodes (I). The displacement degrees of freedom (DOF) q are partitioned into left (q_L) and right (q_R). Similarly, forces are partitioned into left (F_L) and right (F_R). The spatial discretization employs the finite element steps by discretization of one subelement of length (d). The discretization leads to dynamic equilibrium of any substructure in the following manner:

$$(D)\begin{pmatrix} q_L^{\boldsymbol{k}} \\ q_R^{\boldsymbol{k}} \end{pmatrix} = \begin{pmatrix} F_L^{\boldsymbol{k}} \\ F_R^{\boldsymbol{k}} \end{pmatrix} \tag{2.15}$$

where (D) is the complex dynamic stiffness matrix of the substructure. This is condensed on the left and right boundaries DOF at the pulsation ω:

$$(D) = -\omega^2 M + K(1 + i\eta) \tag{2.16}$$

where M, K are the mass and the stiffness matrix, respectively, η is the structural loss factor, i is the unit imaginary number, and ω is the circular frequency. The problem in Eq. (2.15) can be partitioned in the following way:

$$\begin{pmatrix} D_{LL} & D_{LR} \\ D_{RL} & D_{RR} \end{pmatrix}\begin{pmatrix} q_L^{\boldsymbol{k}} \\ q_R^{\boldsymbol{k}} \end{pmatrix} = \begin{pmatrix} F_L^{\boldsymbol{k}} \\ F_R^{\boldsymbol{k}} \end{pmatrix} \tag{2.17}$$

Spectral approaches can be used in two ways: a state space representation form and FE form. The following describes the details of both forms.

Spectral problem: Transfer matrix form

Here the spectral formulation is presented based on the state space representation. This formulation uses a symplectic matrix for the classification of different mode of propagation [Mencik and Ichchou, 2005]. The kinematic variables, q, and F are represented through state vectors as $u_L^{\boldsymbol{k}} = \left(q_L^{\boldsymbol{k}T} \;\; -F_L^{\boldsymbol{k}T}\right)^T$ and $u_R^{\boldsymbol{k}} = \left(q_R^{\boldsymbol{k}T} \;\; F_R^{\boldsymbol{k}T}\right)^T$; and related by the transfer matrix S.

$$u_R^{\boldsymbol{k}} = S.u_L^{\boldsymbol{k}} \tag{2.18}$$

where S connects the displacement vector and is forced on the two surfaces of cell $\boldsymbol{k}$, S is written as:

$$S = \begin{pmatrix} -\left(D_{LR}\right)^{-1} D_{LL} & -\left(D_{LR}\right)^{-1} \\ D_{RL} - D_{RR}\left(D_{LR}\right)^{-1} D_{LL} & -D_{RR}\left(D_{LR}\right)^{-1} \end{pmatrix} \tag{2.19}$$

Then the following eigenvalue problem obtained as:

$$\begin{aligned} S\phi_i &= \mu_i \phi_i \\ |S - \mu_i I_{2n}| &= 0 \end{aligned} \tag{2.20}$$

where $(\mu_i, \phi_i)_{i=1\ldots 2n}$ are the waveguide propagation modes, and n is the number of cross-sectional DOFs. The eigenvalues are related to the wavenumber by $\mu = exp(-jkd)$, where d is the length of the unit cell. For complex cross sections, S may be poor conditioned.

Spectral problem: Finite element form

An alternative formulation based on a finite element model of a typical subsystem is available. According to Bloch's theorem, the dynamic of the global waveguide can be expanded using the wave solution of the following form

$$q_R = \mu q_L \text{ and } F_R = -\mu F_L \tag{2.21}$$

where μ is the propagation constant. The Floquet-Bloch condition applied to the dynamic equation, leads to the classic quadratic eigenvalue problem [Houillon et al., 2005] in terms

of propagation constant:

$$\left(D_{RL} + \mu_i I_{2n} \left(D_{LL} + D_{RR}\right) + \mu_i^2 I_{2n} D_{LR}\right) \left(\Phi_q\right)_i = 0 \tag{2.22}$$

where $i = 1...2n$, and n is the cross sectional DOFs, D_{LL}, D_{RL}, D_{RR} and D_{LR} are the elements of the dynamic stiffness matrix. The wave mode of the global system is $(\mu_i, (\Phi_q)_i)_{i=1...2n}$. These two forms of the eigen problem, state-space form Eq. (2.20) and spectral form Eq. (2.22) are attempted for the stochastic analysis in periodic media in the 1D domain.

2.6.2 Wave finite element method in 2D periodic media

Consider an infinite thin plate lying in the (x, y) plane with a unit cell as shown in Fig. 2.7. The unit cell is divided into four corner nodes. The unit cell DOFs (q) are divided into

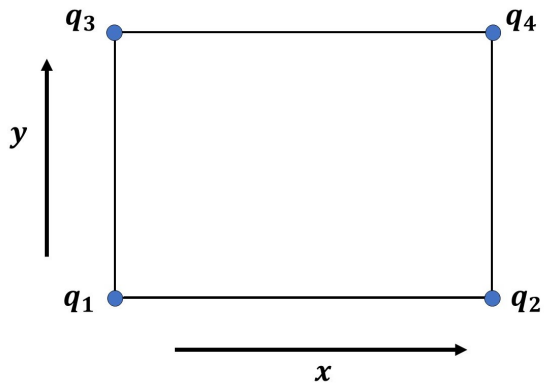

Figure 2.7: Rectangular plate element

four corner nodal DOFs, q_1, q_2, q_3 and q_4. The vector of nodal DOFs are given by $q = \left[q_1^T, q_2^T, q_3^T, q_4^T\right]^T$, similarly, the vector of nodal forces are given by $f = \left[f_1^T, f_2^T, f_3^T, f_4^T\right]^T$. where T denotes the transpose. The time-harmonic equation of motion of the unit cell can be written as

$$\left(K - \omega^2 M\right) q = f \tag{2.23}$$

where K is the stiffness matrices, M is the mass matrices, ω is the circular frequency, f is the nodal forces vector, and q is the nodal displacements vector. This equation is used to form the spectral problem involving wavenumber k_x, k_y and frequency ω.

The dynamic stiffness matrix can be expressed as $D = K - \omega^2 M$. Here, introducing the periodic structure theory for the unit cell and considering a time-harmonic response [Mace and Manconi, 2008], the deterministic harmonic equation of motion can be expressed as

$$\left(K^*\left(\lambda_x, \lambda_y\right) - \omega^2 M^*\left(\lambda_x, \lambda_y\right)\right) q_1 = 0 \tag{2.24}$$

where $K^* = \Lambda_L K \Lambda_R$ and $M^* = \Lambda_L M \Lambda_R$ are the reduced stiffness and mass matrices. λ_x and λ_y are the propagation constants in x- and y- directions, respectively, and Λ_L and Λ_R are matrices that contain the propagation constants from the periodicity conditions.

$$\Lambda_L = \begin{bmatrix} I & \lambda_x^{-1} I & \lambda_y^{-1} I & \lambda_x^{-1}\lambda_y^{-1} I \end{bmatrix}$$

$$\Lambda_R = \begin{Bmatrix} I \\ \lambda_x I \\ \lambda_y I \\ \lambda_x \lambda_y I \end{Bmatrix} \tag{2.25}$$

where I is the identity matrix. The eigenvalue problem of Eq. (2.24) can be expressed as:

$$D^*\left(\omega, \lambda_x, \lambda_y\right) q_1 = 0 \tag{2.26}$$

where $D^*\left(\omega, \lambda_x, \lambda_y\right)$ is the reduced dynamic stiffness matrix. For the sake of clarity, the reduced dynamic stiffness matrix is now represented as D. If the reduced dynamic stiffness matrix is partitioned as:

$$D = \begin{bmatrix} D_{11} & D_{12} & D_{13} & D_{14} \\ D_{21} & D_{22} & D_{23} & D_{24} \\ D_{31} & D_{32} & D_{33} & D_{34} \\ D_{41} & D_{42} & D_{43} & D_{44} \end{bmatrix} \tag{2.27}$$

The eigenproblem in Eq. (2.24) and Eq. (2.26) involves three parameters, λ_x, λ_y, and ω. Depending on the nature of the solution sought the eigenproblem takes various forms.

WFEM 2D: Direct form

If the frequency ω and one wavenumber is known, then the eigenvalue problem in Eq. (2.26) can be written in the following form

$$\begin{aligned}\big[&(D_{11}+D_{22}+D_{33}+D_{44})+(D_{12}+D_{34})\lambda_x+(D_{21}+D_{43})\lambda_x^{-1}+(D_{13}+D_{24})\lambda_y\\&+(D_{31}+D_{42})\lambda_y^{-1}+D_{14}\lambda_x\lambda_y+D_{41}\lambda_x^{-1}\lambda_y^{-1}+D_{32}\lambda_x\lambda_y^{-1}+D_{23}\lambda_x^{-1}\lambda_y)\big]\,q_1=0\end{aligned}\quad(2.28)$$

for the solution of Eq. (2.26) in the case where frequency and one wavenumber in the x- or y- directions are known, the eigenvalue form becomes a quadratic eigenvalue problem. Then the nonlinear Eq. (2.28) can be reduced to a quadratic eigenproblem in λ_x form, when λ_x is unknown and (ω, λ_y) are given.

$$\begin{aligned}\big[&(D_{21}+D_{43}+D_{41}\lambda_y^{-1}+D_{23}\lambda_y)+\mu_i(D_{11}+D_{22}+D_{33}+D_{44}+(D_{31}+D_{42})\lambda_y^{-1}\\&+(D_{13}+D_{24})\lambda_y)+\mu_i^2(D_{12}+D_{34}+D_{32}\lambda_y^{-1}+D_{14}\lambda_y)\big]\,(\Phi_q)_i=0\end{aligned}\quad(2.29)$$

WFEM 2D: Inverse form

The inverse form is used for the case where the wavenumbers in the x-direction, k_x, and in the y-direction, k_y, are given and corresponding frequencies of free wave propagation are to be sought. In the inverse form, the dynamic condensation cannot be performed in a manner that conserves the the internal nodes. Thus, Λ_L and Λ_R are matrices that contain the propagation constants from the periodicity conditions. They are modified to form:

$$\Lambda'_{\mathrm{R}}=\begin{pmatrix}\Lambda_{\mathrm{R}} & 0\\ 0 & \mathrm{I_i}\end{pmatrix}\quad(2.30)$$

$$\Lambda'_{\mathrm{L}}=\begin{pmatrix}\Lambda_{\mathrm{L}} & 0\\ 0 & \mathrm{I_i}\end{pmatrix}\quad(2.31)$$

where I_i is the identity matrix of size i. Then the deterministic harmonic equation of motion becomes:

$$\Lambda'_{\mathrm{L}}*\left(K-\omega^2M\right)*\Lambda'_{\mathrm{R}}\begin{pmatrix}q_1\\ q_I\end{pmatrix}=0\quad(2.32)$$

where q_I is the conserved internal degree of freedom. This becomes a standard, linear algebraic problem in ω^2, as:

$$\left[K'\left(\lambda_{\mathbf{x}}, \lambda_{\mathbf{y}}\right) - \omega^2 M'\left(\lambda_{\mathbf{x}}, \lambda_{\mathbf{y}}\right)\right] \begin{pmatrix} q_1 \\ q_I \end{pmatrix} = 0 \tag{2.33}$$

In the undamped structure, K and M are real positive definite Hermitian matrices. Thereby the K' and M' with $|\lambda_x| = 1$ and $|\lambda_y| = 1$. The eigenvalues ω^2 for which free wave propagation is possible are real and positive.

2.7 Vibroacoustic analysis with uncertainty

In the vibroacoustic problems, the interaction between a solid and fluid field occur in the form of vibration and sound, respectively. The use of the numerical method for numerical modeling and simulation varies, and it depends on the frequency range of interest. A graphical representation is shown (in Fig. 2.8) of the techniques available for vibroacoustic simulation). [Mace et al., 2005b], [Cicirello and Langley, 2014], [Ichchou et al., 2011], [Xu et al., 2014]. When uncertainty is introduced in the vibroacoustic modeling and simulation of periodic media, the low-frequency domain is unaffected (assumption), and the high-frequency domain is modeled using a statistical energy approach that can accommodate uncertainty. However, the mid-frequency domain is in question.

Miles [Miles, 1966] proposed an asymptotic solution for one-dimensional wave propagation in a heterogeneous elastic medium with a variation of Young's modulus and density. The application of the WKB approximation in the structural dynamics for the inhomogeneous system was introduced by Steele [Steele, 1976]. Manohar and Keane [Manohar and Keane, 1993] studied the randomness in the wave propagation in waveguides using spectral element analysis. Langley [Langley, 1995] developed a method that enables the average value of the inverse squared transmission coefficients to be calculated for a one dimensional near periodic structure. Arenas [Arenas and Crocker, 2001] studied an incident plane sound wave travelling along a rigid duct, where the impedance of a particular horn was obtained using the WKB approximation. Sarkar et al. [Sarkar and Ghanem, 2002] presented a parametric stochastic finite

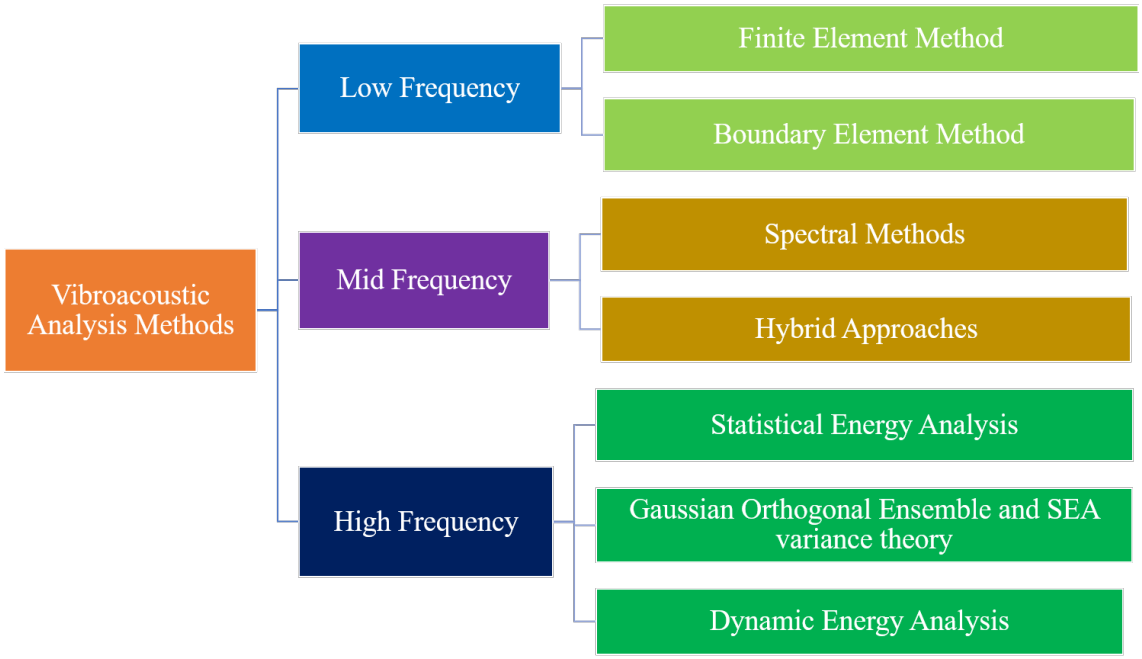

Figure 2.8: Vibroacoustic methods

element approach based on polynomial expansion in conjunction with a proper orthogonal decomposition method and dynamic element method for the mid-frequency vibration analysis. Ichchou et al. [Ichchou et al., 2011] proposed a numerical approach using the WFEM based on the TM considering spatially homogeneous variability in waveguides using first-order perturbation theory for random guided viscoelastic media over a broad frequency range.

Ben Souf et al. [Ben Souf et al., 2013b] presented hybrid WFEM and SWFEM to develop a diffusion matrix of a coupling structure, and also studied the forced response of the random viscoelastic media subject to time-harmonic loading by hybridization of the deterministic WFEM and a parametric probabilistic approach [Ben Souf et al., 2013a]. They also studied uncertainty propagation in the forced response of the periodic coupled structure by hybridization of WFEM and generalized polynomial chaos expansion [Ben Souf et al., 2015c], and investigated the modal uncertainties effect on the random dynamic response of periodic structures [Ben Souf et al., 2015a]. Fabro et al. [Fabro et al., 2015] investigated force response of a finite waveguide undergoing longitudinal and flexural motion using the WKB approximation for random material and geometrical properties. They also derived an approximation by considering a waveguide with piecewise constant material variability to

mitigate the effect of the internal reflections that occur due to any local changes in the material or geometrical properties, and verified this by experimental investigation.

Recently for 1D periodic media, Mencik et al. [Mencik and Duhamel, 2016] presented a method to compute the forced response of periodic structures with many perturbed substructures. Fabro et al. [Fabro et al., 2016] studied the robustness of the band gap by employing WFEM TM with WKB and Karhunen–Loeve expansion for an undulated beam with and without resonators. Li et al. [Li and Xu, 2017] presented a study considering the material and geometrical uncertainty influence on the band structures of an undulated beam with a periodically arched shape. The band gap was calculated using FEM and uncertainty propagated using interval analysis based on the Taylor series expansion. Bouchoucha et al. [Bouchoucha et al., 2017] proposed the second-order perturbation of the 1D SWFEM method proposed by Ichchou et al. [Ichchou et al., 2011]. Fabro et al. [Fabro et al., 2019] proposed a method to extend the applicability of the WKB expansion approach using a finite element method. The latest development by Zhao et al. [Zhao and Zhang, 2019] studied the symplectic eigenvalue problem of the random symplectic matrix employing the Rayleigh quotient method for the study of 1D chains with homogenous randomness.

For 2D periodic media with uncertainty, Vasseur et al. [Vasseur and Deymier, 1997] presented experimental and theoretical results for acoustic wave propagation through periodic and randomly arranged 2D composite material. The experiment result with only one realization indicated that the randomness has only limited influence on the wave propagation through composite media. Cai at al. [Cai and Patil, 2007] studied 2D fiber-reinforced composite panels with quasi-random fiber arrangements that can be qualified as "essentially regular with slight randomness". The numerical simulation used large-scale deterministic simulations of fiber-spacing variation, and showed that band gap phenomena can be enhanced by slight irregularity in the scattered arrangements. The typical scenario in mass-manufactured material represents a slight irregularity. Nakashima et al. [Nakashima et al., 2008] studied the effect of the randomness on 2D unidirectional fiber-reinforced composites using FE analysis. The numerical experiment was performed on a rectangular material with inclusions, and showed that the transmission coefficients fall to low values in stop bands. Recently, Ben Souf et al. [Ben Souf et al., 2015b] studied

the effect of uncertain parameters on sound transmission loss for composite panels using the generalized polynomial chaos expansion applied with a high level of uncertainty in conjunction with WFEM. Zakian et al. [Zakian and Khaji, 2018] proposed a stochastic spectral finite element method for the wave propagation in random media in 2D plates in the time domain in FE framework. Henneberg et al. [Henneberg et al., 2020] investigated the influence of geometrical uncertainties on periodic structures performed on an FE model of an epoxy plate with beam resonators. The stop band behavior under the influence of the material uncertainty was studied using the spectral stochastic method. The uncertainty was propagated using the generalized PEC varying the geometrical parameters. The simulation results suggested the necessity to consider uncertainties in periodic structures.

In non-probabilistic case, Zhu et al. [Zhu and Elis, 1993] studied combined probabilistic and convex theoretic approach for uncertainty in loading parameter. The least favorable stochastic response was estimated by the convex model. A finite span beam was subjected to a random acoustic pressure field and it was considered that the loading parameter belongs to the bounded convex set. The model is a set of functions, and each member function represents a possible realization of uncertain events. The convex model represents uncertain space-wise and time-wise varying excited vectors. The upper and lower bound of the mean square displacement of the structure are expressed by a closed-form solution. Xie et al. [Xie et al., 2017] investigated the topology optimization of 2D PnCs with uncertainties and proposed a surrogate model-based heuristic algorithm. The band diagram computed with the plane wave expansion method and interval model was introduced to handle the uncertainties based on MCS. Ma et al. [Ma and Li, 2018] studied the dynamic response of the uncertainty frame structure and proposed the travelling wave method integrated with interval method considering uncertainty in the geometric dimension and external load.

2.8 Conclusions

This chapter has provided an overview of previous research in the areas of periodic media and uncertainty quantification. The uncertainty in structural response such as dispersion

curve, frequency response function, natural frequency, and mode shapes is the result of propagation of uncertainty, which maybe parametrical or non-parametric. The aim of a parametric approach is to propagate the uncertainty model through the dynamic equations to convert the description of the uncertain input variables into a description of the uncertain response variables. The general classification of UQ is provided, and parametric uncertainty models, both probabilistic and non-probabilistic, have been reviewed with respect to their application to the analysis of structures with uncertain parameters. When information about the uncertainty variables are available, the probabilistic models are applicable. The details of the perturbation, MCS and PCE methods are explained. However, the application of a probabilistic approach faces two difficulties: (i) how to describe uncertain inputs when little information is available; and (ii) how to efficiently compute the uncertainty in the response. There are non-probabilistic models that can be introduced for the uncertainty propagation to overcome these difficulties. Details of the interval approach and fuzzy method are provided in the framework of non-probabilistic models. The deterministic models for periodic media analysis are also reviewed, followed by discussion of the literature on uncertainty analysis in 1D and 2D periodic media.

The picture that emerges from the literature study indicates that more research effort is required for developing vibroacoustic techniques in mid-frequency applications, with the uncertainty modelling being of particular interest. In the next chapter, SWFEM TM [Ichchou et al., 2011] is extended for free wave propagation and FRF in 1D periodic media.

Chapter 3

SWFEM in 1D periodic media

3.1 Introduction

In this chapter SWFEM based on the state space formulation is presented for 1D periodic media, which is an extension of the SWFEM formulation proposed by Ichchou et al. [Ichchou et al., 2011] for random media. The validation is presented for free and forced response. In the 1D case, the extended formulation is applied to free wave propagation and FRF computation of a periodic rod, metamaterial rod, geometrically varying beam, periodic beam, and metamaterial beam. These numerical model are validated with WFEM MCS. An elapsed computation time comparison is presented to determine the computation advantage of the SWFEM over the WFEM MCS.

3.2 SWFEM for free wave propogation

In a 1D periodic structure, the nodes on the boundaries of the periodic structure are denoted as on the left boundary (L), right boundary (R) and the remaining/internal nodes (I). The displacement DOF q is partitioned into left (q_L) and right (q_R). Similarly, forces are partitioned into left (F_L) and right (F_R). To accommodate the uncertainty effects, a random field is considered as a supplementary dimension through spatial discretization employing finite element steps by discretization of one sub-element of length (d). The discretization leads to stochastic dynamic equilibrium of any substructure in the following

manner:

$$(\widetilde{D})\begin{pmatrix}\widetilde{q}_L^{\boldsymbol{k}}\\ \widetilde{q}_R^{\boldsymbol{k}}\end{pmatrix}=\begin{pmatrix}\widetilde{F}_L^{\boldsymbol{k}}\\ \widetilde{F}_R^{\boldsymbol{k}}\end{pmatrix} \tag{3.1}$$

where $(\widetilde{D})$ is the stochastic complex dynamic stiffness matrix of the sub-structure. It is condensed on left and right boundaries degree of freedom at the pulsation ω:

$$(\widetilde{D})=-\omega^2\widetilde{M}+\widetilde{K}(1+i\eta) \tag{3.2}$$

where $\widetilde{M}$, and $\widetilde{K}$ are the stochastic mass and the stiffness matrix, respectively, η is the structural loss factor, i is the unit imaginary number, and ω is the circular frequency. In the probabilistic tools, the parametric approach allows considering the parameters uncertainties (material, geometrical properties, etc.) as random quantities. The random variables are modelled using the first-order perturbation, as Gaussian variables, such that the dynamical equilibrium is expressed as:

$$\left[-\omega^2\left(\overline{M}+\sigma_M\varepsilon\right)+\left(\overline{K}+\sigma_K\varepsilon\right)(1+i\eta)\right]\begin{pmatrix}\overline{q}_L^{(\boldsymbol{k})}+\sigma_{q_L}^{(\boldsymbol{k})}\varepsilon\\ \overline{q}_R^{(\boldsymbol{k})}+\sigma_{q_R}^{(\boldsymbol{k})}\varepsilon\end{pmatrix}=\begin{pmatrix}\overline{F}_L^{(\boldsymbol{k})}+\sigma_F^{(\boldsymbol{k})}\varepsilon\\ \overline{F}_R^{(\boldsymbol{k})}+\sigma_F^{(\boldsymbol{k})}\varepsilon\end{pmatrix} \tag{3.3}$$

The $\overline{(\ )}$ symbol denotes the mean value of the random variable, σ is the standard deviation, and ε is a Gaussian centered variable. In the expression $\overline{M}$, $\overline{K}$, $\overline{q}$, and $\overline{F}$ are mean quantities of the mass matrix, stiffness matrix, displacements vector and load vector, respectively; and σ_M, σ_K, σ_q, and σ_F are their respective standard deviations. The stochastic problem in Eq. (3.1) can be partitioned in the following way:

$$\begin{pmatrix}\widetilde{D}_{LL} & \widetilde{D}_{LR}\\ \widetilde{D}_{RL} & \widetilde{D}_{RR}\end{pmatrix}\begin{pmatrix}\tilde{q}_L^k\\ \tilde{q}_R^k\end{pmatrix}=\begin{pmatrix}\tilde{F}_L^k\\ \tilde{F}_R^k\end{pmatrix} \tag{3.4}$$

Using polynomial chaos projection of the variable in the Eq. (3.4), their mean value and standard deviation can be expressed in following form:

$$\begin{pmatrix}\overline{D}_{LL}+\sigma_{D_{LL}}\varepsilon & \overline{D}_{LR}+\sigma_{D_{LR}}\varepsilon\\ \overline{D}_{RL}+\sigma_{D_{RL}}\varepsilon & \overline{D}_{RR}+\sigma_{D_{RR}}\varepsilon\end{pmatrix}\begin{pmatrix}\overline{q}_L+\sigma_{q_L}\varepsilon\\ \overline{q}_R+\sigma_{q_R}\varepsilon\end{pmatrix}=\begin{pmatrix}\overline{F}_L+\sigma_{F_L}\varepsilon\\ \overline{F}_R+\sigma_{F_R}\varepsilon\end{pmatrix} \tag{3.5}$$

In the above expression $\overline{D}$, $\overline{q}$, and $\overline{F}$ are the mean quantities of the dynamic operators, the displacement vectors, and the loads, respectively; and σ_D, σ_q, and σ_F are their standard deviations. It is to be noted that Eq. (3.5) is valid and can accommodate the stochastic behavior of the stiffness and mass matrices. In the state-space formulation the stochastic kinematic variables, $\widetilde{q}$,and $\widetilde{F}$ are represented through stochastic state vectors as $\widetilde{u}_L = \left(\widetilde{q}_L^T \ -\widetilde{F}_L^T\right)^T$ and $\widetilde{u}_R = \left(\widetilde{q}_R^T \ \widetilde{F}_R^T\right)^T$;and related by the stochastic transfer matrix $\tilde{S}$:

$$\widetilde{u}_R^{\boldsymbol{k}} = \begin{pmatrix} -\left(\widetilde{D}_{LR}\right)^{-1}\widetilde{D}_{LL} & -\left(\widetilde{D}_{LR}\right)^{-1} \\ \widetilde{D}_{RL} - \widetilde{D}_{RR}\left(\widetilde{D}_{LR}\right)^{-1}\widetilde{D}_{LL} & -\widetilde{D}_{RR}\left(\widetilde{D}_{LR}\right)^{-1} \end{pmatrix} \tilde{u}_L^{\boldsymbol{k}}$$

$$\widetilde{u}_R^{\boldsymbol{k}} = \tilde{S}\tilde{u}_L^{\boldsymbol{k}} \tag{3.6}$$

Alternatively

$$\begin{pmatrix} \overline{q}_R + \sigma_{q_R}\varepsilon \\ \overline{F}_R + \sigma_{F_R}\varepsilon \end{pmatrix} = \begin{pmatrix} \overline{S}_{LL} + \sigma_{S_{LL}}\varepsilon & \overline{S}_{LR} + \sigma_{S_{LR}}\varepsilon \\ \overline{S}_{RL} + \sigma_{S_{RL}}\varepsilon & \overline{S}_{RR} + \sigma_{S_{RR}}\varepsilon \end{pmatrix} \begin{pmatrix} \overline{q}_L + \sigma_{q_L}\varepsilon \\ -\overline{F}_L - \sigma_F\varepsilon \end{pmatrix} \tag{3.7}$$

The zeroth-order expansion of the Eq. (3.7) leads to:

$$\begin{pmatrix} \overline{q}_R \\ \overline{F}_R \end{pmatrix} = \begin{pmatrix} \overline{S}_{LL} & \overline{S}_{LR} \\ \overline{S}_{RL} & \overline{S}_{RR} \end{pmatrix} \begin{pmatrix} \overline{q}_L \\ -\overline{F}_L \end{pmatrix} \tag{3.8}$$

Similarly, the zeroth-order development of the Eq. (3.5) leads to the following:

$$\begin{pmatrix} \overline{F}_L \\ \overline{F}_R \end{pmatrix} = \begin{pmatrix} \overline{D}_{LL} & \overline{D}_{LR} \\ \overline{D}_{RL} & \overline{D}_{RR} \end{pmatrix} \begin{pmatrix} \overline{q}_R \\ \overline{q}_R \end{pmatrix} \tag{3.9}$$

The expansion of Eq. (3.9) leads to:

$$\begin{pmatrix} \overline{q}_R \\ \overline{F}_R \end{pmatrix} = -\begin{pmatrix} \overline{D}_{LR} & 0 \\ \overline{D}_{RR} & -1 \end{pmatrix}^{-1} \begin{pmatrix} \overline{D}_{LL} & 1 \\ \overline{D}_{RL} & 0 \end{pmatrix} \begin{pmatrix} \overline{q}_L \\ -\overline{F}_L \end{pmatrix} \tag{3.10}$$

Eqs. (3.8) and (3.10) has similarity and can be written as:

$$\begin{pmatrix} \overline{S}_{LL} & \overline{S}_{LR} \\ \overline{S}_{RL} & \overline{S}_{RR} \end{pmatrix} = - \begin{pmatrix} \overline{D}_{LR} & 0 \\ \overline{D}_{RR} & 1 \end{pmatrix}^{-1} \begin{pmatrix} \overline{D}_{LL} & 1 \\ \overline{D}_{RL} & 0 \end{pmatrix}$$

$$\overline{S} = \begin{pmatrix} -\overline{D}_{LR}{}^{-1}\overline{D}_{LL} & -\overline{D}_{LR}{}^{-1} \\ \overline{D}_{RL} - \overline{D}_{RR}\overline{D}_{LR}{}^{-1}\overline{D}_{LL} & -\overline{D}_{RR}\overline{D}_{LR}{}^{-1} \end{pmatrix} \tag{3.11}$$

Similarly, the first-order development of the Eq. (3.7) leads to:

$$\begin{pmatrix} \sigma_{q_R} \\ \sigma_{F_R} \end{pmatrix} = \begin{pmatrix} \overline{S}_{LL} & \overline{S}_{LR} \\ \overline{S}_{RL} & \overline{S}_{RR} \end{pmatrix} \begin{pmatrix} \sigma_{q_L} \\ -\sigma_{F_L} \end{pmatrix} + \begin{pmatrix} \sigma_{S_{LL}} & \sigma_{S_{LR}} \\ \sigma_{S_{RL}} & \sigma_{S_{RR}} \end{pmatrix} \begin{pmatrix} \overline{q}_L \\ -\overline{F}_L \end{pmatrix} \tag{3.12}$$

The expansion of the Eq. (3.12) leads to:

$$\begin{pmatrix} \overline{D}_{LR} & 0 \\ \overline{D}_{RR} & -1 \end{pmatrix} \begin{pmatrix} \sigma_{q_R} \\ \sigma_{F_R} \end{pmatrix} + \begin{pmatrix} \overline{D}_{LL} & 1 \\ \overline{D}_{RL} & 0 \end{pmatrix} \begin{pmatrix} \sigma_{q_L} \\ -\sigma_{F_L} \end{pmatrix} + \begin{pmatrix} \sigma_{D_{LL}} & 0 \\ \sigma_{D_{RL}} & 0 \end{pmatrix} \begin{pmatrix} \overline{q}_L \\ -\overline{F}_L \end{pmatrix} + \begin{pmatrix} \sigma_{D_{LR}} & 0 \\ \sigma_{D_{RR}} & 0 \end{pmatrix} \begin{pmatrix} \overline{q}_R \\ \overline{F}_R \end{pmatrix} = 0 \tag{3.13}$$

Introducing $\begin{pmatrix} \overline{q}_R \\ \overline{F}_R \end{pmatrix}$ from Eq. (3.8), above equation leads to:

$$\begin{pmatrix} \overline{D}_{LR} & 0 \\ \overline{D}_{RR} & -1 \end{pmatrix} \begin{pmatrix} \sigma_{q_R} \\ \sigma_{F_R} \end{pmatrix} = - \begin{pmatrix} \overline{D}_{LL} & 1 \\ \overline{D}_{RL} & 0 \end{pmatrix} \begin{pmatrix} \sigma_{q_L} \\ -\sigma_{F_L} \end{pmatrix} - \left[\begin{pmatrix} \sigma_{D_{LL}} & 0 \\ \sigma_{D_{RL}} & 0 \end{pmatrix} + \begin{pmatrix} \sigma_{D_{LR}} & 0 \\ \sigma_{D_{RR}} & 0 \end{pmatrix} \begin{pmatrix} \overline{S}_{LL} & \overline{S}_{LR} \\ \overline{S}_{RL} & \overline{S}_{RR} \end{pmatrix} \right] \begin{pmatrix} \overline{q}_L \\ -\overline{F}_L \end{pmatrix} \tag{3.14}$$

By simplification of Eq. (3.14), the standard deviation of the stochastic left state vector expressed as:

$$\begin{pmatrix} \sigma_{q_R} \\ \sigma_{F_R} \end{pmatrix} = - \begin{pmatrix} \overline{D}_{LR} & 0 \\ \overline{D}_{RR} & -1 \end{pmatrix}^{-1} \begin{pmatrix} \overline{D}_{LL} & 1 \\ \overline{D}_{RL} & 0 \end{pmatrix} \begin{pmatrix} \sigma_{q_L} \\ -\sigma_{F_L} \end{pmatrix} - \begin{pmatrix} \overline{D}_{LR} & 0 \\ \overline{D}_{RR} & -1 \end{pmatrix}^{-1} \left[\begin{pmatrix} \sigma_{D_{LL}} & 0 \\ \sigma_{D_{RL}} & 0 \end{pmatrix} + \begin{pmatrix} \sigma_{D_{LR}} & 0 \\ \sigma_{D_{RR}} & 0 \end{pmatrix} \begin{pmatrix} \overline{S}_{LL} & \overline{S}_{LR} \\ \overline{S}_{RL} & \overline{S}_{RR} \end{pmatrix} \right] \begin{pmatrix} \overline{q}_L \\ -\overline{F}_L \end{pmatrix} \tag{3.15}$$

Eq. (3.15) represents the standard deviation of the stochastic left state vectors of Eq. (3.5). Similarly Eq. (3.12) represents the standard deviation of the stochastic left state vectors of Eq. (3.7). Here, comparison of Eq. (3.15) and Eq. (3.12), and identification of σ_S, leads to:

$$\begin{pmatrix} \sigma_{S_{LL}} & \sigma_{S_{LR}} \\ \sigma_{S_{RL}} & \sigma_{S_{RR}} \end{pmatrix} = - \begin{pmatrix} \overline{D}_{LR} & 0 \\ \overline{D}_{RR} & -1 \end{pmatrix}^{-1} \left[\begin{pmatrix} \sigma_{D_{LL}} & 0 \\ \sigma_{D_{RL}} & 0 \end{pmatrix} + \begin{pmatrix} \sigma_{D_{LR}} & 0 \\ \sigma_{D_{RR}} & 0 \end{pmatrix} \begin{pmatrix} \overline{S}_{LL} & \overline{S}_{LR} \\ \overline{S}_{RL} & \overline{S}_{RR} \end{pmatrix} \right] \tag{3.16}$$

Introducing $\overline{S}$ from Eq. (3.11) in the above equation leads to:

$$\begin{pmatrix} \sigma_{S_{LL}} & \sigma_{S_{LR}} \\ \sigma_{S_{RR}} & \sigma_{S_{RR}} \end{pmatrix} = - \begin{pmatrix} \overline{D}_{LR} & 0 \\ \overline{D}_{RR} & -1 \end{pmatrix}^{-1} \left[\begin{pmatrix} \sigma_{D_{DL}} & 0 \\ \sigma_{D_{RL}} & 0 \end{pmatrix} + \begin{pmatrix} \sigma_{D_{LR}} & 0 \\ \sigma_{D_{RR}} & 0 \end{pmatrix} \right] \begin{pmatrix} -\overline{D}_{LR}{}^{-1}\overline{D}_{LL} & -\overline{D}_{LR}{}^{-1} \\ \overline{D}_{RL} - \overline{D}_{RR}\overline{D}_{LR}{}^{-1}\overline{D}_{LL} & -\overline{D}_{RR}\overline{D}_{LR}{}^{-1} \end{pmatrix} \tag{3.17}$$

Then the standard deviation of stochastic transfer matrix is:

$$\sigma_S = \begin{pmatrix} -\overline{D}_{LR} & 0 \\ -\overline{D}_{RR} & 1 \end{pmatrix}^{-1} \begin{pmatrix} \sigma_{D_{LL}} & \sigma_{D_{LR}} \\ \sigma_{D_{RL}} & \sigma_{D_{RR}} \end{pmatrix} \begin{pmatrix} 1 & 0 \\ -\overline{D}_{LR}{}^{-1}\overline{D}_{LL} & -\overline{D}_{LR}{}^{-1} \end{pmatrix} \tag{3.18}$$

Eq. (3.18) is only valid for the single cell. For complex geometry, the internal degree of freedom can be removed using dynamic condensation. The expression for the standard deviation of the condensed dynamic stiffness matrix is derived next.

3.2.1 Derivation for the standard deviation of the condensed dynamic stiffness matrix for 1D periodic media

If the formulation requires the dynamic condensation of the inner DOFs at each frequency step, the standard deviation of the condensed dynamic stiffness matrix has to be evaluated. Having internal DOFs,(I) as shown in Fig. 3.1, the DOFs are partitioned into the left boundary DOFs (D_L), right boundary DOFs (D_R), and internal DOFs (D_I). Introducing

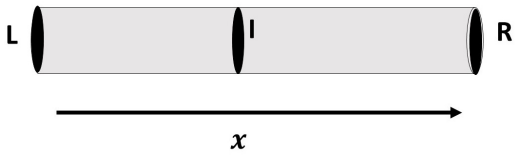

Figure 3.1: 1D element with internal node

uncertainties in the parameters, the stochastic dynamic stiffness matrix has the following form:

$$\widetilde{D} = \begin{bmatrix} \widetilde{\widehat{D}}_{LL} & \widetilde{\widehat{D}}_{LI} & \widetilde{\widehat{D}}_{LR} \\ \widetilde{\widehat{D}}_{IL} & \widetilde{\widehat{D}}_{II} & \widetilde{\widehat{D}}_{IR} \\ \widetilde{\widehat{D}}_{RL} & \widetilde{\widehat{D}}_{RI} & \widetilde{\widehat{D}}_{RR} \end{bmatrix} \tag{3.19}$$

where symbol $\widetilde{\widehat{()}}$ represents the stochastic entity from the original dynamic stiffness matrix. The dynamic condensation and the zeroth-order expansion of the above equation leads to:

$$\overline{\mathrm{D}} = \begin{bmatrix} \overline{D}_{LL} & \overline{D}_{LR} \\ \overline{D}_{RL} & \overline{D}_{RR} \end{bmatrix}$$

$$\overline{\mathrm{D}} = \begin{bmatrix} \overline{\widehat{D}}_{LL} - \overline{\widehat{D}}_{LI}\overline{\widehat{D}}_{II}^{-1}\overline{\widehat{D}}_{IL} & \overline{\widehat{D}}_{LR} - \overline{\widehat{D}}_{LI}\overline{\widehat{D}}_{II}^{-1}\overline{\widehat{D}}_{IR} \\ \overline{\widehat{D}}_{RL} - \overline{\widehat{D}}_{RI}\overline{\widehat{D}}_{II}^{-1}\overline{\widehat{D}}_{IL} & \overline{\widehat{D}}_{RR} - \overline{\widehat{D}}_{RI}\overline{\widehat{D}}_{II}^{-1}\overline{\widehat{D}}_{IR} \end{bmatrix} \tag{3.20}$$

The dynamic condensation and first order expansion of Eq. (3.20) leads to:

$$\sigma_D = \begin{bmatrix} \sigma_{D_{LL}} & \sigma_{D_{LR}} \\ \sigma_{D_{RL}} & \sigma_{D_{RR}} \end{bmatrix} \tag{3.21}$$

where

$$\sigma_{D_{LL}} = \sigma_{\widehat{D}_{LL}} - \overline{\widehat{D}}_{LI}\overline{\widehat{D}}_{II}^{-1}\sigma_{\widehat{D}_{IL}} + \overline{\widehat{D}}_{LI}\overline{\widehat{D}}_{II}^{-2}\sigma_{\widehat{D}_{II}}\overline{\widehat{D}}_{IL} - \sigma_{\widehat{D}_{LI}}\overline{\widehat{D}}_{II}^{-1}\overline{\widehat{D}}_{IL}$$

$$\sigma_{D_{LR}} = \sigma_{\widehat{D}_{LR}} - \overline{\widehat{D}}_{LI}\overline{\widehat{D}}_{II}^{-1}\sigma_{\widehat{D}_{IR}} + \overline{\widehat{D}}_{LI}\overline{\widehat{D}}_{II}^{-2}\sigma_{\widehat{D}_{II}}\overline{\widehat{D}}_{IR} - \sigma_{\widehat{D}_{LI}}\overline{\widehat{D}}_{II}^{-1}\overline{\widehat{D}}_{IR}$$

$$\sigma_{D_{RL}} = \sigma_{\widehat{D}_{RL}} - \overline{\widehat{D}}_{RI}\overline{\widehat{D}}_{II}^{-1}\sigma_{\widehat{D}_{IL}} + \overline{\widehat{D}}_{RI}\overline{\widehat{D}}_{II}^{-2}\sigma_{\widehat{D}_{II}}\overline{\widehat{D}}_{IL} - \sigma_{\widehat{D}_{RI}}\overline{\widehat{D}}_{II}^{-1}\overline{\widehat{D}}_{IL}$$

$$\sigma_{D_{RR}} = \sigma_{\widehat{D}_{RR}} - \overline{\widehat{D}}_{RI}\overline{\widehat{D}}_{II}^{-1}\sigma_{\widehat{D}_{IR}} + \overline{\widehat{D}}_{RI}\overline{\widehat{D}}_{II}^{-2}\sigma_{\widehat{D}_{II}}\overline{\widehat{D}}_{IR} - \sigma_{\widehat{D}_{RI}}\overline{\widehat{D}}_{II}^{-1}\overline{\widehat{D}}_{IR}$$

Above expressions are organized in the matrix form as:

$$\sigma_D = \begin{bmatrix} \sigma_{\widehat{D}_{LL}} & \sigma_{\widehat{D}_{LR}} \\ \sigma_{\widehat{D}_{RL}} & \sigma_{\widehat{D}_{RR}} \end{bmatrix} - \begin{bmatrix} \overline{\widehat{D}}_{LI} & \sigma_{\widehat{D}_{LI}} \\ \overline{\widehat{D}}_{RI} & \sigma_{\widehat{D}_{RI}} \end{bmatrix} \begin{bmatrix} \overline{\widehat{D}}_{II}^{-1} & -\overline{\widehat{D}}_{II}^{-2}\sigma_{\widehat{D}_{II}} \\ 0 & \overline{\widehat{D}}_{II}^{-1} \end{bmatrix} \begin{bmatrix} \sigma_{\widehat{D}_{IL}} & \sigma_{\widehat{D}_{IR}} \\ \overline{\widehat{D}}_{IL} & \overline{\widehat{D}}_{IR} \end{bmatrix} \tag{3.22}$$

To simplify the computation, standard deviation of the condensed dynamic stiffness matrix is arranged as follows:

$$\sigma_D = \begin{bmatrix} \sigma_{\widehat{D}_{LL}} & \sigma_{\widehat{D}_{LR}} \\ \sigma_{\widehat{D}_{RL}} & \sigma_{\widehat{D}_{RR}} \end{bmatrix} - \begin{bmatrix} \overline{\widehat{D}}_{LI} & \sigma_{\widehat{D}_{LI}} \\ \overline{\widehat{D}}_{RI} & \sigma_{\widehat{D}_{RI}} \end{bmatrix} \begin{bmatrix} \overline{\widehat{D}}_{II}^{-1} & -\overline{\widehat{D}}_{II}^{-1}\sigma_{\widehat{D}_{II}}\overline{\widehat{D}}_{II}^{-1} \\ 0 & \overline{\widehat{D}}_{II}^{-1} \end{bmatrix} \begin{bmatrix} \sigma_{\widehat{D}_{IL}} & \sigma_{\widehat{D}_{IR}} \\ \overline{\widehat{D}}_{IL} & \overline{\widehat{D}}_{IR} \end{bmatrix} \tag{3.23}$$

where symbol $\overline{\widehat{()}}$ represents the mean value from the original dynamic stiffness matrix. Following the steps of the deterministic development, a stochastic eigenvalue problem formulated as:

$$\begin{aligned} \widetilde{S}\widetilde{\phi}_i &= \widetilde{\mu}_i\widetilde{\phi}_i \\ \left|\widetilde{S} - \widetilde{\mu}_i I_{2n}\right| &= 0 \end{aligned} \tag{3.24}$$

where $\left(\widetilde{\mu}_i, \widetilde{\phi}_i\right)_{i=1\ldots2n}$ are the stochastic waveguide propagation modes and n is the number of waves, which is equivalent to the cross section DOFs. Then the stochastic eigensolutions of Eq. (3.24) are expressed as follows:

$$\begin{aligned} \widetilde{\mu}_i &= (\overline{\mu}_i + \sigma_{\mu_i}\varepsilon) \\ \widetilde{\phi}_i &= \left(\overline{\phi}_i + \sigma_{\phi_i}\varepsilon\right) \end{aligned} \tag{3.25}$$

The stochastic eigenvalues are associated to eigenvectors. Then, the zeroth-order expansion of Eq. (3.24) leads to:

$$\left(\overline{S} - \overline{\mu}_i I_{2n}\right)\overline{\phi}_i = 0 \tag{3.26}$$

Similarly, the first-order expansion of Eq. (3.24) leads to:

$$\left(\overline{S} - \overline{\mu}_i I_{2n}\right) \sigma_{\phi_i} + \left(\sigma_s - \sigma_{\mu_i} I_{2n}\right) \overline{\phi}_i = 0 \tag{3.27}$$

In order to extract the first-order perturbation of eigenvalues and eigenvectors, we use the left propagation constants. Here $\widetilde{\phi}_i^T J_n$ is a left eigenvector of $\widetilde{S}$ that is associated to the eigenvalue $\frac{1}{\widetilde{\mu}_i}$, where

$$J_n = \begin{pmatrix} 0 & I_n \\ -I_n & 0 \end{pmatrix} \tag{3.28}$$

The left stochastic eigenvalue problem can be established as:

$$\left(\widetilde{\phi}_i^T J_n\right) \widetilde{S} = \frac{1}{\widetilde{\mu}_i} \left(\widetilde{\phi}_i^T J_n\right) \tag{3.29}$$

The first-order expansion of Eq. (3.29) leads to:

$$\left(\sigma_{\phi_i}\right)^T J_n \left(\overline{S} - \frac{1}{\widetilde{\mu}_i} I_{2n}\right) + \overline{\phi}_i^T J_n \left(\sigma_S + \frac{1}{\overline{\mu}_i^2} \sigma_{\mu_i} I_{2n}\right) = 0 \tag{3.30}$$

Simplification of Eq. (3.27) and Eq. (3.30) leads to standard deviation of eigenvalues (σ_{μ_i}) as:

$$\begin{aligned} \sigma_{\mu_i} = &\left[\left(\overline{\phi}_i\right)^T \sigma_S^T \left(\overline{S}^T - \overline{\mu}_i I_{2n}\right)^{-1} J_n \left(\overline{S} - \left(\tfrac{1}{\widetilde{\mu}_i} I_{2n}\right) - \left(\overline{\phi}_i\right)^T J_n \sigma_S\right)\right] \\ &\left[\left(\overline{\phi}_i\right)^T \left(\overline{S}^T - \overline{\mu}_i I_{2n}\right)^{-1} J_n \left(\overline{S} - \left(\overline{\mu}_i\right)^{-1} I_{2n}\right) - \tfrac{1}{\overline{\mu}_i^2} \left(\overline{\phi}_i\right)^T J_n\right]^+ \end{aligned} \tag{3.31}$$

Similarly, the standard deviation of the eigenvectors (σ_{ϕ_i}) as:

$$\sigma_{\phi_i} = -\left[\overline{S} - \overline{\mu}_i I_{2n}\right]^+ \left[\sigma_S - \sigma_{\mu_i} I_{2n}\right] \overline{\phi}_i \tag{3.32}$$

where + is pseudo inverse. Using Eq. (3.31) and Eq. (3.32), the statistics of the wave characteristics can be expressed using the standard deviation of the propagation constants. Let us consider statistics of the wavenumber expressed as:

$$\widetilde{k} = \left(\frac{i}{d}\right) \log \widetilde{\mu} \tag{3.33}$$

where stochastic wavenumber expressed $\widetilde{k} = \overline{k} + \sigma_k \varepsilon$. Once the zeroth and first-order terms of the stochastic eigenvalue are computed, then we can use the statistics of k from Eq. (3.33) to find mean value and dispersion from the mean value. The mean of the wavenumber expressed as:

$$\overline{k} = \left(\frac{i}{d}\right) \log(\overline{\mu}) \tag{3.34}$$

Similarly, the dispersion of the wavenumber from the mean can be expressed as:

$$\sigma_k = \left(\frac{i}{d}\right) \frac{\sigma_\mu}{\overline{\mu}} \tag{3.35}$$

where d is sub-structure length.

3.2.2 Attached resonators

For the low-frequency range, band gaps can be achieved by mounting periodically local resonators. The LR metamaterial-based system consists of a uniform host structure and periodically attached springs ($\boldsymbol{k}_i$) and masses ($\boldsymbol{m}_i$). The number of springs and masses in the resonator can be chosen based on targeted band gap characteristics as per the design of the metamaterial system [Nobrega et al., 2016]. The unit cell of the LR system is shown in Fig. 3.2. The dynamic stiffness matrix (D_0) of the resonator at the attachment point

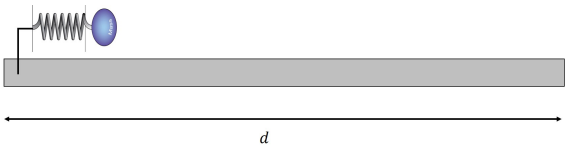

Figure 3.2: Unit cell with local resonator

can be written as [Xiao et al., 2012]:

$$D_0 = \boldsymbol{k}_i - \left(\boldsymbol{k}_i^2 / \left(\boldsymbol{k}_i - \omega^2 \boldsymbol{m}_i\right)\right) \tag{3.36}$$

Once the dynamic stiffness matrix for the LR is obtained, then it needs to be attached to the unit cell of the host structures. The dynamic stiffness matrix of the LR system is obtained as:

$$D = \begin{bmatrix} D_{LL} & D_{LR} \\ D_{RL} & D_{RR} \end{bmatrix} = \begin{bmatrix} D_{LL} + D_0 & D_{LR} \\ D_{RL} & D_{RR} \end{bmatrix} \tag{3.37}$$

In the host structure, the stochastic equation of motion can be expressed as:

$$\begin{pmatrix} \widetilde{D}_{LL} & \widetilde{D}_{LR} \\ \widetilde{D}_{RL} & \widetilde{D}_{RR} \end{pmatrix} \begin{pmatrix} \widetilde{q}_L^{\boldsymbol{k}} \\ \widetilde{q}_R^{\boldsymbol{k}} \end{pmatrix} = \begin{pmatrix} \widetilde{F}_L^{\boldsymbol{k}} \\ \widetilde{F}_R^{\boldsymbol{k}} \end{pmatrix} \tag{3.38}$$

The above expression is similar to the stochastic equation of motion expressed in Eq. (3.4). The stochastic wavenumber characterization can be obtained by using explicit Eq. (3.31), Eq. (3.32).

3.3 SWFEM for forced response

In this section, the harmonic response and effects of uncertainties in terms of kinematic variables, displacement, and forces linked to periodic media, are presented. In reality, structures are not infinite but have finite dimensions. The finite periodic structure is composed of N identical sub-elements. Considering the material properties to have the uncertainties, the frequency response of this system can be expressed by expanding the kinematic variable of the considered sub-system on the basis of eigenvectors [Mencik and Ichchou, 2007] by:

$$\begin{pmatrix} q_L \\ -F_L \end{pmatrix} = \begin{bmatrix} \Phi_q \\ \Phi_F \end{bmatrix} Q_L, \begin{pmatrix} q_R \\ -F_R \end{pmatrix} = \begin{bmatrix} \Phi_q \\ \Phi_F \end{bmatrix} Q_R \tag{3.39}$$

where Φ_q and Φ_F are the matrices of the eigenvector. The terms Q_L and Q_R are the generalized coordinated for the sub-system at the left and right boundaries. Also shown that based on the classification of the eigenvector into incident and reflected waves, generalized coordinate Q_L and Q_L are related by:

$$Q_R = \begin{bmatrix} \boldsymbol{\mu} & 0 \\ 0 & \boldsymbol{\mu}^{-1} \end{bmatrix} Q_L \tag{3.40}$$

where $\boldsymbol{\mu}$ is the matrix of the eigenvalues $\{\mu_i\}_{i=1,\ldots,n}$ using the modal decomposition, the stochastic kinematic variable can be projected on the wave mode base expressed for each

cell $\boldsymbol{k}$. The stochastic state vector is defined as:

$$\tilde{u}_L^{(\boldsymbol{k})} = \begin{pmatrix} \tilde{q}_L^{(\boldsymbol{k})} \\ -\tilde{F}_L^{(\boldsymbol{k})} \end{pmatrix}, \tilde{u}_R^{(\boldsymbol{k})} = \begin{pmatrix} \tilde{q}_R^{(\boldsymbol{k})} \\ \tilde{F}_R^{(\boldsymbol{k})} \end{pmatrix} \tag{3.41}$$

Using the multi-mode method [Mencik and Ichchou, 2005], the stochastic kinematic variable can be projected on the stochastic wave mode bases.

$$\begin{aligned} \tilde{u}_L^{(\boldsymbol{k})} &= \tilde{\Phi}\tilde{Q}^{(\boldsymbol{k})} \\ \tilde{u}_R^{(\boldsymbol{k})} &= \tilde{\Phi}\tilde{Q}^{(\boldsymbol{k}+1)} \quad \forall \quad \boldsymbol{k} \in \{1 \dots N\} \end{aligned} \tag{3.42}$$

where $\tilde{\Phi}=\begin{pmatrix} \tilde{\Phi}_q^{inc} & \tilde{\Phi}_q^{ref} \\ \tilde{\Phi}_F^{inc} & \tilde{\Phi}_F^{ref} \end{pmatrix}$ is the matrix of the stochastic eigenvectors, which are independent and $\tilde{Q}=\begin{pmatrix} \tilde{Q}^{inc} \\ \tilde{Q}^{ref} \end{pmatrix}^{(\boldsymbol{k})}$ is the vector of the stochastic wave mode amplitude for substructure $\boldsymbol{k}$. $\tilde{Q}^{inc}$ is the stochastic amplitude of the incident mode and $\tilde{Q}^{ref}$ for the reflected mode. Using Bloch's theorem, the stochastic amplitude of the $\boldsymbol{k}$th element in the waveguide can be obtained from the stochastic amplitude of the wave of the first element by:

$$\tilde{Q}^{(\boldsymbol{k})} = \begin{pmatrix} \tilde{\mu}^{inc} & 0 \\ 0 & \tilde{\mu}^{ref} \end{pmatrix}^{(\boldsymbol{k}-1)} \tilde{Q}^{(1)} \tag{3.43}$$

Considering that the periodic structure is free-fixed, and exited with a sinusoidal forces. Then the projection of the kinematic variables on the waves basis. The boundary conditions are as follows: Boundary condition at $x = 0$:

$$\tilde{\Phi}_F^{inc}\tilde{Q}^{inc(1)} + \tilde{\Phi}_F^{ref}\tilde{Q}^{ref(1)} = -\tilde{F}_L^{(1)} \tag{3.44}$$

Boundary condition at $x = L$:

$$\tilde{\Phi}_q^{inc}\tilde{Q}^{inc(N+1)} + \tilde{\Phi}_q^{ref}\tilde{Q}^{ref(N+1)} = \tilde{q}_R^{(N)} \tag{3.45}$$

Now using the condition expressed in Eq. (3.43), the second boundary condition becomes:

$$\tilde{\Phi}_q^{inc}\tilde{\mu}^{N}\tilde{Q}^{inc(1)} + \tilde{\Phi}_q^{ref}\tilde{\mu}^{-N}\tilde{Q}^{ref(1)} = \tilde{q}_R^{(N)} \tag{3.46}$$

The above boundary conditions are expressed in the matrix form as:

$$\begin{pmatrix} \tilde{\Phi}_F^{inc} & \tilde{\Phi}_F^{ref} \\ \tilde{\Phi}_q^{inc}\tilde{\mu}^{(inc)N} & \tilde{\Phi}_q^{ref}\tilde{\mu}^{(ref)N} \end{pmatrix} \begin{pmatrix} \tilde{Q}^{inc(1)} \\ \tilde{Q}^{ref(1)} \end{pmatrix} = \begin{pmatrix} -\tilde{F} \\ \tilde{q} \end{pmatrix} \tag{3.47}$$

Then, projection of Eq. (3.47) leads to identify the zeroth-order term (mean value) as:

$$\overline{Q}^{(1)} = \begin{pmatrix} \overline{\Phi}_F^{inc} & \overline{\Phi}_F^{ref} \\ \overline{\Phi}_q^{inc}\overline{\mu}^{(inc)N} & \overline{\Phi}_q^{ref}\overline{\mu}^{(ref)N} \end{pmatrix} \begin{pmatrix} \overline{Q}^{inc(1)} \\ \overline{Q}^{ref(1)} \end{pmatrix} = \begin{pmatrix} -\overline{F} \\ \overline{q} \end{pmatrix} \tag{3.48}$$

The direct inversion of above matrix is not possible, so, to better condition the matrix, appropriate scaling is needed by decoupling the ill-conditioned matrix into two matrices; first matrix, well-conditioned and second with diagonal matrix. Then from well-conditioned matrix the mean value of wave amplitude can be calculated with following expression:

$$\begin{pmatrix} \overline{Q}^{inc(1)} \\ \overline{Q}^{ref(1)} \end{pmatrix} = \begin{pmatrix} I_n & 0 \\ 0 & \overline{\mu}^{(inc)N} \end{pmatrix} \begin{pmatrix} \overline{\Phi}_F^{inc} & \overline{\Phi}_F^{ref}\overline{\mu}^N \\ \overline{\Phi}_q^{inc}\overline{\mu}^N & \overline{\Phi}_q^{ref} \end{pmatrix}^+ \begin{pmatrix} -\overline{F} \\ \overline{q} \end{pmatrix} \tag{3.49}$$

Also the first-order projection of Eq. (3.47) leads to identification of the first-order term (standard deviation) of the wave amplitude as:

$$(\sigma_Q)^{(1)} = \begin{pmatrix} I_n & 0 \\ 0 & \overline{\mu}^{(inc)N} \end{pmatrix} \begin{pmatrix} \overline{\Phi}_F^{inc} & \overline{\Phi}_F^{ref}\overline{\mu}^N \\ \overline{\Phi}_q^{inc}\overline{\mu}^N & \overline{\Phi}_q^{ref} \end{pmatrix}^+ \left[\begin{pmatrix} -\sigma_F \\ \sigma_q \end{pmatrix} - \sigma_A \begin{pmatrix} \overline{Q}^{inc(1)} \\ \overline{Q}^{ref(1)} \end{pmatrix} \right] \tag{3.50}$$

where term

$$\sigma_A = \begin{pmatrix} \sigma_{\Phi_f^{inc}} & \sigma_{\Phi_f^{ref}} \\ \sigma_{\Phi_q^{inc}} \left(\overline{\mu}^{inc}\right)^N + N\overline{\Phi}_q^{inc} \left(\overline{\mu}^{inc}\right)^{(N-1)} \sigma_\mu inc & \sigma_{\Phi_q^{ref}} \left(\overline{\mu}^{ref}\right)^N + N\overline{\Phi}_q^{ref} \left(\overline{\mu}^{ref}\right)^{(N-1)} \sigma_\mu ref \end{pmatrix}$$

where + is pseudo inverse. Knowing the statistics of the amplitude of the first sub-element, the statistics at any element in the structure is expressed using Eq. (3.43) as:

$$\begin{pmatrix} \sigma_{Q^{inc}} \\ \sigma_{Q^{ref}} \end{pmatrix}^{(\boldsymbol{k})} = \begin{pmatrix} \overline{\mu}^{inc} & 0 \\ 0 & \overline{\mu}^{ref} \end{pmatrix}^{(\boldsymbol{k}-1)} \begin{pmatrix} \sigma_{Q^{inc}} \\ \sigma_{Q^{ref}} \end{pmatrix}^{(1)} + (\boldsymbol{k}-1) \begin{pmatrix} \left(\overline{\mu}^{inc}\right)^{(\boldsymbol{k}-2)} \sigma_{\mu^{inc}} & 0 \\ 0 & \left(\overline{\mu}^{ref}\right)^{(\boldsymbol{k}-2)} \sigma_{\mu^{ref}} \end{pmatrix} \begin{pmatrix} \overline{Q}^{inc} \\ \overline{Q}^{inc} \end{pmatrix}^{(1)} \tag{3.51}$$

The equation connecting the stochastic state vector to the stochastic amplitude of the modes, expressed as:

$$(\tilde{q})^{(\boldsymbol{k})} = \begin{pmatrix} \tilde{\Phi}_q^{inc} & \tilde{\Phi}_q^{ref} \\ \tilde{\Phi}_q^{inc}\tilde{\mu}^{inc} & \tilde{\Phi}_q^{ref}\tilde{\mu}^{ref} \end{pmatrix} (\tilde{Q})^{(\boldsymbol{k})} \tag{3.52}$$

The projection of Eq. (3.52)lead to zeroth-order terms (mean value) as:

$$(\overline{q})^{(\boldsymbol{k})} = \begin{pmatrix} \overline{\Phi}_q^{inc} & \overline{\Phi}_q^{ref} \\ \overline{\Phi}_q^{inc}\overline{\mu}^{inc} & \overline{\Phi}_q^{ref}\overline{\mu}^{ref} \end{pmatrix} (\overline{Q})^{(\boldsymbol{k})} \tag{3.53}$$

And, first-order term as the standard deviation of the the nodal displacement of the both side of the element $\boldsymbol{k}$ as:

$$(\sigma_q)^{(\boldsymbol{k})} = \begin{pmatrix} \overline{\Phi}_q^{inc} & \overline{\Phi}_q^{ref} \\ \overline{\Phi}_q^{inc}\overline{\mu}^{inc} & \overline{\Phi}_q^{ref}\overline{\mu}^{ref} \end{pmatrix} (\sigma_Q)^{(\boldsymbol{k})} + \begin{pmatrix} \sigma_{\Phi_q^{inc}} & \sigma_{\Phi_q^{ref}} \\ \sigma_{\Phi_q^{inc}}\overline{\mu}^{inc} + \Phi_q^{inc}\sigma_{\mu^{inc}} & \sigma_{\Phi_q^{ref}} + \Phi_q^{ref}\sigma_{\mu ref} \end{pmatrix} \overline{Q}^{(\boldsymbol{k})} \tag{3.54}$$

Eq. (3.54) is used to find the statistics of the displacement at each node for the sub-element $\boldsymbol{k}$ in the periodic structure.

3.4 Numerical results

This section shows the validation of the SWFEM formulation considering a binary periodic rod and periodic beam. The periodic rod and beam consist of section A of length l_1 and

section B of length l_2 as depicted in Fig. 3.3. Here, sections A and B are made of different materials. In the first case, longitudinal waves are studied, while in the second case flexural waves are studied in a beam of circular section.

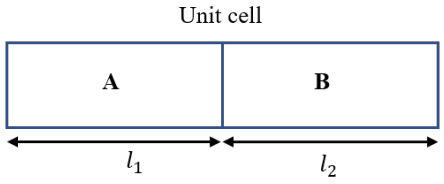

Figure 3.3: Symmetric unit cell

3.4.1 Monte Carlo simulation

As the number of samples is increased, the sampling error is decreased; so 10,000 samples are chosen to obtain the reference results. The analytical sampling and MCS results are treated as reference results for validation purpose. The workflow of the MCS is shown in Fig. 3.4.

3.4.2 Analysis of free wave propagation

In this subsection, the SWFEM is used to study the effect of parametric uncertainty on the dispersion relation of the longitudinal wavenumber in a periodic rod with sections A and B.

Periodic rod

The reference analytical solution of a periodic rod is based on the following expression of the wavenumber [Tian et al., 2011]:

$$\cos(kl) = \cos\left(\frac{\omega}{c_a} l_a\right) \cos\left(\frac{\omega}{c_b} l_b\right) - \frac{1}{2}\left(\frac{\rho_a c_a}{\rho_b c_b} + \frac{\rho_b c_b}{\rho_a c_a}\right) \sin\left(\frac{\omega}{c_a} l_a\right) \sin\left(\frac{\omega}{c_b} l_b\right) \tag{3.55}$$

where c_a, and, c_b are the wave velocity in sections A and B, respectively, and expressed as $c_a = \sqrt{E_a/\rho_a}$ and $c_b = \sqrt{E_b/\rho_b}$, E_a, ρ_a, and l_a are the Young's modulus, density and length for section A and E_b, ρ_b, and l_b are those for section B. l is the total length of

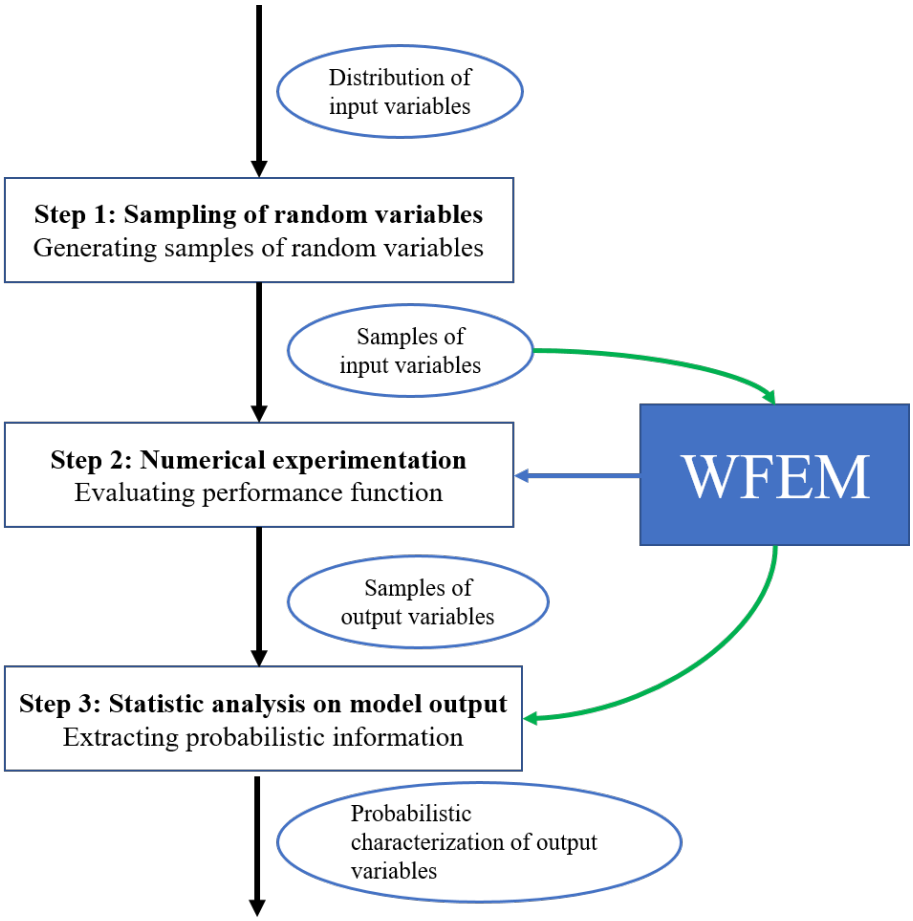

Figure 3.4: WFEM MCS workflow

the unit cell. The uncertainty effect is studied considering a variation of (4%) of Young's modulus nominal values. It is to be mentioned that the input uncertainties are represented inside the bracket (). The frequency range is 10-1500 Hz. The sampling method is used to obtain the wave characteristics of the analytical wavenumber obtained using Eq. (3.55). A two-node rod element with one DOF per node is considered that allows treatments of longitudinal wave. The local stiffness and mass matrices are assembled into global stiffness and mass matrices in the MATLAB environment, with 200 elements in the unit cell of the periodic rod. In this way, the wavelength contains at least 20 elements in the frequency range. The material and geometric properties are reported in Table 3.1.

The results obtained with analytical sampling, SWFEM TM and WFEM MCS are compared. Comparision of the mean values is shown in Fig. 3.5(a); there exists one full band gap at approximately 418-928 Hz. The comparison of the standard deviation is presented in Fig. 3.5(b). The mean value and standard deviation are in good agreement. The

Table 3.1: Material and geometric properties of periodic rod

Geometry/Property	Value
Rod length (A)	1 m
Rod length (B)	1 m
Radius of rod	0.0644 m
Young's modulus (A)	4.50 $\times 10^9$ Pa
Young's modulus (B)	70 $\times 10^9$ Pa
Mass density (A)	1200 kg/m^3
Mass density (B)	2700 kg/m^3
Loss factor (A) and (B)	0.001

SWFEM standard deviation is computed considering loss factor, whilst on the other hand the analytical sampling is computed without damping. It is observed that the effect of the uncertainty on the longitudinal wavenumber, is nearly 3% at the start of the band gap, and nearly 10% nearly at the end of the band gap. With increasing frequency, the uncertainty effect is growing, as it can be seen that variation is around 33% at the start of the second bandgap frequency. This suggests that the effect of the uncertainty is increasing with increasing frequency range for longitudinal wavenumber. The uncertainty effect is also studied considering a variation of (4%) of the nominal values of mass density. The results obtained with analytical sampling, SWFEM TM, and WFEM MCS are compared. The mean values comparison is shown in Fig. 3.6(a) and the standard deviation comparison is presented in Fig. 3.6(b). The results are in good agreement.

Periodic beam

The uncertainty effect on the flexural wave in a periodic beam is studied by considering the Euler-Bernoulli beam theory. The material and geometric properties are reported in Table 3.2. For the numerical formulation, the two-node beam element with two degrees of freedom per node is considered. The frequency range of computation is 10-1500 Hz. Considering the uncertainty in Young's modulus of the binary periodic beam to be (4%) about the nominal value, the numerical experiment is performed with SWFEM formulation. To validate the obtained result, an MCS study is carried out. Fig. 3.7(a) shows the comparison of the mean value of the flexural wavenumber obtained from SWFEM and MCS on the WFEM simulation. In Fig. 3.7(b), the standard deviation comparison is shown from SWFEM and MCS results. The results are in good agreement, which confirmed the

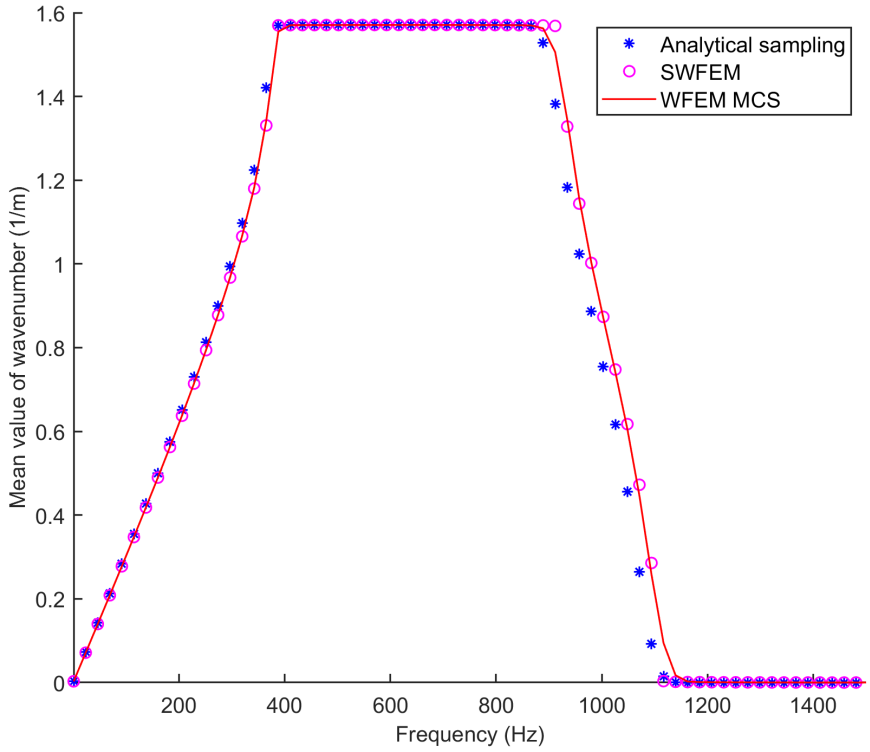

(a) Mean value comparison

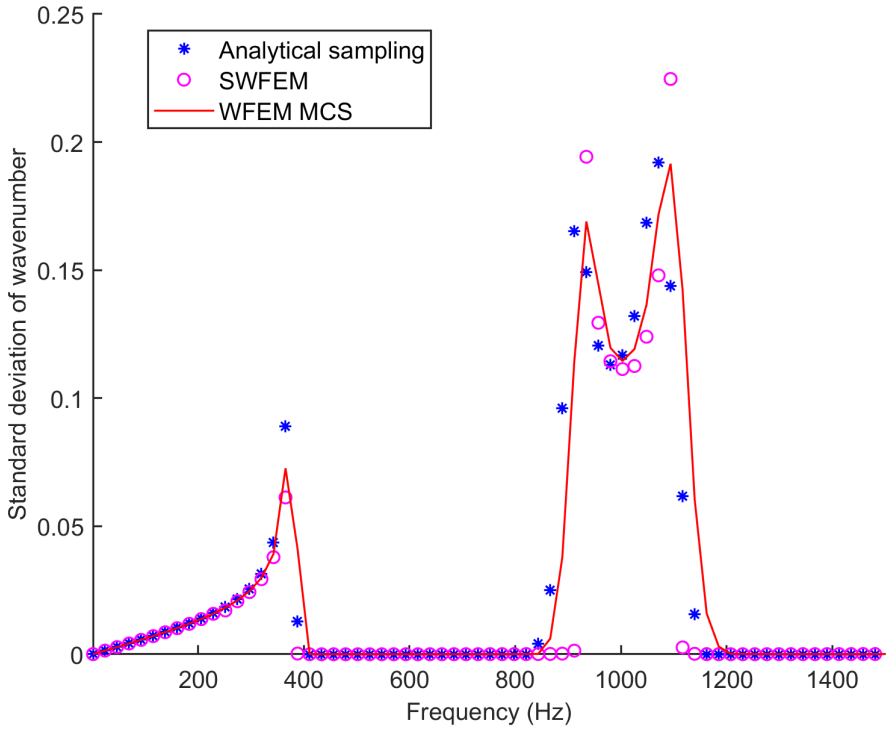

(b) Standard deviation comparison

Figure 3.5: Validation of the periodic rod with 4% stochastic elasticity

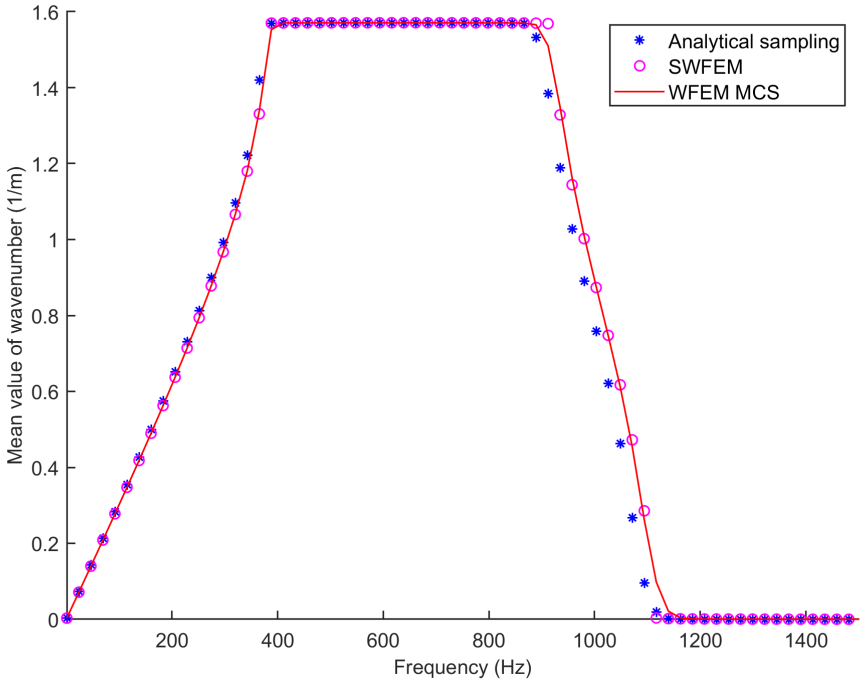

(a) Mean value comparison

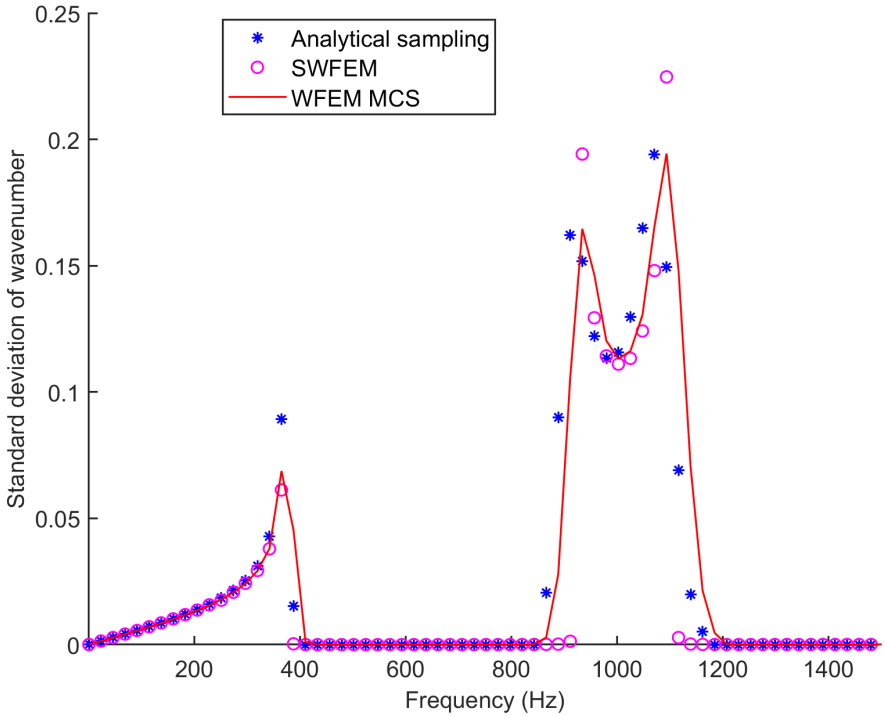

(b) Standard deviation comparison

Figure 3.6: Validation of the periodic rod with 4% stochastic density

validity of the SWFEM formulation applied to flexural wave analysis.

The uncertainty effect is also studied considering a variation of (4%) of the nominal values

Table 3.2: Material and geometric properties of periodic beam

Geometry/Property	Value
Beam length (A)	0.25 m
Beam length (B)	0.25 m
Radius of beam	0.00945 m
Young's modulus (A)	210 $\times 10^9$ Pa
Young's modulus (B)	0.72 $\times 10^9$ Pa
Mass density (A)	7800 kg/m^3
Mass density (B)	935 kg/m^3
Loss factor (A) and (B)	0.001

of mass density. The results obtained with analytical sampling, SWFEM TM, and WFEM MCS are compared. The mean values comparison is shown in Fig. 3.8(a) and the standard deviation comparison is presented in Fig. 3.8(b). The results are in good agreement.

3.4.3 Analysis of frequency response function

In this section, the FRF response of the 1D periodic case is considered as follows for a periodic rod, metamaterial rod, geometrically varying beam, and metamaterial beam.

Periodic rod for the bounded case

A 1D periodic structure which is made up of N=10 substructure is considered. The substructure material and geometric properties are detailed in Table 3.3. The structure is

Table 3.3: Material and geometric properties of periodic rod (FRF case)

Geometry/Property	Value
Rod length (A)	1 m
Rod length (B)	1 m
Radius of Rod	0.06 m
Young's modulus (A)	210 $\times 10^9$ Pa
Young's modulus (B)	77 $\times 10^9$ Pa
Mass density (A)	7800 kg/m^3
Mass density (B)	2700 kg/m^3
Loss factor (A) and (B)	0.01

fixed at its right end, and at left end, it is subjected to a longitudinal point force. The FRF, i.e., the frequency evaluation of the magnitude of the logitudinal displacement at the excitation point, is computed at 4990 discrete frequencies. The frequencies are uniformly

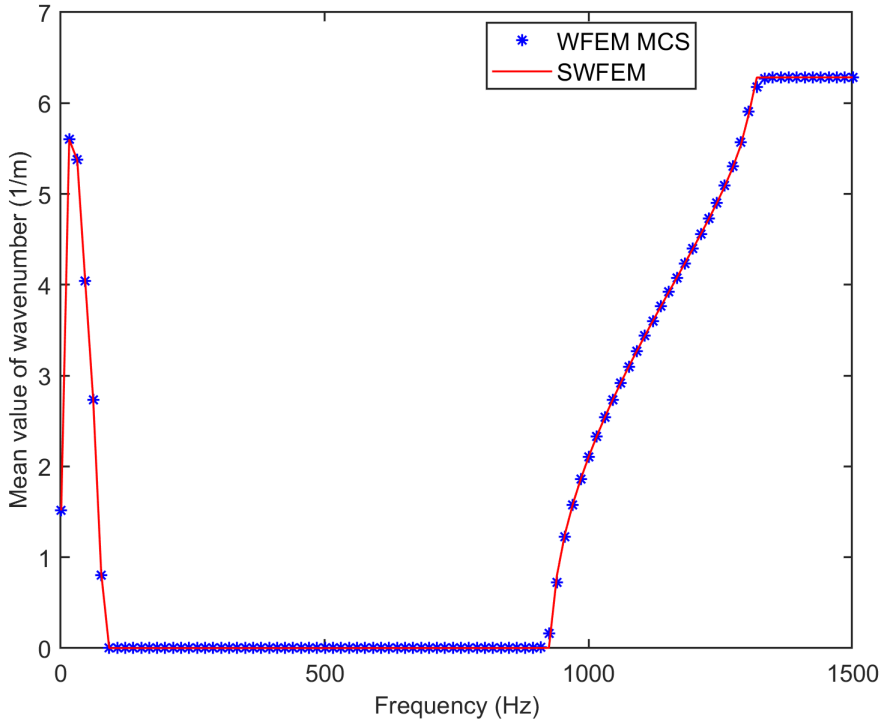

(a) Mean value comparison

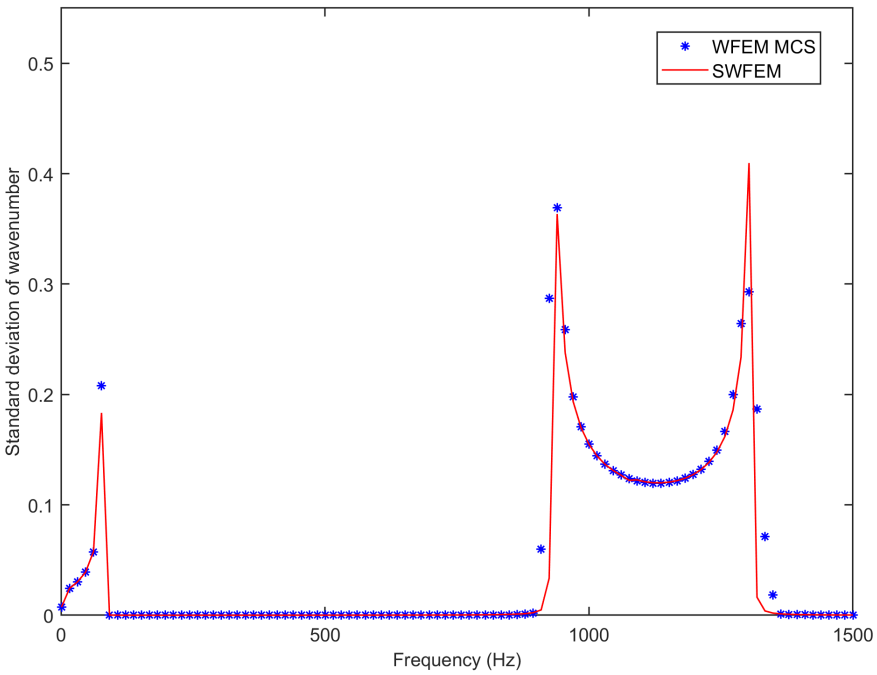

(b) Standard deviation comparison

Figure 3.7: Validation of the periodic beam with 2% stochastic elasticity

spread over the frequency range of 10-5000 Hz. In this case, the Young's modulus is considered as a stochastic parameter with (2%) variation about the nominal value. The

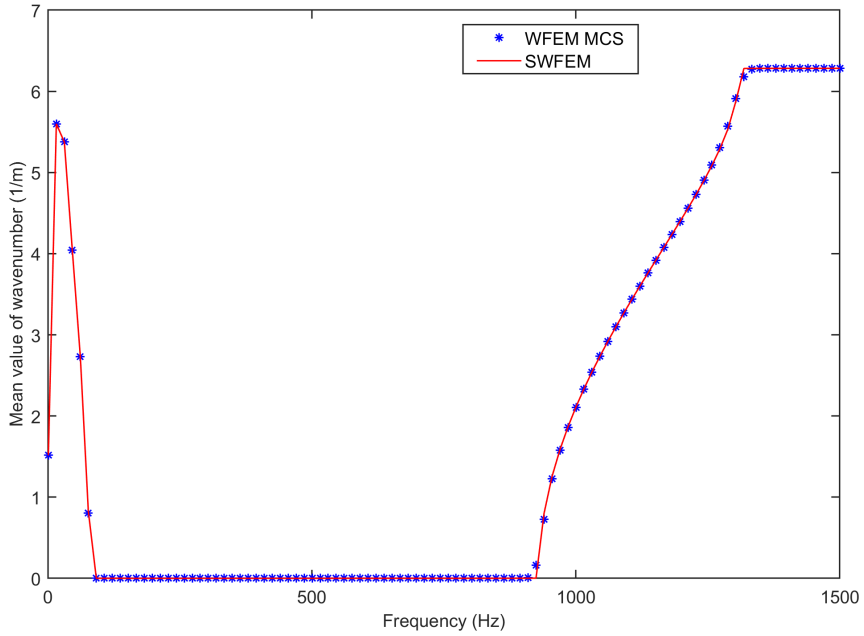

(a) Mean value comparison

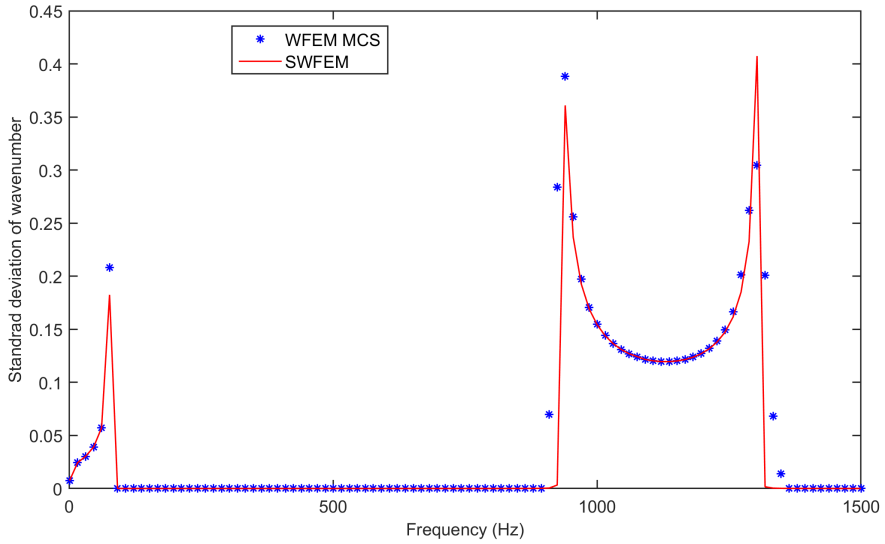

(b) Standard deviation comparison

Figure 3.8: Validation of the periodic beam with 2% stochastic density

mean value of the FRF is obtained by solving Eq.(3.53) and the standard deviation of the longitudinal displacement is obtained by solving Eq. (3.54). The results obtained with WFEM MCS are compared with SWFEM results. The mean values comparison of the band gap is shown in Fig. 3.9(a) and FRF is shown in Fig. 3.9(b). The standard deviation comparison is presented in Fig. 3.10(a) for the band gap and correspondingly in Fig. 3.10(b) for the FRF. The results are in good agreement. It can be seen that the band

gap can be also identified easily in the FRF.

Metamaterial rod for the bounded cases validation

To validate the SWFEM and demonstrate its capacity to compute the band gaps and FRF dispersion in an elastic metamaterial rod with attached single-DOF local resonators, numerical experiments are performed. A 1D periodic structure that is made up of N=10 substructures is considered. The metamaterial, material, and geometric properties are detailed in Table 3.4. To show the metamaterial band gaps, FRF is measured. The meta-

Table 3.4: Material and geometric properties of metamaterial rod (FRF case)

Geometry/Property	Value
Rod length (A)	0.5 m
Rod length (B)	0.5 m
Radius of Rod	0.01 m
Young's modulus (A)	210 $\times 10^9$ Pa
Young's modulus (B)	210 $\times 10^9$ Pa
Mass density (A)	7800 kg/m^3
Mass density (B)	7800 kg/m^3
Loss factor (A) and (B)	0.01
Resonator frequecy	1250 Hz
Resonator mass density ratio	0.2

material rod is fixed at its right end, and at the left end, it is subjected to a longitudinal point force. The FRF is computed at 2990 discreted frequencies. The frequencies are uniformaly spread over the frequency range of 10-3000 Hz. In this case, the uncertainty in the host structure Young's modulus is considered with (2%) variation about the nominal value. The results obtained with WFEM MCS are compared with SWFEM results. The mean values comparison of the band gap is shown in Fig. 3.11(a) and FRF is shown in Fig. 3.11(b). The standard deviation comparison is presented in Fig. 3.12(a) for the band gap and correspondingly in Fig. 3.12(b) for the FRF. The results are in good agreement. It can be seen that the resonance band gap can be also identified easily in the FRF around the resonance frequency.

Geometrically varying beam for the bounded cases validation

A 1D geometrically varying structure that is made up of N= 10 substructures is considered. The substructure material and geometric properties are detailed in Table 3.5. The global

Table 3.5: Material and geometric properties of geometrically varying beam (FRF case)

Geometry/Property	Value
Beam length (A)	0.05 m
Beam length (B)	0.05 m
Width of beam (A)	0.003 m
Width of beam (B)	0.003 m
Height of beam (A)	0.002 m
Height of beam (B)	0.003 m
Young's modulus (A) and (B)	71 $\times 10^9$ Pa
Mass density (A) and (B)	2700 kg/m^3
Loss factor (A) and (B)	0.001

structure is fixed at its right end, and at the left end, it is subjected to a flexural point force. The substructures are meshed with two-node beam element with two DOFs per node, to allow the treatments of flexural wave. The FRF is computed at 2490 discrete frequencies uniformly spread over the freuqncy range of 10-2500 Hz. In this case, the Young's modulus is considered as a stochastic parameter with (2%) variation about the nominal value. The results obtained with WFEM MCS are compared with SWFEM results. The mean values comparison of the band gap is shown in Fig. 3.13(a) and FRF is shown in Fig. 3.13(b). The standard deviation comparison is presented in Fig. 3.14(a) for the band gap and correspondingly in Fig. 3.14(b) for the FRF. The results are in good agreement. It can be seen that results are in good agreement and the band gap can be also identified easily in the FRF.

Metamaterial beam for the bounded cases validation

To validate the SWFEM and demonstrate its capacity to compute the band gaps and FRF dispersion in an elastic metamaterial beam with attached single-DOF local resonators, a numerical experiment is performed. A 1D periodic structure which is made up of N=10 substructures is considering. The metamaterial material and geometric properties are detailed in Table 3.6. Initially the bare beam is simulated, and no band gap exists in the obtained dispersion curve shown in Fig. 3.15. Then, a single DOF resonator is attached

Table 3.6: Material and geometric properties of metamaterial beam (FRF case)

Geometry/Property	Value
Beam length (A)	0.25 m
Beam length (B)	0.25 m
Radius of beam	0.01 m
Young's modulus (A)	210 $\times 10^9$ Pa
Young's modulus (B)	210 $\times 10^9$ Pa
Mass density (A)	7800 kg/m^3
Mass density (B)	7800 kg/m^3
Loss factor (A) and (B)	0.01
Resonator frequecy	350 Hz
Resonator mass density ratio	0.2

to the beam. The metamaterial beam is fixed at its right end, and at the left end, it is subjected to a flexural point force. The FRF is computed at 990 discrete frequencies spread over 10-1000 Hz. The Young's modulus of the host structure is considered as a stochastic parameters with (2%) variation about the nominal value. The results obtained with WFEM MCS are compared with SWFEM results. The mean values comparison of the band gap is shown in Fig. 3.16(a) and FRF is shown in Fig. 3.16(b). The standard deviation comparison is presented in Fig. 3.17(a) for the band gap and correspondingly in Fig. 3.17(b) for the FRF. It can be seen that the results are in good agreement and the band gap can be also identified in the FRF.

3.5 Elapsed time comparison for SWFEM 1D periodic media

In the context of uncertainty quantification in periodic media, in crude MCS, the sample selection mainly depends on the maximum number of simulations, elapsed time, and desired accuracy. To establish the preeminence of SWFEM over the WFEM MCS, the numerical costs involved in computation is compared with that of crude MCS. The test ran on a mobile workstation with, an Intel® Core™ i7 7820 HQ CPU clocked at 2.90 GHz and 32 GB RAM. The comparison of elapsed time is reported in Table 3.7. Where it can be seen that computational effort by application of SWFEM is much smaller compared to WFEM MCS. The employed perturbation method computation efficiency results from the fact that, very few additional matrix factorization are performed to compute the re-

Table 3.7: Elapsed time comparison for SWFEM 1D periodic media

	WFEM MCS (10000 samples)	SWFEM (single run)
1D periodic media	3840 seconds	9.34 seconds

sponse variability. The SWFEM formulation uses the deterministic results to evaluate the response variability of the wavenumber. Thus, SWFEM formulation has superiority over the WFEM MCS in computation cost, which has great advantages for modeling complex periodic structures.

3.6 Conclusions

In this chapter, SWFEM based on the state-space form is extended to periodic media in 1D cases. The formulation is detailed for free wave propagation and FRF. Various numerical cases are presented and validated with MCS, for free wave propagation in a periodic rod and periodic beam. In the FRF cases, the periodic rod, metamaterial rod, geometrically varying beam, and metamaterial beam result validate the use of SWFEM. In the context of uncertainty quantification in periodic media, an elapsed computational time comparison is presented. The result of the simulation shows the computation advantage of the SWFEM over the MCS.

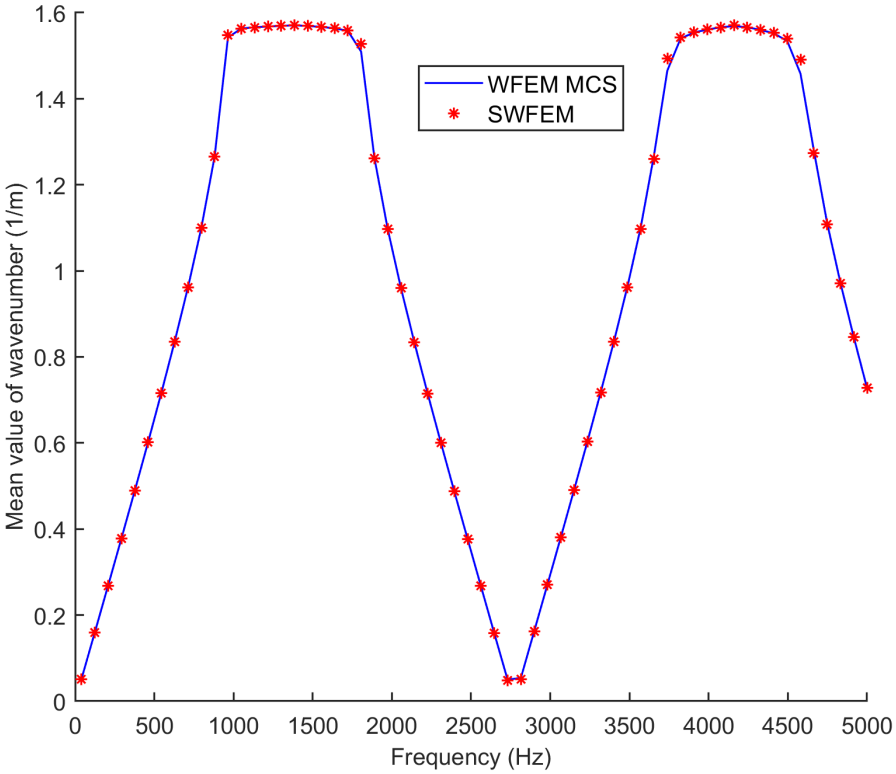

(a) Mean value comparison of band gap

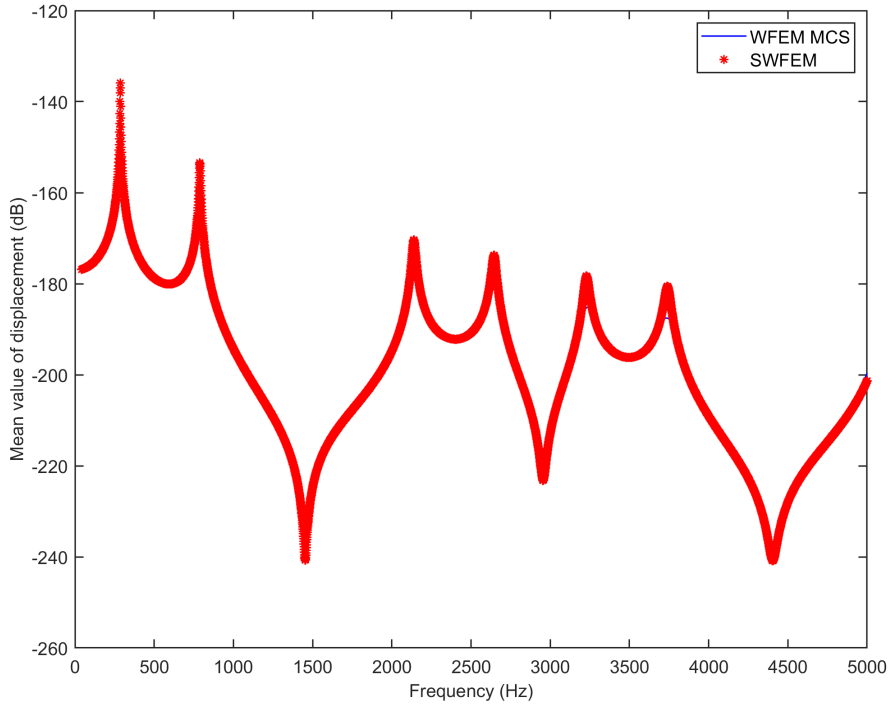

(b) Mean value comparison of FRF

Figure 3.9: Validation of the mean value of the periodic rod with 2% stochastic elasticity

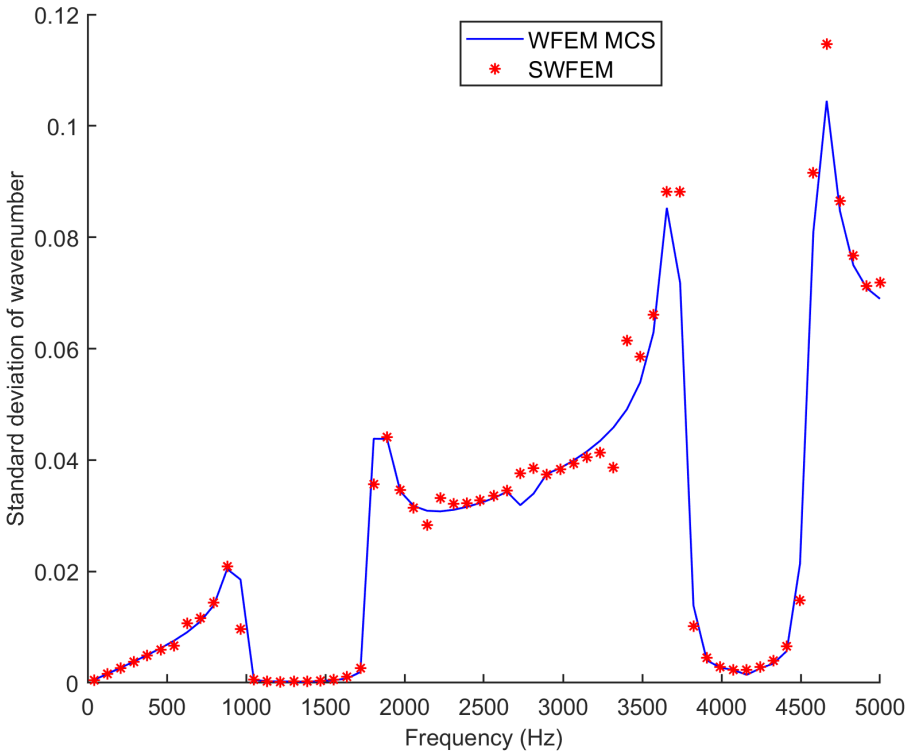

(a) Standard deviation comparison of band gap

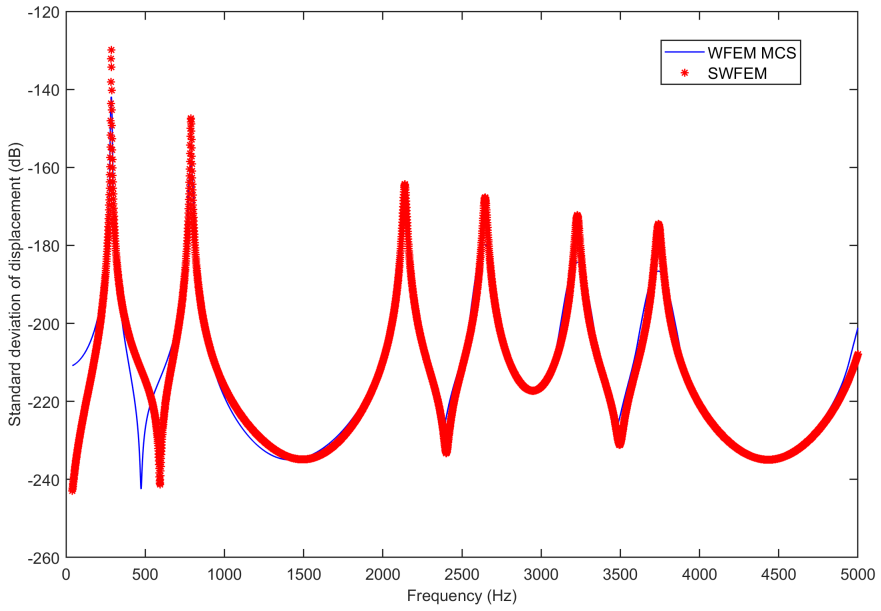

(b) Standard deviation comparison of FRF

Figure 3.10: Validation of the standard deviation of the periodic rod with 2% stochastic elasticity

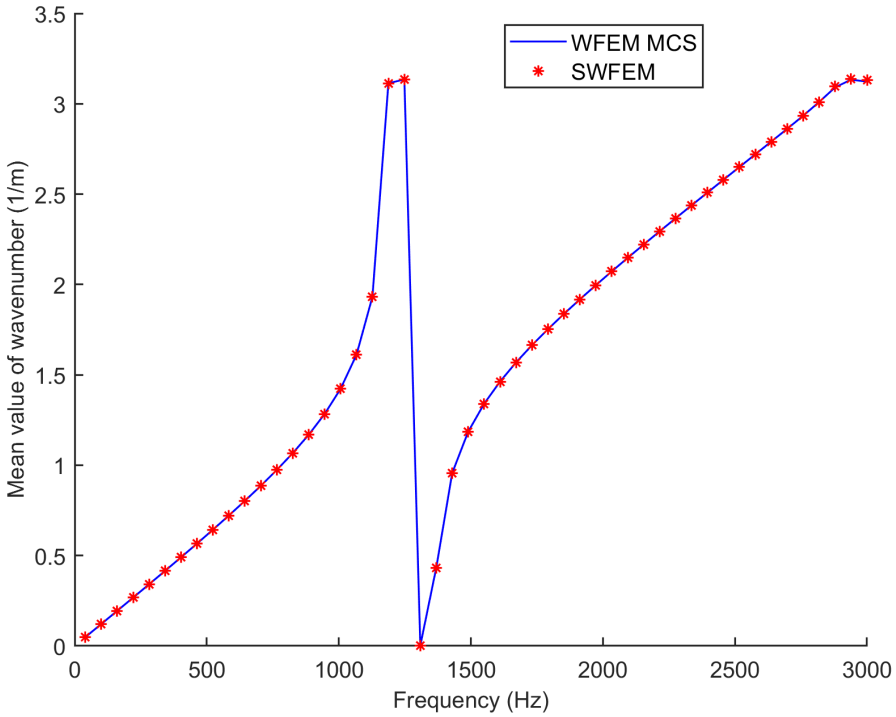

(a) Mean value comparison of band gap

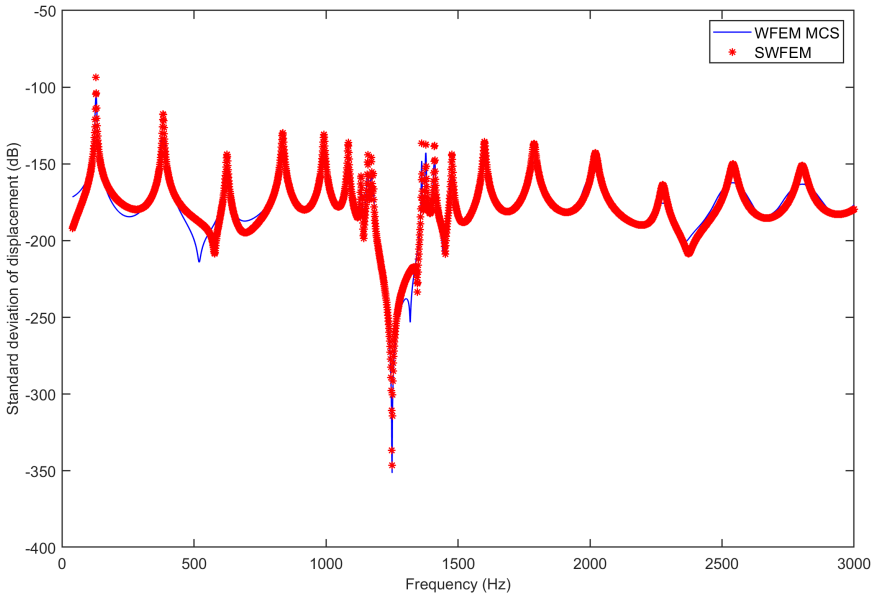

(b) Mean value comparison of FRF

Figure 3.11: Validation of the mean value of the metamaterial rod with 2% stochastic elasticity

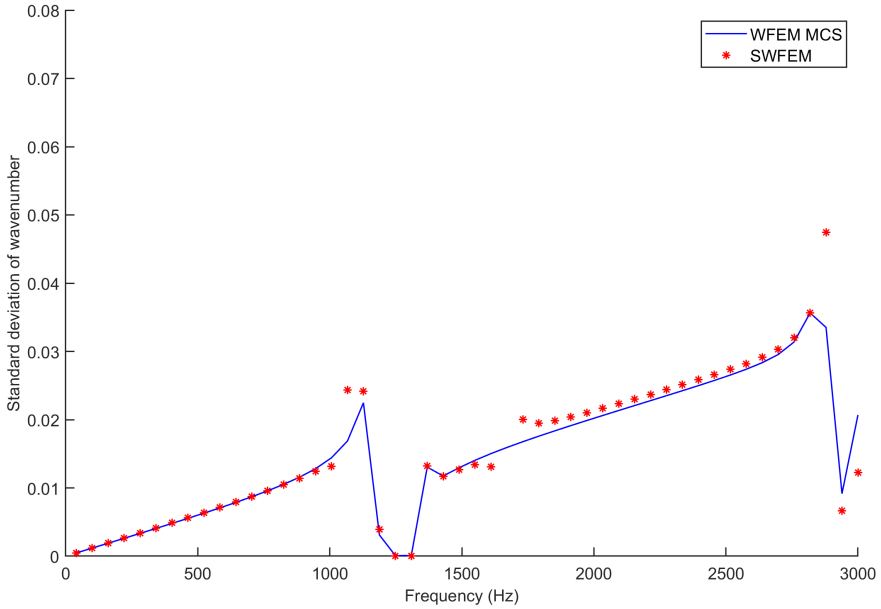

(a) Standard deviation comparison for the band gap

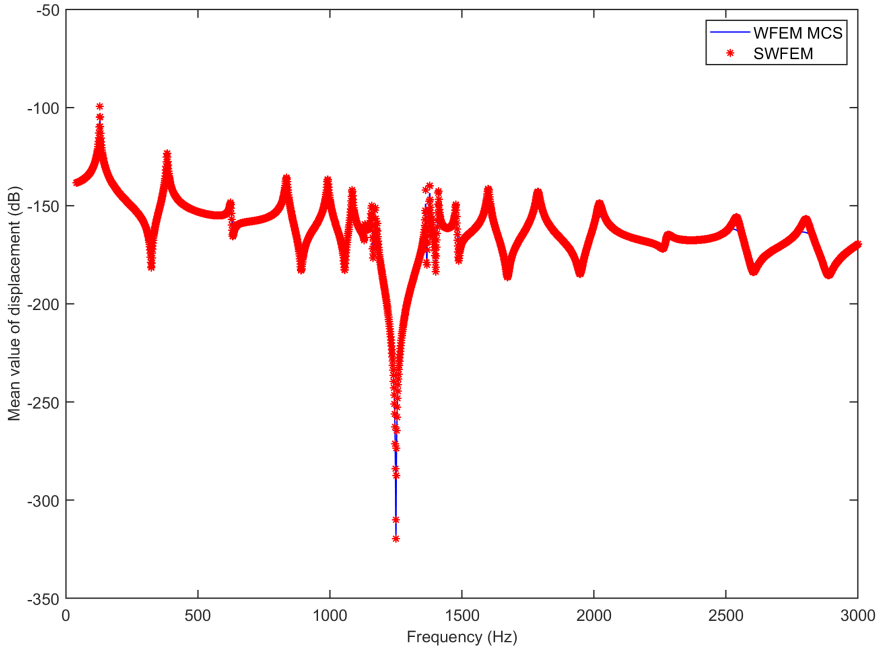

(b) Standard deviation comparison for the FRF

Figure 3.12: Validation of the standard deviation of the metamaterial rod with 2% stochastic elasticity

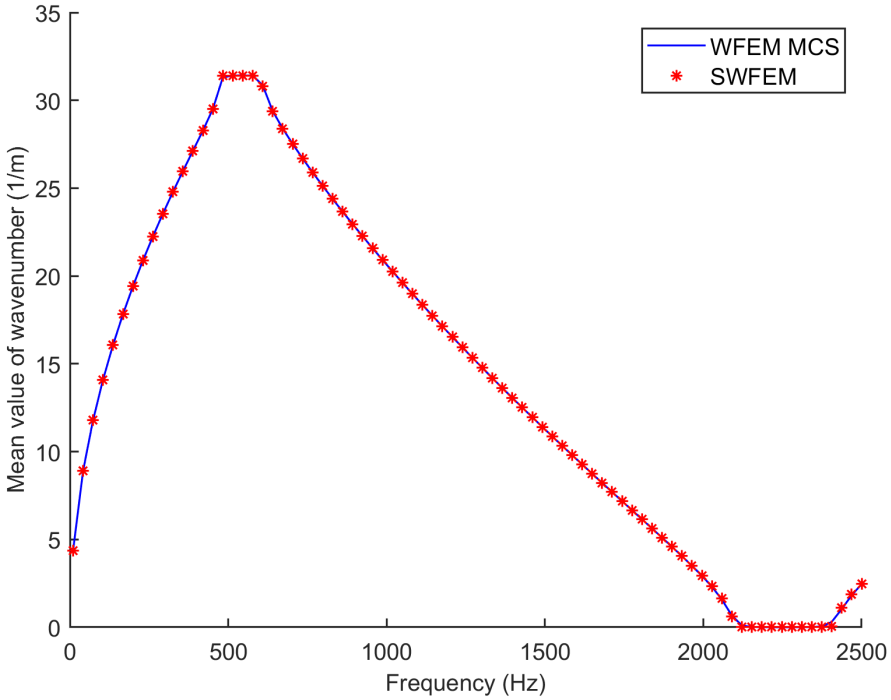

(a) Mean value comparison of band gap

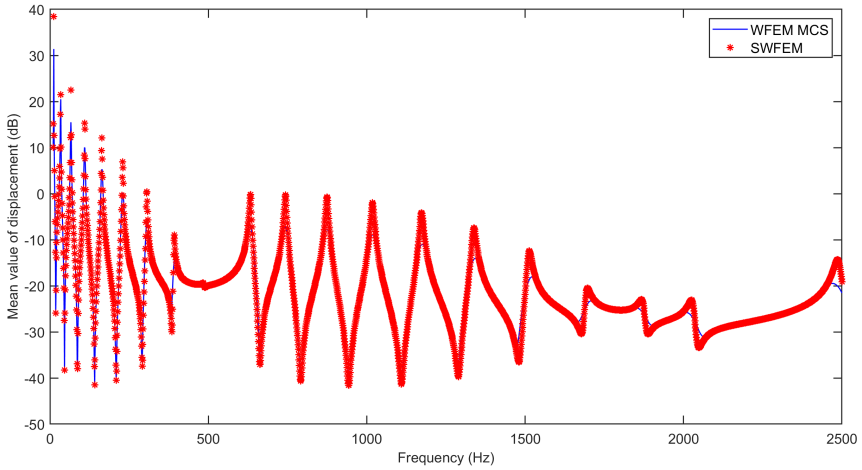

(b) Mean value comparision of FRF

Figure 3.13: Validation of the mean value of the periodic step beam with 2% stochastic elasticity

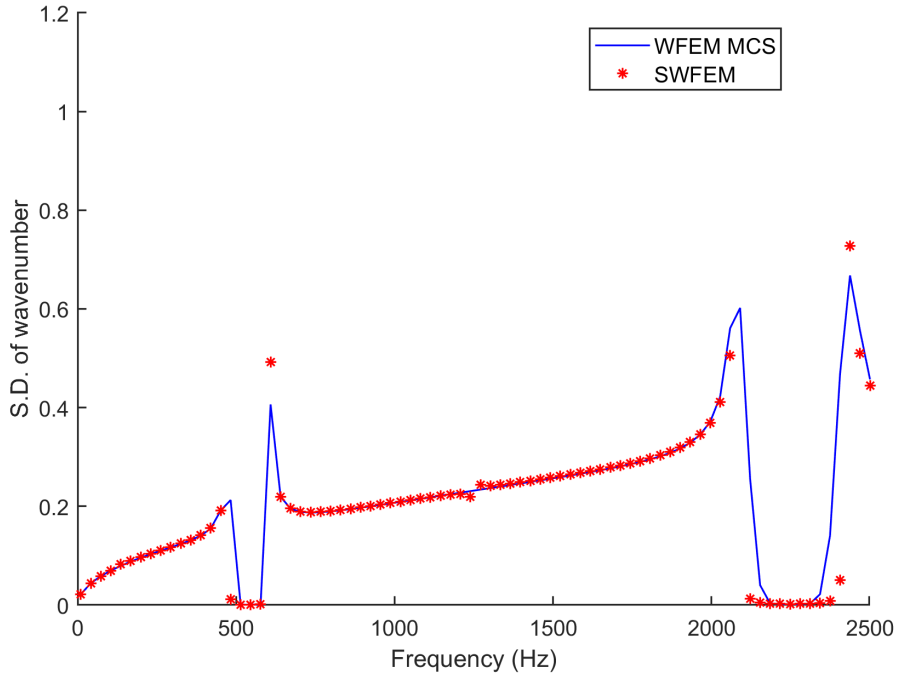

(a) Standard deviation comparison of band gap

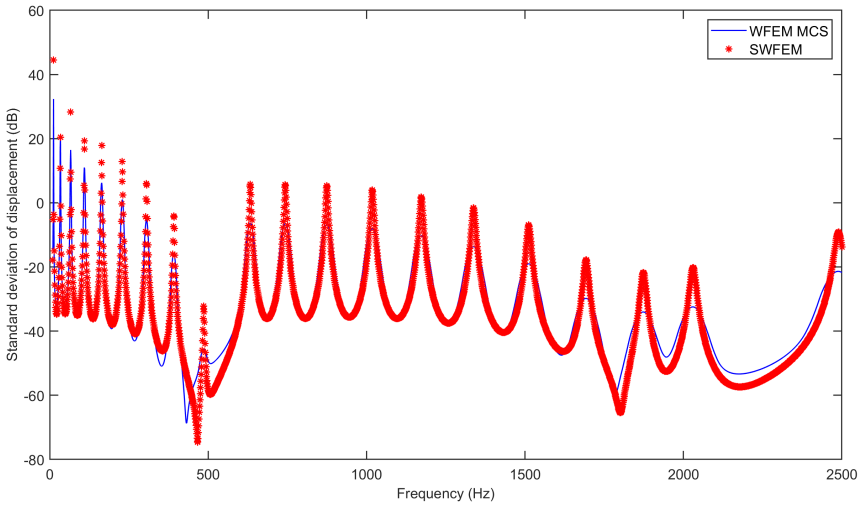

(b) Standard deviation comparison of FRF

Figure 3.14: Validation of the standard deviation of the periodic step beam with 2% stochastic elasticity

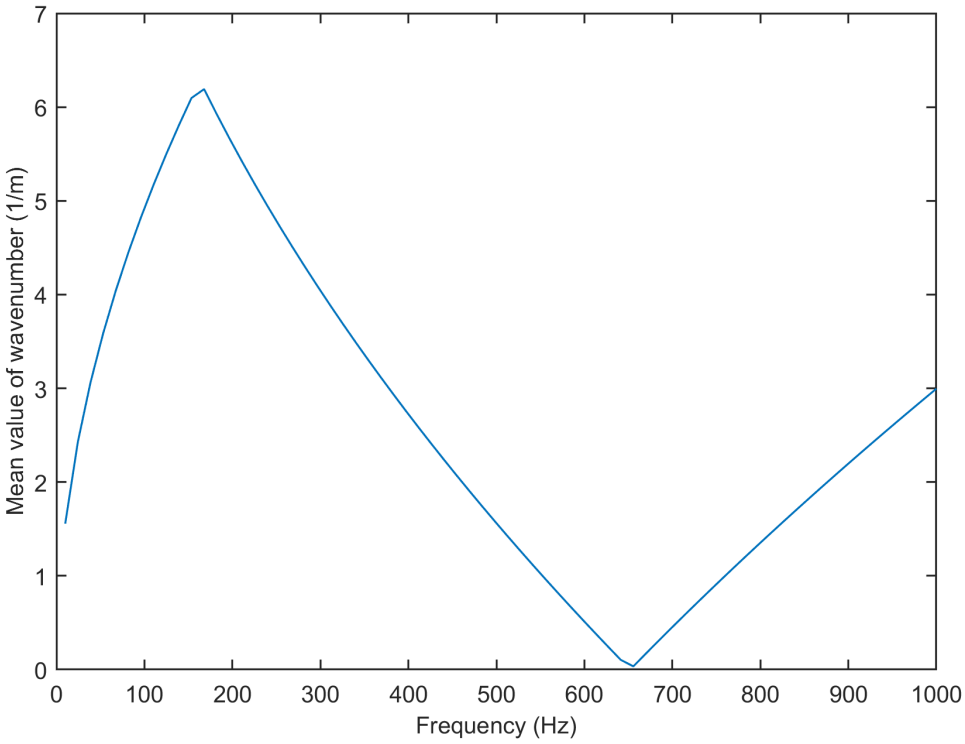

Figure 3.15: Mean value comparison of band gap

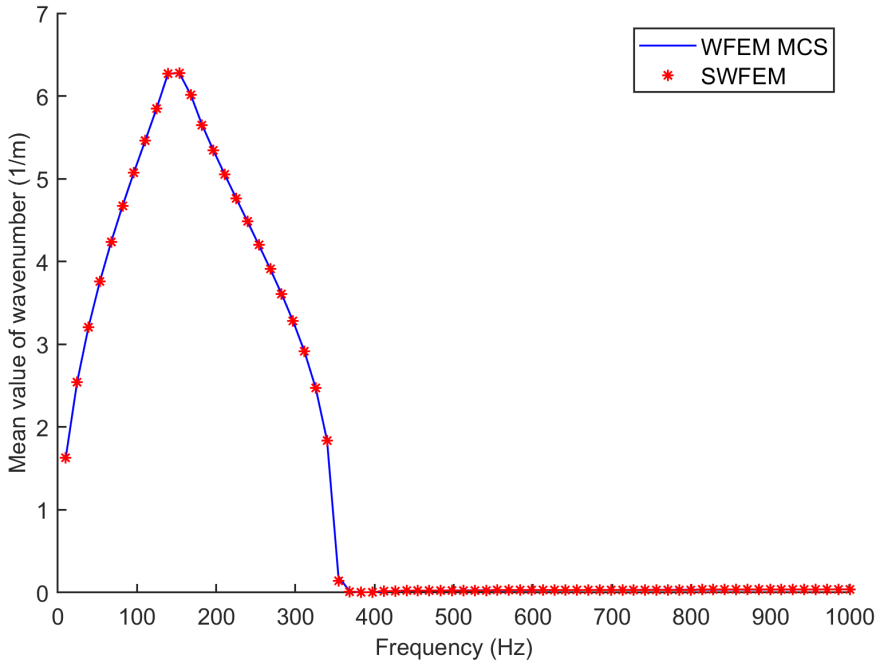

(a) Mean value comparison of band gap

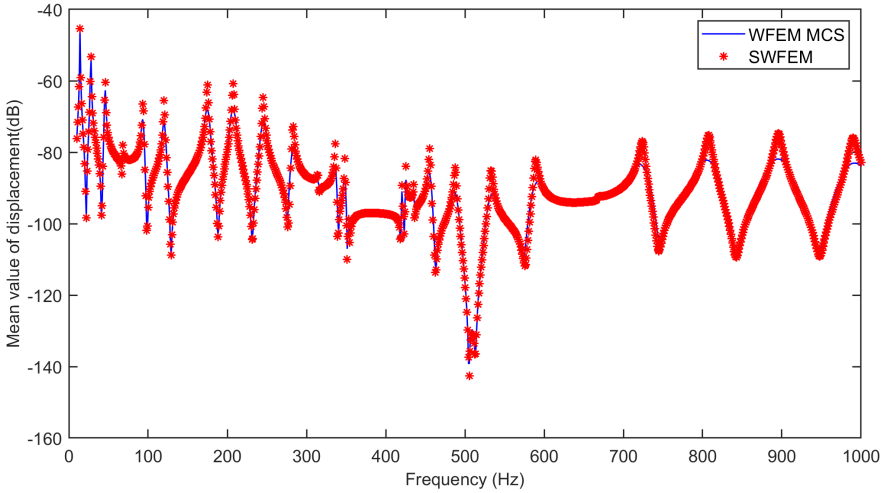

(b) Mean value comparison of FRF

Figure 3.16: Validation of the mean value of the metamaterial beam with 2% stochastic elasticity

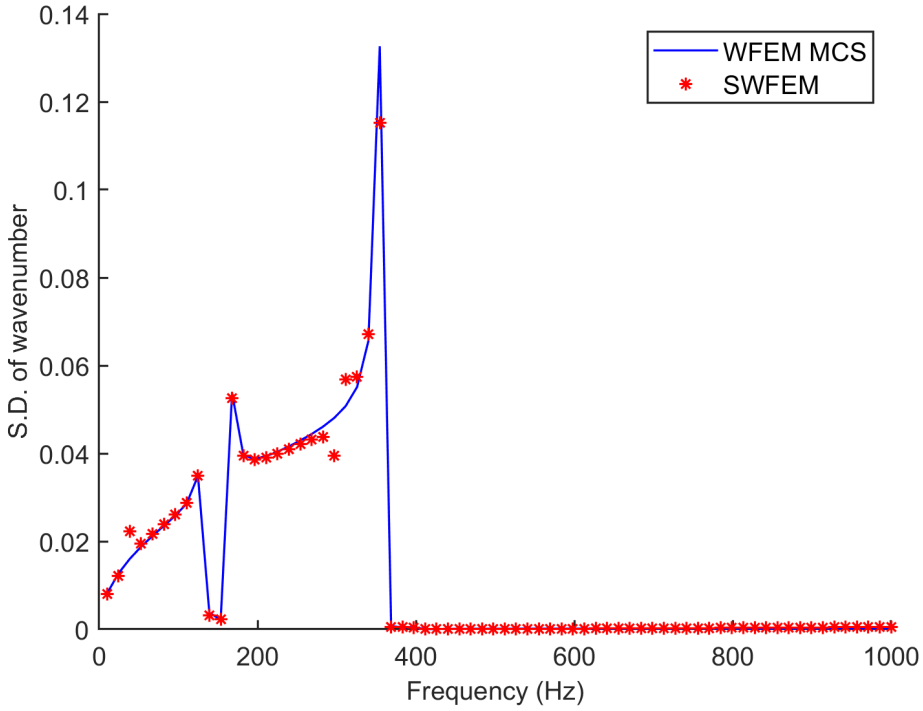

(a) Standard deviation comparison of band gap

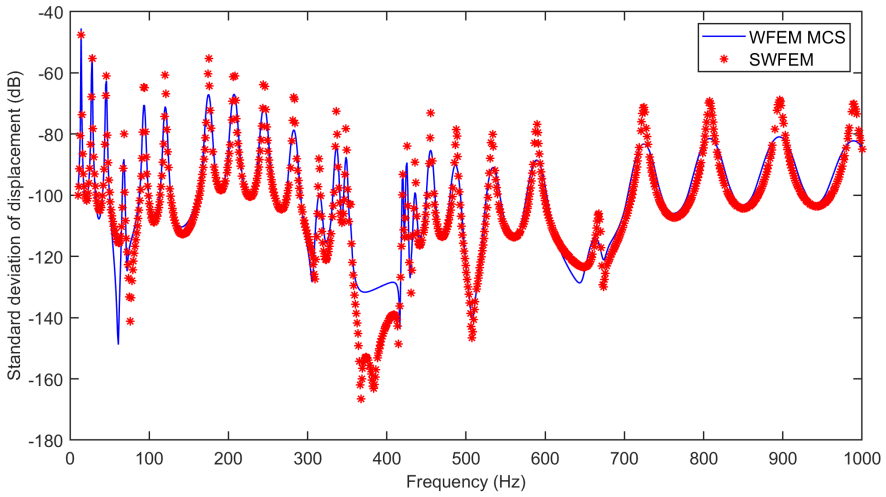

(b) Standard deviation comparison of FRF

Figure 3.17: Validation of the standard deviation of the metamaterial beam with 2% stochastic elasticity

Chapter 4

SWFEM QEV: 1D and 2D periodic media

4.1 Introduction

In the deterministic case, the dispersion curve is extracted by spectral analysis. The use of a state-space representation is an interesting alternative to spectral analysis. However, when using the state-space method, numerical ill-conditioning may occur when a large number of the unit cells are involved in the periodic system model [Waki et al., 2009]. To overcome this shortcoming, for stochastic modelling, a stochastic spectral approach with the quadratic formulation is presented in this section for 1D and 2D periodic media. In addition, the formulation is adopted for the metamaterial structure. In 1D cases, the proposed formulation is applied to a periodic rod and metamaterial rod. In 2D cases, homogeneous, and periodic plates are investigated. The solutions were validated by comparison with MCS. The effect of uncertain parameters on the wavenumber dispersion is investigated considering stochasticity indicator and COV study. An elapsed computational time comparison is presented to show the efficiency advantage of the SWFEM QEV over the MCS.

4.2 SWFEM quadratic formulation: 1D periodic media

Consider a one-dimensional periodic system, as shown in Fig.4.1. One-dimensional pe-

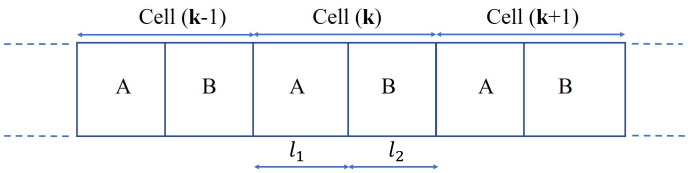

Figure 4.1: Schematic representation of the periodic structure

riodic structures are obtained by formulating the unit cell and then repeating in the propagation direction. Then, the study of this structure is converted into a study of the unit cell based on the Floquet-Bloch theorem [Mead, 1973].

The variables are displacements as q and forces as F. The dynamic stiffness matrix $(D) = -\omega^2 M + K(1 + i\eta)$, where K is the stiffness matrix, M is the mass matrix, η is the loss factor, i is the unit imaginary number, and ω is the circular frequency. The nodes on the boundaries of the periodic structure are denoted as on the left boundary (L), right boundary (R) and the remaining/internal nodes (I). The displacement DOFs q are partitioned into left (q_L) and right (q_R). Similarly, forces are partitioned into left (F_L) and right (F_R). Firstly, the deterministic form of the quadratic eigenvalue problem is obtained. The dynamic of the global waveguide can be expanded on the wave solution as follows:

$$q_R = \mu q_L, F_R = -\mu F_L \tag{4.1}$$

where μ is the propagation constant. The Floquet-Bloch condition applied to the dynamic equation, leads to the classic quadratic eigenvalue problem [Houillon et al., 2005] in terms of propagation constant:

$$\left(D_{RL} + \mu_i I_{2n} \left(D_{LL} + D_{RR}\right) + \mu_i^2 I_{2n} D_{LR}\right) \left(\Phi_q\right)_i = 0 \tag{4.2}$$

where $i = 1...2n$, n is the cross sectional DOFs, and D_{LL}, D_{RL}, D_{RR}, and D_{LR} are the elements of the dynamic stiffness matrix. The wave mode of the global system is $(\mu_i, (\Phi_q)_i)_{i=1...2n}$.

Based on the quadratic eigenvalue form, to accommodate the effects of uncertainties,

stochastic equation of motion can be expressed in the form:

$$\widetilde{D}\ \widetilde{q} = \widetilde{F} \tag{4.3}$$

where symbol $\widetilde{()}$ denotes the stochastic entity. The Eq. (4.3) can be partitioned as follows:

$$\begin{pmatrix} \widetilde{D}_{LL} & \widetilde{D}_{LR} \\ \widetilde{D}_{RL} & \widetilde{D}_{RR} \end{pmatrix} \begin{pmatrix} \widetilde{q}_L^{\boldsymbol{k}} \\ \widetilde{q}_R^{\boldsymbol{k}} \end{pmatrix} = \begin{pmatrix} \widetilde{F}_L^{\boldsymbol{k}} \\ \widetilde{F}_R^{\boldsymbol{k}} \end{pmatrix} \tag{4.4}$$

Using the dynamic stiffness matrix symmetry, stochastic quadratic eigenvalue problem can be written as:

$$\left(\widetilde{D}_{RL} + \widetilde{\mu}_i I_{2n}(\widetilde{D}_{LL} + \widetilde{D}_{RR}) + \widetilde{\mu}_i^2 I_{2n}\widetilde{D}_{LR}\right)\left(\widetilde{\Phi}_q\right)_i = 0 \tag{4.5}$$

Using polynomial chaos projection of the variables in Eq. (4.5), we can extract their mean value $\overline{()}$ and standard deviation (σ). Stochastic eigenvalues ($\widetilde{\mu}_i$) and stochastic eigenvectors $\left(\widetilde{\Phi}_q\right)_i$ are the solution of the stochastic quadratic equation Eq. (4.5). The zeroth-order chaos expansion of Eq. (4.5) leads to:

$$\left(\overline{D}_{RL} + \overline{\mu}_i I_{2n}(\overline{D}_{LL} + \overline{D}_{RR}) + \overline{\mu}_i^2 I_{2n}\overline{D}_{LR}\right)\left(\overline{\Phi}_q\right)_i = 0 \tag{4.6}$$

The first-order chaos expansion of the stochastic quadratic Eq. (4.5) leads to:

$$\begin{aligned} &\left[\overline{D}_{RL} + \overline{\mu}_i I_{2n}(\overline{D}_{LL} + \overline{D}_{RR}) + \overline{\mu}_i^2 I_{2n}\overline{D}_{LR}\right]\sigma_{\left(\Phi_{qL}\right)_i} \\ &+\left[\sigma_{D_{RL}} + \sigma_{\mu_i} I_{2n}(\overline{D}_{LL} + \overline{D}_{RR}) + \overline{\mu}_i I_{2n}(\sigma_{D_{LL}} + \sigma_{D_{RR}} + 2\overline{\mu}_i I_{2n}\sigma_{\mu_i}\overline{D}_{LR} + \overline{\mu}_i^2 I_{2n}\sigma_{D_{LR}})\right]\left(\overline{\Phi}_q\right)_i = 0 \end{aligned} \tag{4.7}$$

From the above equation the standard deviation of eigenvectors $\sigma_{(\Phi_q)_i}$ can be expressed as:

$$\begin{aligned} &\sigma_{(\Phi_q)_i} = -\left[\overline{D}_{RL} + \overline{\mu}_i I_{2n}(\overline{D}_{LL} + \overline{D}_{RR}) + \overline{\mu}_i^2 I_{2n}\overline{D}_{LR}\right]^{-1} \\ &\left[\sigma_{D_{RL}} + \sigma_{\mu_i I_{2n}}(\overline{D}_{LL} + \overline{D}_{RR}) + \overline{\mu}_i I_{2n}\left(\sigma_{D_{LL}} + \sigma_{D_{RR}}\right) + 2\overline{\mu}_i I_{2n}\sigma_{\mu_i}\overline{D}_{LR} + \overline{\mu}_i^2 I_{2n}\sigma_{D_{LR}}\right]\left(\overline{\Phi}_q\right)_i \end{aligned} \tag{4.8}$$

$\left(\widetilde{\Phi}_q\right)_i^T$, the stochastic left eigenvectors linked with stochastic left eigenvalues $\widetilde{\mu}_i^{-1}$, which form the stochastic left quadratic eigenvalue problem as:

$$\left(\widetilde{\Phi}_q\right)_i^T \left(\widetilde{D}_{RL} + \widetilde{\mu}_i^{-1} I_{2n}(\widetilde{D}_{LL} + \widetilde{D}_{RR}) + \widetilde{\mu}_i^{-2} I_{2n}\widetilde{D}_{LR}\right) = 0 \tag{4.9}$$

The first-order chaos expansion of stochastic left quadratic eigenvalue leads to:

$$\begin{aligned}\sigma_{(\Phi_q)_i}{}^T \left[\overline{D}_{RL} + \overline{\mu}_i{}^{-1} I_{2n}(\overline{D}_{LL} + \overline{D}_{RR}) + \overline{\mu}_i{}^{-2} I_{2n}\overline{D}_{LR}\right] + \left(\overline{\Phi}_q\right)_i^T \left[\sigma_{D_{RL}} - \overline{\mu}_i{}^{-2} I_{2n}\sigma_{\mu_i}(\overline{D}_{LL}\right.\\ \left. + \overline{D}_{RR}) + \overline{\mu}_i{}^{-1} I_{2n}(\sigma_{D_{LL}} + \sigma_{D_{RR}}) - 2\overline{\mu}_i{}^{-3} I_{2n}\sigma_{\mu_i}\overline{D}_{LR} + \overline{\mu}_i{}^{-2} I_{2n}\sigma_{DR}\right] = 0\end{aligned} \tag{4.10}$$

In the above equation, identification of the targeted terms $\sigma_{(\Phi_q)_i}, \sigma_{\mu_i}$ and replacement of $\sigma_{(\Phi_q)_i}$ leads to:

$$\begin{aligned}&- \Big[\left[\overline{D}_{RL} + \overline{\mu}_i I_{2n}(\overline{D}_{LL} + \overline{D}_{RR}) + \overline{\mu}_i^2 I_{2n}\overline{D}_{LR}\right]^{-1} \left[\sigma_{D_{RL}} + \sigma_{\mu_i} I_{2n}(\overline{D}_{LL} + \overline{D}_{RR})\right.\\ &\left. + \overline{\mu}_i I_{2n}(\sigma_{D_{LL}} + \sigma_{D_{RR}}) + 2\overline{\mu}_i\sigma_{\mu_i} I_{2n}\overline{D}_{LR} + \overline{\mu}_i^2 I_{2n}\sigma_{D_{LR}}](\overline{\Phi}_q)_i\right]^T \left[\overline{D}_{RL} + \overline{\mu}_i{}^{-1} I_{2n}(\overline{D}_{LL} + \overline{D}_{RR})\right.\\ &\left. + \overline{\mu}_i{}^{-2} I_{2n}\overline{D}_{LR}\right] + \left(\overline{\Phi}_q\right)_i^T \left[\sigma_{D_{RL}} - \overline{\mu}_i^{-2} I_{2n}\sigma_{\mu_i}(\overline{D}_{LL} + \overline{D}_{RR}) + \mu_i^{-1} I_{2n}(\sigma_{D_{LL}} + \sigma_{D_{RR}})\right.\\ &\left. -2\mu_i^{-3} I_{2n}\sigma_{\mu_i} D_{LR} + \mu_i^{-2} I_{2n}\sigma_{D_{LR}}\right] = 0\end{aligned} \tag{4.11}$$

Simplification of the above equation for σ_{μ_i} leads to:

$$\begin{aligned}&\sigma_{\mu_i} I_{2n}\Big[\left(\overline{\Phi}_q\right)_i^T \left[- (\overline{D}_{LL} + \overline{D}_{RR})^T - 2\overline{\mu}_i I_{2n}\overline{D}_{LR}^T\right]\left[\overline{D}_{RL} + \mu_i I_{2n}(\overline{D}_{LL} + \overline{D}_{RR})\right.\\ &\left. + \overline{\mu}_i^2 I_{2n}\overline{D}_{LR}\right]^{-1}\left[\overline{D}_{RL} + \overline{\mu}_i{}^{-1} I_{2n}(\overline{D}_{LL} + \overline{D}_{RR}) + \overline{\mu}_i{}^{-2} I_{2n}\overline{D}_{LR}\right] - \left(\Phi_q\right)_i^T \left[\overline{\mu}_i{}^{-2} I_{2n}(\overline{D}_{LL} + \overline{D}_{RR})\right.\\ &\left. + 2\overline{\mu}_i{}^{-3} I_{2n}\overline{D}_{LR}\right]\Big] = \left(\overline{\Phi}_q\right)_i^T \left[\sigma_{D_{RL}}^T + \overline{\mu}_i I_{2n}\left(\sigma_{D_{LL}} + \sigma_{D_{RR}}\right)^T + \overline{\mu}_i^2 I_{2n}\sigma_{D_{LR}}^T\right]\left[\overline{D}_{RL}\right.\\ &\left. + \overline{\mu}_i I_{2n}\left(\overline{D}_{LL} + \overline{D}_{RR}\right) + \overline{\mu}_i^2 I_{2n}\overline{D}_{LR}\right]^{-1}\left[\overline{D}_{RL} + \overline{\mu}_i{}^{-1} I_{2n}\left(\overline{D}_{LL} + \overline{D}_{RR}\right) + \overline{\mu}_i{}^{-2} I_{2n}\overline{D}_{LR}\right]\\ &- \left(\overline{\Phi}_q\right)_i^T \left[\sigma_{D_{RL}} + \overline{\mu}_i{}^{-1} I_{2n}\left(\sigma_{D_{LL}} + \sigma_{D_{RR}}\right) + \overline{\mu}_i{}^{-2}\sigma_{D_{LR}}\right]\end{aligned} \tag{4.12}$$

Finally, the analytical expression for the standard deviation of the eigenvalues (σ_{μ_i}) is:

$$\sigma_{\mu_i} = \left(\overline{\Phi}_q\right)_i^T \left[\sigma_{D_{RL}}^T + \overline{\mu}_i I_{2n}\left(\sigma_{D_{LL}} + \sigma_{D_{RR}}\right)^T + \overline{\mu}_i^2 I_{2n}\sigma_{D_{LR}}^T\right]\left[\overline{D}_{RL} + \overline{\mu}_i I_{2n}(\overline{D}_{LL} + \overline{D}_{RR}) + \overline{\mu}_i^2 I_{2n}\overline{D}_{LR}\right]^{-1}\left[\overline{D}_{RL} + \overline{\mu}_i{}^{-1} I_{2n}(\overline{D}_{LL} + \overline{D}_{RR}) + \overline{\mu}_i{}^{-2} I_{2n}\overline{D}_{LR}\right] - \left(\overline{\Phi}_q\right)_i^T \left[\sigma_{D_{RL}} + \overline{\mu}_i{}^{-1} I_{2n}\left(\sigma_{D_{LL}} + \sigma_{D_{RR}}\right) + \overline{\mu}_i{}^{-2} I_{2n}\sigma_{D_{LR}}\right]\Bigg[\left(\overline{\Phi}_q\right)_i^T\left[-(\overline{D}_{LL} + \overline{D}_{RR})^T - 2\overline{\mu}_i I_{2n}\overline{D}_{LR}^T\right]\left[\overline{D}_{RL} + \overline{\mu}_i I_{2n}(\overline{D}_{LL} + \overline{D}_{RR}) + \overline{\mu}_i^2 I_{2n}\overline{D}_{LR}\right]^{-1}\left[\overline{D}_{RL} + \overline{\mu}_i{}^{-1} I_{2n}(\overline{D}_{LL} + \overline{D}_{RR}) + \overline{\mu}_i{}^{-2} I_{2n}\overline{D}_{LR}\right] - \left(\overline{\Phi}_q\right)_i^T\left[\overline{\mu}_i{}^{-2} I_{2n}(\overline{D}_{LL} + \overline{D}_{RR}) + 2\overline{\mu}_i{}^{-3} I_{2n}D_{LR}\right]\Bigg]^{-1} \tag{4.13}$$

Also, the analytical expression for the standard deviation of the eigenvectors $\left(\sigma_{(\Phi_q)_i}\right)$ is:

$$\sigma_{(\Phi_q)_i} = -\left[\overline{D}_{RL} + \overline{\mu}_i I_{2n}(\overline{D}_{LL} + \overline{D}_{RR}) + \overline{\mu}_i^2 I_{2n}\overline{D}_{LR}\right]^{-1}\left[\sigma_{D_{RL}} + \sigma_{\mu_i I_{2n}}(\overline{D}_{LL} + \overline{D}_{RR}) + \overline{\mu}_i I_{2n}\left(\sigma_{D_{LL}} + \sigma_{D_{RR}}\right) + 2\overline{\mu}_i\sigma_{\mu_i} I_{2n}\overline{D}_{LR} + \overline{\mu}_i^2 I_{2n}\sigma_{D_{LR}}\right]\left(\overline{\Phi}_q\right)_i \tag{4.14}$$

Eq. (4.13) and Eq. (4.14) are the explicit expressions for the statistical characterization of wavenumber using deterministic eigenvalue solutions in the 1D periodic media.

4.2.1 Internal nodes

If the formulation requires the dynamic condensation of the inner DOFs at each frequency step, the standard deviation of the condensed dynamic stiffness matrix has to be evaluated. Having internal DOFs, as shown in Fig. 4.2, the DOFs are partitioned into the left

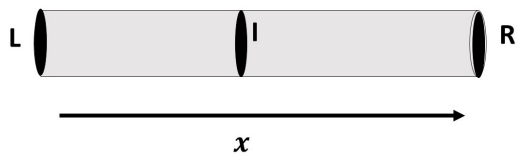

Figure 4.2: Unit cell with internal node

boundary DOFs (D_L), right boundary DOFs (D_R), and internal DOFs (D_I). Introducing uncertainties in the parameters, the stochastic dynamic stiffness matrix has the following

form:

$$\widetilde{D} = \begin{bmatrix} \widetilde{\widehat{D}}_{LL} & \widetilde{\widehat{D}}_{LI} & \widetilde{\widehat{D}}_{LR} \\ \widetilde{\widehat{D}}_{IL} & \widetilde{\widehat{D}}_{II} & \widetilde{\widehat{D}}_{IR} \\ \widetilde{\widehat{D}}_{RL} & \widetilde{\widehat{D}}_{RI} & \widetilde{\widehat{D}}_{RR} \end{bmatrix} \tag{4.15}$$

where symbol $\widetilde{\widehat{()}}$ represents the stochastic entity from the original dynamic stiffness matrix. The dynamic condensation and the zeroth-order expansion of the above Eq. (4.15) leads to:

$$\overline{\mathrm{D}} = \begin{bmatrix} \overline{D}_{LL} & \overline{D}_{LR} \\ \overline{D}_{RL} & \overline{D}_{RR} \end{bmatrix}$$

$$\overline{\mathrm{D}} = \begin{bmatrix} \overline{\widehat{D}}_{LL} - \overline{\widehat{D}}_{LI}\overline{\widehat{D}}_{II}^{-1}\overline{\widehat{D}}_{IL} & \overline{\widehat{D}}_{LR} - \overline{\widehat{D}}_{LI}\overline{\widehat{D}}_{II}^{-1}\overline{\widehat{D}}_{IR} \\ \overline{\widehat{D}}_{RL} - \overline{\widehat{D}}_{RI}\overline{\widehat{D}}_{II}^{-1}\overline{\widehat{D}}_{IL} & \overline{\widehat{D}}_{RR} - \overline{\widehat{D}}_{RI}\overline{\widehat{D}}_{II}^{-1}\overline{\widehat{D}}_{IR} \end{bmatrix} \tag{4.16}$$

The first-order expansion leads to the standard deviation of the condensed dynamic stiffness matrix:

$$\sigma_D = \begin{bmatrix} \sigma_{\widehat{D}_{LL}} & \sigma_{\widehat{D}_{LR}} \\ \sigma_{\widehat{D}_{RL}} & \sigma_{\widehat{D}_{RR}} \end{bmatrix} - \begin{bmatrix} \overline{\widehat{D}}_{LI} & \sigma_{\widehat{D}_{LI}} \\ \overline{\widehat{D}}_{RI} & \sigma_{\widehat{D}_{RI}} \end{bmatrix} \begin{bmatrix} \overline{\widehat{D}}_{II}^{-1} & -\overline{\widehat{D}}_{II}^{-1}\sigma_{\widehat{D}_{II}}\overline{\widehat{D}}_{II}^{-1} \\ 0 & \overline{\widehat{D}}_{II}^{-1} \end{bmatrix} \begin{bmatrix} \sigma_{\widehat{D}_{IL}} & \sigma_{\widehat{D}_{IR}} \\ \overline{\widehat{D}}_{IL} & \overline{\widehat{D}}_{IR} \end{bmatrix} \tag{4.17}$$

where symbol $\overline{\widehat{()}}$ represents the mean value from the original dynamic stiffness matrix. Eq. (4.17) is used for accommodating the contribution of the standard deviation of the condensed DOFs on the boundary DOFs.

4.2.2 Attached resonators

For the low-frequency range, the band gaps can be achieved by mounting periodically local resonators. The LR metamaterial-based system consists of a uniform host structure and periodically attached springs ($\boldsymbol{k}_i$) and masses ($\boldsymbol{m}_i$). The number of springs and masses in the resonator can be chosen based on targeted band gap characteristics as per design of the metamaterial system [Nobrega et al., 2016]. The unit cell of the LR system is shown in Fig.4.3. The dynamic stiffness matrix (D_0) of the resonator at the attachment point can be written as [Xiao et al., 2012]:

$$D_0 = \boldsymbol{k}_i - \left(\boldsymbol{k}_i^2 / \left(\boldsymbol{k}_i - \omega^2 \boldsymbol{m}_i\right)\right) \tag{4.18}$$

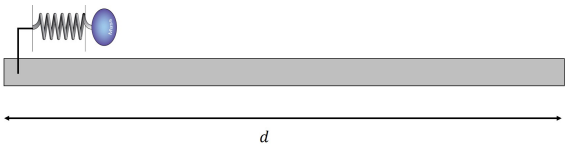

Figure 4.3: Unit cell with local resonator

Once the dynamic stiffness matrix for the LR is obtained, then it needs to be attached to the unit cell of the host structures. The dynamic stiffness matrix of the LR rod is obtained as:

$$D = \begin{bmatrix} D_{LL} & D_{LR} \\ D_{RL} & D_{RR} \end{bmatrix} = \begin{bmatrix} D_{LL} + D_0 & D_{LR} \\ D_{RL} & D_{RR} \end{bmatrix} \tag{4.19}$$

In the host structure, the stochastic equation of motion can be expressed as:

$$\begin{pmatrix} \widetilde{D}_{LL} & \widetilde{D}_{LR} \\ \widetilde{D}_{RL} & \widetilde{D}_{RR} \end{pmatrix} \begin{pmatrix} \widetilde{q}_L^{\boldsymbol{k}} \\ \widetilde{q}_R^{\boldsymbol{k}} \end{pmatrix} = \begin{pmatrix} \widetilde{F}_L^{\boldsymbol{k}} \\ \widetilde{F}_R^{\boldsymbol{k}} \end{pmatrix} \tag{4.20}$$

The above expression is similar to the stochastic equation of motion expressed in Eq. (4.4). The stochastic wavenumber characterization can be obtained by explicitly using Eq. (4.13) and Eq. (4.14).

4.3 SWFEM quadratic formulation: 2D periodic media

4.3.1 Four noded rectangular element

Consider an infinite thin plate lying in the (x, y) plane and its unit cell as shown in Fig. 4.4. The unit cell is divided into four corner nodes. The unit cell DOFs (q) are divided into four corner nodal DOFs,: q_1, q_2, q_3 and q_4. The vector of nodal DOFs are given by $q = \left[q_1^T, q_2^T, q_3^T, q_4^T\right]^T$. Similarly, the vectors of nodal forces are given by $f = \left[f_1^T, f_2^T, f_3^T, f_4^T\right]^T$. where T denotes the transpose. Then the time-harmonic equation of motion of the unit cell can be written as:

$$\left(K - \omega^2 M\right) q = f \tag{4.21}$$

where K is the stiffness matrix, M is the mass matrix, ω is the circular frequency, f is the nodal forces vector, and q is the nodal displacements vector. This equation is used

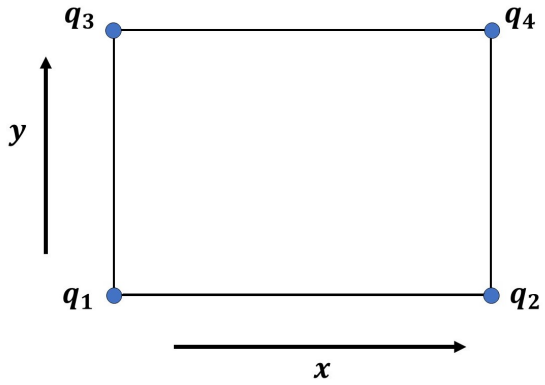

Figure 4.4: Rectangular plate element

to form the spectral problem involving wavenumber in the x-direction (k_x), wavenumber in y-direction (k_y), and frequency ω. The dynamic stiffness matrix can be expressed as $D = K - \omega^2 M$. Here, introducing the periodic structure theory for the unit cell and considering a time-harmonic response [Mace and Manconi, 2008], the deterministic harmonic equation of motion can be expressed as:

$$\left(K^*\left(\lambda_x, \lambda_y\right) - \omega^2 M^*\left(\lambda_x, \lambda_y\right)\right) q_1 = 0 \tag{4.22}$$

where $K^* = \Lambda_L K \Lambda_R$ and $M^* = \Lambda_L M \Lambda_R$ are the reduced stiffness and mass matrices, respectively. λ_x and λ_y are the propagation constants in x- and y-directions, respectively. Λ_L and Λ_L are matrices that contain the propagation constants from the periodicity conditions:

$$\Lambda_L = \begin{bmatrix} I & \lambda_x^{-1} I & \lambda_y^{-1} I & \lambda_x^{-1}\lambda_y^{-1} I \end{bmatrix}$$

$$\Lambda_R = \begin{Bmatrix} I \\ \lambda_x I \\ \lambda_y I \\ \lambda_x \lambda_y I \end{Bmatrix} \tag{4.23}$$

where I is the identity matrix. The eigenvalue problem of Eq. (4.22) can be expressed as:

$$D^*\left(\omega, \lambda_x, \lambda_y\right) q_1 = 0 \tag{4.24}$$

where $D^*(\omega, \lambda_x, \lambda_y)$ is the reduced dynamic stiffness matrix. For the sake of clarity, the reduced dynamic stiffness matrix is now represented as D. If the reduced dynamic stiffness matrix is partitioned as:

$$D = \begin{bmatrix} D_{11} & D_{12} & D_{13} & D_{14} \\ D_{21} & D_{22} & D_{23} & D_{24} \\ D_{31} & D_{32} & D_{33} & D_{34} \\ D_{41} & D_{42} & D_{43} & D_{44} \end{bmatrix} \tag{4.25}$$

Then, the eigenvalue problem in Eq. (4.24) can be written in the following form:

$$\begin{aligned} &\big[(D_{11} + D_{22} + D_{33} + D_{44}) + (D_{12} + D_{34})\lambda_x + (D_{21} + D_{43})\lambda_x^{-1} + (D_{13} + D_{24})\lambda_y \\ &+(D_{31} + D_{42})\lambda_y^{-1} + D_{14}\lambda_x\lambda_y + D_{41}\lambda_x^{-1}\lambda_y^{-1} + D_{32}\lambda_x\lambda_y^{-1} + D_{23}\lambda_x^{-1}\lambda_y)\big]\, q_1 = 0 \end{aligned} \tag{4.26}$$

For the solution of Eq. (4.24) in the case where frequency and one wavenumber in x or y-directions are known, the eigenvalue form becomes a quadratic eigenvalue problem. Then, the nonlinear Eq. (4.26) can be reduced to a quadratic eigenproblem in λ_x form when λ_x is unknown and (ω, λ_y) are given by:

$$\begin{aligned} &\big[(D_{21} + D_{43} + D_{41}\lambda_y^{-1} + D_{23}\lambda_y) + \mu_i(D_{11} + D_{22} + D_{33} + D_{44} + (D_{31} + D_{42})\lambda_y^{-1} \\ &+ +(D_{13} + D_{24})\lambda_y)\mu_i^2(D_{12} + D_{34} + D_{32}\lambda_y^{-1} + D_{14}\lambda_y)\big]\,(\Phi_q)_i = 0 \end{aligned} \tag{4.27}$$

For the stochastic modelling, we assume that uncertainties are spatially homogeneous to guarantees the periodicity assumption is respected in the stochastic case. The stochastic equation of motion can be expressed as:

$$\widetilde{D}\,(\omega, \lambda_x, \lambda_y)\, q_1 = 0 \tag{4.28}$$

where the stochastic dynamic stiffness matrix $(\widetilde{D})$ has the form $\widetilde{D} = (\overline{D} + \sigma_D\varepsilon)$. (ε) is the centred and reduced Gaussian variable. The above Eq. (4.28) extends Eq. (4.24) to the

stochastic case. Then, the stochastic spectral problem is expressed as:

$$\Big[(\widetilde{D}_{21}+\widetilde{D}_{43}+\widetilde{D}_{41}\lambda_y^{-1}+\widetilde{D}_{23}\lambda_y)+\widetilde{\mu}_i I_{2n}(\widetilde{D}_{11}+\widetilde{D}_{22}+\widetilde{D}_{33}+\widetilde{D}_{44}+(\widetilde{D}_{31}+\widetilde{D}_{42})\lambda_y^{-1} +(\widetilde{D}_{13}+\widetilde{D}_{24})\lambda_y)+\widetilde{\mu}_i^2 I_{2n}(\widetilde{D}_{12}+\widetilde{D}_{34}+\widetilde{D}_{32}\lambda_y^{-1}+\widetilde{D}_{14}\lambda_y)\Big]\left(\widetilde{\Phi}_q\right)_i=0 \quad (4.29)$$

where $\left(\widetilde{\mu}_i,\widetilde{\phi}_i\right)_{i=1\ldots 2n}$ are the stochastic waveguide propagation modes, and n is the cross sectional DOFs. Then stochastic eigensolutions of Eq. (4.29) are expressed as follows:

$$\begin{aligned}\widetilde{\mu}_i &= (\overline{\mu}_i+\sigma_{\mu_i}\varepsilon)\\ \widetilde{\phi}_i &= \left(\overline{\phi}_i+\sigma_{\phi_i}\varepsilon\right)\end{aligned} \quad (4.30)$$

Using polynomial chaos projection of variables in the Eq. (4.29), extract their mean value $\overline{()}$ and standard deviation (σ). The first-order chaos expansion of stochastic spectral problem in Eq. (4.29) leads to:

$$\begin{aligned}&\Big[(\overline{D}_{21}+\overline{D}_{43}+\overline{D}_{41}\lambda_y^{-1}+\overline{D}_{23}\lambda_y)+\overline{\mu}_i I_{2n}(\overline{D}_{11}+\overline{D}_{22}+\overline{D}_{33}+\overline{D}_{44}+(\overline{D}_{31}+\overline{D}_{42})\lambda_y^{-1}\\ &+(\overline{D}_{13}+\overline{D}_{24})\lambda_y)+\overline{\mu}_i^2 I_{2n}(\overline{D}_{12}+\overline{D}_{34}+\overline{D}_{32}\lambda_y^{-1}+\overline{D}_{14}\lambda_y)\Big]\sigma_{\left(\Phi_q\right)_i}+\Big[(\sigma_{D_{21}}+\sigma_{D_{43}}+\sigma_{D_{41}}\lambda_y^{-1}\\ &+\sigma_{D_{23}}\lambda_y)+\sigma_{\mu_i I_{2n}}(\overline{D}_{11}+\overline{D}_{22}+\overline{D}_{33}+\overline{D}_{44}+(\overline{D}_{31}+\overline{D}_{42})\lambda_y^{-1}+(\overline{D}_{13}+\overline{D}_{24})\lambda_y)+\overline{\mu}_i I_{2n}(\sigma_{D_{11}}\\ &+\sigma_{D_{22}}+\sigma_{D_{33}}+\sigma_{D_{44}}+\sigma_{D_{31}}\lambda_y^{-1}+\sigma_{D_{42}}\lambda_y^{-1}+\sigma_{D_{13}}\lambda_y+\sigma_{D_{24}}\lambda_y)+2\overline{\mu}_i I_{2n}\sigma_{\mu_i}(\overline{D}_{12}+\overline{D}_{34}\\ &+\overline{D}_{32}\lambda_y^{-1}+\overline{D}_{14}\lambda_y)+\overline{\mu}_i^2 I_{2n}(\sigma_{D_{12}}+\sigma_{D_{34}}+\sigma_{D_{32}}\lambda_y^{-1}+\sigma_{D_{14}}\lambda_y)\Big]\left(\overline{\Phi}_q\right)_i=0\end{aligned} \quad (4.31)$$

From above equation the standard deviation of the eigenvectors is:

$$\begin{aligned}\sigma_{\left(\Phi_q\right)_i}=&-\Big[(\sigma_{D_{21}}+\sigma_{D_{43}}+\sigma_{D_{41}}\lambda_y^{-1}+\sigma_{D_{23}}\lambda_y)+\sigma_{\mu_i}I_{2n}(\overline{D}_{11}+\overline{D}_{22}+\overline{D}_{33}+\overline{D}_{44}+(\overline{D}_{31}+\overline{D}_{42})\lambda_y^{-1}\\ &+(\overline{D}_{13}+\overline{D}_{24})\lambda_y)+\overline{\mu}_i I_{2n}(\sigma_{D_{11}}+\sigma_{D_{22}}+\sigma_{D_{33}}+\sigma_{D_{44}}+\sigma_{D_{31}}\lambda_y^{-1}+\sigma_{D_{42}}\lambda_y^{-1}+\sigma_{D_{13}}\lambda_y+\sigma_{D_{24}}\lambda_y)\\ &+2\overline{\mu}_i I_{2n}\sigma_{\mu_i}(\overline{D}_{12}+\overline{D}_{34}+\overline{D}_{32}\lambda_y^{-1}+\overline{D}_{14}\lambda_y)+\overline{\mu}_i^2 I_{2n}(\sigma_{D_{12}}+\sigma_{D_{34}}+\sigma_{D_{32}}\lambda_y^{-1}+\sigma_{D_{14}}\lambda_y)\Big]\\ &\left(\overline{\Phi}_q\right)_i\Big[(\overline{D}_{21}+\overline{D}_{43}+\overline{D}_{41}\lambda_y^{-1}+\overline{D}_{23}\lambda_y)+\overline{\mu}_i I_{2n}(\overline{D}_{11}+\overline{D}_{22}+\overline{D}_{33}+\overline{D}_{44}\\ &+(\overline{D}_{31}+\overline{D}_{42})\lambda_y^{-1}+(\overline{D}_{13}+\overline{D}_{24})\lambda_y)+\overline{\mu}_i^2 I_{2n}(\overline{D}_{12}+\overline{D}_{34}+\overline{D}_{32}\lambda_y^{-1}+\overline{D}_{14}\lambda_y)\Big]^{-1}\end{aligned} \quad (4.32)$$

$\left(\widetilde{\Phi}_q\right)_i^T$, the left stochastic eigenvectors linked with stochastic left eigenvalues $\widetilde{\mu}_i^{-1}$, which form the stochastic left quadratic eigenvalue problem as:

$$\begin{aligned}(\Phi_q)_i^T \Big[&(\widetilde{D}_{21}+\widetilde{D}_{43}+\widetilde{D}_{41}\lambda_y^{-1}+\widetilde{D}_{23}\lambda_y)+\widetilde{\mu}_i^{-1}I_{2n}(\widetilde{D}_{11}+\widetilde{D}_{22}+\widetilde{D}_{33}+\widetilde{D}_{44}\\ &+(\widetilde{D}_{31}+\widetilde{D}_{42})\lambda_y^{-1}+(\widetilde{D}_{13}+\widetilde{D}_{24})\lambda_y)+\widetilde{\mu}_i^{-2}I_{2n}(\widetilde{D}_{12}+\widetilde{D}_{34}+\widetilde{D}_{32}\lambda_y^{-1}+\widetilde{D}_{14}\lambda_y)\Big]=0\end{aligned} \tag{4.33}$$

First-order chaos expansion of the stochastic left eigenvalue problem leads to:

$$\begin{aligned}&\sigma_{\left(\Phi_q\right)_i}{}^T\Big[(\overline{D}_{21}+\overline{D}_{43}+\overline{D}_{41}\lambda_y^{-1}+\overline{D}_{23}\lambda_y)+\overline{\mu}_i{}^{-1}I_{2n}(\overline{D}_{11}+\overline{D}_{22}+\overline{D}_{33}+\overline{D}_{44}+(\overline{D}_{31}+\overline{D}_{42})\lambda_y^{-1}\\ &+(\overline{D}_{13}+\overline{D}_{24})\lambda_y)+\overline{\mu}_i{}^{-2}I_{2n}(\overline{D}_{12}+\overline{D}_{34}+\overline{D}_{32}\lambda_y^{-1}+\overline{D}_{14}\lambda_y)\Big]+\left(\Phi_q\right)_i^T\Big[(\sigma_{D_{21}}+\sigma_{D_{43}}+\sigma_{D_{41}}\lambda_y^{-1}\\ &+\sigma_{D_{23}}\lambda_y)-\overline{\mu}_i{}^{-2}I_{2n}\sigma_{\mu_i}(\overline{D}_{11}+\overline{D}_{22}+\overline{D}_{33}+\overline{D}_{44}+(\overline{D}_{31}+\overline{D}_{42})\lambda_y)+\overline{\mu}_i{}^{-1}I_{2n}(\sigma_{D_{11}}+\sigma_{D_{22}}\\ &+\sigma_{D_{33}}+\sigma_{D_{44}}+\sigma_{D_{31}}\lambda_y^{-1}+\sigma_{D_{42}}\lambda_y^{-1}+\sigma_{D_{13}}\lambda_y+\sigma_{D_{24}}\lambda_y)\\ &-2\overline{\mu}_i{}^{-3}I_{2n}\sigma_{\mu_i}(\overline{D}_{12}+\overline{D}_{34}+\overline{D}_{32}\lambda_y^{-1}+\overline{D}_{14}\lambda_y)+\overline{\mu}_i{}^{-2}I_{2n}(\sigma_{D_{12}}+\sigma_{D_{34}}+\sigma_{D_{32}}\lambda_y^{-1}+\sigma_{D_{14}}\lambda_y)\Big]=0\end{aligned} \tag{4.34}$$

Inserting $\sigma_{(\Phi_q)_i}$ in the above equation and simplification leads to standard deviation of the eigenvalue as:

$$\sigma_{\mu_i} = \left(\overline{\Phi}_q\right)_i^T \Big[(\sigma_{D_{21}}^T + \sigma_{D_{43}}^T + (\sigma_{D_{41}}\lambda_y^{-1})^T + (\sigma_{D_{23}}\lambda_y)^T) + \overline{\mu}_i I_{2n}(\sigma_{D_{11}}^T + \sigma_{D_{22}}^T + \sigma_{D_{33}}^T + \sigma_{D_{44}}^T$$
$$+ (\sigma_{D_{31}}\lambda_y^{-1})^T + (\sigma_{D_{42}}\lambda_y^{-1})^T + (\sigma_{D_{13}}\lambda_y)^T + (\sigma_{D_{24}}\lambda_y)^T) + \overline{\mu}_i^2 I_{2n}(\sigma_{D_{12}}^T + \sigma_{D_{34}}^T + (\sigma_{D_{32}}\lambda_y^{-1})^T$$
$$+ (\sigma_{D_{14}}\lambda_y)^T)\Big] \Big[(\overline{D}_{21}^T + \overline{D}_{43}^T + (\overline{D}_{41}\lambda_y^{-1})^T + (\overline{D}_{23}\lambda_y)^T) + \sigma_{\mu_i} I_{2n}(\overline{D}_{11}^T + \overline{D}_{22}^T + \overline{D}_{33}^T + \overline{D}_{44}^T +$$
$$((\overline{D}_{31} + \overline{D}_{42})\lambda_y^{-1})^T + ((\overline{D}_{13} + \overline{D}_{24})\lambda_y)^T) + \overline{\mu}_i^2 I_{2n}(\overline{D}_{12}^T + \overline{D}_{34}^T + (\overline{D}_{32}\lambda_y^{-1})^T + (\overline{D}_{14}\lambda_y)^T\Big]^{-1}$$
$$+ \Big[(\overline{D}_{21} + \overline{D}_{43} + (\overline{D}_{41}\lambda_y^{-1})(\overline{D}_{23}\lambda_y)) + \overline{\mu}_i{}^{-1} I_{2n}(\overline{D}_{11} + \overline{D}_{22} + \overline{D}_{33} + \overline{D}_{44} + (\overline{D}_{31} + \overline{D}_{42})\lambda_y^{-1}$$
$$+ (\overline{D}_{13} + \overline{D}_{24})\lambda_y) + \overline{\mu}_i{}^{-2} I_{2n}(\overline{D}_{12} + \overline{D}_{34} + \overline{D}_{32}\lambda_y^{-1} + \overline{D}_{14}\lambda_y)\Big]$$
$$- \left(\overline{\Phi}_q\right)_i^T \Big[(\sigma_{D_{21}} + \sigma_{D_{43}} + \sigma_{D_{41}}\lambda_y^{-1} + \sigma_{D_{23}}\lambda_y) + \overline{\mu}_i{}^{-1} I_{2n}(\sigma_{D_{11}} + \sigma_{D_{22}} + \sigma_{D_{33}} + \sigma_{D_{44}} + \sigma_{D_{31}}\lambda_y^{-1}$$
$$+ \sigma_{D_{42}}\lambda_y^{-1} + \sigma_{D_{13}}\lambda_y + \sigma_{D_{24}}\lambda_y) + \overline{\mu}_i{}^{-2} I_{2n}\big(\sigma_{D_{12}} + \sigma_{D_{34}} + \sigma_{D_{32}}\lambda_y^{-1} + \sigma_{D_{14}}\lambda_y\big)\Big]$$
$$\Big[\left(\overline{\Phi}_q\right)_i^T \Big[-(\overline{D}_{11}^T + \overline{D}_{22}^T + \overline{D}_{33}^T + \overline{D}_{44}^T + (\overline{D}_{31}\lambda_y^{-1})^T + (\overline{D}_{42}\lambda_y^{-1})^T) - 2\overline{\mu}_i I_{2n}(\overline{D}_{12}^T + \overline{D}_{34}^T$$
$$+(\overline{D}_{32}\lambda_y^{-1})^T + (\overline{D}_{14}\lambda_y)^T)\Big]\Big[(\overline{D}_{21}^T + \overline{D}_{43}^T + (\overline{D}_{41}\lambda_y^{-1})^T + (\overline{D}_{23}\lambda_y)^T) + \overline{\mu}_i I_{2n}(\overline{D}_{11}^T + \overline{D}_{22}^T + \overline{D}_{33}^T + \overline{D}_{44}^T$$
$$+ ((\overline{D}_{31} + \overline{D}_{42})\lambda_y^{-1})^T + (\overline{D}_{13} + \overline{D}_{24})\lambda_y^T) + \overline{\mu}_i^2 I_{2n}(\overline{D}_{12}^T + \overline{D}_{34}^T + (\overline{D}_{32}\lambda_y^{-1})^T + (\overline{D}_{14}\lambda_y))^T\Big]^{-1}$$
$$\Big[(\overline{D}_{21} + \overline{D}_{43} + (\overline{D}_{41}\lambda_y^{-1}) + (\overline{D}_{23}\lambda_y)) + \overline{\mu}_i{}^{-1} I_{2n}(\overline{D}_{11} + \overline{D}_{22} + \overline{D}_{33}$$
$$+ \overline{D}_{44} + (\overline{D}_{31} + \overline{D}_{42})\lambda_y^{-1} + (\overline{D}_{13} + \overline{D}_{24})\lambda_y) + \overline{\mu}_i{}^{-2} I_{2n}(\overline{D}_{12} + \overline{D}_{34} + \overline{D}_{32}\lambda_y^{-1} + \overline{D}_{14}\lambda_y)\Big]$$
$$- \left(\overline{\Phi}_q\right)_i^T \Big[\overline{\mu}_i{}^{-2} I_{2n}(\overline{D}_{11} + \overline{D}_{22} + \overline{D}_{33} + \overline{D}_{44} + (\overline{D}_{31} + \overline{D}_{42})\lambda_y^{-1} + (\overline{D}_{13} + \overline{D}_{24})\lambda_y)$$
$$+ 2\overline{\mu}_i{}^{-3} I_{2n}(\overline{D}_{12} + \overline{D}_{34} + \overline{D}_{32}\lambda_y^{-1} + \overline{D}_{14}\lambda_y)\Big]\Big]^{-1} \quad (4.35)$$

The explicit expression for the standard deviation of the eigvenvectors is:

$$\sigma_{\left(\Phi_q\right)_i} = -\Big[(\sigma_{D_{21}}+\sigma_{D_{43}}+\sigma_{D_{41}}\lambda_y^{-1}+\sigma_{D_{23}}\lambda_y)+\sigma_{\mu_i}I_{2n}(\overline{D}_{11}+\overline{D}_{22}+\overline{D}_{33}+\overline{D}_{44}+(\overline{D}_{31}+\overline{D}_{42})\lambda_y^{-1}$$
$$+(\overline{D}_{13}+\overline{D}_{24})\lambda_y)+\overline{\mu}_i I_{2n}(\sigma_{D_{11}}+\sigma_{D_{22}}+\sigma_{D_{33}}+\sigma_{D_{44}}+\sigma_{D_{31}}\lambda_y^{-1}+\sigma_{D_{42}}\lambda_y^{-1}+\sigma_{D_{13}}\lambda_y+\sigma_{D_{24}}\lambda_y)$$
$$+2\overline{\mu}_i I_{2n}\sigma_{\mu_i}(\overline{D}_{12}+\overline{D}_{34}+\overline{D}_{32}\lambda_y^{-1}+\overline{D}_{14}\lambda_y)+\overline{\mu}_i^2 I_{2n}(\sigma_{D_{12}}+\sigma_{D_{34}}+\sigma_{D_{32}}\lambda_y^{-1}+\sigma_{D_{14}}\lambda_y)\Big]$$
$$\left(\overline{\Phi}_q\right)_i \Big[(\overline{D}_{21}+\overline{D}_{43}+\overline{D}_{41}\lambda_y^{-1}+\overline{D}_{23}\lambda_y)+\overline{\mu}_i I_{2n}(\overline{D}_{11}+\overline{D}_{22}+\overline{D}_{33}+\overline{D}_{44}$$
$$+(\overline{D}_{31}+\overline{D}_{42})\lambda_y^{-1}+(\overline{D}_{13}+\overline{D}_{24})\lambda_y)+\overline{\mu}_i^2 I_{2n}(\overline{D}_{12}+\overline{D}_{34}+\overline{D}_{32}\lambda_y^{-1}+\overline{D}_{14}\lambda_y)\Big]^{-1} \quad (4.36)$$

The above Eq. (4.35) and Eq. (4.36) are the explicit expressions for the statistics of wave propagation using deterministic eigenvalue solutions in 2D periodic media.

4.3.2 Internal nodes

If the modeling of unit cells require inner DOFs, a condensed dynamic stiffness matrix is necessary. In the case of internal nodes (I) as shown in Fig. 4.5, the DOFs are partitioned into boundary DOFs (D_{bd}) and internal DOFs (D_I). The dynamic stiffness matrix has

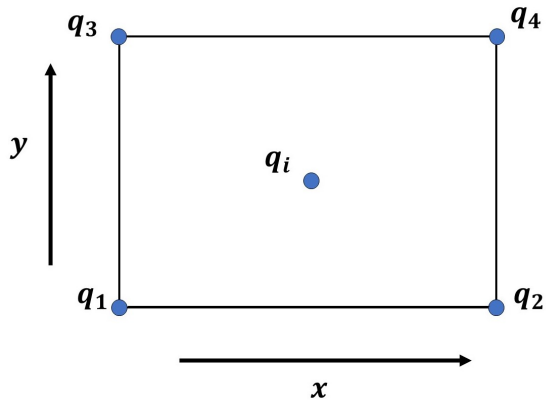

Figure 4.5: Schematic diagram of a thin plate element with inner nodes

the following form:

$$D = \begin{bmatrix} \widehat{D}_{bdbd} & \widehat{D}_{bdI} \\ \widehat{D}_{Ibd} & \widehat{D}_{II} \end{bmatrix} \quad (4.37)$$

where symbol $\widehat{()}$ represents the elements from the original dynamic stiffness matrix. The standard deviation of the condensed dynamic stiffness matrix,can be expressed as:

$$\sigma_{D_{bd}} = \left[\sigma_{\widehat{D}_{bdbd}}\right] - \left[\overline{\widehat{D}}_{bdI} \quad \sigma_{\widehat{D}_{bdI}}\right] \begin{bmatrix} \overline{\widehat{D}}_{II}^{-1} & -\overline{\widehat{D}}_{II}^{-1}\sigma_{\widehat{D}_{II}}\overline{\widehat{D}}_{II}^{-1} \\ 0 & \overline{\widehat{D}}_{II}^{-1} \end{bmatrix} \begin{bmatrix} \sigma_{\widehat{D}_{Ibd}} \\ \overline{\widehat{D}}_{Ibd} \end{bmatrix} \tag{4.38}$$

where symbol $\overline{\widehat{()}}$ that represents the mean value from the original dynamic stiffness matrix.

4.4 Numerical results

The proposed numerical scheme is summarized in the workflow in Fig. 4.6. In this section,

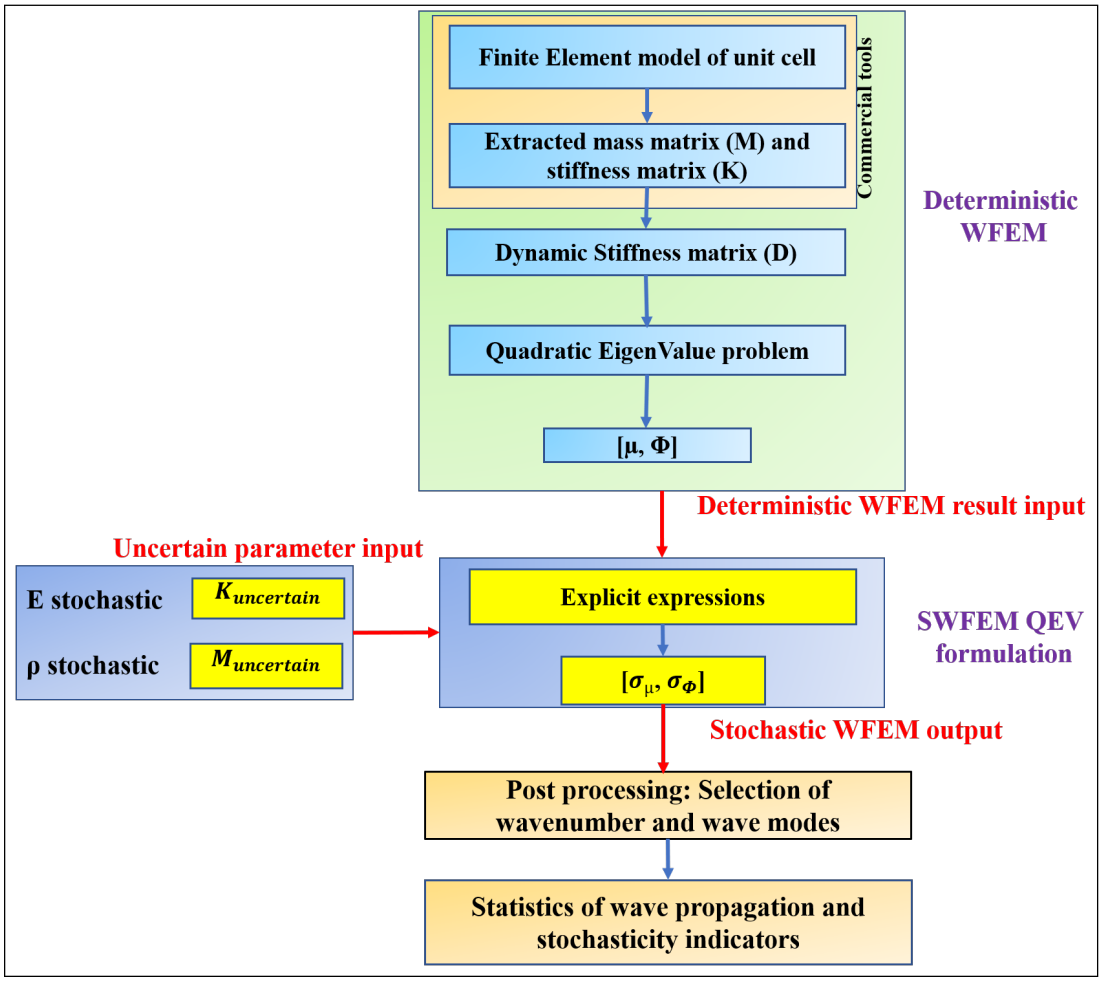

Figure 4.6: Workflow of developed SWFEM QEV

the validation of the developed SWFEM QEV formulation is performed. In the first part, the validation of SWFEM QEV for the 1D periodic rod with band gap is presented.

Furthermore, the validation of the metamaterial case is discussed. In the second part, the SWFEM QEV formulation is validated for the homogeneous and periodic plate and the applicability and accuracy of the formulation is checked.

4.4.1 Validation of SWFEM QEV: 1D

This subsection includes the validation of the SWFEM QEV formulation applied to a 1D periodic rod considering the material uncertainty. In addition, the variation of the longitudinal wavenumber is analyzed with the variation of the input properties.

Dispersion analysis of periodic rod

The periodic rod consists of section A of length l_1, and section B of length l_2 as depicted in the Fig. 4.7. Here sections A and B are made of different materials. The validation of the present developed formulation is demonstrated by comparing the result with those available from analytical sampling and MCS. The SWFEM QEV is used to study the effect of parametric uncertainties on the dispersion relation of the longitudinal wave in the periodic rod. The reference analytical solution of a periodic rod is based on the following

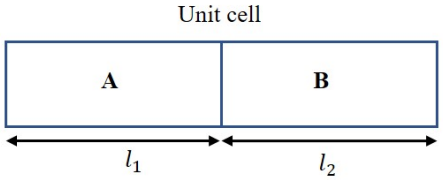

Figure 4.7: Symmetric unit cell of 1D periodic rod

expression of the wavenumber [Tian et al., 2011]:

$$\cos(kl) = \cos\left(\frac{\omega}{c_a} l_a\right) \cos\left(\frac{\omega}{c_b} l_b\right) - \frac{1}{2}\left(\frac{\rho_a c_a}{\rho_b c_b} + \frac{\rho_b c_b}{\rho_a c_a}\right) \sin\left(\frac{\omega}{c_a} l_a\right) \sin\left(\frac{\omega}{c_b} l_b\right) \tag{4.39}$$

where c_a, and c_b are the wave velocities in the sections A and B, respectively, and expressed as $c_a = \sqrt{E_a/\rho_a}$ and $c_b = \sqrt{E_b/\rho_b}$, E_a, ρ_a, and l_a are the respective Young's modulus, density and length for section A and E_b, ρ_b, and l_b are those for section B. l is the total length of the unit cell. The uncertainty effect is studied considering a variation of (4%) of Young's modulus nominal values. It is to be mentioned that the input uncertainties

are represented inside bracket (). The frequency range is 10-2000 Hz. The sampling method is used to obtain the wave characteristics of the analytical wavenumber using Eq. (4.39). The analytical sampling and MCS results are treated as reference result for validation purpose. A two-node rod element is considered. This element allows treatments of a longitudinal wave. The local stiffness and mass matrices are assembled into global stiffness and mass matrices in the MATLAB environment with 200 elements in the unit cell of the periodic rod. In this manner, the wavelength contains at least 20 elements in the frequency range. The material and geometric properties are reported in Table 4.1. The

Table 4.1: Material and geometric properties of periodic rod (SWFEM QEV)

Geometry/Property	Value
Rod length (A)	1 m
Rod length (B)	1 m
Radius of rod	0.0644 m
Young's modulus (A)	4.50 $\times 10^9$ Pa
Young's modulus (B)	70 $\times 10^9$ Pa
Mass density (A)	1200 kg/m^3
Mass density (B)	2700 kg/m^3
Loss factor (A) and (B)	0.001

results obtained with analytical sampling, SWFEM TM, SWFEM QEV, and WFEM MCS are compared. The mean values comparison is shown in Fig. 4.8; there exist two full band gaps, first at approximately 418-928 Hz and the other at 1184-1847 Hz. It is to be noted that the WFEM MCS are performed using the WFEM quadratic form. The comparison of the standard deviation is presented in Fig. 4.9, showing that the results are in good agreement. The SWFEM QEV standard deviation is computed considering loss factor; however, the analytical sampling is computed without damping. It is observed that the effect of the uncertainty on the longitudinal wavenumber, is nearly 3% at the start of the first band gap,and 10% nearly at the end of the band gap. The uncertainty effect increases with increasing frequency; it can be seen that variation is around 33% at the start of second band gap frequency and 35% at the end of the second band gap frequency.

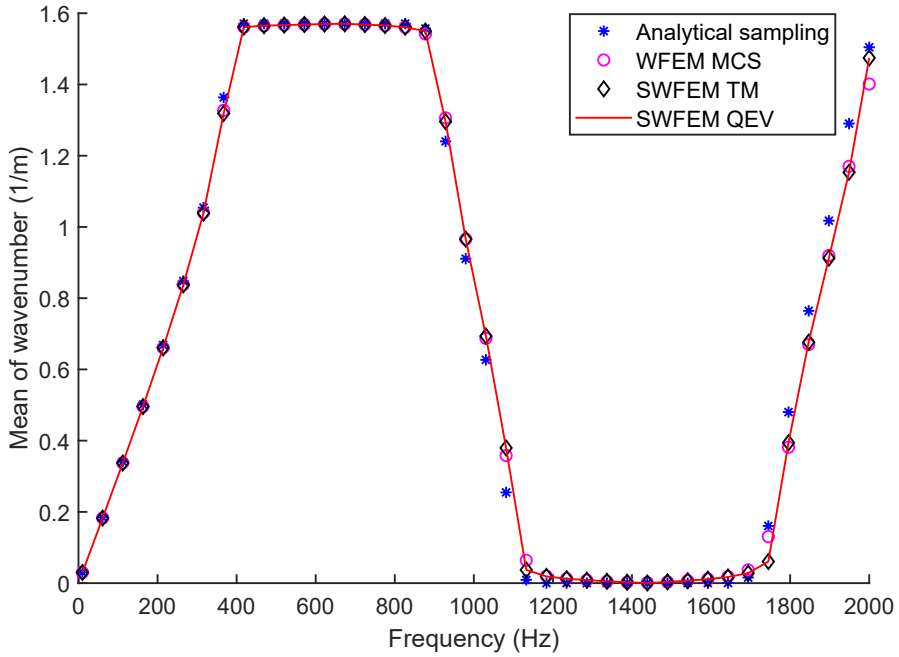

Figure 4.8: Mean value of longitudinal wavenumber comparison (Young's modulus stochastic)

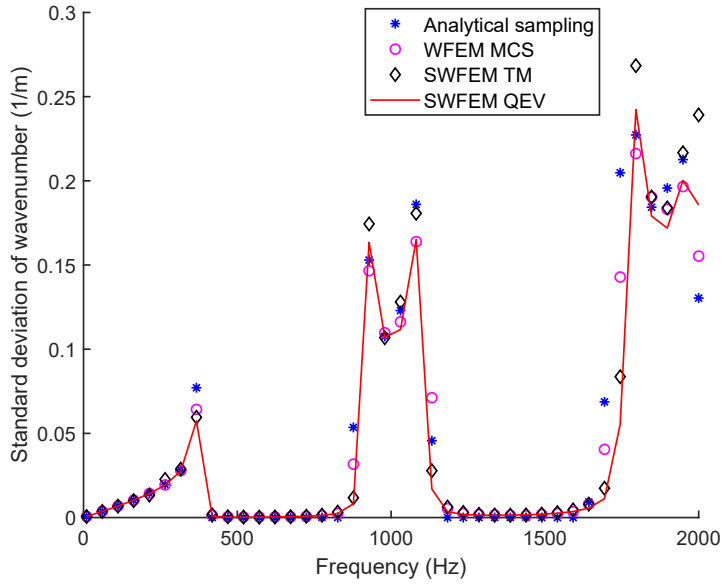

Figure 4.9: Standard deviation of longitudinal wavenumber comparison (Young's modulus stochastic)

Effect of the parameter uncertainties on the wavenumber in the periodic rod

The variation of material parameter scatters the longitudinal wavenumber. Here, the focus is to quantify the variation of COV that is defined as (standard deviation /mean value) for

the longitudinal wavenumber with the variation of COV of the material properties. This also helps to judge the capacity of the developed formulation for the range of variation it can accommodate. In the numerical experiment, the material properties, namely Young's modulus and density, are varying with a Gaussian distribution. For the comparison 10,000 samples are used for the WFEM MCS. The input in term of COV is varying up to (7%) about the mean value of the considered parameter. In the first case, Young's modulus is stochastic. The comparison of the COV of the input parameter (Young's modulus stochastic) at discrete frequencies is shown in Fig. 4.10. From the figure, it is observed that in the propagation frequency region, the variation of the wavenumber is linear; however, this relationship breaks down at the edge of the band gap. In the low frequency range, the variation of wavenumber is significantly affected by the variation of the input uncertainty. The highest variation is recorded at the second band gap edge frequency. The comparison

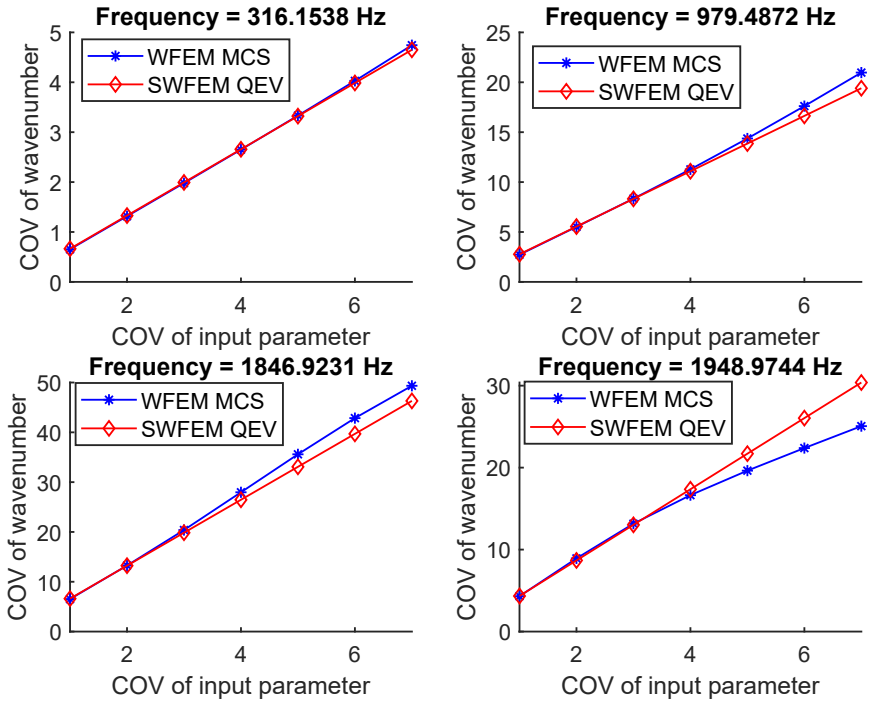

Figure 4.10: Variation of the longitudinal wavenumber with varying Young's modulus, MCS (blue star line) and, present formulation (red diamond line) at discrete frequencies

of stochastic density is shown in Fig. 4.11, for which the same trend is visible. At (3%) input uncertainty, the longitudinal wavenumber COV is 1.997 with stochastic elasticity and 1.991 with stochastic density at 316 Hz; and 19.855 in case of stochastic elasticity and 19.840 with stochastic density at 1846 Hz. This confirms the the effect of elasticity

stochasticity is slightly higher than the stochastic density. Furthermore, the significance of the uncertain wavenumber is increasing with increasing frequency. The validity of the developed formulation is limited to roughly 4% variation. This is because the formulation is based on the first-order expansion.

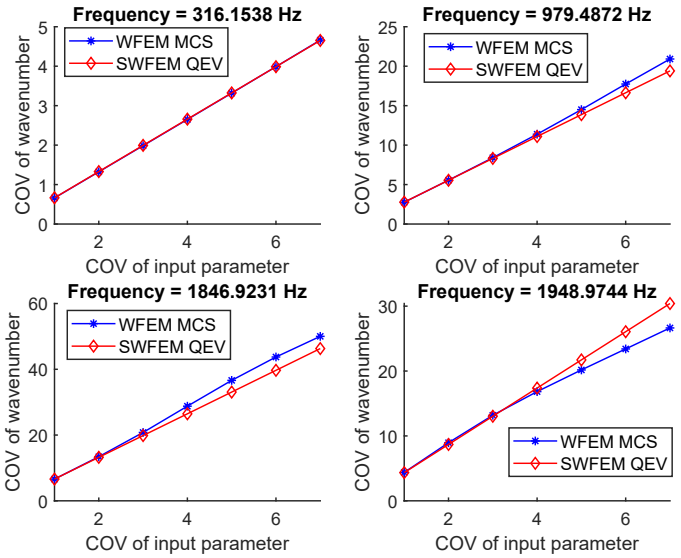

Figure 4.11: Variation of the longitudinal wavenumber with varying density, MCS (blue star line), and present formulation (red diamond line) at discrete frequencies

Dispersion analysis of metamaterial rods

To demonstrate the capability of the developed stochastic formulation of accurately analyzing a metamaterial system; a simple metamaterial-based rod system is considered. A system consisting of a uniform rod with periodically attached SDOF local resonators is evaluated. The system material and geometrical parameters are presented in Table 4.2. The local resonator frequency of the SDOF resonator is tuned to 500 Hz with a mass ratio

Table 4.2: Metamaterial rod material and geometric properties

Geometry/Property	Value
Rod length	1 m
Radius of rod	0.01 m
Young's modulus	70 $\times 10^9$ Pa
Mass density	2700 kg/m^3
Loss factor	0.01

of 20% of the host system. A resonator with stiffness of $1.6743 \times 10^6 N/m$, and mass of

0.1696 kg is attached to the left end of the host rod. The uncertainty in the host rod is considered (4%) around the nominal value of the Young's modulus. A comparison for WFEM MCS, SWFEM QEV, and SWFEM TM is presented. The comparison of mean value is shown in Fig. 4.12, and of standard deviation in Fig. 4.13. It can be seen from the graphs that; the curves are in excellent agreement, which confirms the validity of the formulation for the simulation of uncertainty in the metamaterial system. In Fig. 4.12, a typical asymmetric resonance gap is observed with sharp attenuation at the resonator tuned frequency (500 Hz) of the SDOF resonator. At the lower frequency, the nature of such attenuation is asymmetric. An indicator is used to check the effects of uncertainties. Stochasticity indicator is defined as the ratio of the standard deviation of the wavenumber and the mean of the wavenumber at a discrete frequency. It is also expressed as COV:

$$COV = \sigma_k / \overline{k} \tag{4.40}$$

where σ_k is the standard deviation of the wavenumber and $\overline{k}$ is the mean value of wavenumber. It indicates the spread of the wavenumber at discrete frequency steps. The stochastic indicator for the metamaterial system is presented in Fig. 4.14. From the graph it is visible that the propagative longitudinal wavenumber varies by approximately 2%. The wavenumber varies by 2.63% at the start of the resonance band gap frequency (492 Hz), and a maximum variation of 2.7% of the wavenumber occurs at the end of the resonance band gap frequency (552 Hz). Inside the resonance band gap, the variation attains a minimum value of 1.4%. However; it is not completely zero. As a matter of fact, the results show that the uncertainty alters the wave states inside the resonance band gap and the effects of uncertainties are increasing at higher frequency. Moreover, the results obtained from the SWFEM QEV are in excellent agreement with the WFEM MCS results inside the resonance band gap.

Effect of the parameter uncertainties on the wavenumber of metamaterial rod

To assess the effect of the uncertain input on the variation of the wavenumber of the metamaterial rod system, the uncertainty in the host structure is considered. The dependence of the variation of the wavenumber on the variation of Young's modulus is plotted in

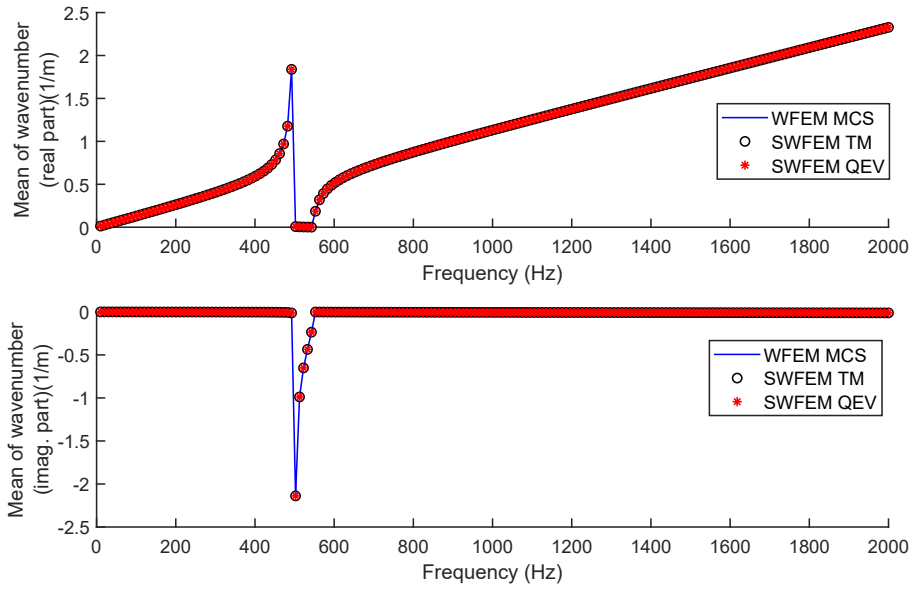

Figure 4.12: Mean value of the real and imaginary part of longitudinal wavenumber comparison (Young's modulus stochastic)

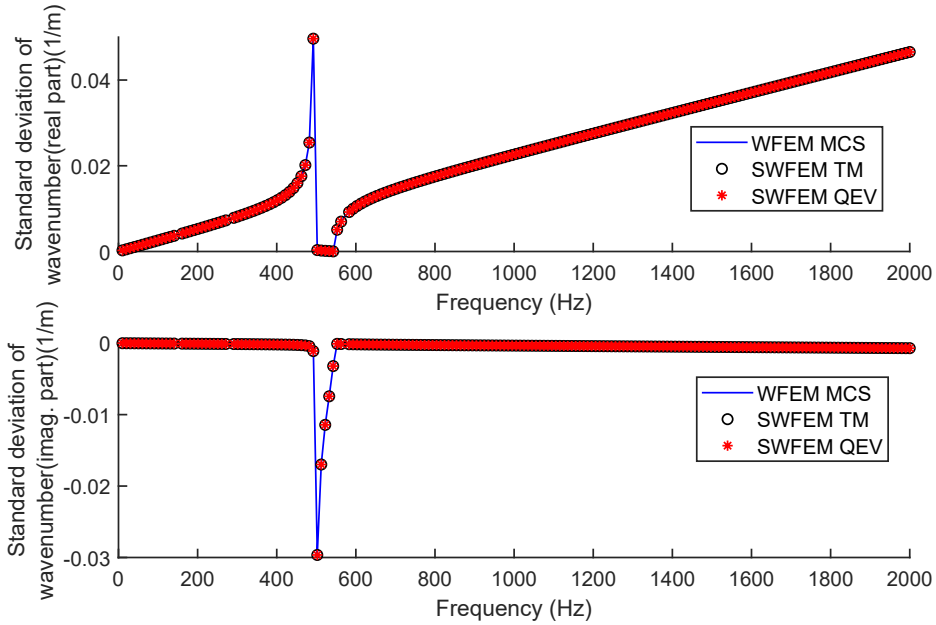

Figure 4.13: Standard deviation of the real and imaginary part of longitudinal wavenumber comparison (Young's modulus stochastic)

Fig. 4.15. In the case of stochastic density, the variations are shown in Fig. 4.16. From the graphs, it can be observed that with stochastic Young's modulus, the effect on wavenumber is showing linear trends. However; with uncertainty density, the band gap widens slightly. Also, around the resonance frequency, effect of the uncertainty is nearly mini-

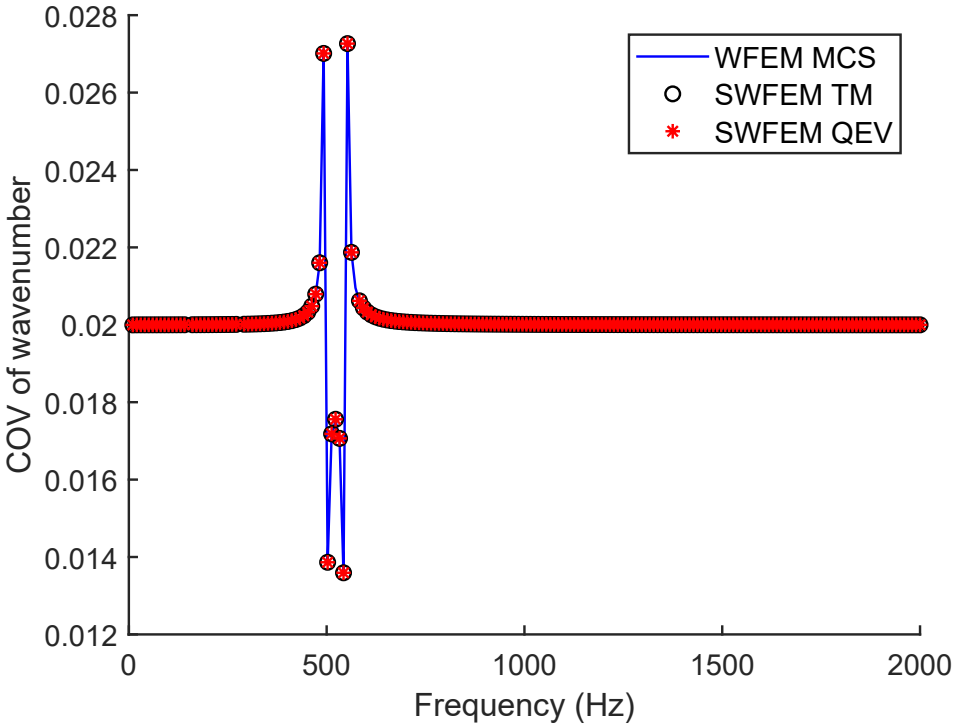

Figure 4.14: Stochasticity indicator for metamaterial rod system (Young's modulus stochastic)

mum. It is noteworthy, that in the case of the metamaterial and stochastic host structure, the quadratic formulation results are consistent with MCS with (7%) uncertainty. That suggests, the SWFEM QEV handle a higher level of uncertainties.

4.4.2 Validation of SWEFM QEV: 2D

In this subsection, numerical studies are presented to demonstrate the validity and applicability of the stochastic quadratic formulation developed in this chapter. A homogenous plate case and periodic plate case are discussed; and the wavenumber dispersion is analyzed with variation of the input parameters.

Homogeneous plate

To demonstrate the validity of the formulation in the simple homogenous plate case, numerical simulations are performed. A thin plate unit cell is modelled with four-node elements with three DOFs at each node. The material properties are reported in Table 4.3.

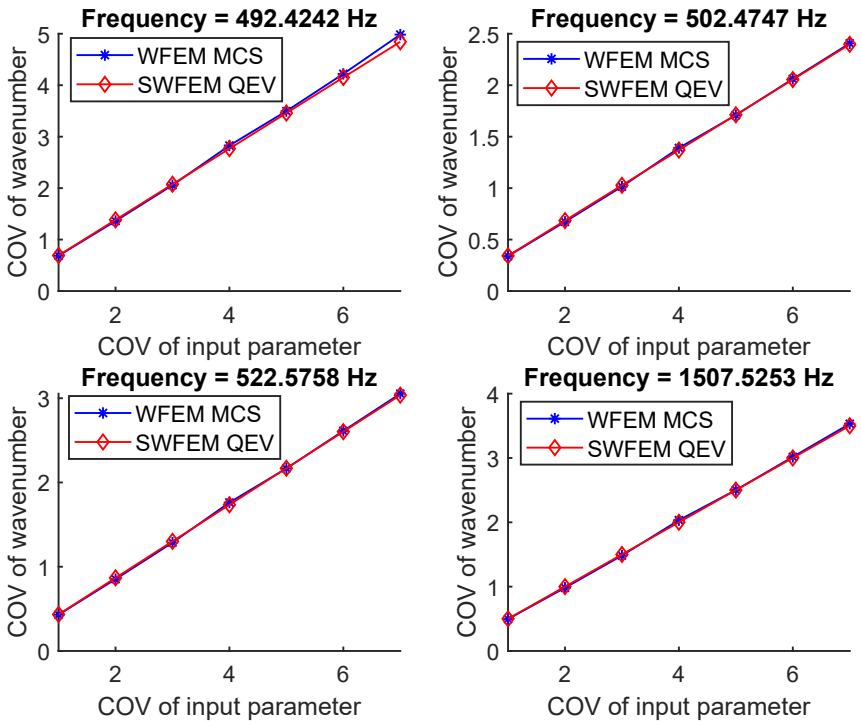

Figure 4.15: Variation of the longitudinal wavenumber with host structure uncertainty (Young's modulus stochastic), MCS (blue star line) and present formulation (red diamond line) at discrete frequencies

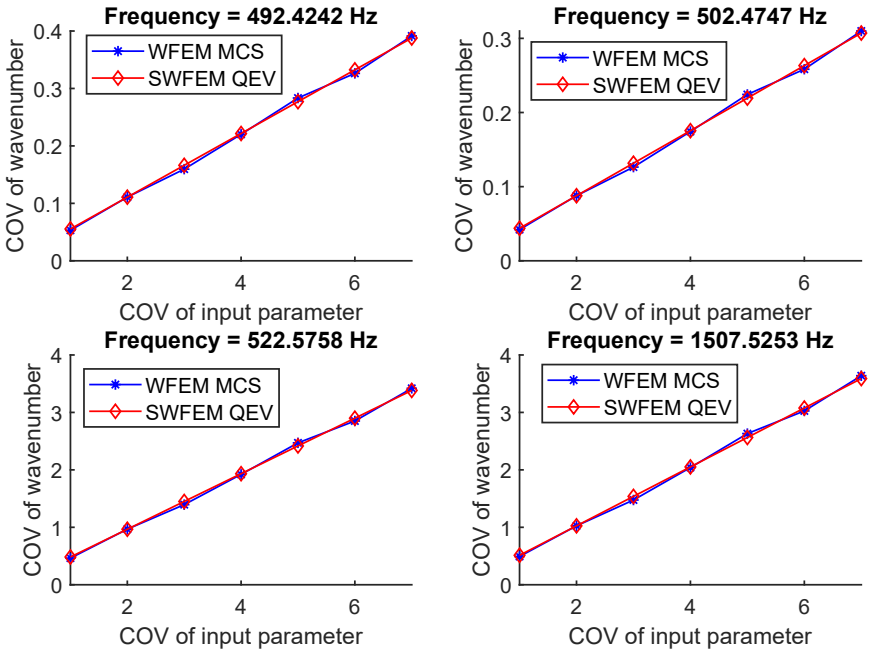

Figure 4.16: Variation of the longitudinal wavenumber with host structure uncertainty (density stochastic), MCS (blue star line) and present formulation (red diamond line) at discrete frequencies

The dimensions of the unit cell are $L_x = L_y = 0.005m$ with thickness $h = 0.0005m$.

Table 4.3: Material properties of homogeneous plate

Geometry/Property	Value
Young's modulus	$210 \times 10^9\ Pa$
Poission's ratio	0.3
Mass density	$7800\ kg/m^3$
Loss factor	0.01

The reference analytical solution of a plate is based on the following expression of the wavenumber:

$$k_f = \sqrt[4]{\rho h \omega^2 / D_{bending}} \tag{4.41}$$

where the plate bending stiffness is $D_{\text{bending}} = Eh^3/12\left(1-\nu^2\right)$. E is the Young's modulus, ρ is the density, ν is the Poisson's ratio, h is the plate thickness, and ω is the circular frequency. The uncertainty effect is studied with (4%) variation of Young's modulus around the nominal value. The out-of-plane flexural wave is responsible for transmitting most of the acoustic energy. Therefore, the out-of-plane flexural wave is the primary wave type considered during the numerical analysis. The analytical sampling and WFEM MCS are treated as reference results for validation purposes. The mean value comparison of the flexural wavenumber is presented in Fig. 4.17, and the standard deviation comparison is shown in Fig. 4.18. The standard deviation obtained from the SWFEM QEV is in excellent agreement with analytical sampling and WFEM MCS results. It verifies the validity of the stochastic quadratic formulation for the homogenous plate. The stochasticity indicator for the (4%) variation in Young's modulus is plotted and shown in Fig. 4.19. From the figure it can be inferred that Young's modulus uncertainty does not cause any variation on the out-of-plane flexural wavenumber with the frequency. The dispersion curve in the (k_x, k_y) plane at discrete frequencies is presented in Fig. 4.20. The mean value and standard deviation comparison are also shown in Fig. 4.20. From Fig. 4.20 it can be observed that the contour curves are independent of propagation direction. This is caused by the isotropic nature of the plate;Thus, the material properties are independent of the direction, and, this is also predicted in the simulated results.

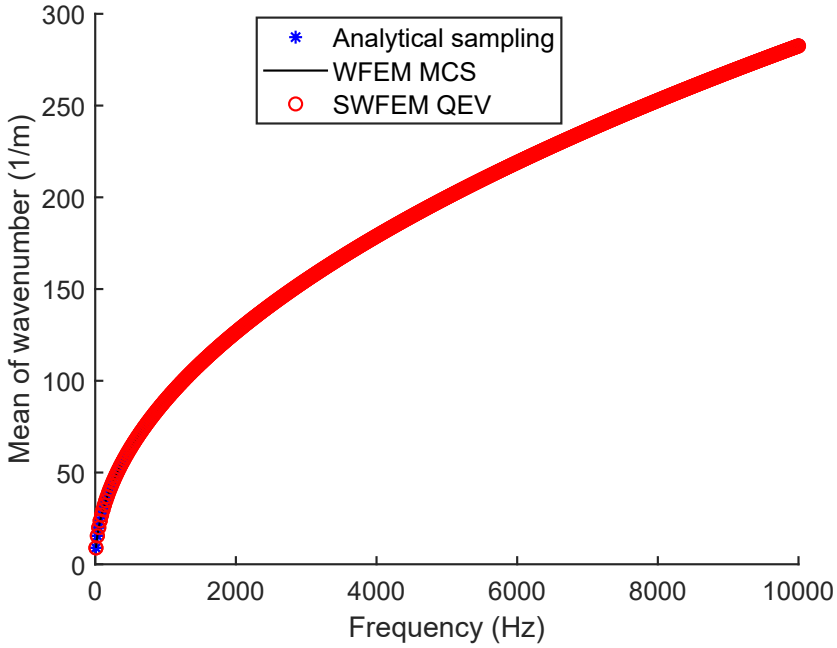

Figure 4.17: Mean value of out-of-plane flexural wavenumber in x-direction (Young's modulus stochastic)

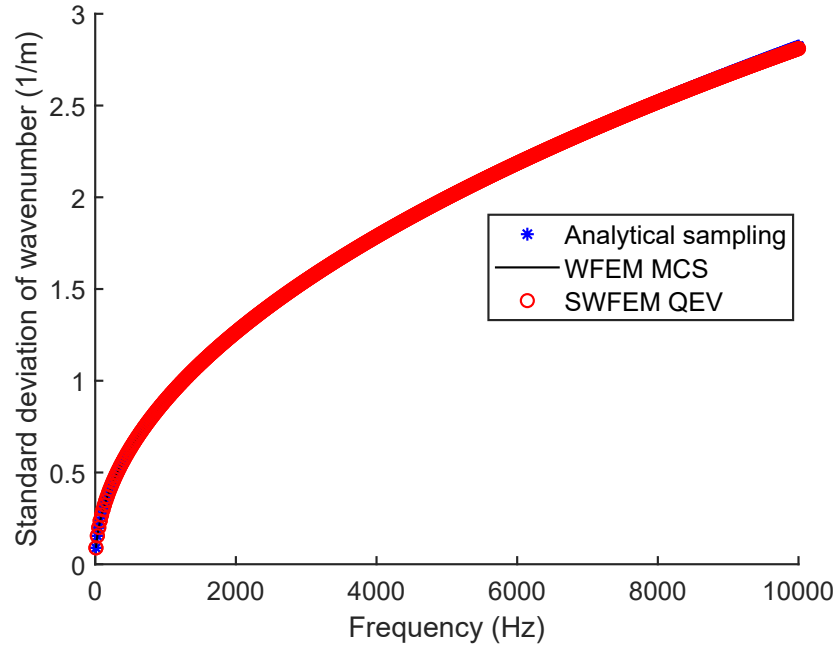

Figure 4.18: Standard deviation out-of-plane flexural wavenumber in x-direction (Young's modulus stochastic)

Effect of the parameter uncertainties on out-of-plane flexural wavenumber of homogeneous plate

The influence of the uncertainties in the material properties on the variation of out-of-plane flexural wavenumber is discussed. The COV of the wavenumber with change of input COV

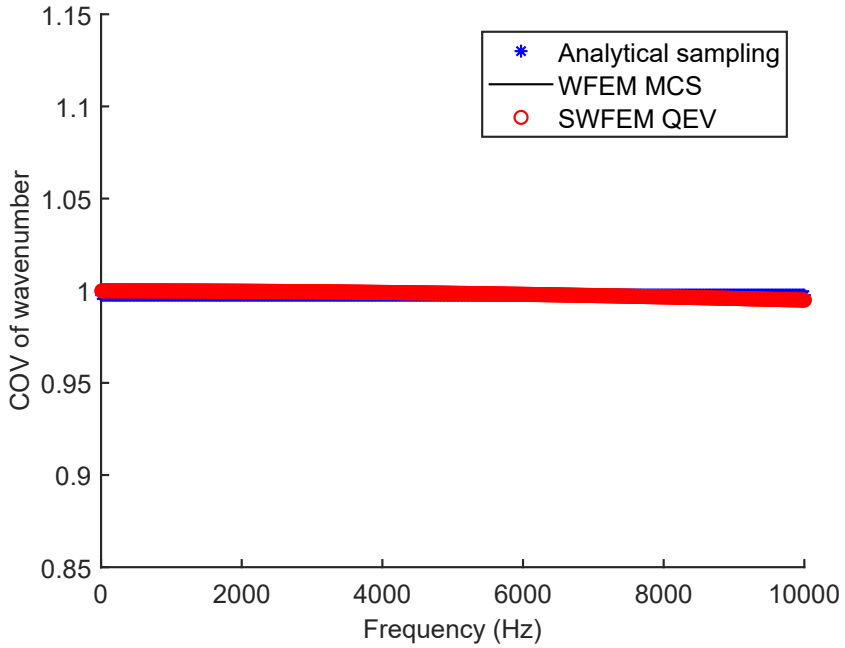

Figure 4.19: Stochasticity indicator for out-of-plane flexural wavenumber in x-direction (Young's modulus stochastic)

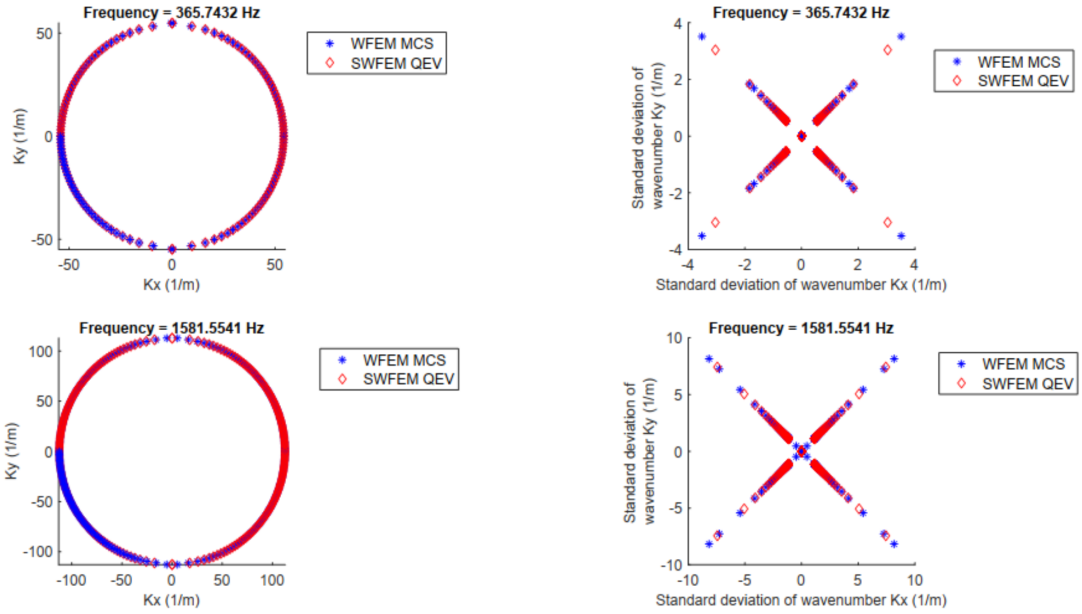

Figure 4.20: k-space mean value and standard deviation (Young's modulus stochastic), MCS results (blue star) and present formulation (red diamond) at discrete frequencies

is analyzed for the range from (1%) to (7%). In the first case, only Young's modulus is considered as an uncertain input. The comparison of the COV of the flexural wavenumber obtained from SWFEM QEV and COV of the WFEM MCS results is presented in Fig. 4.21,

where it can be seen that the flexural wavenumber variation is linear. In the second case, the density is considered as the uncertain input parameter. The comparison is presented in Fig. 4.22; where linear variation of the flexural wavenumber is observed. In both cases, the results obtained from SWFEM QEV are very close to the reference WFEM MCS results, which demonstrates the accuracy of the formulation for the range of COV considered. From Fig. 4.21 and Fig. 4.22, it can also be seen that the variations of the flexural wavenumber are slightly higher with uncertain Young's modulus than with uncertain density.

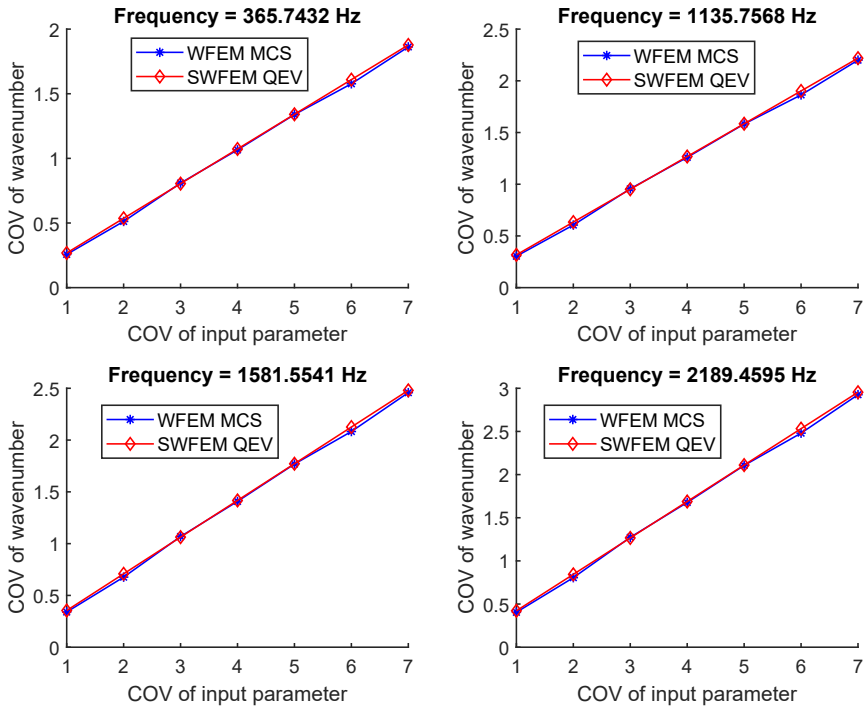

Figure 4.21: Variation of the out-of-plane flexural wavenumber (Young's modulus stochastic), MCS (blue star line) and present formulation (red diamond line) at discrete frequencies

Periodic plate

In this subsection, validation of the SWFEM QEV formulation is performed for a 2D periodic plate. In addition, the flexural wavenumber dispersion statistics are analyzed with variation of the input parameters. The periodic plate consists of N repetitions of alternating sub-plate type A and sub-plate type B in x-direction. The sub-plate type A

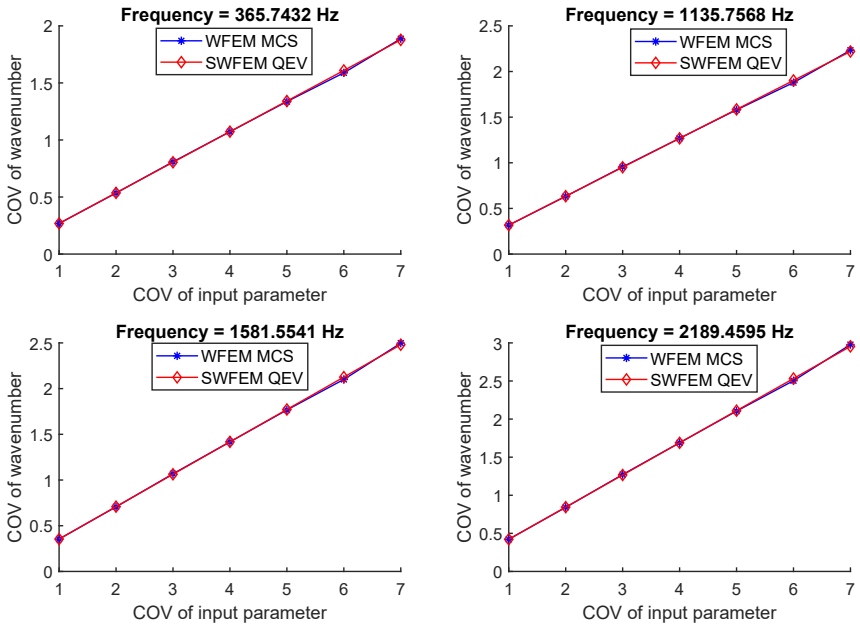

Figure 4.22: Variation of the out-of-plane flexural wavenumber (density stochastic), MCS (blue star line) and present formulation (red diamond line) at discrete frequencies

and sub-plate type B can be of different material properties and or different geometric dimensions. Here in the numerical simulation periodic plate made of different material properties are considered. The schematic of a periodic plate and corresponding unit cell model are shown in Fig. 4.23. The periodic plate unit cell consists of an assembly of a 2x2 array of unit cells comprised of sub-plate type A and sub-plate type B. The periodic plate material properties are reported in Table 4.4. The periodic plate unit cell is modelled with

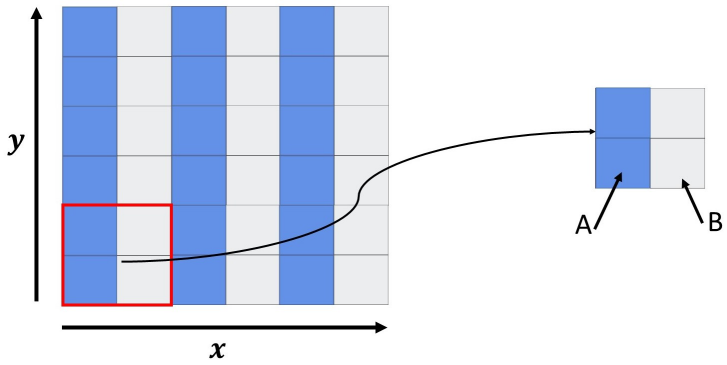

Figure 4.23: Schematic of the periodic plate and unit cell of the periodic plate

four-noded elements with three DOFs at each node. The dimensions of the unit cell are $L_x = L_y = 0.1m$ with thickness $h = 0.01m$. The validation of the developed formulation is presented for out-of-plane flexural wavenumber. The considered frequency range is 10-3000

Table 4.4: Material properties of the periodic plate

Geometry/Property	Value
Young's modulus of sub-plate type A	$70 \times 10^9\ Pa$
Young's modulus of sub-plate type B	$4.5 \times 10^9\ Pa$
Poisson's ratio of sub-plate type A and B	0.3
Mass density of sub-plate type A	$2700\ kg/m^3$
Mass density of sub-plate type B	$1200\ kg/m^3$
Loss factor of sub-plate type A and B	0.01

Hz. The Young's modulus of sub-plates type A and B are considered as the uncertainties iwth variation of (4%) about the nominal values. Since there are no results reported in the literature for a periodic plate with uncertainties, the WFEM MCS is considered as the reference solution. Using the (ω, k_y) formulation, the out-of-plane flexural wavenumber dispersion is computed, and comparisons of the mean value and standard derivation are shown in Fig. 4.24 and Fig. 4.25, respectively. The comparison shows the agreement of the SWFEM QEV results with the reference results. This verifies the applicability of the formulation for the periodic plate case.

From the mean value comparison shown in Fig. 4.24, the start of the band gap is approximately 2352 Hz. At the same frequency, the maximum value of standard deviation is observed in the standard deviation comparison graph shown in Fig. 4.25. Furthermore, the stochasticity indicator presented in Fig. 4.26, shows that the maximum variation of 6.5% of the wavenumber is observed at 2352 Hz. Inside the band gap zone, the variation of wavenumber shows the decrease in value of the standard deviation. The dispersion curve in the (k_x, k_y) plane at discrete frequencies is shown in Fig.4.27. Where it can be seen that the contour curves are dependent on the propagation direction, which is due to the periodicity of the plate. It can be summarized that the uncertainties affect the out-of-plane flexural wavenumber scattering, and that the maximum value of the variation of out-of-plane flexural wavenumber occurs at the band gap edge frequencies.

Effect of the parameter uncertainties on the out-of-plane flexural wavenumber of periodic plate

The COV of the out-of-plane flexural wavenumber with uncertain Young's modulus and uncertain density are analyzed. The scattering of the out-of-plane flexural wavenumber

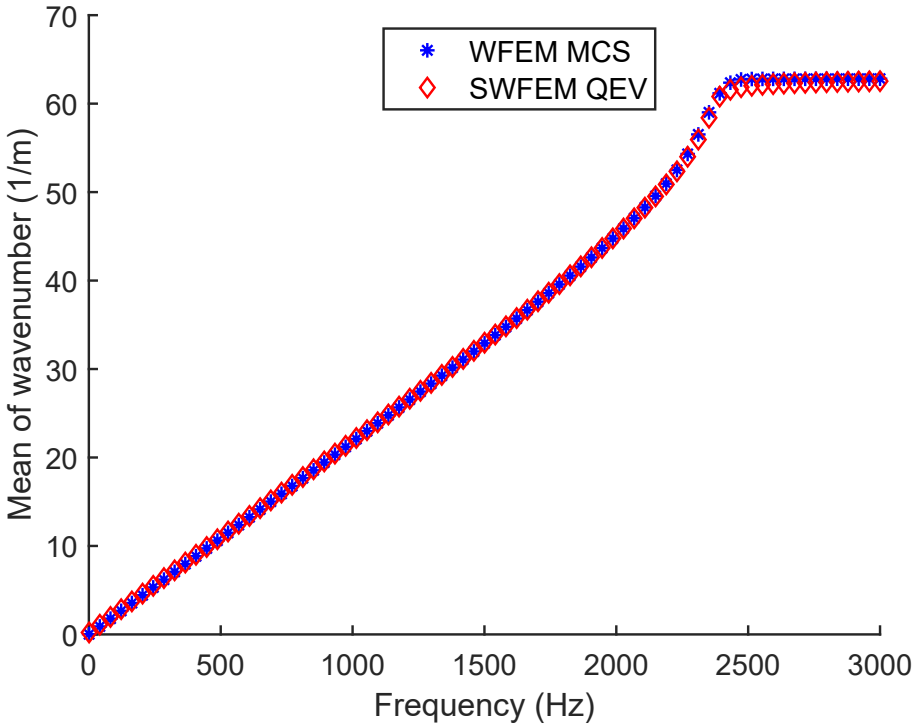

Figure 4.24: Mean value of out-of-plane flexural wavenumber in x-direction (Young's modulus stochastic)

can be calculated by allowing the COV of the material parameters from (1%) to (7%). In this range, the presented results would be enough to extrapolate the results for the COV, keeping in mind the limitation of the first-order perturbation method. The variation of the out-of-plane flexural wavenumber for the periodic plate with uncertainty in Young's modulus is shown in Fig. 4.28, and with uncertainty in density in Fig. 4.29. It is observed that at (3%) input uncertainty, the out-of-plane flexural wavenumber COV is 2.895 with stochastic elasticity and 2.835 with stochastic density at 2030 Hz; and 1.525 in case of stochastic elasticity and 1.521 with stochastic density at 469 Hz. The flexural wavenumber COV for uncertain elasticity is higher than for uncertain density. This difference in COV is very minimal and stronger with increasing frequency. The COV plots show the linear variation of out-of-plane flexural wavenumber in low frequency regions and shifting to higher variation with increasing frequency.

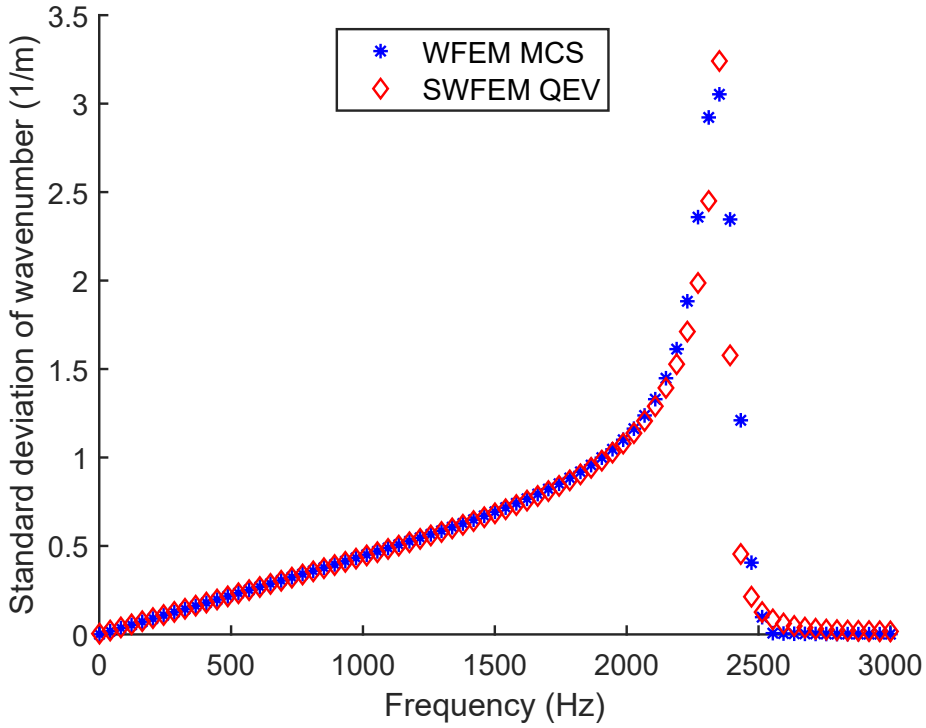

Figure 4.25: Standard deviation out-of-plane flexural wavenumber in x-direction (Young's modulus stochastic)

4.5 Elapsed time comparison for SWFEM QEV 1D and 2D periodic media

In the context of uncertainty quantification in periodic media, in crude MCS, the sample selection mainly depends on the maximum number of simulations, elapsed time, and desired accuracy. In order to establish the preeminence of SWFEM QEV over the WFEM MCS, the numerical costs of computation is compared with that of crude MCS. One test case each for 1D and 2D cases are presented to exhibit the elapsed time comparison, because different parameter elapsed time trends are approximately equivalent in all cases. The test ran on a mobile workstation with Intel® Core™ i7 7820 HQ CPU clocked at 2.90

Table 4.5: Elapsed time comparison for 1D and 2D SWFEM QEV

	WFEM MCS (10000 samples)	SWFEM QEV (single run)
1D periodic media	3840 seconds	5.45 seconds
2D periodic media	14400 seconds	21.57 seconds

GHz with 32 GB RAM. The comparison of elapsed time is reported in Table 4.5, showing

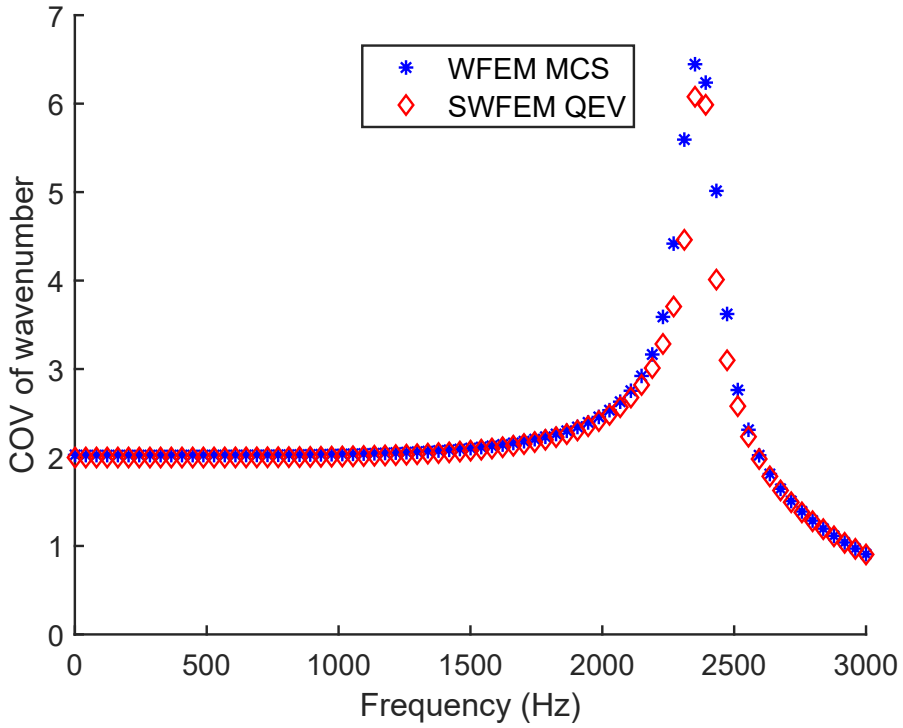

Figure 4.26: Stochasticity indicator for out-of-plane flexural wavenumber in x-direction (Young's modulus stochastic)

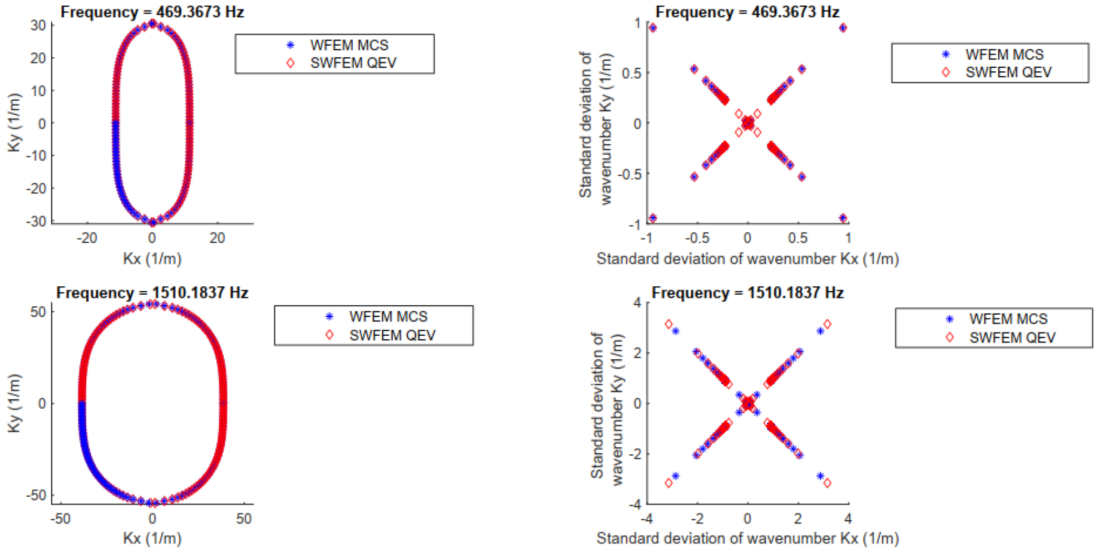

Figure 4.27: k-space mean value and standard deviation of wavenumber (Young's modulus stochastic)

that computational effort by application of SWFEM QEV is much smaller compared to WFEM MCS. The SWFEM QEV formulation uses the deterministic results to evaluate the response variability of the wavenumber. Thus, the SWFEM QEV formulation is more

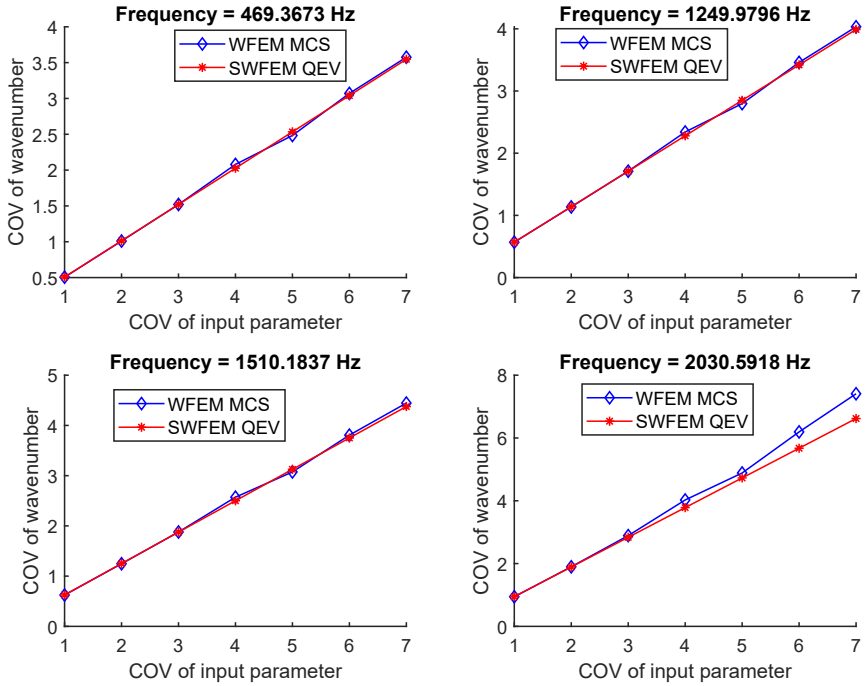

Figure 4.28: Variation of the out-of-plane flexural wavenumber (Young's modulus stochastic), MCS (blue diamond line) and present formulation (red star line) at discrete frequencies

computationally efficient than the WFEM MCS, which can turn to great advantages for complicated geometries of periodic structures.

4.6 Conclusions

This chapter presents a computationally inexpensive stochastic spectral approach to study the effects of uncertainties in 1D and 2D periodic media. In 1D cases, the proposed formulation is applied to a periodic rod and metamaterial rod at frequencies up to 2000 Hz. The results are compared with SWFEM TM, WFEM MCS, and analytical solutions. It shows an excellent agreement and a substantial reduction in computation cost. The effect of uncertain parameters on the longitudinal wavenumber dispersion is investigated considering stochasticity indicator and COV study. The effect on variation of longitudinal wavenumber is higher with elastic stochasticity than with stochastic density. It is noteworthy, that in the metamaterial system, the developed formulation can handle a higher level of uncertainties. In 2D cases, the formulation is applied to a homogeneous plate up

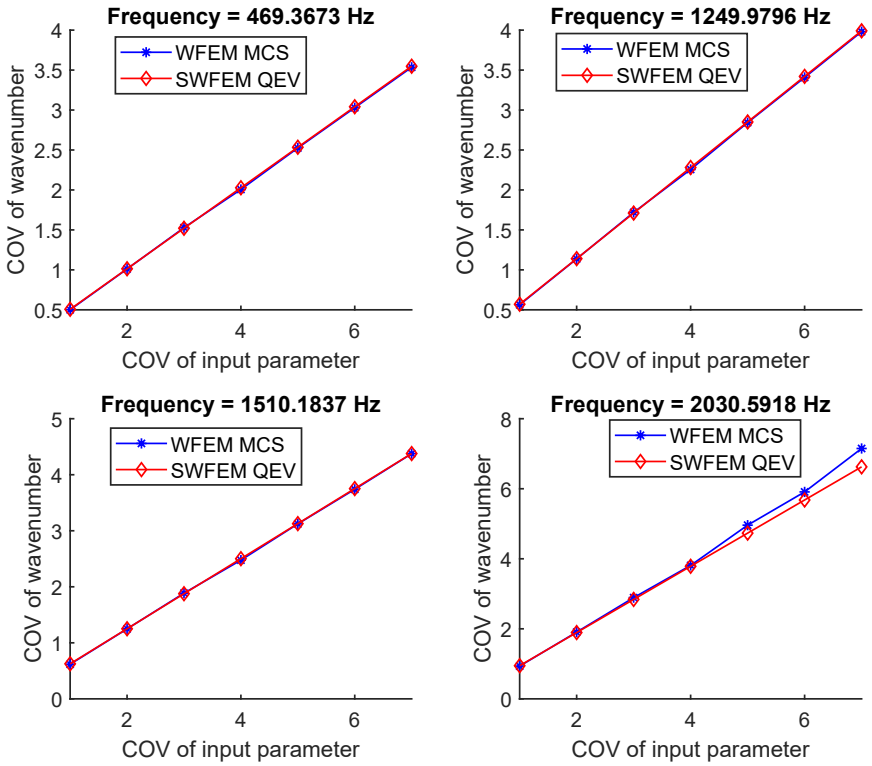

Figure 4.29: Variation of the out-of-plane flexural wavenumber (density stochastic), MCS (blue star line) and present formulation (red diamond line) at discrete frequencies

to 10,000 Hz and a periodic plate up to 3000 Hz. In the homogenous plate case, it is found that variation of out-of-plane flexural wavenumber is slightly higher with uncertain elasticity than with uncertain density. For the periodic plate case, uncertainties affect the out-of-plane flexural wavenumber scattering, and the maximum value of the variation of flexural wavenumber occurs at the band gap edge frequency. The COV study highlights the linear variation of flexural wavenumber in the low-frequency region and shifts to higher variation with increasing frequency. The developed formulation offers huge cost savings in terms of computation cost. The computational cost savings are very interesting and can be a good point for optimisation, reliability studies and uncertainties of complex periodic structures. Also it can be applied for damage detection and sensitivity analysis. Furthermore, the formulation can be employed for layered media, laminated, fiber-reinforced and complicated cross-section geometries, for determining the variation of dispersion properties, wavemodes, and group and phase velocities.

Chapter 5

FWFEM for 1D and 2D periodic media

5.1 Introduction

The aim of a parametric approach is to propagate the uncertainty model through the dynamic equations to convert the description of the uncertain input variables into a description of the uncertain response variables. When information about the uncertainty variables is available, the probabilistic models are applicable. However, the application of probabilistic approach faces two difficulties: (i) when little information is available, how to describe uncertain inputs; and (ii) how to efficiently compute the uncertainty in the response. There are non-probabilistic models, that can be introduced for the uncertainty propagation to overcome the difficulties. Due to imprecision and non-availability of the information about the uncertain variable, uncertainty in the variable, they are being modelled as fuzzy variables. In this chapter, FWFEM is formulated for 1D and 2D periodic structures. In 1D case, FWFEM based on the state space formulation is presented for free and forced wave propogation. In 2D case, formulation for the Bloch analysis with fuzzy uncertainties is presented for the direct and inverse forms of WFEM. The validations are presented for the free and forced response in 1D and 2D cases. The developed formulation is applied to the free wave propagation and FRF computation of a periodic rod and periodic beam. The direct form of FWFEM is applied for free wave propagation for

the homogeneous plate and periodic plate cases; and the inverse form of FWFEM with a bi-material square plate. These numerical results are compared with WFEM MCS for the validation purpose. Furthermore, the effect of the varying uncertainty on the band gap is also presented. The elapsed time comparison is presented to determine the computation advantage of the developed FWFEM over the WFEM MCS.

5.1.1 Fuzzy arithmetic operations definitions

In this subsection, the preliminary requirements for the fuzzy method, i.e., fuzzy set theory, fuzzy number, and membership function, are introduced. The membership of a classical set (U) of object, is defined as u. Then the membership of a classical subset A from the universe (U) can be represented as a characteristic function μ_A with valuation set defined as $0, 1$; considering the validation set is characterized by a real interval $[0, 1]$, then set A is defined as the fuzzy set. The fuzzy set is represented as:

$$\mu_A(u) = \left\{ \begin{array}{ll} 1, & \text{if } u \in A \\ 0, & \text{if } u \notin A \end{array} \right\} \tag{5.1}$$

Considering the valuation set is characterized by a real interval $[0, 1]$, then the fuzzy set is considered as set A and characterized by a set of pairs as:

$$A = \{[u, \mu_A(u)], u \in U\} \quad 0 \leq \mu_A(u) \leq 1 \tag{5.2}$$

where $\mu_A(u)$ is the level of the membership u in fuzzy set $'A'$. The closer the value of $\mu_A(u)$ is to 1, more it is represented as u belonging to A.

A triangular membership function is shown in Fig. 5.1. One example of the case could be the representation of the sound pressure level inside an aircraft. Let $X = \{80, 83, 84, 86, 88, 90, 94\}$ be the possible sound pressure setting of the indicator (in dBA) in a commercial airplane. Then the fuzzy set A "comfortable sound pressure level for human activity in the plane" can be defined as:

$$A = (80, 0), (83, 0.8), (84, 0.7), (86, 0.5), (88, 0.4), (90, 0.2), (94, 0.1) \tag{5.3}$$

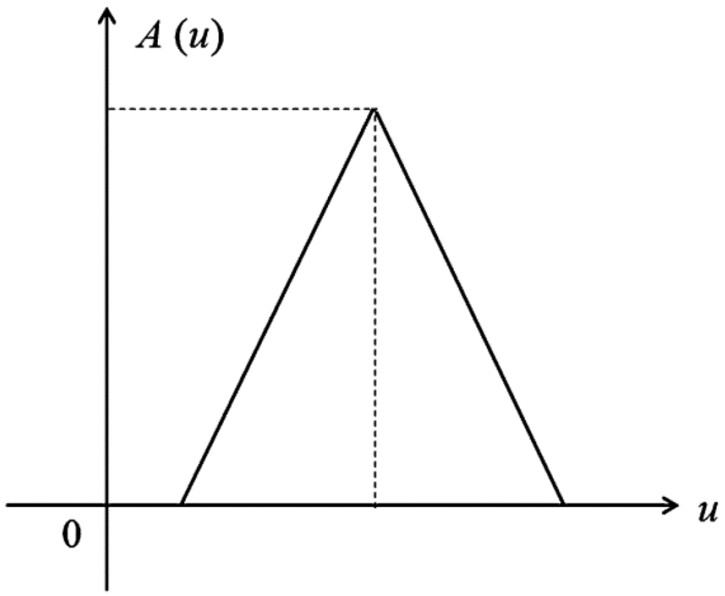

Figure 5.1: Triangular membership function

Where the level of the membership 0 implies complete discomfort, and 1 implies complete comfort. A is a subset of X with no sharp boundaries. Before moving to the formulation, the definition of the α-cut is detailed. In α-cut: An element belonging to a fuzzy set, is called the α-cut of a fuzzy set A, and is represented as A_α, which is a fuzzy set of crisp values $'U'$ moreover, it belongs to the original set of the membership level surpassing some threshold in α as $\alpha \in [0\ 1]$. The fuzzy arithmetic operations involved in deriving the mathematical expression and fuzzy arithmetic operation, namely fuzzy addition, fuzzy subtraction, fuzzy multiplication, and fuzzy division are performed. It is to be noted that the deterministic arithmetic operations are represented as $+, -, *, /$, and the fuzzy arithmetical operations as $(+), (-), (.), (/)$. In dealing with fuzzy sets A, and B the arithmetic operation are performed with the α-cut approach. The fuzzy arithmetic operation of the two fuzzy numbers A and B are as follows [Rao and Liu, 2004]:

Fuzzy addition (+):

$$A_\alpha(+)B_\alpha = [a_1^\alpha\ a_2^\alpha]\,(+)\,[b_1^\alpha\ b_2^\alpha] = [a_1^\alpha + b_1^\alpha\ a_2^\alpha + b_2^\alpha] \tag{5.4}$$

Fuzzy subtraction (-):

$$A_\alpha(-)B_\alpha = [a_1^\alpha \ a_2^\alpha]\,(-)\,[b_1^\alpha \ b_2^\alpha] = [a_1^\alpha - b_2^\alpha \ a_2^\alpha - b_1^\alpha] \tag{5.5}$$

Fuzzy multiplication (.):

$$\begin{aligned} A_\alpha(\cdot)B_\alpha &= [a_1^\alpha \ a_2^\alpha]\,(\cdot)\,[b_1^\alpha \ b_2^\alpha] \\ &= [\min\left(a_1^\alpha \cdot b_1^\alpha, a_1^\alpha \cdot b_2^\alpha, a_2^\alpha \cdot b_1^\alpha, a_2^\alpha \cdot b_2^\alpha\right) \\ &\quad \max\left(a_1^\alpha \cdot b_1^\alpha, a_1^\alpha \cdot b_2^\alpha, a_2^\alpha \cdot b_2^\alpha, a_2^\alpha \cdot b_2^\alpha\right)] \end{aligned} \tag{5.6}$$

Fuzzy division (/):

$$\begin{aligned} A_\alpha(/)B_\alpha &= [a_1^\alpha \ a_2^\alpha]\,(/)\,[b_1^\alpha \ b_2^\alpha] \\ &= \left[\min\left(\tfrac{a_1^\alpha}{b_1^\alpha}, \tfrac{a_1^\alpha}{b_2^\alpha}, \tfrac{a_2^\alpha}{b_1^\alpha}, \tfrac{a_2^\alpha}{b_2^\alpha}\right) \ \ \max\left(\tfrac{a_1^\alpha}{b_1^\alpha}, \tfrac{a_1^\alpha}{b_2^\alpha}, \tfrac{a_2^\alpha}{b_1^\alpha}, \tfrac{a_2^\alpha}{b_2^\alpha}\right)\right] \end{aligned} \tag{5.7}$$

where A_α and B_α are the interval of confidence of A and B for the considered level of membership function (α). The multiplication of a deterministic number $\kappa \in R^+$ with a fuzzy number $x_\alpha = [x_1^\alpha x_2^\alpha]$ can be expressed by

$$\kappa(\cdot)\,(x_\alpha) = [\kappa \ \kappa](\cdot)\,[x_1^\alpha \ x_2^\alpha] = [\kappa \cdot x_1^\alpha \ \kappa \cdot x_2^\alpha] \tag{5.8}$$

5.2 FWFEM formulation for free wave propagation in 1D periodic media

The fuzzy approach is used to formulate the FWFEM for the free wave propagation in the 1D periodic structure. The membership function are used to model the parametric fuzzy variables. In the 1D periodic structure shown in Fig 5.2, the nodes are located on the left boundary (L), right boundary (R), and remaining/internal nodes (I).

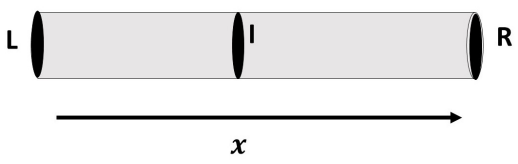

Figure 5.2: Unit cell of periodic structure

The displacement DOFs, q, are partitioned into left (q_L), internal (q_I), and right (q_R). Similarly, forces are partitioned into left (F_L), internal (F_I), and right (F_R). Periodic structures exhibit a considerable amount of scattering in material properties including Young's modulus, Poisson's ratio, and density caused by manufacturing processes and mechanical properties evaluations. As these uncertainties involve in various processes, the exact values of these properties and parameters are impossible to determine. Due to the imprecision and non-availability of the information about the uncertain variables, they are being modelled as fuzzy variables. If fuzziness is present in the material properties, the stiffness and mass matrix become fuzzy, which contributes to the fuzziness in the dynamic equation and leads to a fuzzy dispersion diagram and FRF. The realistic response is obtained by quantifying the uncertainties in terms of the bound of responses (lower and upper bounds) arising due to fuzziness in the design parameters.

In the fuzzy approach, the fuzzy parametric approach considers the uncertainties in the parameters (material, geometrical properties) as fuzzy parameters. The fuzzy variables are modelled using the membership function. Every term in the formulation denoted with subscript α is the fuzzy term, and it is linked with the membership level. The symbol () denotes the fuzzy arithmetic operation. The material properties are modelled as fuzzy variables. Due to uncertainties presents in the material parameters, the stiffness, and mass matrix becomes fuzzy that introduce fuzzy uncertainty in the dynamic matrix. The fuzzy complex dynamic stiffness matrix of the substructure $\boldsymbol{k}$, at the pulsation ω is:

$$D_\alpha = -\omega_\alpha^2 M_\alpha(+) K_\alpha(1 + i\eta) \tag{5.9}$$

where M_α is the fuzzy mass matrix, and K_α is the fuzzy stiffness matrix, η is the structural loss factor, i is the unit imaginary number, and ω_α is the fuzzy circular frequency. The fuzzy dynamical equilibrium of any substructure $\boldsymbol{k}$ is precisely formulated in this way without loss of generality [Rao and Liu, 2004], [Liu and Rao, 2005], [Pawar et al., 2012], [Patle et al., 2018] as:

$$\begin{bmatrix} D_{LL_\alpha} & D_{LI_\alpha} & D_{LR_\alpha} \\ D_{IL_\alpha} & D_{II_\alpha} & D_{IR_\alpha} \\ D_{RL_\alpha} & D_{RI_\alpha} & D_{RR_\alpha} \end{bmatrix} (.) \begin{pmatrix} q_{L_\alpha}^{(\boldsymbol{k})} \\ q_{I_\alpha}^{(\boldsymbol{k})} \\ q_{R_\alpha}^{(\boldsymbol{k})} \end{pmatrix} = \begin{pmatrix} F_{L_\alpha}^{(\boldsymbol{k})} \\ 0 \\ F_{R_\alpha}^{(\boldsymbol{k})} \end{pmatrix} \tag{5.10}$$

The dynamic condensation of the fuzzy dynamical equilibrium leads to:

$$\begin{bmatrix} D_{LL_\alpha}(-)D_{LI_\alpha}(.)D_{II_\alpha}^{-1}(.)D_{IL_\alpha} & D_{LR_\alpha}(-)D_{LI_\alpha}(.)D_{II_\alpha}^{-1}(.)D_{IR_\alpha} \\ D_{RL_\alpha}(-)D_{RI_\alpha}(.)D_{II_\alpha}^{-1}(.)D_{IL_\alpha} & D_{RR_\alpha}(-)D_{RI_\alpha}(.)D_{II_\alpha}^{-1}(.)D_{IR_\alpha} \end{bmatrix} (.) \begin{pmatrix} q_{L_\alpha}^{(\boldsymbol{k})} \\ q_{R_\alpha}^{(\boldsymbol{k})} \end{pmatrix} = \begin{pmatrix} F_{L_\alpha}^{(\boldsymbol{k})} \\ F_{R_\alpha}^{(\boldsymbol{k})} \end{pmatrix} \tag{5.11}$$

that is,

$$\begin{pmatrix} D_{LL_\alpha}^* & D_{LR_\alpha}^* \\ D_{RL_\alpha}^* & D_{RR_\alpha}^* \end{pmatrix} (.) \begin{pmatrix} q_{L_\alpha}^{\boldsymbol{k}} \\ q_{R_\alpha}^{\boldsymbol{k}} \end{pmatrix} = \begin{pmatrix} F_{L_\alpha}^{\boldsymbol{k}} \\ F_{R_\alpha}^{\boldsymbol{k}} \end{pmatrix} \tag{5.12}$$

In the above expression D_{LL_α}, D_{LR_α}, D_{RL_α}, and D_{RR_α} are the fuzzy quantities of the fuzzy dynamic operators, $q_{L_\alpha}^{\boldsymbol{k}}$, $q_{L_\alpha}^{\boldsymbol{k}}$ are the fuzzy displacement vectors and $F_{L_\alpha}^{\boldsymbol{k}}$, $F_{R_\alpha}^{\boldsymbol{k}}$ are the fuzzy load vectors. The fuzzy kinematic variables, q_α, and F_α are represented through fuzzy state vectors, $u_{L_\alpha}^{\boldsymbol{k}} = \left((q_{L_\alpha}^{\boldsymbol{k}})^T \ (-F_{L_\alpha}^{\boldsymbol{k}})^T\right)^T$ and $u_{R_\alpha}^{\boldsymbol{k}} = \left((q_{R_\alpha}^{\boldsymbol{k}})^T \ (F_{R_\alpha}^{\boldsymbol{k}})^T\right)^T$; and related by the fuzzy transfer matrix S_α as:

$$u_{R_\alpha}^{\boldsymbol{k}} = \begin{pmatrix} -{D_{LR_\alpha}^*}^{-1}(.)D_{LL_\alpha}^* & -{D_{LR_\alpha}^*}^{-1} \\ D_{RL_\alpha}^*(-)D_{RR_\alpha}^*(.){D_{LR_\alpha}^*}^{-1}(.)D_{LL_\alpha}^* & -D_{RR_\alpha}^*(.){D_{LR_\alpha}^*}^{-1} \end{pmatrix} (.) u_{L_\alpha}^{\boldsymbol{k}}$$

$$u_{R_\alpha}^{\boldsymbol{k}} = S_\alpha(.)u_{L_\alpha}^{\boldsymbol{k}} \tag{5.13}$$

where

$$S_\alpha = \begin{pmatrix} -{D_{LR_\alpha}^*}^{-1}(.)D_{LL_\alpha}^* & -{D_{LR_\alpha}^*}^{-1} \\ D_{RL_\alpha}^*(-)D_{RR_\alpha}^*(.){D_{LR_\alpha}^*}^{-1}(.)D_{LL_\alpha}^* & -D_{RR_\alpha}^*(.){D_{LR_\alpha}^*}^{-1} \end{pmatrix} \tag{5.14}$$

is the fuzzy transfer matrix.

The structural parameters namely, stiffness and mass matrices are fuzzy, thus, a fuzzy eigenvalue problem [Massa et al., 2008], [Xia and Friswell, 2014],[Zhang et al., 2015] formulated as:

$$\begin{aligned} S_\alpha(.)\phi_{i\alpha} &= \mu_{i\alpha}(.)\phi_{i\alpha} \\ |S_\alpha - \mu_{i\alpha}(.)I_{2n}| &= 0 \end{aligned} \tag{5.15}$$

where $(\mu_{i\alpha}, \phi_{i\alpha})_{i=1\ldots2n}$ are the fuzzy wave modes and n is the number of cross sectional DOFs. The solution of the fuzzy eigenvalue problem in Eq. (5.15) can be obtained several ways [Faes and Moens, 2019]. One to solve the fuzzy eigenvalues problem is by converting the fuzzy eigenvalue problem into the interval eigenvalue problem for all levels of the α-cut [Faes and Moens, 2019], [Xu et al., 2014]. Once the fuzzy eigenvalue problem is solved, the

resulting fuzzy eigenvalues ($\mu_{i\alpha}$) are directly related to the fuzzy wavenumber k_α through the relation:

$$\mu_{i\alpha} = \exp(-j(.)k_\alpha(.)d) \tag{5.16}$$

where d is the unit cell length and $j^2 = -1$. Then, the fuzzy wavenumber is expressed as:

$$k_\alpha = \left(\frac{j}{d}\right)(.)\log(\mu_{i\alpha}) \tag{5.17}$$

Furthermore, the fuzzy eigenvector matrix Φ_α can be written as:

$$\Phi_\alpha = \begin{bmatrix} \Phi^{inc}_{q_\alpha} & \Phi^{ref}_{q_\alpha} \\ \Phi^{inc}_{F_\alpha} & \Phi^{ref}_{F_\alpha} \end{bmatrix} \tag{5.18}$$

where subscripts q_α and F_α indicate that the component corresponds to the fuzzy displacements and fuzzy forces. The terms are denoted (inc) for the incident waves and (ref) for the reflected waves.

5.3 FWFEM formulation for forced response in 1D periodic media

The real structures are not infinite but have finite dimensions. Here, a formulation for the harmonic response with fuzzy uncertainties is presented. The periodic waveguide is composed of N identical substructure $\boldsymbol{k}$ and belonging to the global system. The material parameters are considered to have fuzzy uncertainties. The fuzzy kinematic variables for every cell, q_α, and F_α are expressed using state-space formulation, as fuzzy state vectors:

$$u^{\boldsymbol{k}}_{L_\alpha} = \left((q^{\boldsymbol{k}}_{L_\alpha})^T\ (-F^{\boldsymbol{k}}_{L_\alpha})^T\right)^T ; u^{\boldsymbol{k}}_{R_\alpha} = \left((q^{\boldsymbol{k}}_{R_\alpha})^T\ (F^{\boldsymbol{k}}_{R_\alpha})^T\right)^T \tag{5.19}$$

where T denotes the transpose. Using the multi-mode method [Mencik and Ichchou, 2005], the fuzzy kinematic variable can be projected on the fuzzy wave mode bases as follows:

$$\begin{aligned} u^{(\boldsymbol{k})}_{L_\alpha} &= \Phi_\alpha(.)Q^{(\boldsymbol{k})}_\alpha \\ u^{(\boldsymbol{k})}_{R_\alpha} &= \Phi_\alpha(.)Q^{(\boldsymbol{k}+1)}_\alpha \quad \forall \quad \boldsymbol{k} \in \{1 \dots N\} \end{aligned} \tag{5.20}$$

where Φ_α is the matrix of the fuzzy eigenvectors as expressed in Eq. (5.18), that are independent. In addition, the vector of the fuzzy wave mode amplitude for substructure $\boldsymbol{k}$ is expressed as:

$$Q_\alpha = \begin{pmatrix} {Q_\alpha}^{inc} \\ {Q_\alpha}^{ref} \end{pmatrix}^{(\boldsymbol{k})} \tag{5.21}$$

where Q_α^{inc} is the fuzzy amplitude of the incident mode and Q_α^{ref} is that of the reflected mode. Applying the Bloch's theorem, the fuzzy amplitude of the $\boldsymbol{k}$th substructure in the waveguide can be obtained from the fuzzy amplitude of the wave of the first element by relation:

$$Q_\alpha^{(\boldsymbol{k})} = \begin{pmatrix} \mu_\alpha^{inc} & 0 \\ 0 & \mu_\alpha^{ref} \end{pmatrix}^{(\boldsymbol{k}-1)} (.) Q_\alpha^{(1)} \tag{5.22}$$

Considering that the periodic structure is free-fixed, and excited with a sinusoidal forces, the boundary conditions are as follows:

Boundary condition at $x = 0$:

$$\Phi_{F_\alpha}^{inc}(.){Q_\alpha}^{inc(1)}(+)\Phi_{F_\alpha}^{ref}(.){Q_\alpha}^{ref(1)} = -F_{L_\alpha}^{(1)} \tag{5.23}$$

Boundary condition at $x = L$:

$$\Phi_{q_\alpha}^{inc}(.){Q_\alpha}^{inc(N+1)}(+)\Phi_{q_\alpha}^{ref}(.){Q_\alpha}^{ref(N+1)} = q_{R_\alpha}^{(N)} \tag{5.24}$$

Using the relation in Eq. (5.22), the second boundary condition is transformed to:

$$\Phi_{q_\alpha}^{inc}(.){\mu_\alpha}^{N}(.){Q_\alpha}^{inc(1)}(+)\Phi_{q_\alpha}^{ref}(.){\mu_\alpha}^{-N}(.){Q_\alpha}^{ref(1)} = q_{R_\alpha}^{(N)} \tag{5.25}$$

The boundary condition expressed in Eq. (5.23) and Eq. (5.25) is, written in the matrix form as:

$$\begin{pmatrix} \Phi_{F_\alpha}^{inc} & \Phi_{F_\alpha}^{ref} \\ \Phi_{q_\alpha}^{inc}(.){\mu_\alpha}^{(inc)N} & \Phi_{q_\alpha}^{ref}(.){\mu_\alpha}^{(ref)-N} \end{pmatrix} (.) \begin{pmatrix} {Q_\alpha}^{inc(1)} \\ {Q_\alpha}^{ref(1)} \end{pmatrix} = \begin{pmatrix} -F_\alpha \\ q_\alpha \end{pmatrix} \tag{5.26}$$

The above matrix is not well conditioned, and so an appropriate scaling in required. This is performed by decoupling the ill-conditioned matrix into two matrices, one matrix with

better conditioned and the second with diagonal, expressed as:

$$\begin{pmatrix} \Phi_{F_\alpha}^{inc} & \Phi_{F_\alpha}^{ref} \\ \Phi_{q_\alpha}^{inc}(.){\mu_\alpha}^{(inc)N} & \Phi_{q_\alpha}^{ref}(.){\mu_\alpha}^{(ref)-N} \end{pmatrix} (.) \begin{pmatrix} I_n & 0 \\ 0 & \overline{\mu}^{(inc)N} \end{pmatrix} (.) \begin{pmatrix} {Q_\alpha}^{inc(1)} \\ {Q_\alpha}^{ref(1)} \end{pmatrix} = \begin{pmatrix} -F_\alpha \\ q_\alpha \end{pmatrix} \tag{5.27}$$

Then, the fuzzy wave amplitude can be calculated as:

$$\begin{pmatrix} {Q_\alpha}^{inc(1)} \\ {Q_\alpha}^{ref(1)} \end{pmatrix} = \begin{pmatrix} I_n & 0 \\ 0 & {\mu_\alpha}^{(inc)N} \end{pmatrix} (.) \begin{pmatrix} \Phi_{F_\alpha}^{inc} & \Phi_{F_\alpha}^{ref}(.){\mu_\alpha}^{N} \\ \Phi_{q_\alpha}^{inc}(.){\mu_\alpha}^{N} & \Phi_{q_\alpha}^{ref} \end{pmatrix}^{+} (.) \begin{pmatrix} -F_\alpha \\ q_\alpha \end{pmatrix} \tag{5.28}$$

Thus, the fuzzy amplitude of the wave at the $\boldsymbol{k}$th substructure can be obtained by Eq. (5.28) and Eq.(5.22).

The fuzzy kinematic variables (displacements and forces) are derived from the equation connecting the fuzzy state vectors to the fuzzy amplitude of the modes. The fuzzy nodal displacement for the sub-element $\boldsymbol{k}$ is expressed as:

$$q_\alpha^{(\boldsymbol{k})} = \begin{pmatrix} \Phi_{q_\alpha}^{inc} & \Phi_{q_\alpha}^{ref} \\ \Phi_{q_\alpha}^{inc}(.){\mu_\alpha}^{inc} & \Phi_{q_\alpha}^{ref}(.){\mu_\alpha}^{ref} \end{pmatrix} (.)(Q_\alpha)^{(\boldsymbol{k})} \tag{5.29}$$

Similar way, the fuzzy nodal forces for the sub-element $\boldsymbol{k}$ are expressed as:

$$F_\alpha^{(\boldsymbol{k})} = \begin{pmatrix} \Phi_{F_\alpha}^{inc} & \Phi_{F_\alpha}^{ref} \\ \Phi_{F_\alpha}^{inc}{\mu_\alpha}^{inc} & \Phi_{F_\alpha}^{ref}{\mu_\alpha}^{ref} \end{pmatrix} (.)(Q_\alpha)^{(\boldsymbol{k})} \tag{5.30}$$

Eq. (5.29) and Eq. (5.30) are used to find the nodal fuzzy displacements and nodal fuzzy forces on both sides of the substructure $\boldsymbol{k}$ of the global system.

5.4 FWFEM formulation for 2D periodic media

The approach followed here is to first, build a finite element model of the unit cell; that will then be used to define a fuzzy dynamic equation that leads to a fuzzy eigenvalue problem. By solving the fuzzy eigenvalue problem, the wave characteristics are determined, and their fuzzy bounds of variation are predicted.

Consider an infinite thin plate lying in the (x, y) plane with a unit cell as shown in Fig. 5.3. The unit cell is divided into five nodes. The nodes are located on the left corner (1), right

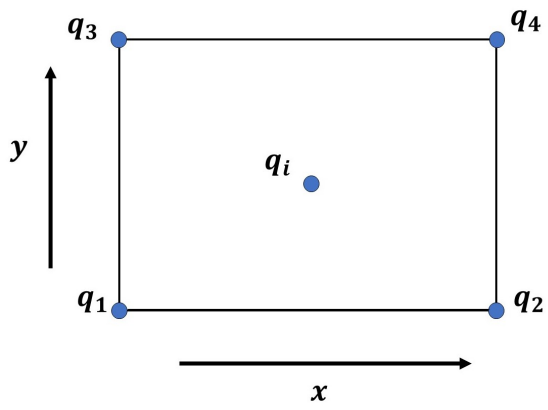

Figure 5.3: Rectangular plate element

corner (2), top left corner (3), and top left right (4), and remaining/internal nodes (i). The unit cell DOFs (q) are divided into four corner nodal DOFs, q_1, q_2, q_3, q_4 and internal node DOFs as q_i.

The vector of nodal DOFs are given by $q = \left[q_1^T, q_2^T, q_3^T, q_4^T, q_i^T\right]^T$. Similarly, the vector of nodal forces are given by $f = \left[f_1^T, f_2^T, f_3^T, f_4^T, f_i^T\right]^T$. where T denotes the transpose. The stiffness and mass matrix are calculated using analytical expression or by using a commercial FE program. If fuzziness is present in the material properties, which contribute to the fuzziness in the stiffness and mass matrix, then fuzzy uncertainty is introduced into the dynamic matrix. Then, the global fuzzy dynamic equilibrium [Rao and Liu, 2004],[Liu and Rao, 2005] of a substructure represented as the time-harmonic equation of motion can be written as:

$$\left(K_\alpha(-)\omega_\alpha^2(.)M_\alpha\right)(.)q_\alpha = f_\alpha \tag{5.31}$$

where K_α is the fuzzy stiffness matrix, M_α is the fuzzy mass matrx, ω_α is the fuzzy circular frequency, f_α is the fuzzy nodal forces vector, and q_α is the fuzzy nodal displacements vector. Eq. (5.31) is used to form the fuzzy spectral problem involving wavenumber in x-direction k_x, wavenumber in y-direction k_y and frequency ω. The fuzzy dynamic stiffness matrix can be expressed as $D_\alpha = K_\alpha(-)\omega_\alpha^2(.)M_\alpha$.

Introducing the periodic structure theory for the unit cell and considering a time-harmonic

response [Mace and Manconi, 2008] the fuzzy harmonic equation of motion can be formulated as:

$$\left(K_\alpha{}^*\left(\lambda_{x_\alpha},\lambda_{y_\alpha}\right)(-)\omega_\alpha^2(.)M_\alpha^*\left(\lambda_{x_\alpha},\lambda_{y_\alpha}\right)\right)(.)q_{1_\alpha}=0 \tag{5.32}$$

where $K_\alpha{}^* = \Lambda_{L_\alpha}(.)K_\alpha(.)\Lambda_{R_\alpha}$ and $M_\alpha{}^* = \Lambda_{L_\alpha}(.)M_\alpha(.)\Lambda_{R_\alpha}$ are the fuzzy reduced stiffness and mass matrices, respectively, and ω_α is the fuzzy circular frequency. λ_{x_α} and λ_{y_α} are the fuzzy propagation constants in x- and y-directions respectively. Λ_{L_α} and Λ_{R_α} are matrices containing the fuzzy propagation constants from the periodicity conditions as:

$$\begin{aligned}\Lambda_{L_\alpha} &= \begin{bmatrix} I & \lambda_{x_\alpha}^{-1}(.)I & \lambda_{y_\alpha}^{-1}(.)I & \lambda_{x_\alpha}^{-1}(.)\lambda_{y_\alpha}^{-1}(.)I \end{bmatrix} \\ \Lambda_{R_\alpha} &= \begin{Bmatrix} I \\ \lambda_{x_\alpha}(.)I \\ \lambda_{y_\alpha}(.)I \\ \lambda_{x_\alpha}(.)\lambda_{y_\alpha}(.)I \end{Bmatrix}\end{aligned} \tag{5.33}$$

where I is the identity matrix. The fuzzy eigenvalue problem of Eq. (5.32) can be expressed as:

$$D_\alpha{}^*\left(\omega_\alpha,\lambda_{x_\alpha},\lambda_{y_\alpha}\right)(.)q_{1_\alpha}=0 \tag{5.34}$$

where $D_\alpha{}^*\left(\omega_\alpha,\lambda_{x_\alpha},\lambda_{y_\alpha}\right)$ is the fuzzy reduced dynamic stiffness matrix. For the sake of clarity, the fuzzy reduced dynamic stiffness matrix is now represented as D_α. If the reduced dynamic stiffness matrix is partitioned as:

$$D_\alpha = \begin{bmatrix} D_{11_\alpha} & D_{12_\alpha} & D_{13_\alpha} & D_{14_\alpha} \\ D_{21_\alpha} & D_{22_\alpha} & D_{23_\alpha} & D_{24_\alpha} \\ D_{31_\alpha} & D_{32_\alpha} & D_{33_\alpha} & D_{34_\alpha} \\ D_{41_\alpha} & D_{42_\alpha} & D_{43_\alpha} & D_{44_\alpha} \end{bmatrix} \tag{5.35}$$

The fuzzy eigenvalue problem in Eq. (5.32) and Eq. (5.34) involving three parameters, $\lambda_{x_\alpha}, \lambda_{y_\alpha}$ and ω_α. Depending on the nature of the solution sought, the fuzzy eigenproblem takes various forms.

5.4.1 FWFEM 2D: Direct form

Consider that the frequency ω and one wavenumber is known; in this case the fuzzyeigenvalue problem in Eq. (5.34) can be written in the following form:

$$\begin{aligned}\big[&(D_{11_\alpha}(+)D_{22_\alpha}(+)D_{33_\alpha}(+)D_{44_\alpha})(+)(D_{12_\alpha}(+)D_{34_\alpha})(.)\lambda_{x_\alpha}(+)(D_{21_\alpha}(+)D_{43_\alpha})(.)\lambda_{x_\alpha}^{-1}\\ &(+)(D_{13_\alpha}(+)D_{24_\alpha})(.)\lambda_{y_\alpha}(+)(D_{31_\alpha}(+)D_{42_\alpha})(.)\lambda_{y_\alpha}^{-1}(+)D_{14_\alpha}(.)\lambda_{x_\alpha}(.)\lambda_{y_\alpha}\\ &(+)D_{41_\alpha}(.)\lambda_{x_\alpha}^{-1}(.)\lambda_{y_\alpha}^{-1}(+)D_{32_\alpha}(.)\lambda_{x_\alpha}(.)\lambda_{y_\alpha}^{-1}(+)D_{23_\alpha}(.)\lambda_{x_\alpha}^{-1}(.)\lambda_{y_\alpha})\big]\,(.)q_{1_\alpha}=0\end{aligned} \quad (5.36)$$

Then, the fuzzy nonlinear Eq. (5.36) can be reduced to fuzzy quadratic eigenproblem in λ_{x_α} form when λ_{x_α} is unknown and $(\omega_\alpha, \lambda_{y_\alpha})$ are given, as:

$$\begin{aligned}\big[&(D_{21_\alpha}(+)D_{43_\alpha}(+)D_{41_\alpha}(.)\lambda_{y_\alpha}^{-1}(+)D_{23_\alpha}(.)\lambda_{y_\alpha})(+)\mu_{i_\alpha}(.)(D_{11_\alpha}(+)D_{22_\alpha}(+)D_{33_\alpha}(+)D_{44_\alpha}\\ &(+)(D_{31_\alpha}(+)D_{42_\alpha})(.)\lambda_{y_\alpha}^{-1}(+)(D_{13_\alpha}(+)D_{24_\alpha})(.)\lambda_{y_\alpha})\mu_{i_\alpha}^2(.)(D_{12_\alpha}(+)D_{34_\alpha}(+)D_{32_\alpha}(.)\lambda_{y_\alpha}^{-1}\\ &(+)D_{14_\alpha}(.)\lambda_{y_\alpha})\big](.)\,(\Phi_{q_\alpha})_i=0\end{aligned} \quad (5.37)$$

The fuzzy quadratic eigenproblem is solved and eigenvalues representing the wavenumber propagating along the x-, and y-directions are complex values. The propagating wavenumber in the x-direction (k_{x_α}) and y-direction (k_{y_α}) are calculated using following relation:

$$\begin{aligned}k_{x_\alpha}&=\left(\frac{j}{d_x}\right)(.)\log(\mu_{i\alpha})\\ k_{y_\alpha}&=\left(\frac{j}{d_y}\right)(.)\log(\mu_{i\alpha})\end{aligned} \quad (5.38)$$

where d_x is the unit cell length in the x-direction, d_y is the unit cell length in the y-direction and j^2=-1.

5.4.2 FWFEM 2D: Inverse form

The second case is called the inverse forms, for which the wavenumber in the x-direction, k_x, and in the y-direction, k_y, are known, and corresponding frequencies of free wave propagation are to be sought. In the inverse form, the dynamic condensation cannot be performed and internal nodes are conserved. Thus, the Λ_{L_α} and Λ_{R_α} are matrices

containing the propagation constants from the periodicity conditions that are modified to form:

$$\Lambda'_{R_\alpha} = \begin{pmatrix} \Lambda_{\alpha R} & 0 \\ 0 & I_i \end{pmatrix} \tag{5.39}$$

$$\Lambda'_{L_\alpha} = \begin{pmatrix} \Lambda_{L_\alpha} & 0 \\ 0 & I_i \end{pmatrix} \tag{5.40}$$

where I_i is the identity matrix of size i. Then fuzzy harmonic equation of motion becomes:

$$\Lambda'_{L_\alpha}(.)\left(K_\alpha(-)\omega_\alpha^2(.)M_\alpha\right)(.)\Lambda'_{R_\alpha}(.)\begin{pmatrix} q_{1_\alpha} \\ q_{I_\alpha} \end{pmatrix} = 0 \tag{5.41}$$

where q_{I_α} are the conserved internal degree of freedom. Which become fuzzy linear algerbric problem in ω_α^2, as:

$$\left[{K_\alpha}'(\lambda_{x_\alpha}, \lambda_{y_\alpha})(-)\omega_\alpha^2(.){M_\alpha}'(\lambda_{x_\alpha}, \lambda_{y_\alpha})\right](.)\begin{pmatrix} q_{1_\alpha} \\ q_{I_\alpha} \end{pmatrix} = 0 \tag{5.42}$$

In the undamped structure, K_α and M_α are real positive definite Hermitian matrices. Thereby the K'_α and M'_α with $|\lambda_{x_\alpha}| = 1$ and $|\lambda_{y_\alpha}| = 1$. The fuzzy eigenvalue problem leads to the solution $(\omega_\alpha^2, \phi_\alpha)$ with fuzzy eigenvalues for which free wave propagation is possible, ω_α^2, that are real and positive, and the fuzzy eigenvectors, ϕ_α, that are orthogonal.

The representations of result: band structure

In a 2D periodic structure, the behavior is described with the help of the propagation constants μ_x, and μ_y and linked to the wavenumbers k_x and k_y through relations [Ruzzene and Tsopelas, 2003], [Mace and Manconi, 2008] :

$$\lambda_x = e^{\mu_x}, \lambda_y = e^{\mu_y}, \mu_x = -ik_xL_x, \mu_y = -ik_yL_y \tag{5.43}$$

where L_x, L_y are the size of unit cells in the x- and y-directions, respectively.

The relation in Eq. (5.43) can be translated for the fuzzy description of the parameter

with the help of fuzzy set theory [DuBois and Prade, 1980] as:

$$\lambda_{x_\alpha} = e^{\mu_{x\alpha}}, \lambda_{y_\alpha} = e^{\mu_{y\alpha}}, \mu_{x_\alpha} = -ik_{x_\alpha}(.)L_x, \mu_{y_\alpha} = -ik_{y_\alpha}(.)L_y \tag{5.44}$$

The eigen solutions of ω in Eq.(5.42) can be expressed in various ways through different coordinate systems [Ruzzene and Tsopelas, 2003],[Hussein, 2009]. The numerical experiments results in this thesis are presented in the coordinate system $(k_{x_\alpha}, k_{y_\alpha})$, which is termed as fuzzy slowness surface.

When damping is not considered and only free propagative waves are studied, the wavenumber $(k_{x\alpha}, k_{y_\alpha})$ are real values and vary in the first Brillouin zone $[(-\pi/L_x, \pi/L_x), (-\pi/L_y, \pi/L_y)]$ [Brillouin, 1946]. When x and y are symmetric axes of the structure, the symmetric nature of the slowness surfaces are realized with respect to the $k_{x_\alpha} = 0$ and $k_{y_\alpha} = 0$ axes. The symmetric property can be exploited to limit the variation of the wavenumbers to the IBZ. In the IBZ, k_{x_α} and k_{y_α} are positive. A 2D representation of the slowness surface is the "band structure". The band structure is obtained by varying the wavenumbers along the contour of the IBZ (O-A-B-O) as shown in Fig. 5.4

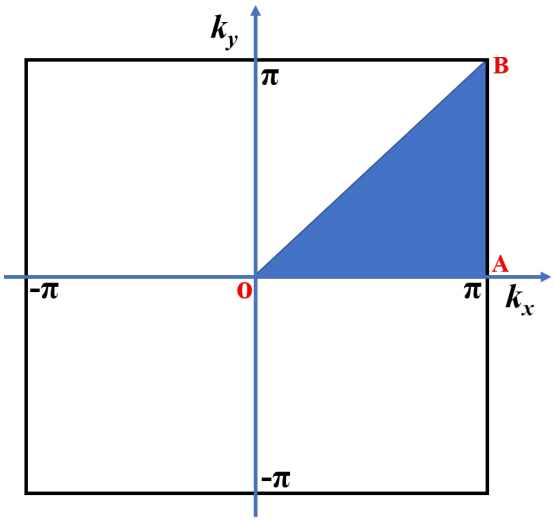

Figure 5.4: The IBZ within a unit cell showing the wave vector path $(O - A - B - O)$

5.5 Numerical results

The fuzzy uncertainties are propogated by various methods in the literature, with one common implementation being using the α-cut level [Moens and Hanss, 2011] strategy. In the α-cut method, the fuzzy parameter that is being modelled by fuzzy membership function, is divided into a number of α-cut levels. The output response in terms of fuzzy output for a specific membership level is found for the particular α-cut, by searching the input level by performing interval analysis in each α-cut. The response variable is finally assembled from results obtained from the α-level interval. The proposed numerical scheme is summarized in the workflow in Fig. 5.5. This section shows the validation of

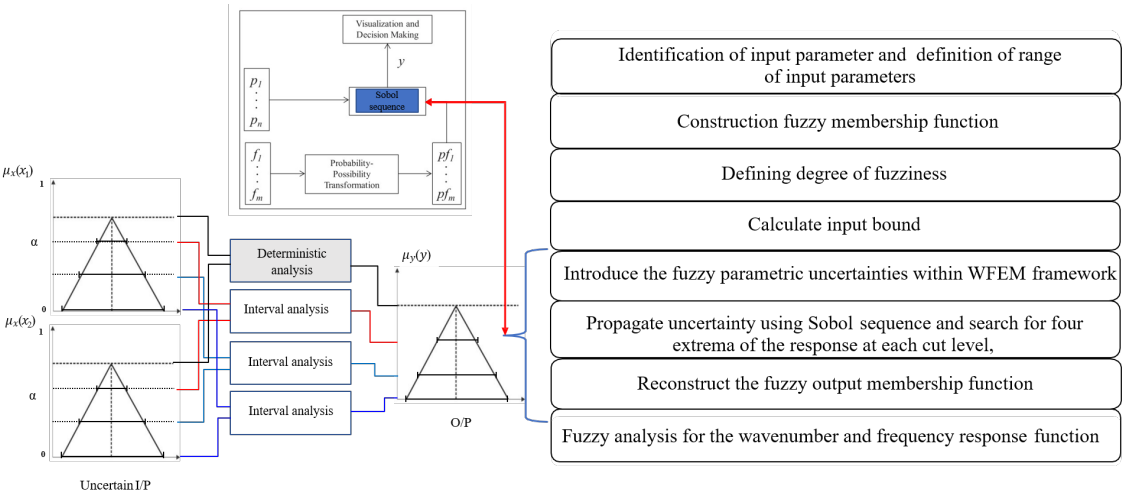

Figure 5.5: FWFEM workflow

the FWFEM formulation presented in the previous section. The analysis is performed for periodic rod and periodic beam cases. The periodic rod and beam consist of a section A of length l_1 and section B of length l_2 with different constituent materials, as depicted in Fig 5.6. Firstly, longitudinal waves studied for the band gap and FRF; then, the flexural waves in the beam are studied.

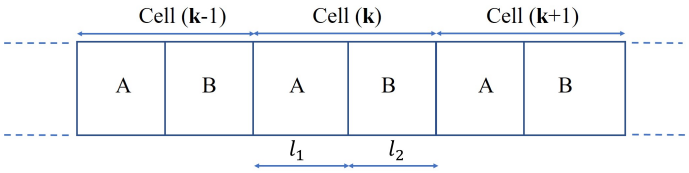

Figure 5.6: Schematic representation of 1D periodic media

5.5.1 Periodic rod

The FWFEM is used to study the effect of fuzzy parametric uncertainty on the band gap and FRF of a longitudinal wave in the periodic rod. To validate FWFEM results, a comparison is made between the result from the proposed FWFEM upper and lower bounds, and those obtained from MCS. The uncertainty effect is studied considering fuzzy uncertain material properties modeled with triangular fuzzy membership function with lower and upper variation fixed at (10%) of the nominal value. The considered frequency range is 10- 5500 Hz. The MCS is performed to obtain the reference wave characteristics of the lower and upper bounds of longitudinal wavenumber and FRF.

Two-node rod elements with one DOF per node are considered. The global stiffness and mass matrices are formed with 100 elements in the unit cell of the periodic rod in the MATLAB environment. The input material and geometrical properties are shown in Table 5.1. The value of fuzzy Young's modulus of section A (material 1) and section B

Table 5.1: Geometrical and material properties of the periodic rod

Geometry/Property	Value
Young's modulus (A)	70×10^9 Pa
Young's modulus (B)	210×10^9 Pa
Mass density (A)	2700 kg/m^3
Mass density (B)	7800 kg/m^3
Loss factor (A) and (B)	0.001
Rod length (A)	1 m
Rod length (B)	1 m
Radius of rod (A) and (B)	0.0644 m

(material 2) are modelled using the triangular membership function, as shown in Fig. 5.7. The FWFEM result at α-cut=0 (largest interval) in terms of upper and lower bounds of the wavenumber is compared with MCS upper and lower bound. The comparison results are presented in Fig. 5.8, and show excellent agreement. The band gap envelops are extracted from the fuzzy elasticity in the 11 α-cut levels and shown in Fig. 5.9. It can be seen that the effect of input uncertainty on the bandgap bounds is increasing with increasing frequency, as the upper and lower bound width is clearly increasing. The variation bound of the longitudinal wavenumber obtained with fuzzy elasticity at α-cut=0 at the discrete frequencies are shown in Fig. 5.10. It can be inferred that the response membership function is not always symmetric about the mean/crisp value. It is observed

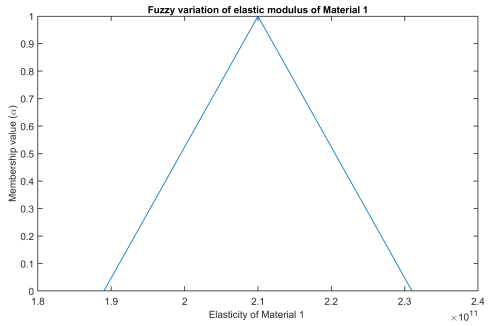

(a) Fuzzy membership function for material 1

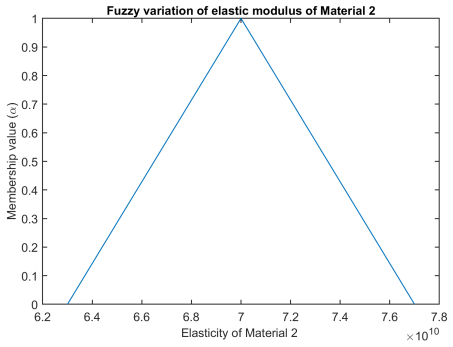

(b) Fuzzy membership function for material 2

Figure 5.7: Input fuzzy membership with 10% uncertainty, The units are (Pa)

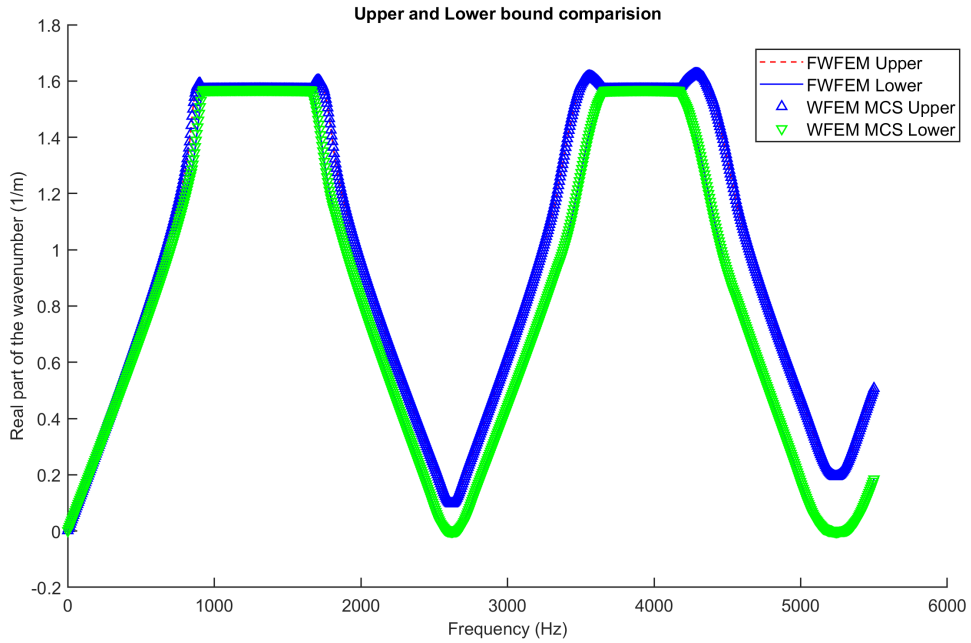

Figure 5.8: Longitudinal wavenumber comparison (fuzzy Young's moduls)

that in the propagation region, the variation of the longitudinal wavenumber is linear. However, near the band gap edge frequency it is non-symmetric. Therefore, the upper bound of longitudinal wavenumber is more sensitive to the uncertain elasticity. The FRF of a periodic rod of the finite extent of 20 m is excited by unit harmonic force. The FRF of the magnitude of the longitudinal displacement at the excitation point, is computed at 5490 discrete frequencies uniformaly spread over 10-5500 Hz. In this case, the Young's modulus is stochastic with 10% variation about the nominal value. In Fig. 5.11, the FWFEM for the bounded case is compared with WFEM MCS, indicating the upper and lower bound comparison at α-cut=0 (maximum bound) are in good agreement. To demonstrate the

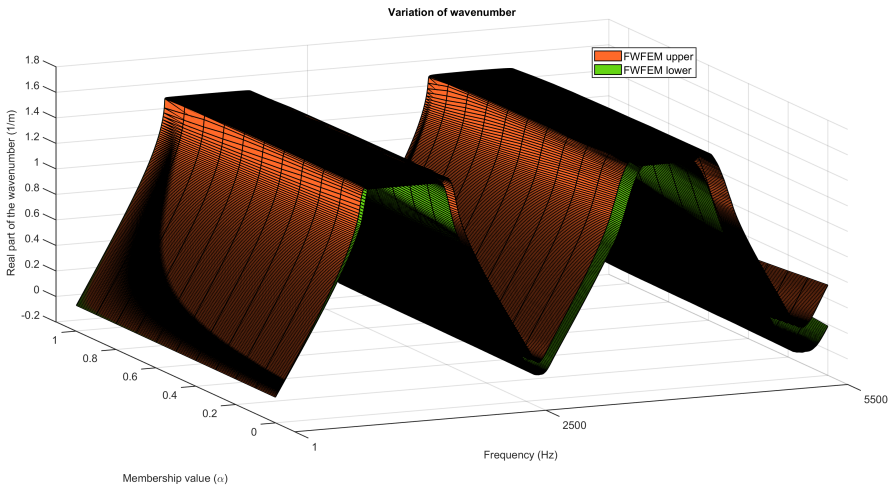

Figure 5.9: Fuzzy bounds of the periodic rod with 10% uncertainty

effect of fuzzy variation on the fuzzy FRF bound, at different membership values, the results are plotted in Fig. 5.12, Fig. 5.13, and Fig. 5.14. It can be seen in Fig. 5.12 that as the value of α-cut increases, the fuzzy bound of FRF decreases, and finally at α=1, without any simulation bound as expected, α=1.

5.5.2 Periodic beam

Here, the validation of the FWFEM is presented for the periodic beam case, by studying the fuzzy uncertainty effect on the flexural wave in the periodic beam. For numerical simulation, the Euler-Bernoulli beam theory is considered. The input material and geometric properties are shown in Table 5.2. A two-node beam element with two DOFs

Table 5.2: Geometrical and material properties for the periodic beam

Geometry/Property	Value
Young's modulus (A)	210 $\times 10^9$ Pa
Young's modulus (B)	0.72 $\times 10^9$ Pa
Mass density (A)	7800 kg/m^3
Mass density (B)	935 kg/m^3
Loss factor (A) and (B)	0.01
Beam length (A)	0.25 m
Beam length (B)	0.25 m
Height of beam (A) and (B)	0.003 m
Width of beam (A) and (B)	0.003 m

per node is considered. The global matrices (stiffness and mass) in the unit cell of the

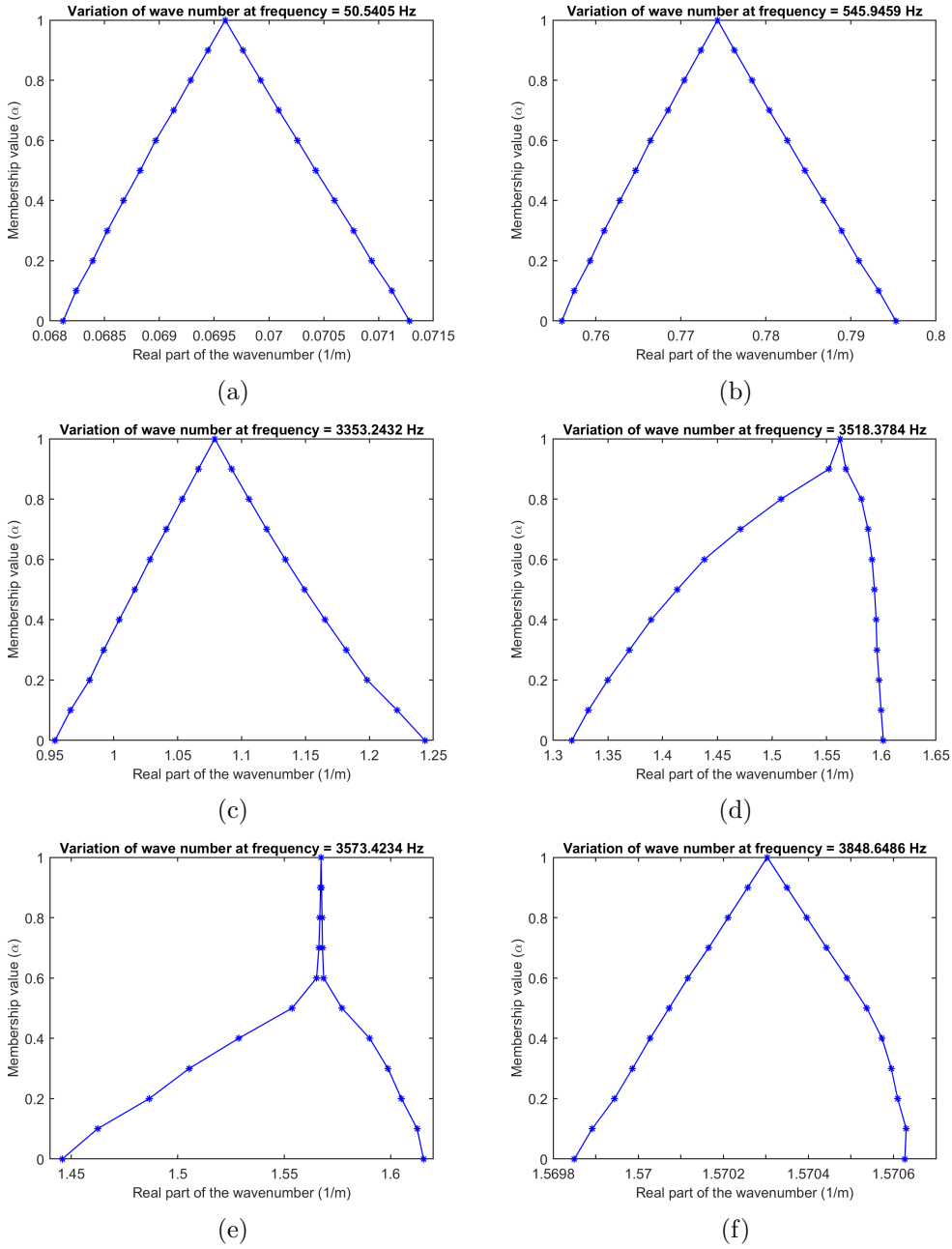

Figure 5.10: Longitudinal wavenumber variation with 10% uncertainty at discrete frequencies

periodic beam are evaluated in the MATLAB environment. The frequency range of computation is 10-2000 Hz. For the fuzzy uncertainty propagation, the elasticity of material 1 and material 2 is fuzzified using the triangular membership function; the membership functions are shown in Fig. 5.15. It can be seen that the effect of the fuzzy uncertainty on the band gap bounds is increasing with increased frequency. The FWFEM result at α-cut=0 is computed and compared with upper and lower bounds obtained with WFEM MCS and shown in Fig. 5.16, and shows good agreement. The FRF of the magnitude of

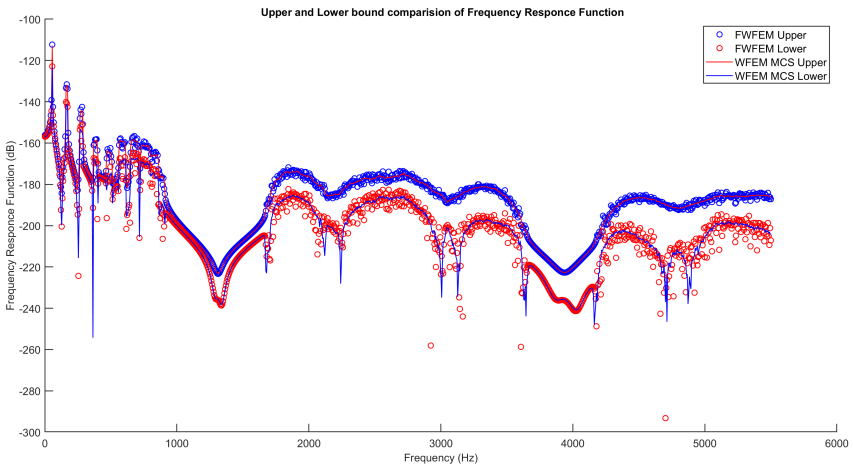

Figure 5.11: Validation of the FRF of periodic rod with 10% uncertainty

the flexural displacement at the excitation point, is computed at 1990 discrete frequencies spread uniformaly over 10-2000 Hz. In this case, the Young's modulus is stochastic with 10% variation about the nominal value. The fuzzy bound for flexural wavenumber and FRF for different membership values are plotted in Fig. 5.17, Fig. 5.18 and Fig. 5.19. As the α-cut value increases the fuzzy bound of flexural wavenumber and FRF are expected to decrease. The same behavior can be seen in Fig. 5.17, Fig. 5.18, and Fig. 5.19. In Fig. 5.17, the fuzzy bounds do not exist in the wavenumber and FRF at α-cut=1. It can be summarized that the fuzzy envelop is widening with increasing frequency. The variation bound of the flexural wavenumber obtained with fuzzy elasticity at α-cut=0 at the discrete frequencies is shown in Fig. 5.20. It is observed that in the propagation region, the variation of the longitudinal wavenumber is linear. However, near the band gap edge frequency it is non-symmetric; thus, the upper bound of flexural wavenumber is more sensitive to the uncertain elasticity.

5.5.3 FWFEM Direct form

Homogeneous plate case

To demonstrate the validity of the FWFEM direct formulation, the homogeneous plate case is considered, and numerical experiments are performed. A thin plate unit cell is modelled with four-node elements with three DOFs at each node. The material properties

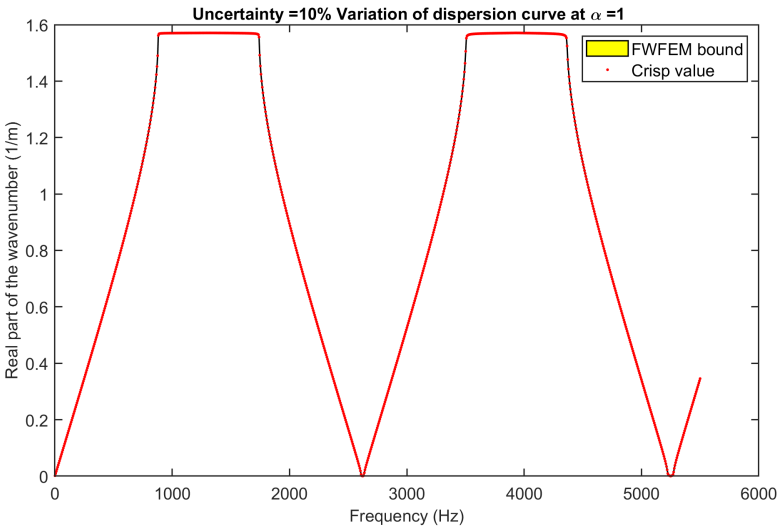

(a) Band gap bound

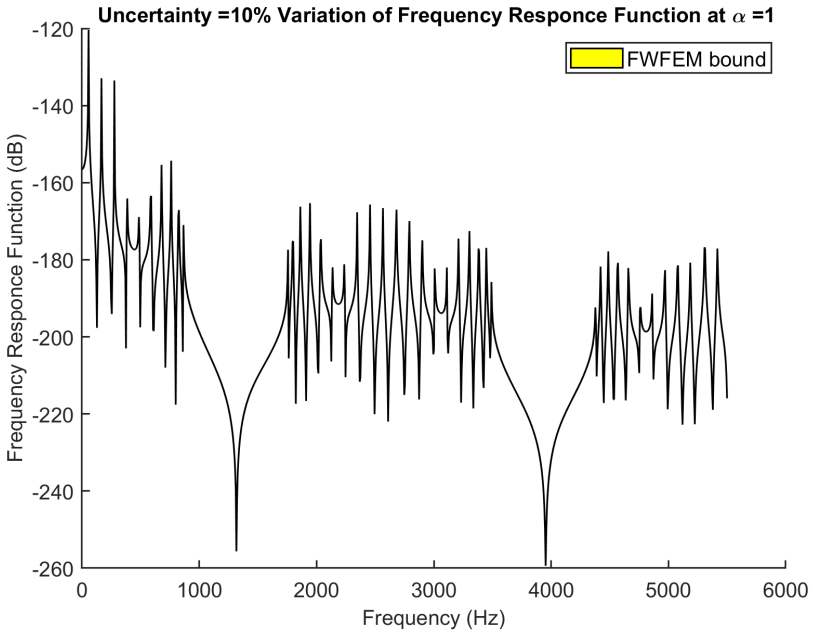

(b) FRF bound

Figure 5.12: Band gap bound and FRF bound with 10% uncertainty at $\alpha = 1$

are reported in Table 5.3.

Table 5.3: Material properties of homogeneous plate (fuzzy case)

Geometry/Property	Value
Young's modulus	210 $\times 10^9$ Pa
Poission's ratio	0.3
Mass density	7800 kg/m^3
Loss factor	0.01

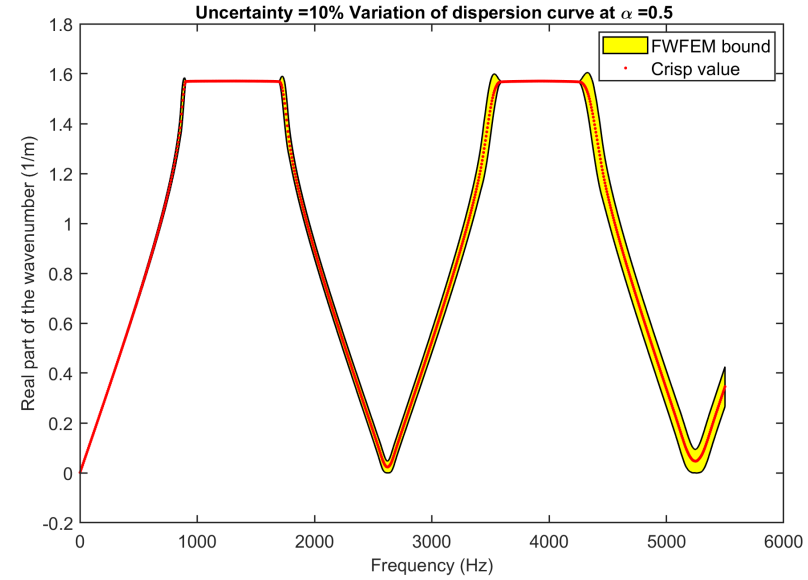

(a) Band gap bound

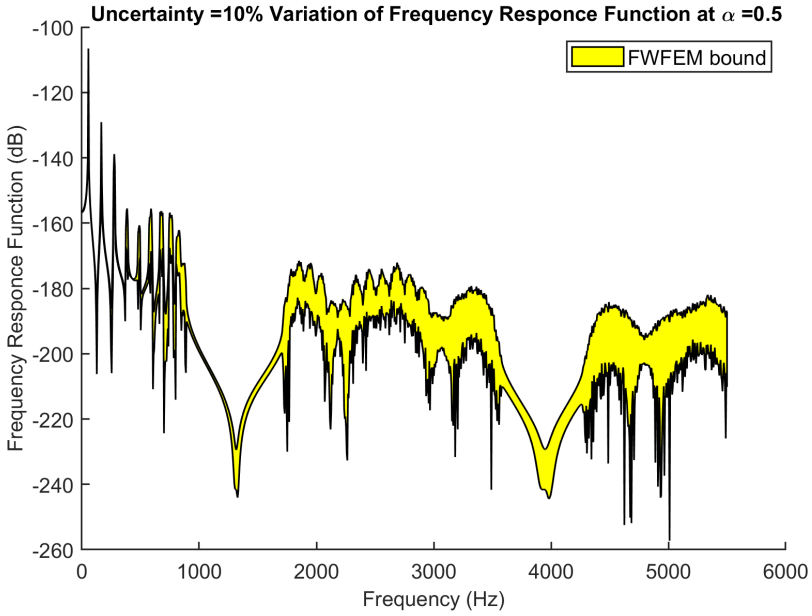

(b) FRF bound

Figure 5.13: Band gap bound and FRF bound with 10% uncertainty at $\alpha = 0.5$

The dimensions of the unit cell are $L_x = L_y = 0.005\ m$ with thickness $h = 0.0005\ m$. The fuzzy uncertainty effects are studied with variation of (10%) of the Young's modulus with reference to the deterministic value. The fuzzy parameter is modeled using the triangular membership function shown in Fig. 5.21. Most of the acoustic energy is transmitted by out-of-plane flexural waves. Therefore the out-of-plane flexural waves are considered during the numerical experiments. The MCS of the WFEM results are treated as reference results comparison and validation purposes. The comparison of the out-of-plane flexural

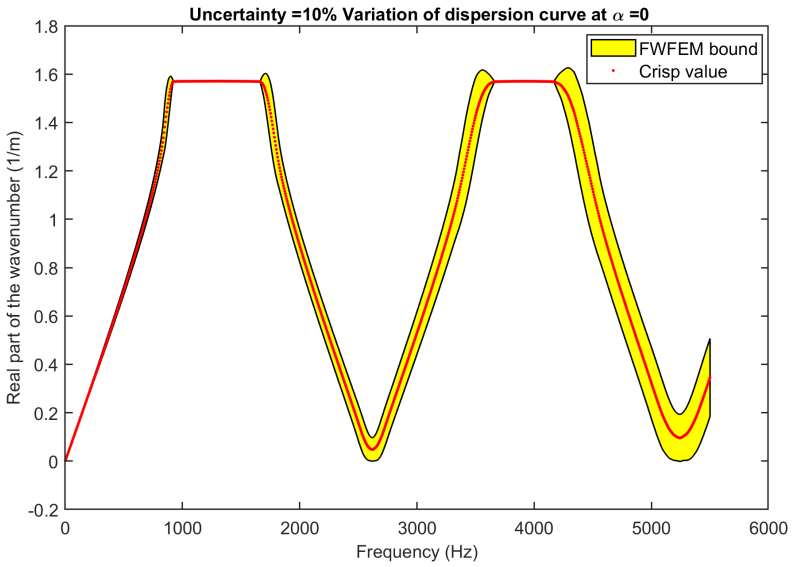

(a) Band gap bound

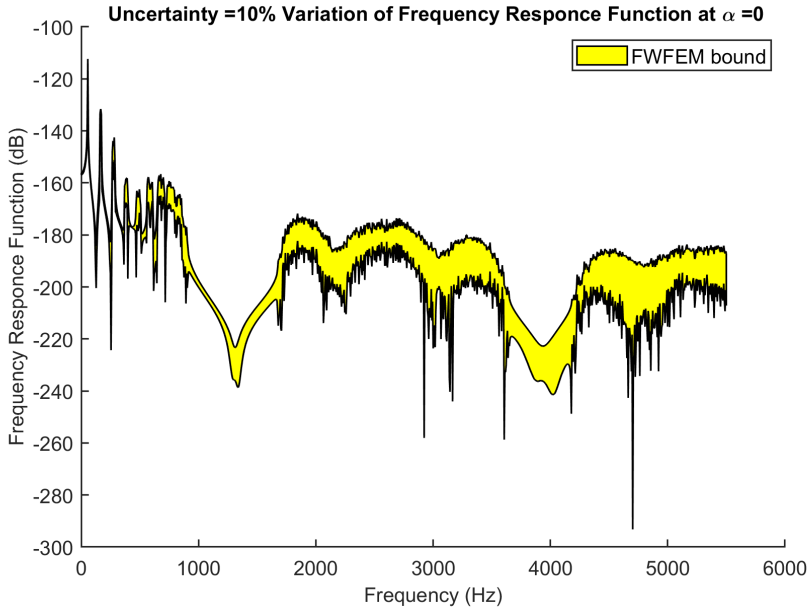

(b) FRF bound

Figure 5.14: Band gap bound and FRF bound with 10% uncertainty at $\alpha = 0$

wavenumber upper and lower bounds obtained from the FWFEM at α-cut=0 (maximum variation) and WFEM MCS are plotted in Fig. 5.22. The upper and lower bounds obtained from the FWFEM formulation show good agreement with the MCS results. This confirms the validity of the FWFEM formulation for the homogeneous plate case. The bounds of the out-of-plane flexural wavenumber are extracted from the FWFEM at 11 α-cut level and shown in Fig. 5.23. It can be seen from the Fig. 5.23 that the out-of-plane flexural wavenumber bounds are widening at higher frequency.

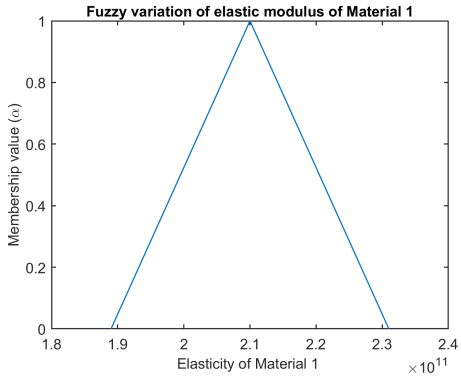

(a) Fuzzy membership function material 1

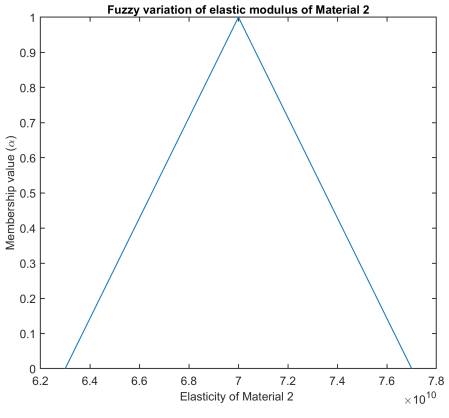

(b) Fuzzy membership function material 2

Figure 5.15: Input fuzzy membership variable 10% uncertainty, The units are (Pa)

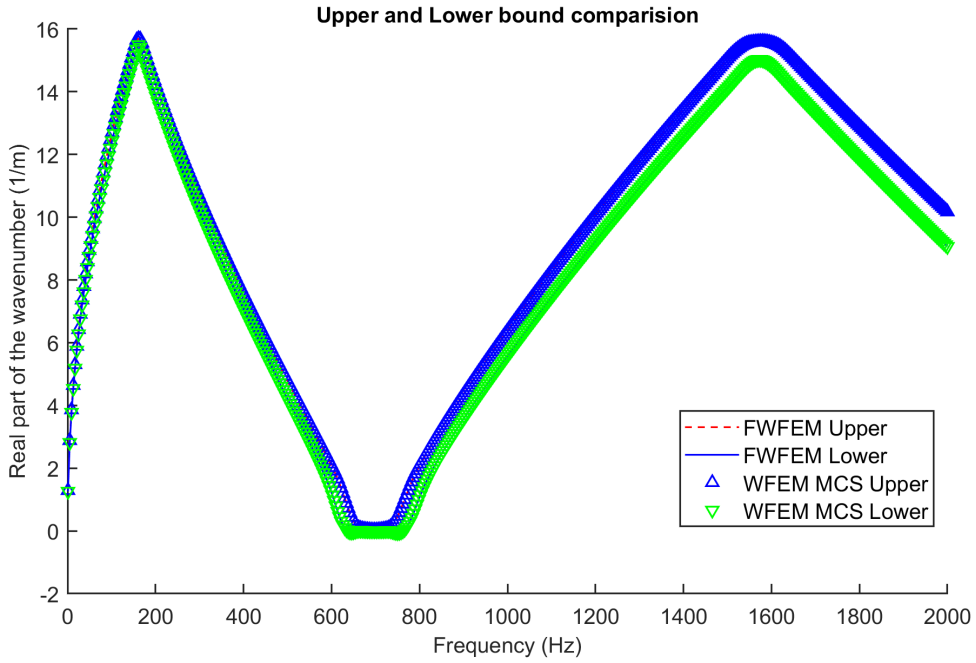

Figure 5.16: Flexural wavenumber comparison (fuzzy Young's modulus)

To demonstrate the influence of variation of uncertain material properties (Young's modulus) on the flexural wavenumber, different membership values of the fuzzy elasticity are simulated. The fuzzy bounds at different membership values for (5%), (10%), (15%), and (25%) variation in the Young's modulus are in Fig. 5.24,Fig. 5.25, Fig. 5.26, and Fig. 5.27, respectively. It can be seen in Fig. 5.25 that as the value of membership (α-cut) increases the fuzzy bound of out-of-plane flexural wavenumber decrease. At α=1, without any bounds as expected, α=1, represents the determinist result.

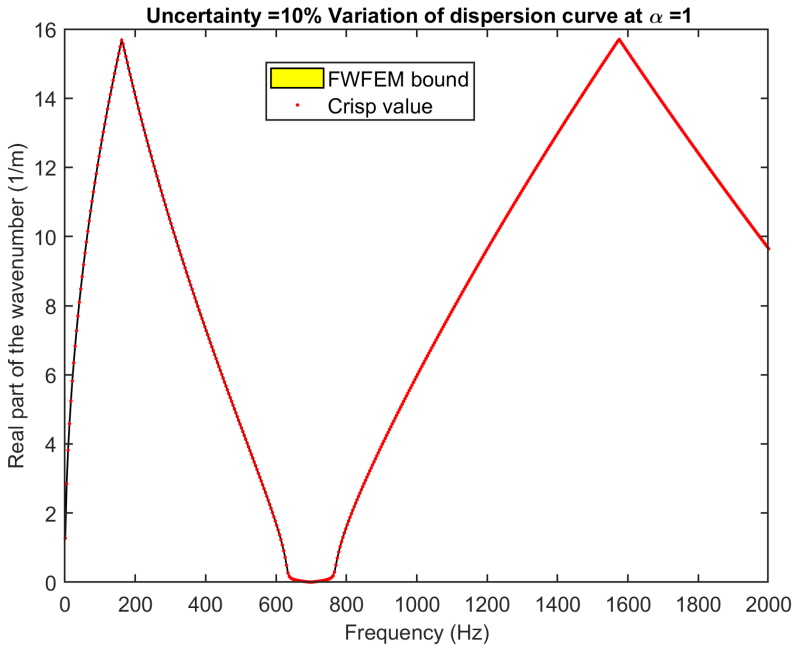

(a) Band gap bound

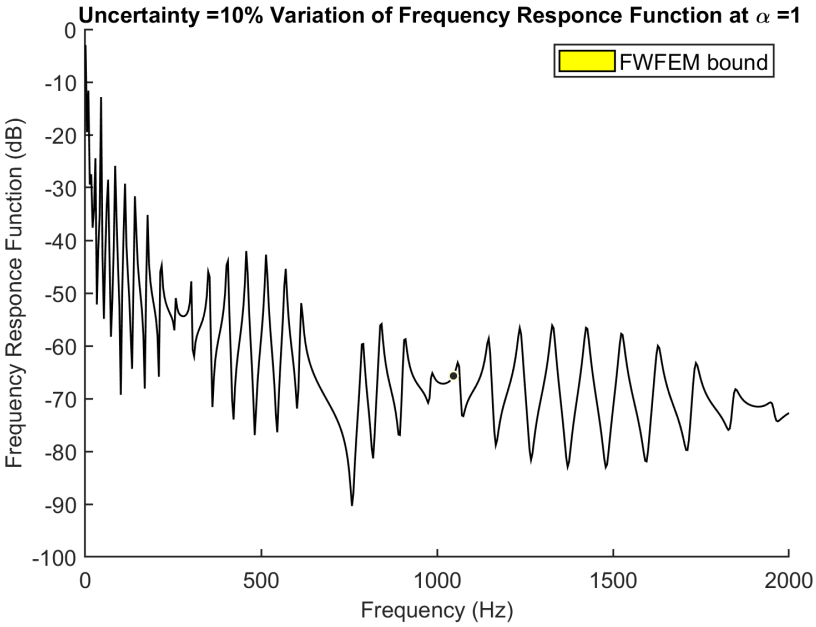

(b) FRF bound

Figure 5.17: Band gap bound and FRF bound with 10% uncertainty at $\alpha = 1$

It can also be inferred from the figures that Young's modulus uncertainty causes the increase in the fuzzy bounds of the out-of-plane flexural wavenumber in the higher frequency region, because the uppper and lower bounds are widening in the higher frequency region. The fuzzy bounds of the out-of-plane flexural wavenumber at discrete frequencies with fuzzy elasticity (10% variation) in 11 α-cut level are extracted and plotted in Fig. (5.28). It is visible from Fig. (5.28) that the fuzzy bound envelope is nearly constant

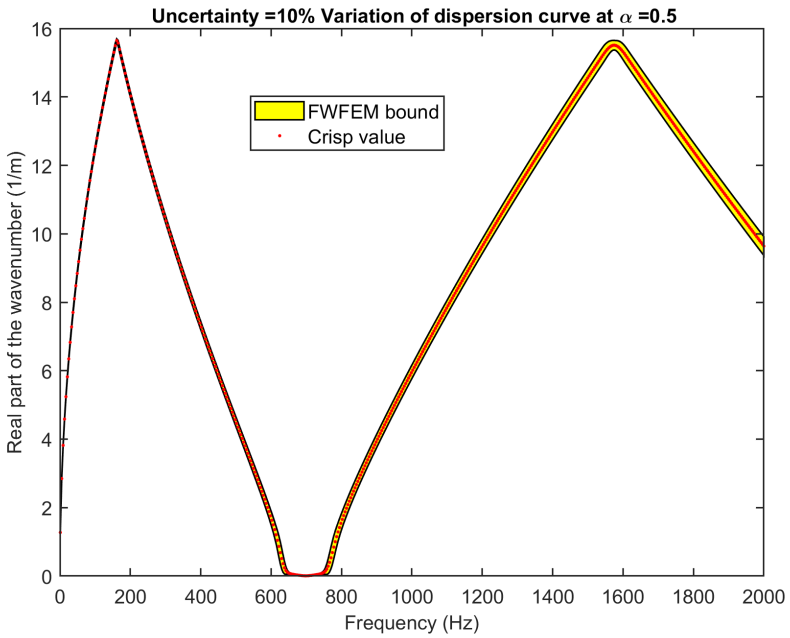

(a) Band gap bound

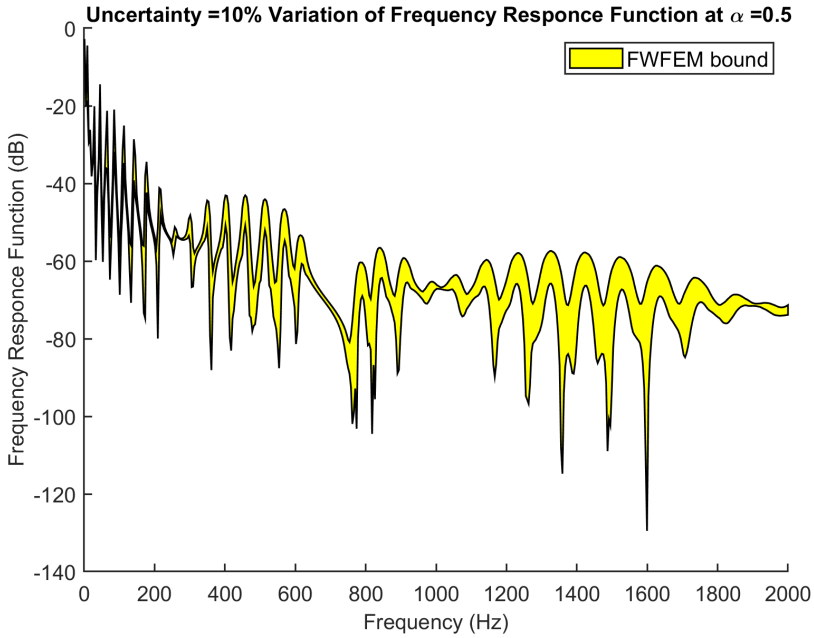

(b) FRF bound

Figure 5.18: Band gap bound and FRF bound with 10% uncertainty at $\alpha = 0.5$

with increasing frequency. This means that at the same level of fuzziness, the out-of-plane flexural wavenumber in the homogeneous plate is equisensitive to the fuzzy upper and lower bounds.

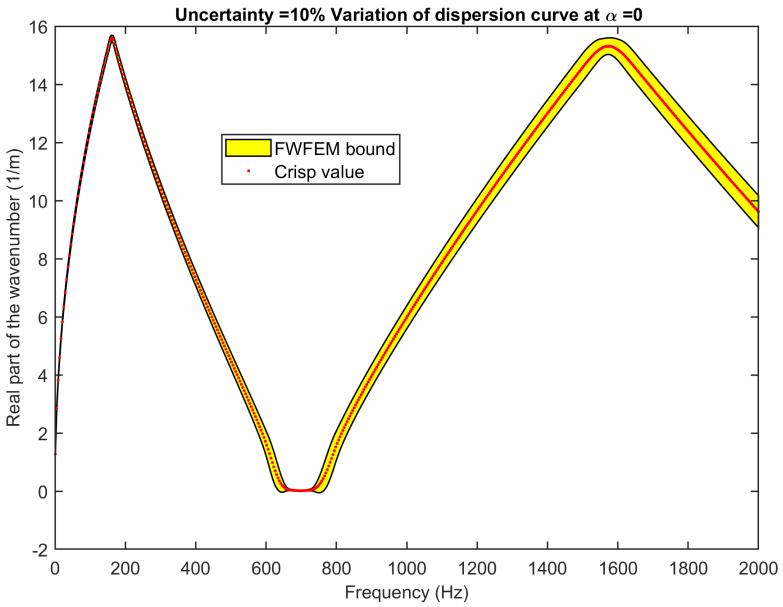

(a) Band gap bound

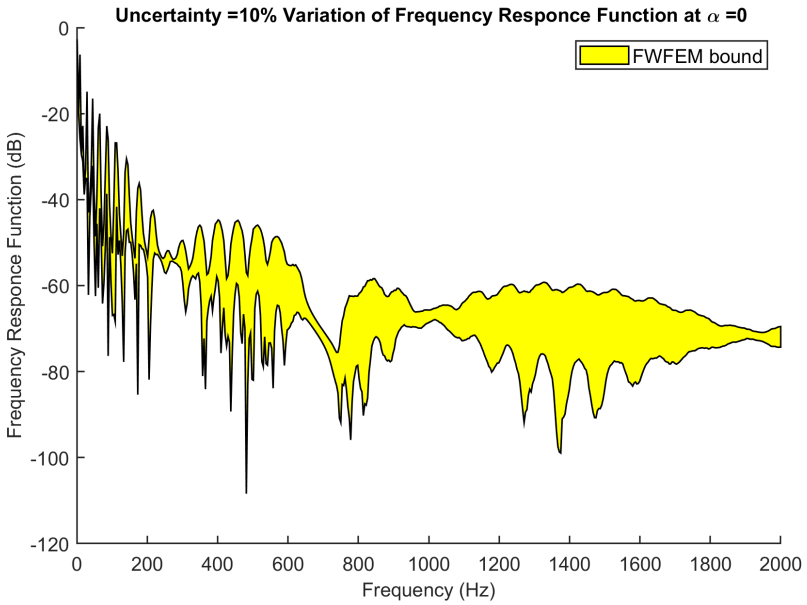

(b) FRF bound

Figure 5.19: Band gap bound and FRF bound with 10% uncertainty at $\alpha = 0$

Periodic plate case

The validation of the FWFEM formulation is performed for the 2D periodic plate case. The periodic plate consists of N repetitions of alternating sub-plate type A and sub-plate type B in x-direction. The sub-plate type A and sub-plate type B can be of different material properties and or different geometric dimensions. Here in the numerical simulation periodic plate made of different material properties are considered. A schematic

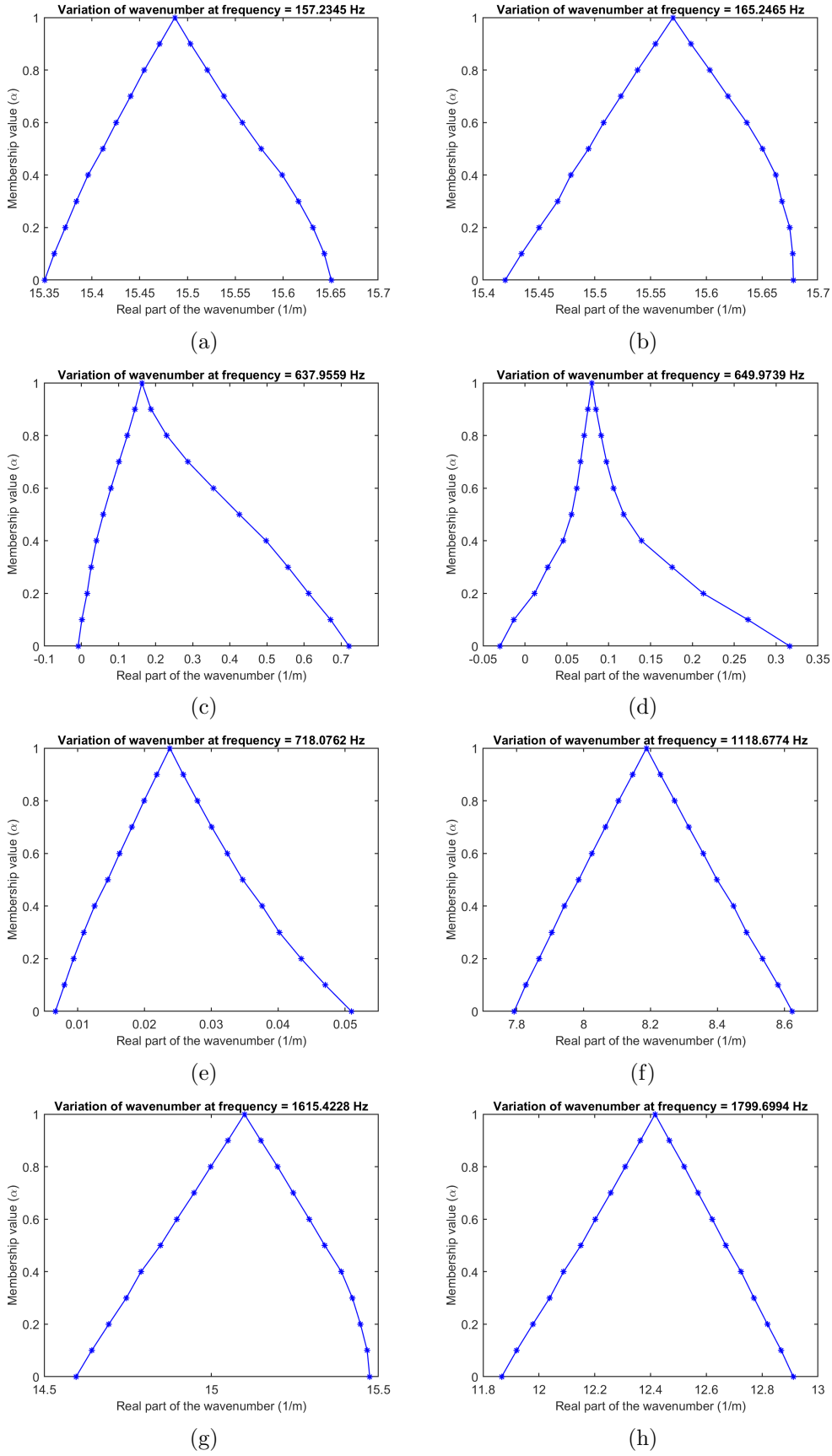

Figure 5.20: Flexural wavenumber variation with 10% uncertainty at discrete frequencies

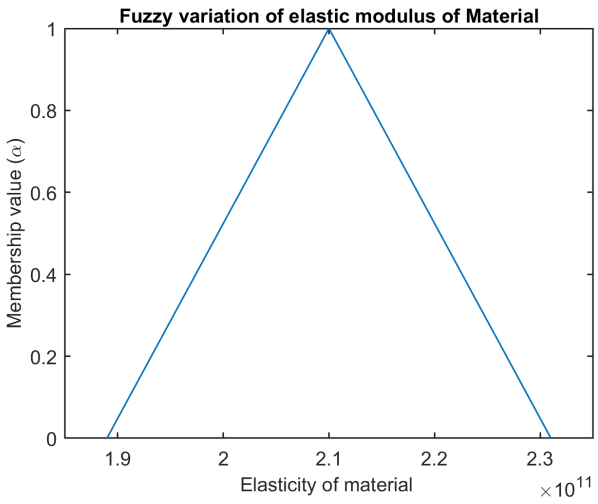

Figure 5.21: Input fuzzy membership function with 10% uncertainty. The unit is (Pa)

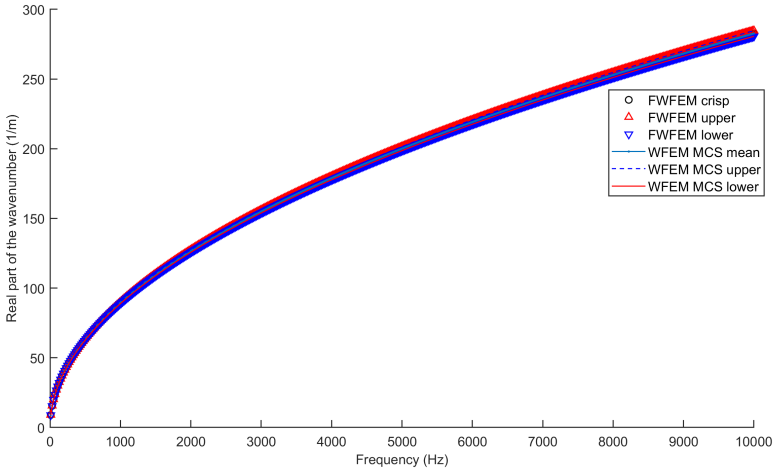

(a) Comparison of out-of-plane flexural wavenumber (fuzzy Young's modulus)

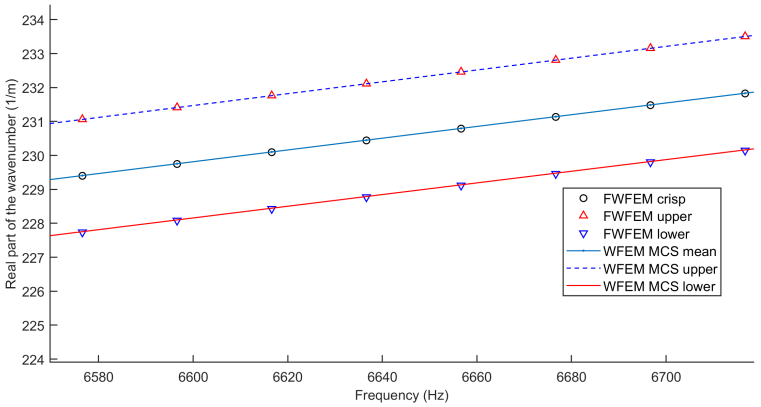

(b) Zoomed part

Figure 5.22: Homogeneous plate validation

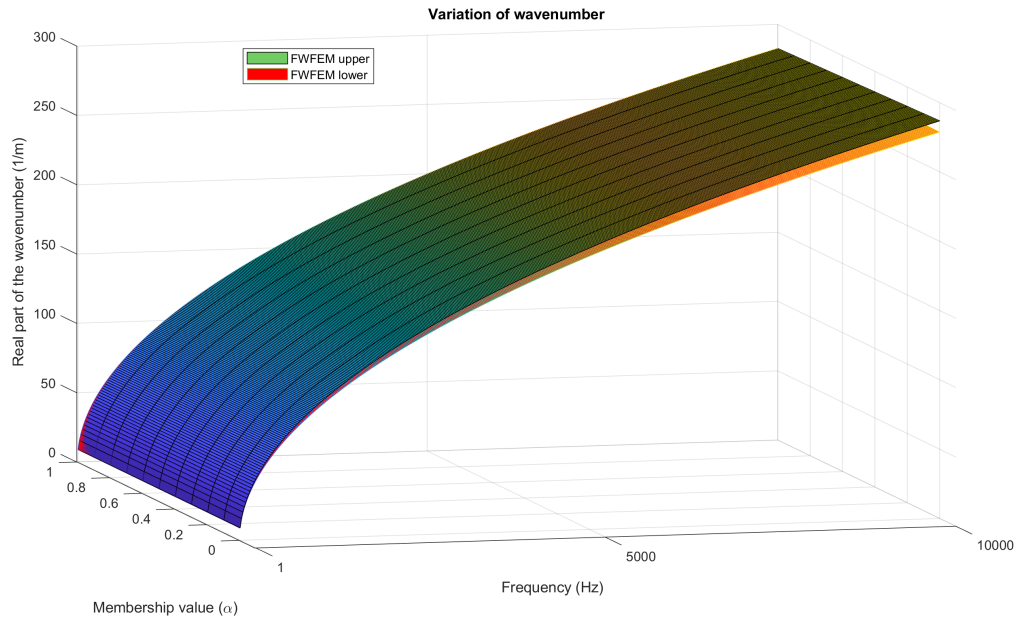

(a)

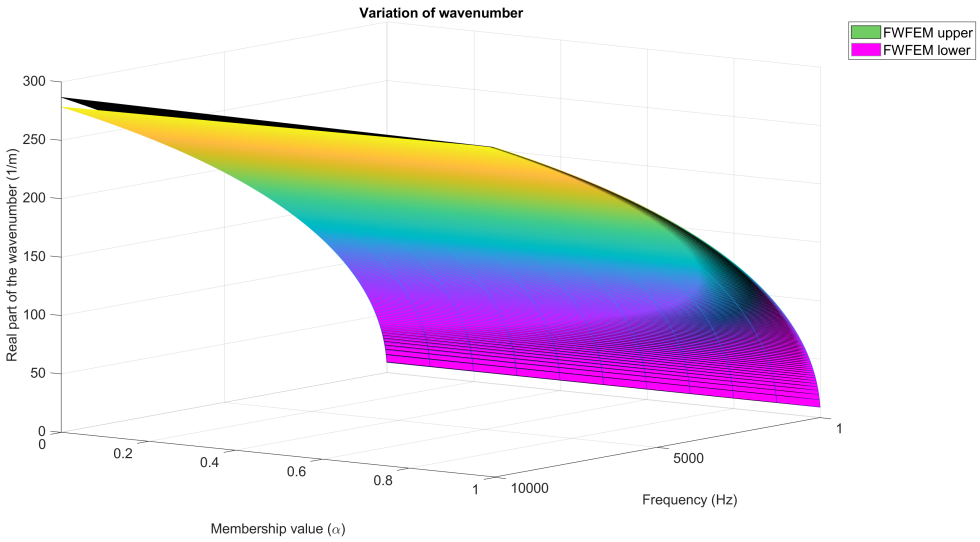

(b)

Figure 5.23: Fuzzy bound of out-of-plane flexural wavenumber of the homogeneous plate with 10% uncertainty

of the periodic plate and corresponding unit cell model is shown in Fig. 5.29. The considered material properties are reported in Table 5.4. The periodic plate unit cell is modeled with four-node elements with three DOFs at each node. The dimensions of the unit cell are $L_x = L_y = 0.1\ m$ with thickness $h = 0.005\ m$. The validation of the developed FWFEM formulation is presented for the out-of-plane flexural wavenumber in the considered periodic plate. The considered frequency range is 10-3000 Hz. The Young's modulus of sub-plate type A and sub-plate type B are considered uncertain, with variation

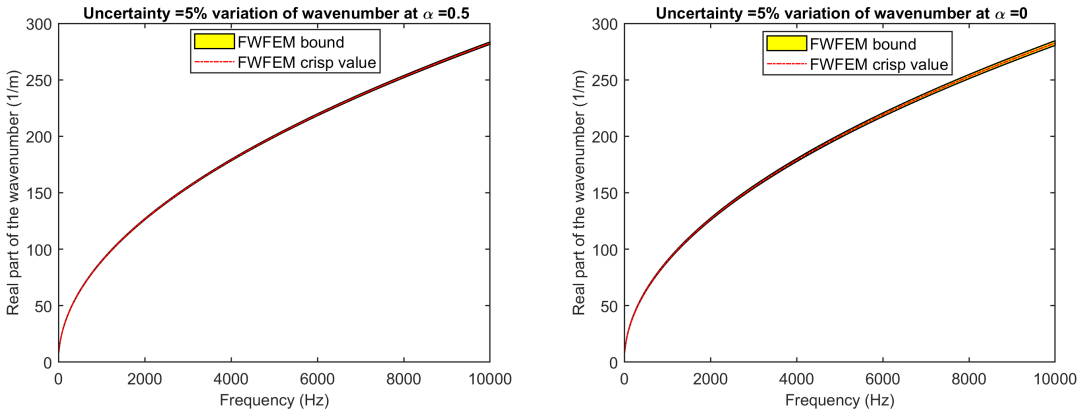

(a) (b)

Figure 5.24: The out-of-plane flexural wavenumber bound with 5% uncertainty

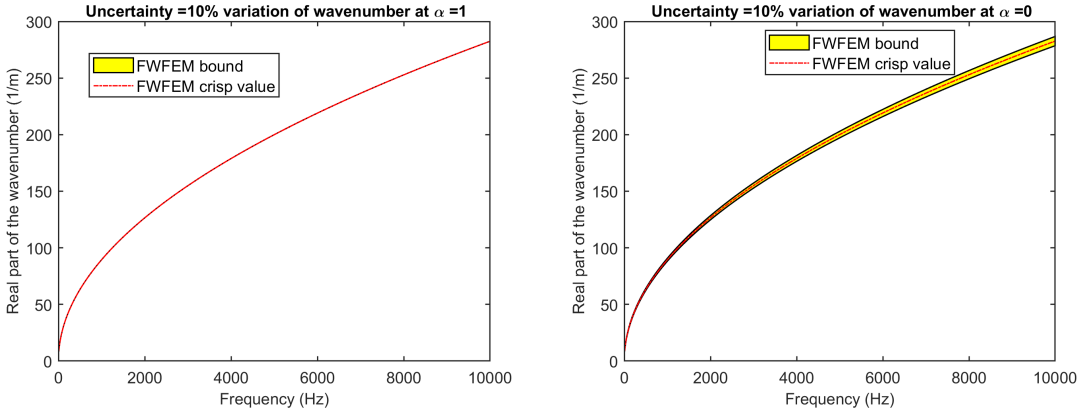

(a) (b)

Figure 5.25: The out-of-plane flexural wavenumber bound with 10% uncertainty

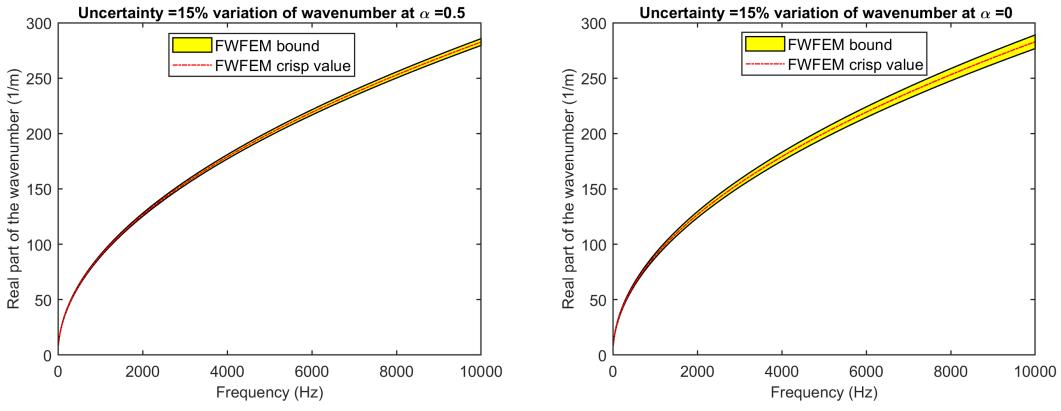

(a) (b)

Figure 5.26: The out-of-plane flexural wavenumber bound with 15% uncertainty

of (10%) about the nominal values. For the fuzzy uncertainty propagation, the elasticity of sub-plate type A (material 1) and sub-plate type B (material 2) are fuzzified using a triangular membership function as shown in Fig. 5.30. The WFEM MCS is consid-

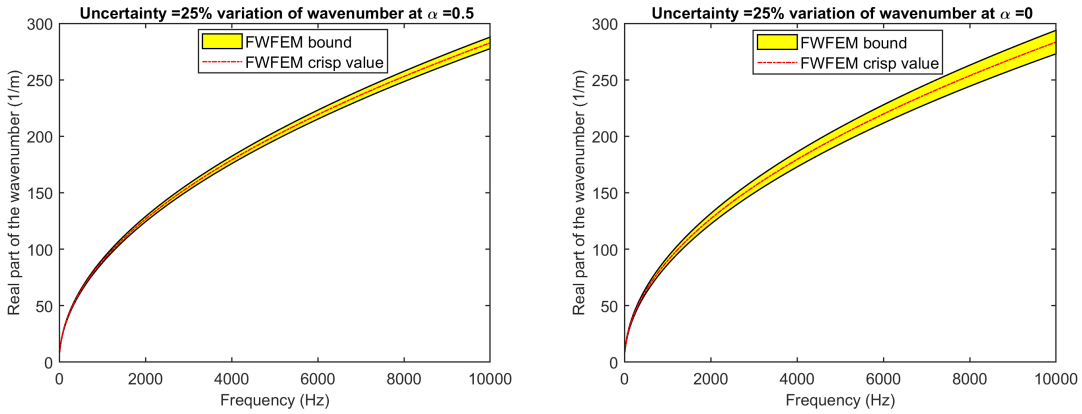

(a) (b)

Figure 5.27: The out-of-plane flexural wavenumber bound with 25% uncertainty

Table 5.4: Material properties of periodic plate (fuzzy case)

Geometry/Property	Value
Young's modulus of sub-plate type A	70 $\times 10^9$ Pa
Young's modulus of sub-plate type B	210 $\times 10^9$ Pa
Poission's ratio of sub-plate type A and B	0.3
Mass density of sub-plate type A	2700 kg/m^3
Mass density of sub-plate type B	7800 kg/m^3
Loss factor of sub-plate type A and B	0.001

ered as the reference solution for the validation. The out-of-plane flexural wavenumber dispersion is computed from the FWFEM formulation at α-cut=0 (maximum variation), and the obtained fuzzy upper and lower bounds are compared with the upper and lower bounds obtained from MCS. The comparison of the upper and lower bounds is shown in Fig. 5.31, demonstrating excellent agreement of the FWFEM results with the reference results. This verifies the applicability of the FWFEM formulation for the periodic plate case. In Fig. 5.31, the band gap can be observed starting around 2352 Hz. Near the same frequency, the variation of the upper and lower bounds is maximum, as seen in Fig. 5.31(b). Moreover, inside the band gap zone there is very small variation of out-of-plane flexural wavenumber. This confirm the validity of the FWFEM formulation for the periodic plate case. The fuzzy bounds of the out-of-plane flexural wavenumber for the periodic plate are shown Fig. 5.32.

The effect of uncertainty of the material properties on the out-of-plane flexural wavenumber bounds is demonstrated by calculating different variations of the elasticity. The fuzzy bounds at different membership values for the (5%),(10%),(20%), and (25%) variation in

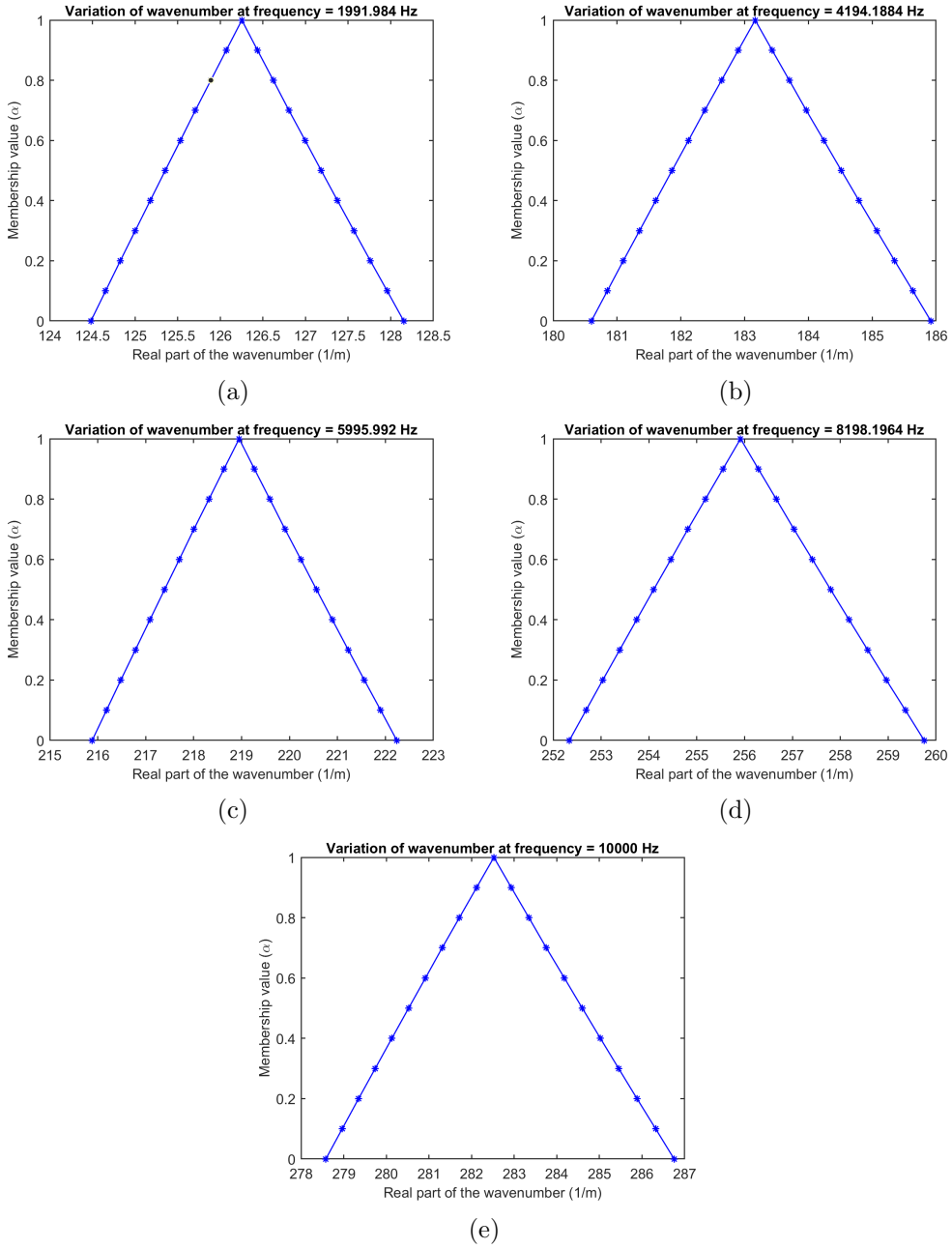

Figure 5.28: Fuzzy bound of the out-of-plane flexural wavenumber with 10% uncertainty at discrete frequencies

the Young's modulus are plotted in Fig. 5.33,Fig. 5.34, Fig. 5.35, and Fig. 5.36, respectively. It is visible from Fig. 5.34(a) that at α=1, the FWFEM results shows the crisp value, that is equivalent to deterministic results. From Fig. 5.33, Fig. 5.34, Fig. 5.35, and Fig. 5.36, it can be seen that with increase of uncertainty level, at constant α-cut, the upper bound of the out-of-plane flexural wavenumber descends gradually; however, the lower bound of the out-of-plane flexural wavenumber rises slowly. As the uncertainty rises, the flexural wavenumber bounds increase gradually. The out-of-plane flexural wavenumber

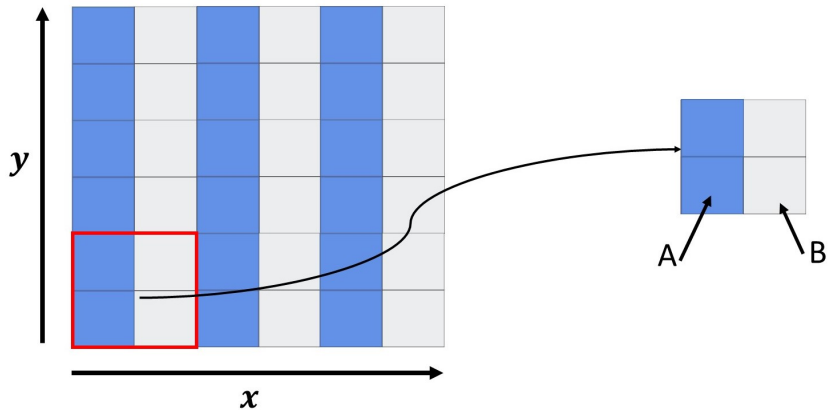

Figure 5.29: Schematic representation of the periodic plate and unit cell

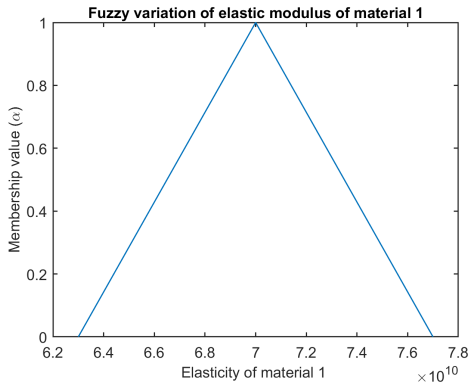

(a) Fuzzified material property for sub-plate type A

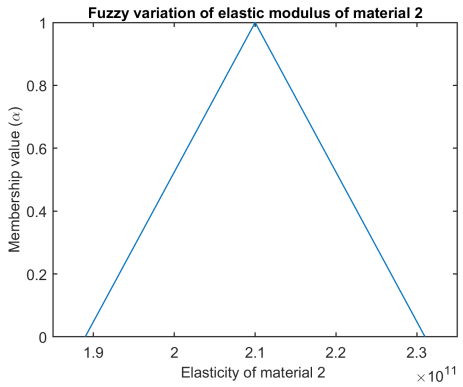

(b) Fuzzified material property for sub-plate type B

Figure 5.30: Input fuzzy membership function with 10% uncertainty. The units are (Pa)

bounds for the periodic plate at the discrete frequencies with 11 α-cut levels are extracted and plotted in Fig. 5.37. The uncertainty is considered as 10% of the Young's modulus. It can be observed in Fig. 5.37(b) that the lower bound rises slowly before the band gap edge frequency. From Fig. 5.37(c), it can be seen that at the band gap edge frequency, the lower bound rises gradually and upper bound descends slowly. Furthermore, inside the band gap in Fig. 5.37(e), the upper and lower bounds are equisensitive to out-of-plane flexural wavenumber.

5.5.4 FWFEM Inverse form

In this subsection, the validation of the FWFEM inverse form is performed through a linear elastic, continuum model of 2D. The mass and stiffness matrices are computed using COMSOL Multiphysics® software [Comsol, 2017]. A square lattice is considered

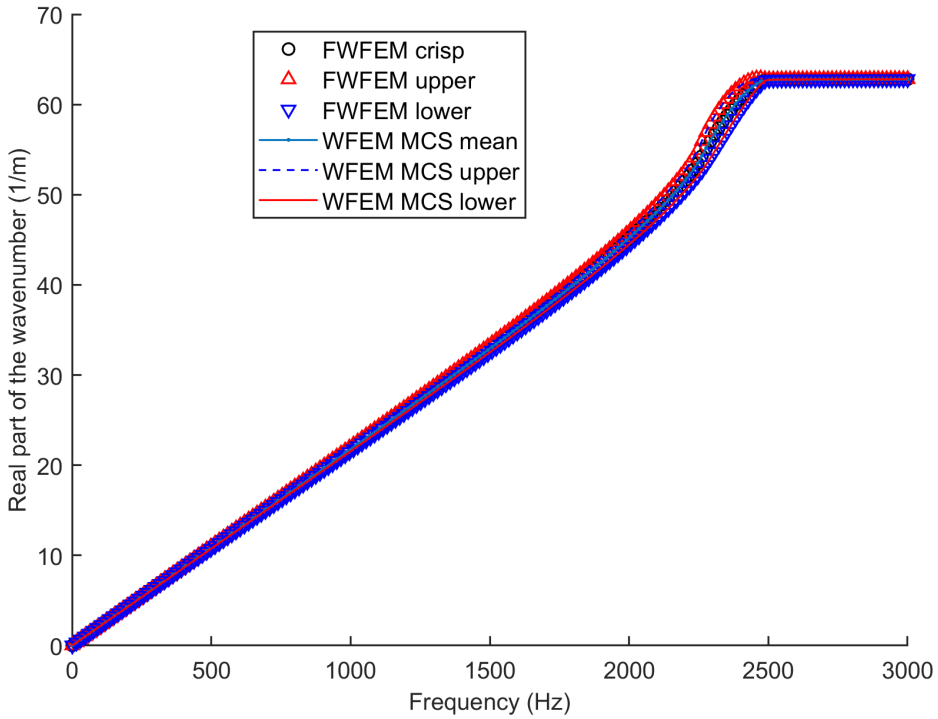

(a) Comparison of out-of-plane flexural wavenumber (fuzzy Young's modulus)

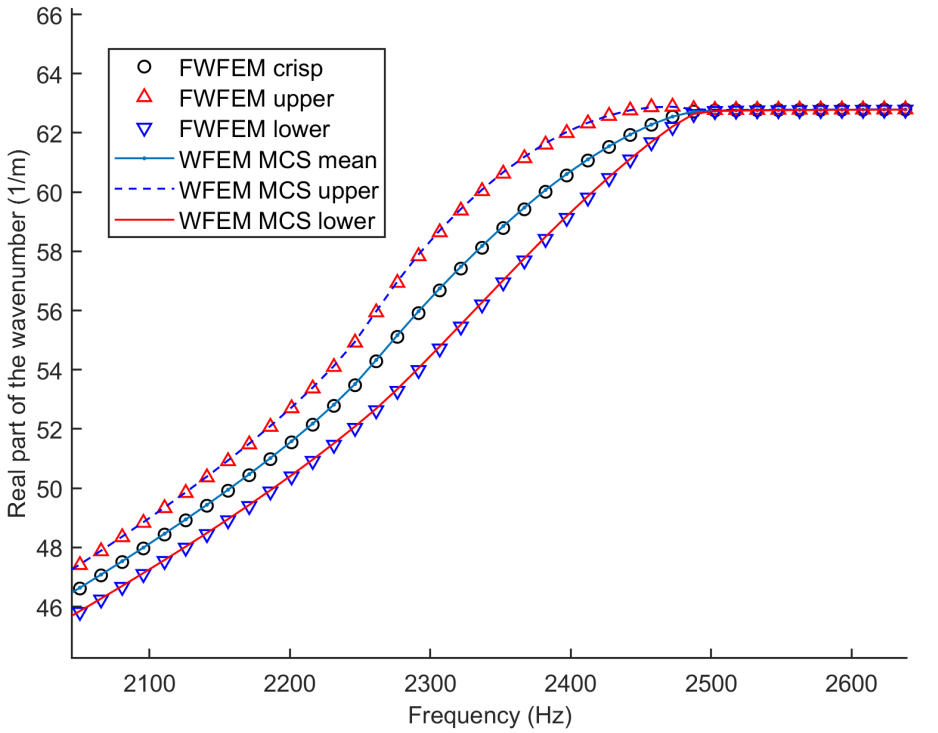

(b) Zoomed part

Figure 5.31: Periodic plate validation

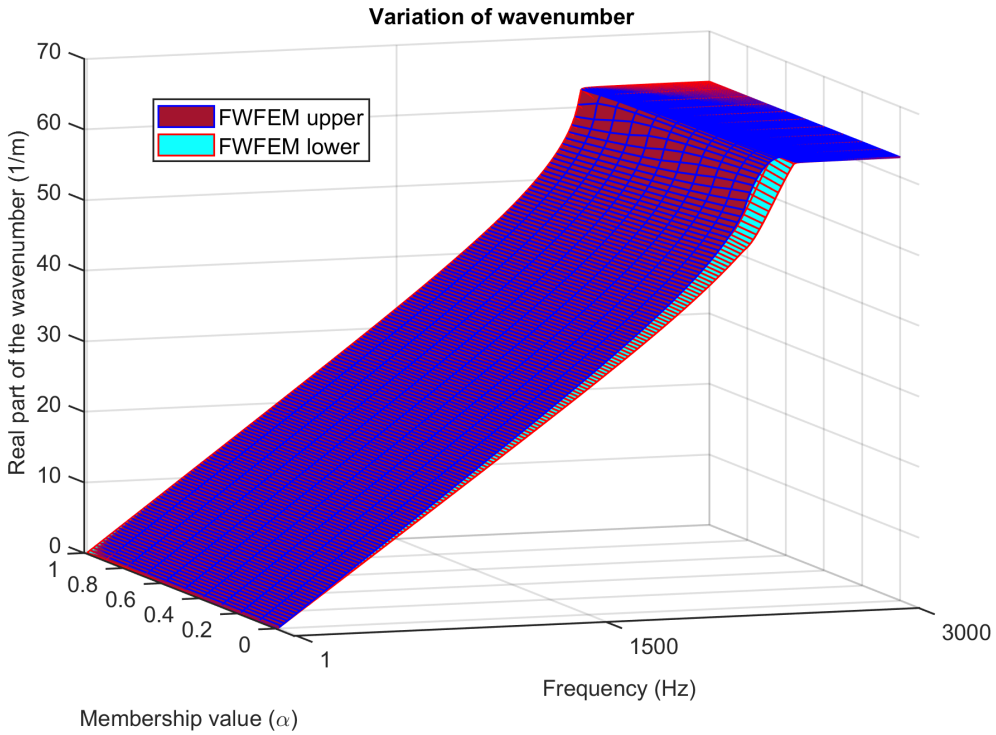

(a)

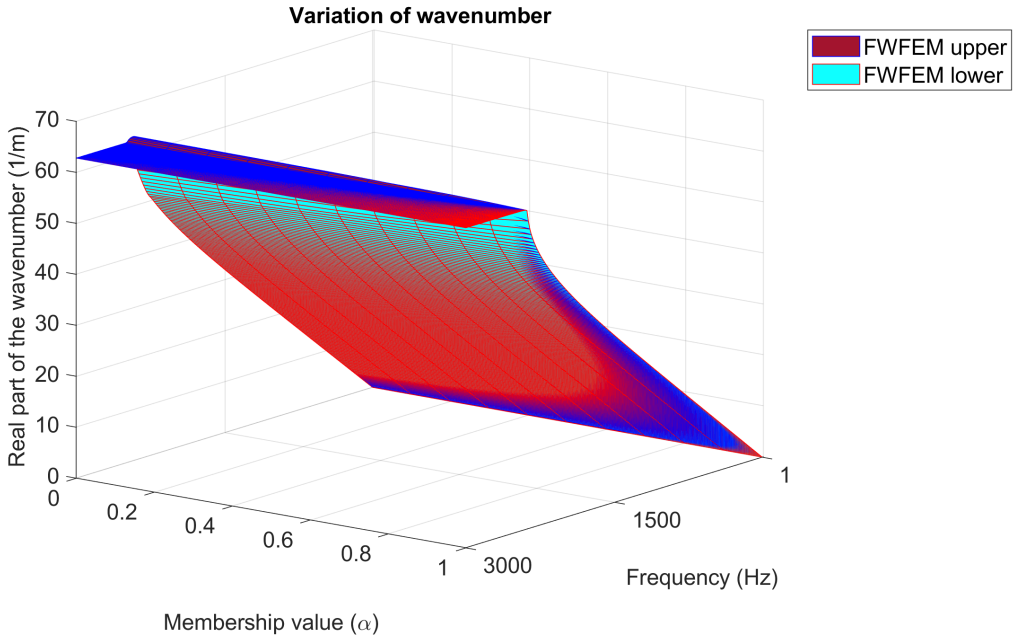

(b)

Figure 5.32: Fuzzy bound of the out-of-plane flexural wavenumber of the periodic plate with 10% uncertainty

with a bi-material unit cell to validate the developed FWFEM inverse form formulation. One material phase is chosen to be stiff and dense (material 2) and the other compliant and light (material 1). The schematic of the square lattice unit cell model is shown in Fig. 5.38. The lattice constant for material 1 (l_1)= 0.1 m and for material 2 (l_2)=0.04

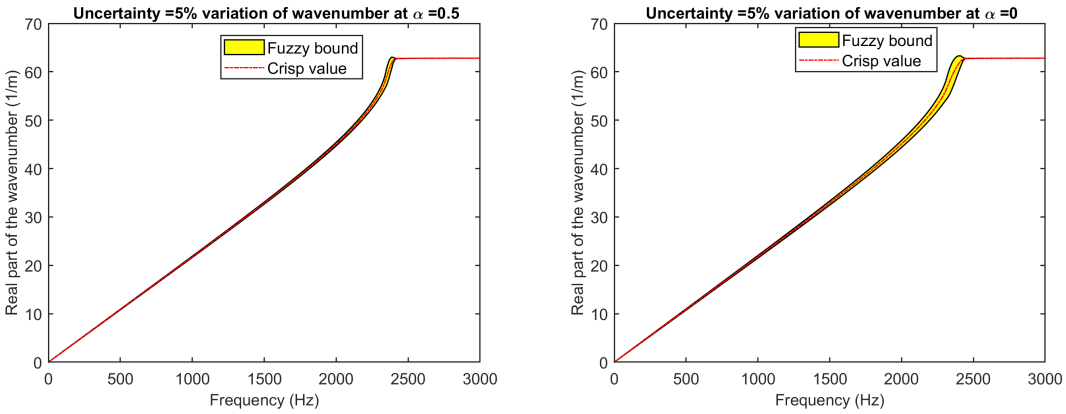

(a) (b)

Figure 5.33: The out-of-plane flexural wavenumber bound for periodic plate with 5% uncertainty

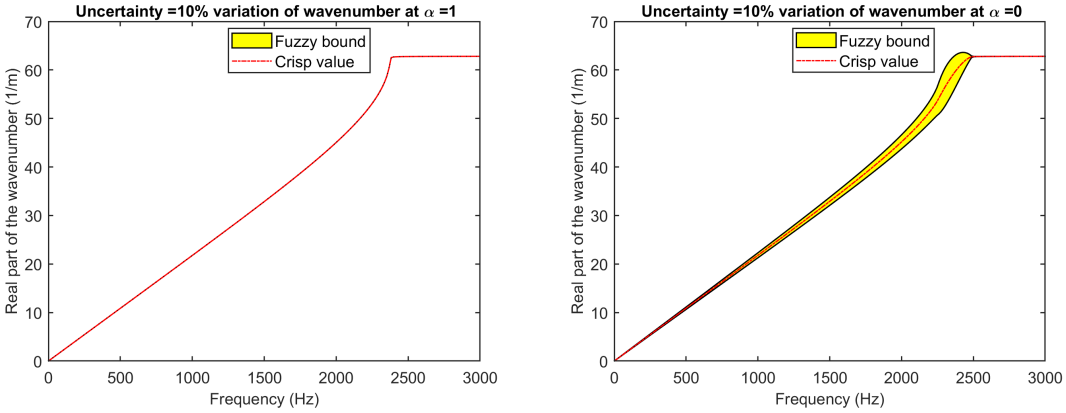

(a) (b)

Figure 5.34: The out-of-plane flexural wavenumber bound for periodic plate with 10% uncertainty

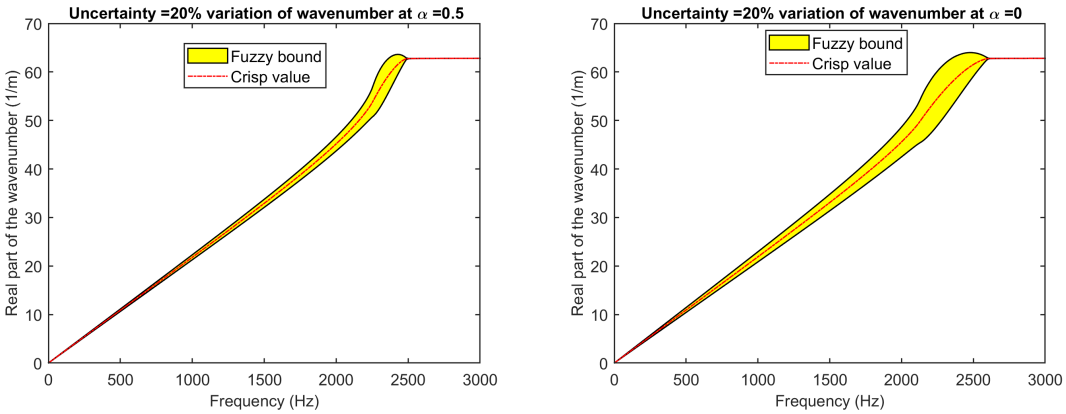

(a) (b)

Figure 5.35: The out-of-plane flexural wavenumber bound for periodic plate with 20% uncertainty

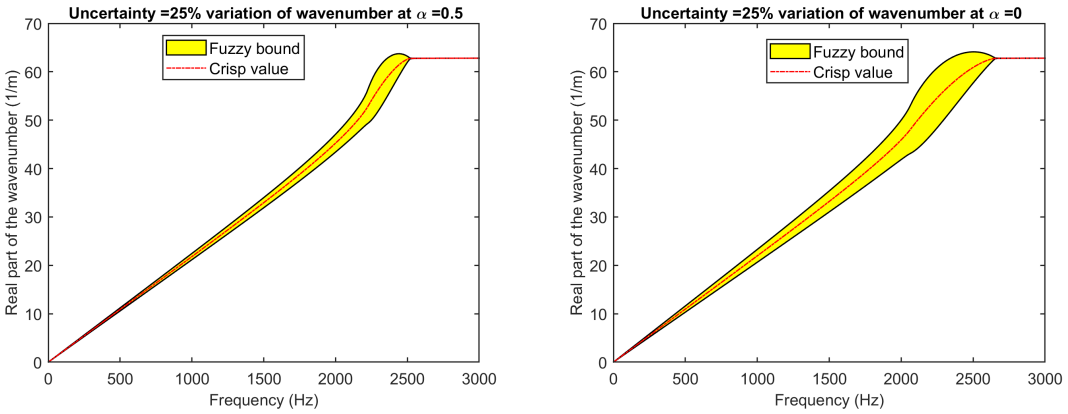

(a) (b)

Figure 5.36: The out-of-plane flexural wavenumber bound for periodic plate with 25% uncertainty

m. The considered material properties are reported in Table 5.5. The square unit

Table 5.5: Material properties for square lattice (fuzzy case)

Geometry/Property	Value
Young's modulus of Material 1	4.5×10^9 Pa
Young's modulus of Material 2	70×10^9 Pa
Poission's ratio of Material 1 and Material 2	0.35
Mass density of Material 1	1200 kg/m^3
Mass density of Material 2	2700 kg/m^3

cell has free triangular finite element, with total number of element as = 2802 (mesh shown in Fig. 5.39). The periodic boundary conditions are applied, and, the number of DOFs is 2802. The k-space is discretized and total of 427 sampling across the IBZ are considered. For the fuzzy uncertainty propagation, the elasticity of material 1 and material 2 are fuzzified using the triangular membership function shown in Fig. 5.40. By solving the equations of the fuzzy eigenproblem Eq. (5.42), various orders of the fuzzy eigen frequency $\omega_{i\alpha}$ are achieved. In the numerical simulation, the first seven orders of eigen frequencies are used to illustrate the band structures of the bi-material unit cell. The WFEM MCS is considered as the reference solution for validation purposes. The dispersion curve is computed from the FWFEM inverse form formulation with 10% uncertainty of the Young's modulus at α-cut=0 (maximum variation). The obtained fuzzy upper and lower bounds are compared with the upper and lower bounds obtained from the MCS and shown in Fig. 5.41, and shows excellent agreement. This verifies the validity of the FWFEM inverse form formulation for the 2D case. In Fig. 5.42 (a) every colored curve represents fuzzy

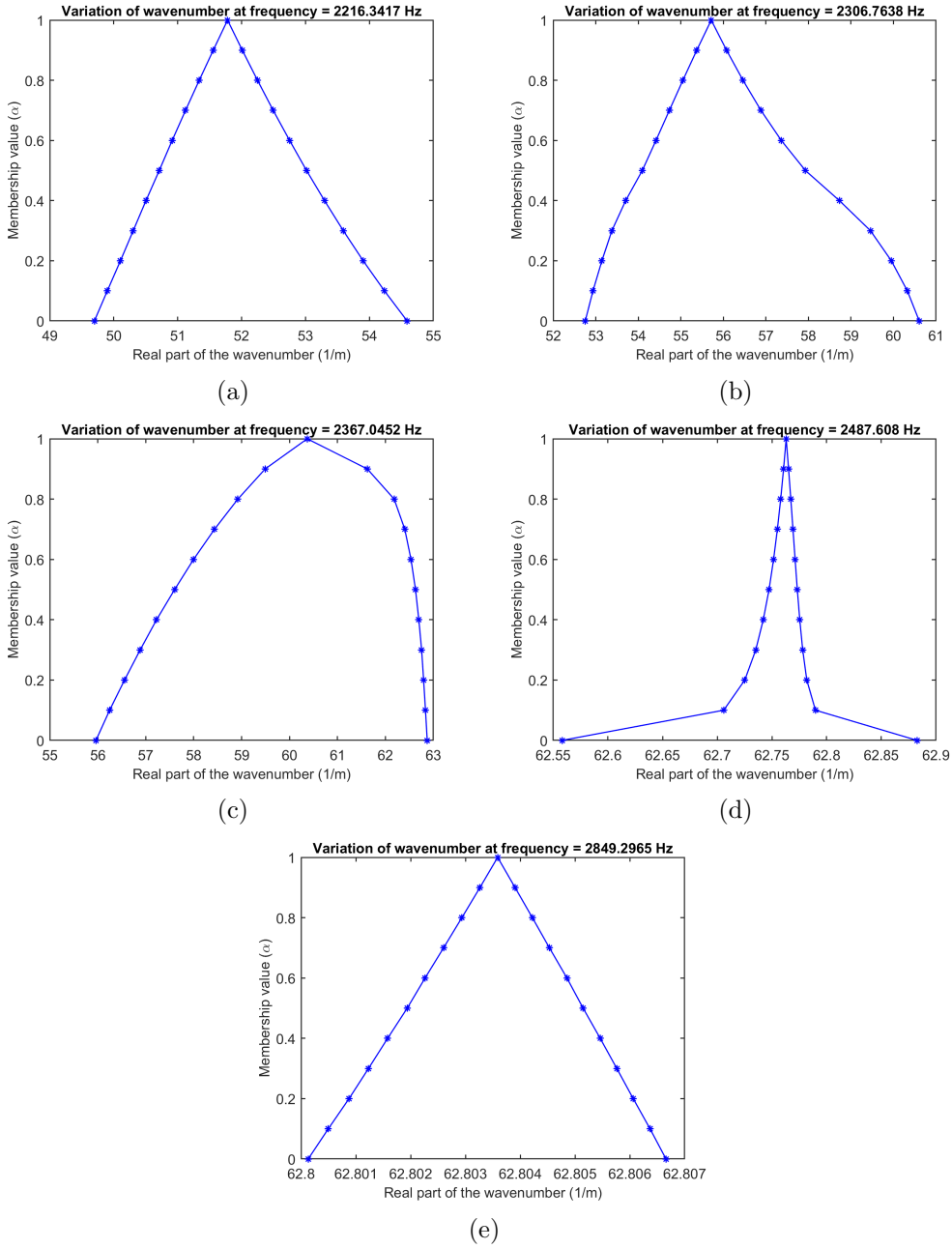

Figure 5.37: Fuzzy bound of the out-of-plane flexural wavenumber for the periodic plate with 10% uncertainty at discrete frequencies

eigen frequency, ω_α. If the maximum of the fuzzy eigen frequency $\omega_{n_\alpha-1}$ is less than the minimum of the fuzzy eigen frequency ω_{n_α}, there exists a partial band gap (the shaded area in Fig. 5.42(a), where the propagation of elastic waves is prohibited. The effects of fuzziness of the Young's modulus on bang gap with the variation of the elasticity (5%), (10%), (15%), (20%), and (25%) are shown in Fig. 5.42, Fig. 5.43, Fig. 5.44, Fig. 5.45, and Fig 5.46, respectively. In those figures, if the maximal upper bound of the fuzzy eigen frequency $\omega_{n_\alpha-1}$ is less than the lower bound of the fuzzy eigen frequency ω_n, then a band

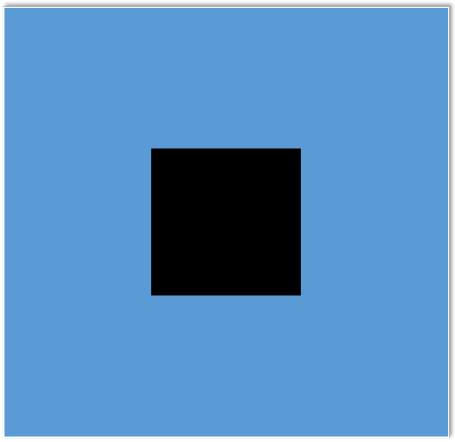

Figure 5.38: Schematic of the square lattice unit cell

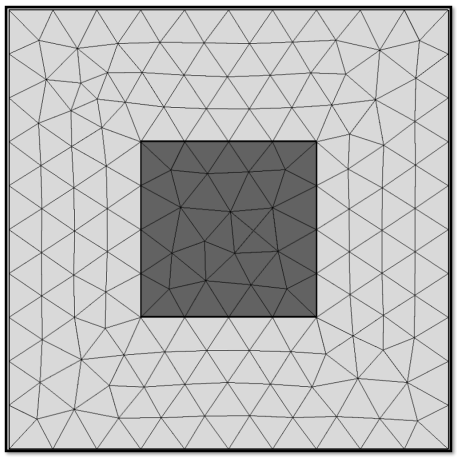

Figure 5.39: Unit cell mesh

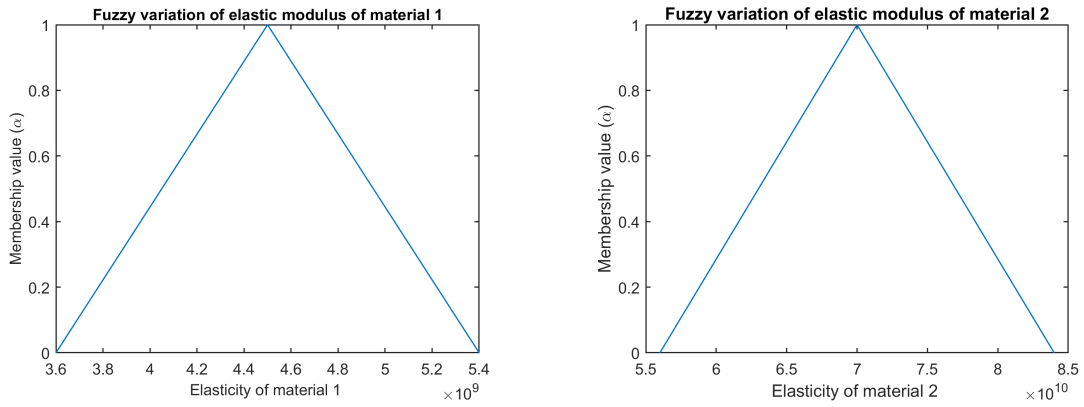

(a) Fuzzified material 1 (b) Fuzzified material 2

Figure 5.40: Input fuzzy membership function with 10% uncertainty. The units are (Pa)

gap exists with fuzzy uncertainties. From Fig. 5.43(b), it can be observed that with the increase of uncertainty, the upper bounds of the band gaps descend gradually, whilst at the same time the lower bounds rise very slowly. The fuzzy eigen frequencies bounds for

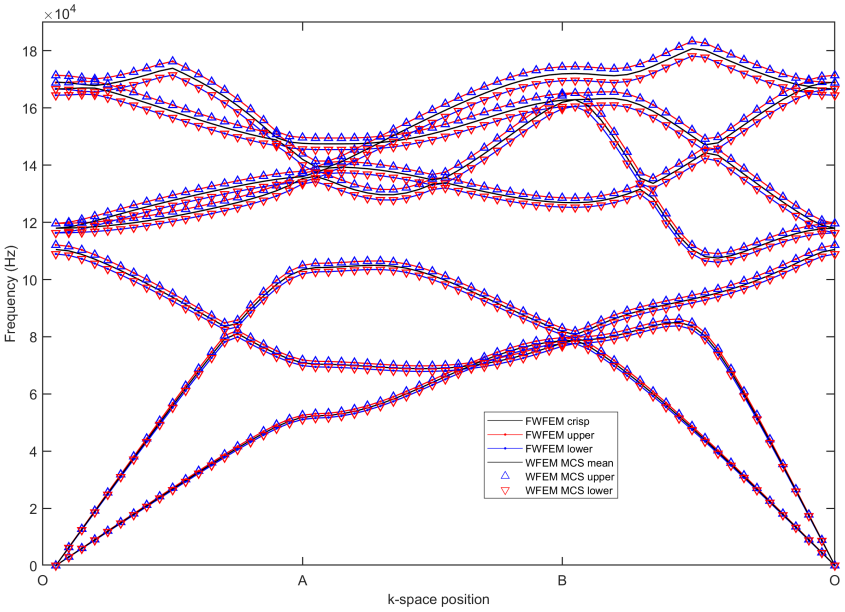

(a) Comparison of out-of-plane flexural wavenumber (fuzzy Young's modulus)

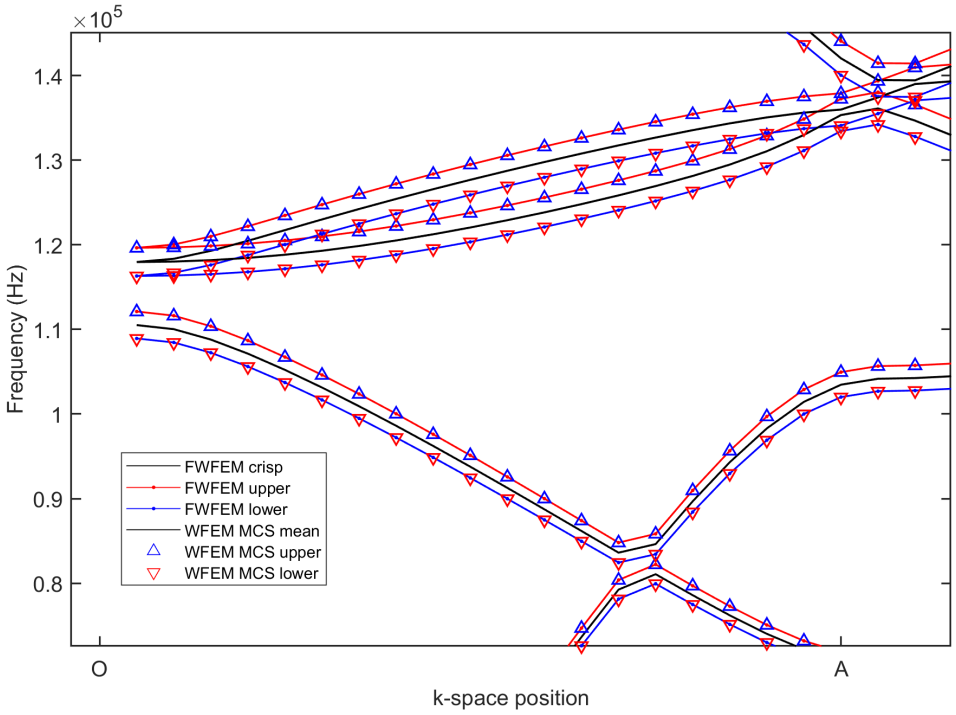

(b) Zoomed part

Figure 5.41: Bi-material square lattice validation

the square plate at the discrete wave vector with 11 α-cut levels are plotted in Fig. 5.47, Fig. 5.48, and Fig. 5.49. The uncertainty is considered to be 10% of the Young's modulus. It can be observed in Fig. 5.47(a) that the fuzzy frequency bounds rise with increasing frequency.

5.6 Elapsed time comparison for FWFEM 1D and 2D periodic media

The numerical costs involved in computation of fuzzy response with 11 α-cut levels is compared with that of WFEM MCS. The numerical test ran on a mobile workstation containing an Intel® Core^{TM} i7 7820 HQ CPU clocked at 2.90 GHz and 32 GB RAM. The comparison of elapsed time is reported in Table 5.6. It can be seen from Table 5.6

Table 5.6: Elapsed time comparison for FWFEM 1D periodic media

	WFEM MCS (10000 samples)	FWFEM
1D Periodic media	3840 seconds	234 seconds
2D Periodic media: Direct form	14400 seconds	122.52 seconds
2D Periodic media: Invers form	25490 seconds	2840 seconds

that computational effort by application of FWFEM is smaller than to WFEM MCS. In the case of the FWFEM inverse form, computation cost is higher because the internal nodes are conserved in the WFEM inverse formulation. Thus, it can be summarized that FWFEM direct and inverse form formulations have superiority over the WFEM MCS in terms of computation cost, which is highly advantageous for modeling complex periodic structures.

5.7 Conclusions

In this chapter, a computationally inexpensive fuzzy approach for uncertainty propagation in 1D and 2D periodic media is presented. The method allows wave characteristic to be defined by using a fuzzy parametric approach integrated with WFEM. In 1D case the state space formulation is basis for FWFEM formulation and in 2D case, direct and inverse formulation is presented. In 1D, the study proposes a new approach to predict fuzzy bounds of the band gap and FRF of periodic rod and periodic beam with fuzzy parametric uncertainties. The uncertainty quantification of longitudinal and flexural wavenumber and FRF with fuzzy variable are simulated. The maximum fuzzy bound of FRF is obtained at α=0, which decreases with increase in α-cuts value. The approach was presented for very simplified test cases, but it is found to be more efficient when compared with the

conventional MCS approach in terms of computational cost.

In the 2D direct formulation case, the formulation is applied to a homogeneous plate up to 10,000 Hz, and to a periodic plate at frequency up to 3000 Hz. The FWFEM results are compared with traditional WFEM MCS results, and show excellent agreement and a substantial reduction in computation cost. In the homogenous plate case, it is found that variation of out-of-plane flexural wavenumber is slightly higher with uncertain elasticity. For the periodic plate case, uncertainties affect the out-of-plane flexural wavenumber, and the maximum bound of the flexural wavenumber occurs near the band gap edge frequency. In the 2D inverse formulation case, the formulation is applied to a bi-material square lattice. The FWFEM inverse form results are compared with traditional WFEM MCS results, and again show excellent agreement.

The analysis presented in this chapter suggest that the uncertainties have a significant impact on the band structures. These effects are seen in shift of the bag gap edge frequencies that result into narrowing the band gap width. It is highly desirable to include the uncertainties when designing and analyzing the lattice and complex periodic structures. In terms of computation cost, the developed formulations offer substantial cost savings and can be a good starting point for optimization and reliability studies of complex periodic structures with uncertainties.

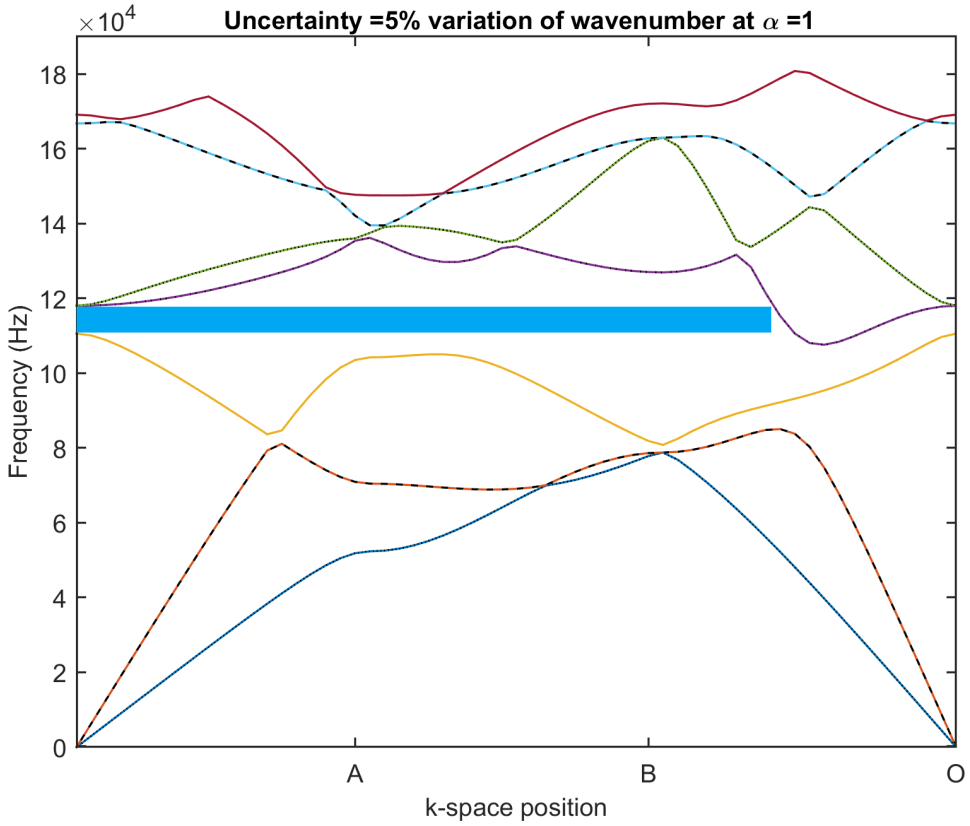

(a) Fuzzy crisp value

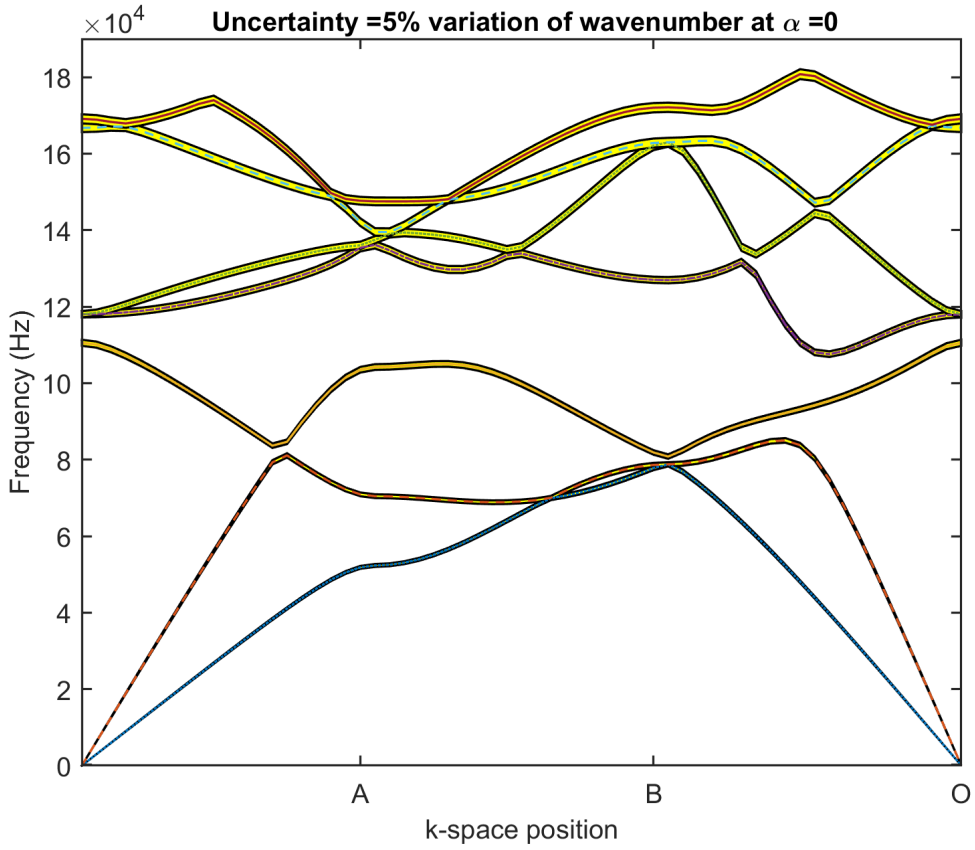

(b)

Figure 5.42: Band structure with 5% uncertainty

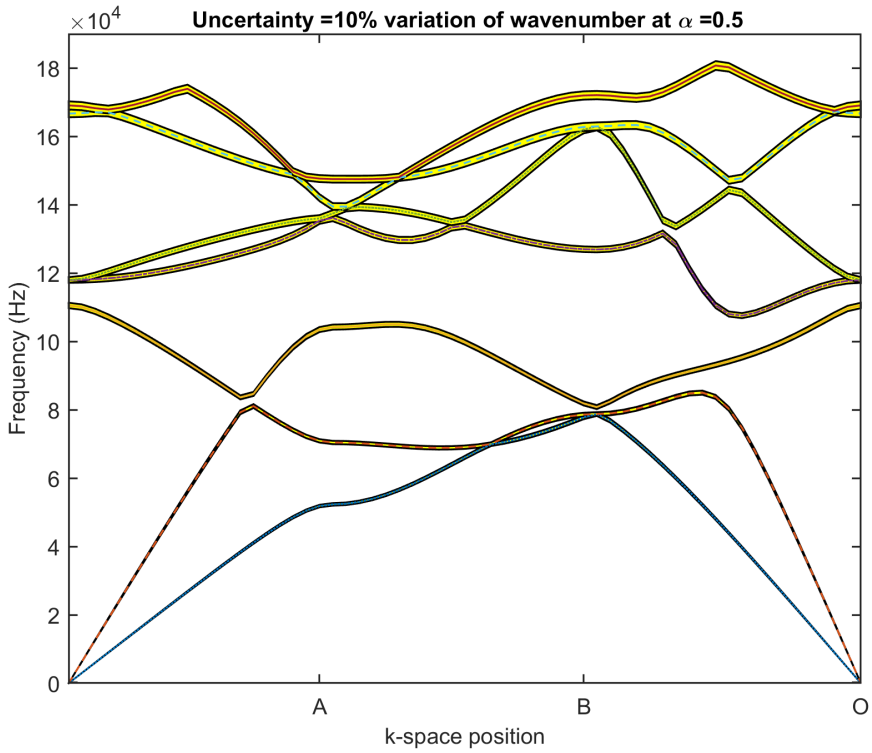

(a)

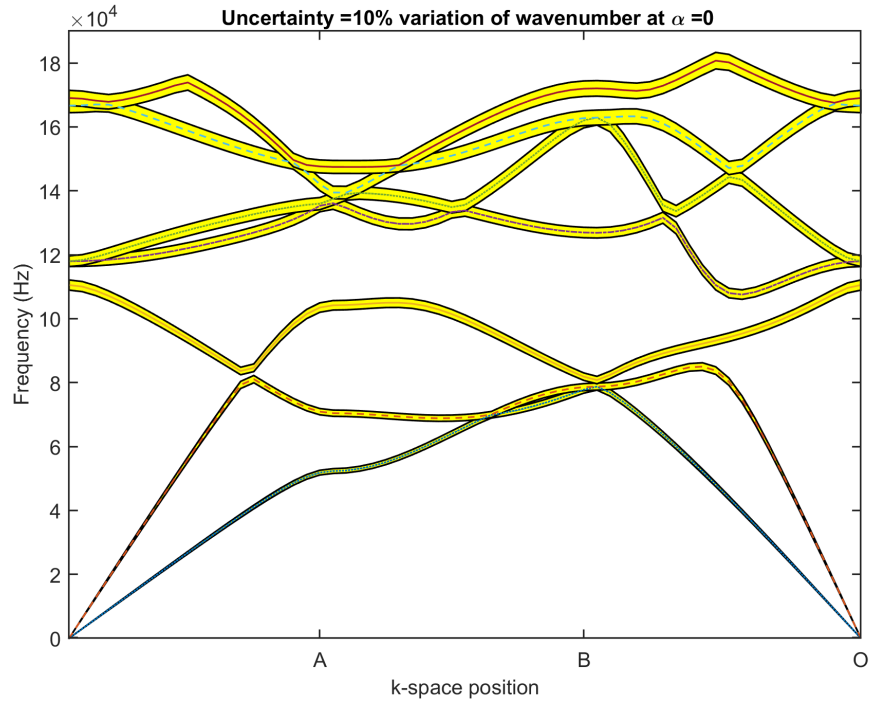

(b)

Figure 5.43: Band structure with 10% uncertainty

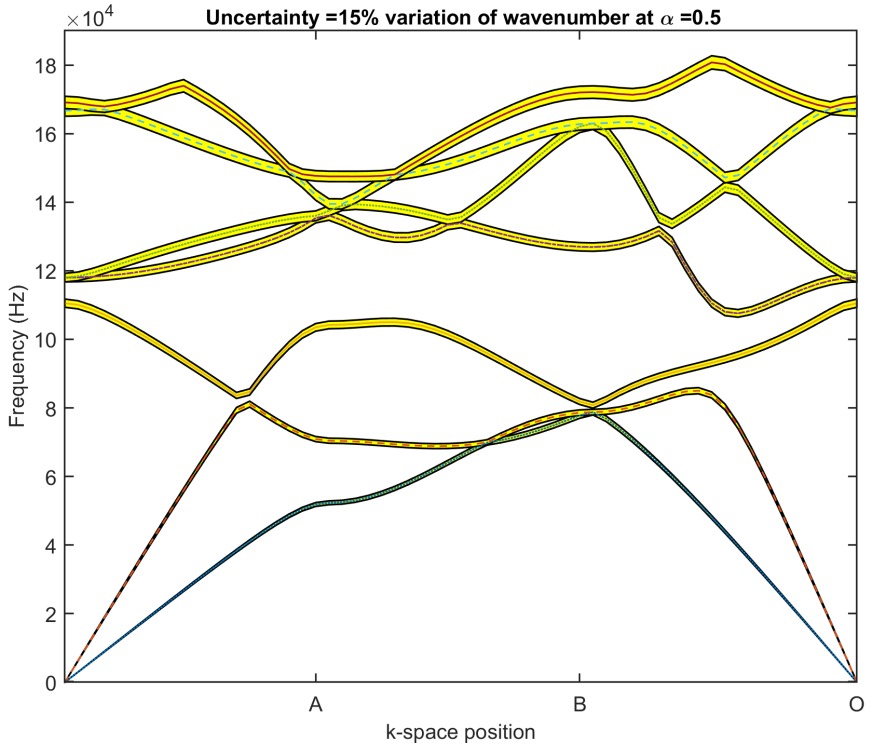

(a)

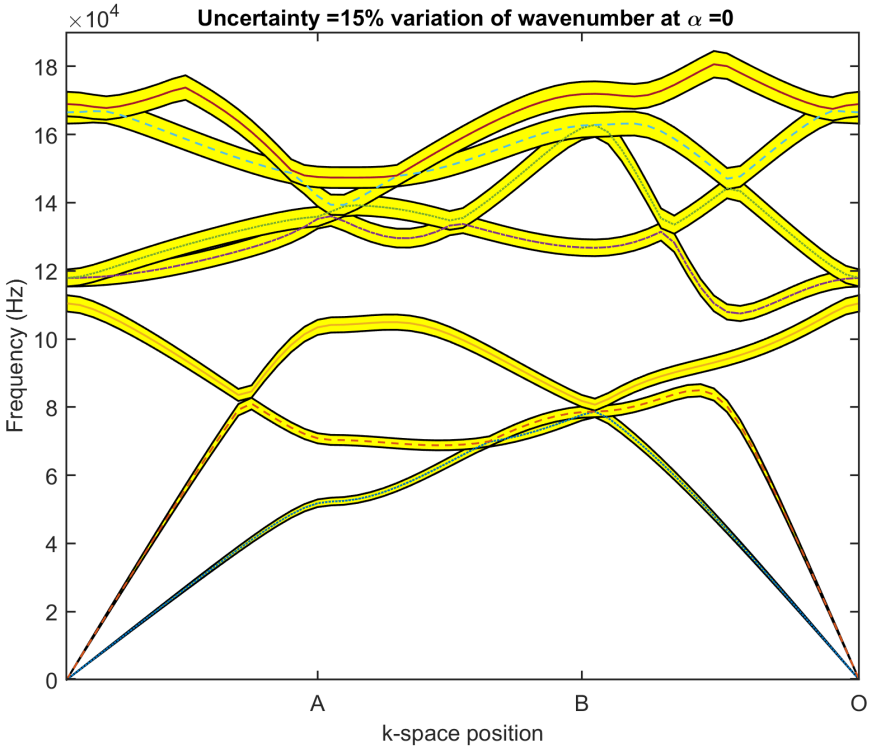

(b)

Figure 5.44: Band structure with 15% uncertainty

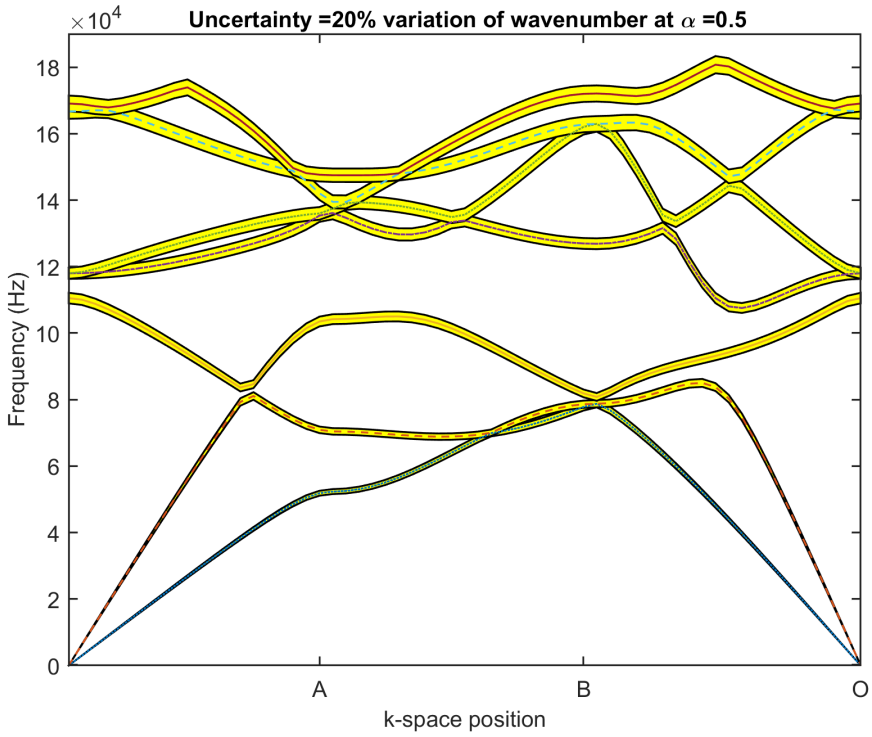

(a)

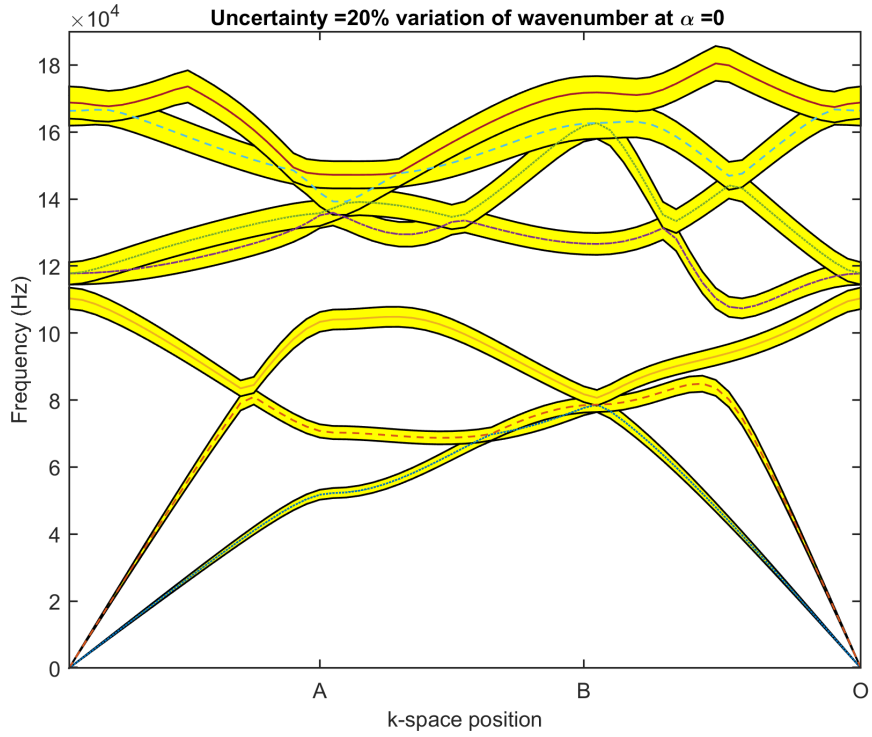

(b)

Figure 5.45: Band structure with 20% uncertainty

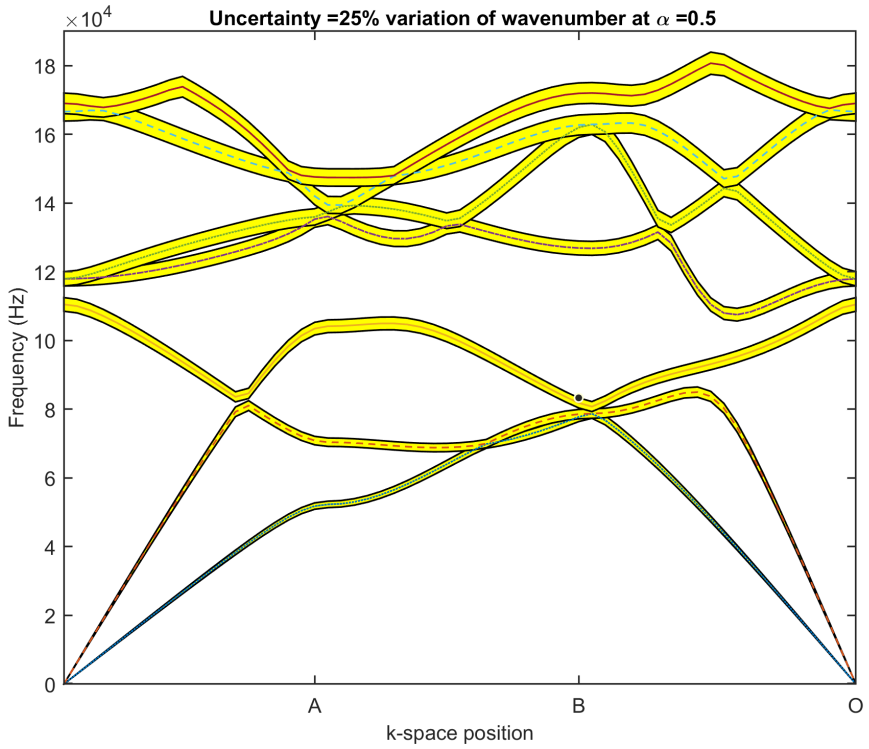

(a)

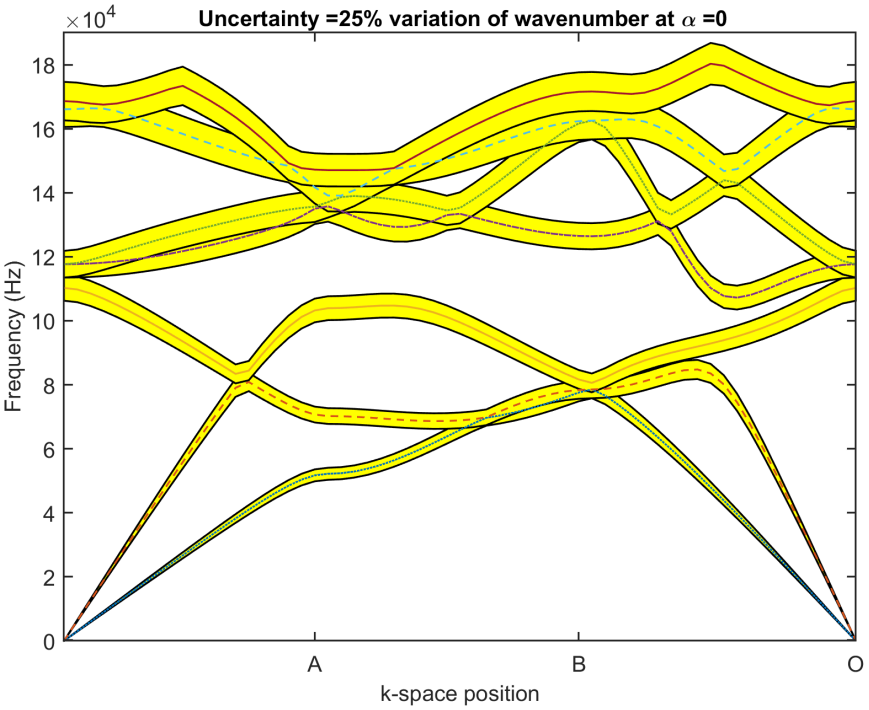

(b)

Figure 5.46: Band structure with 25% uncertainty

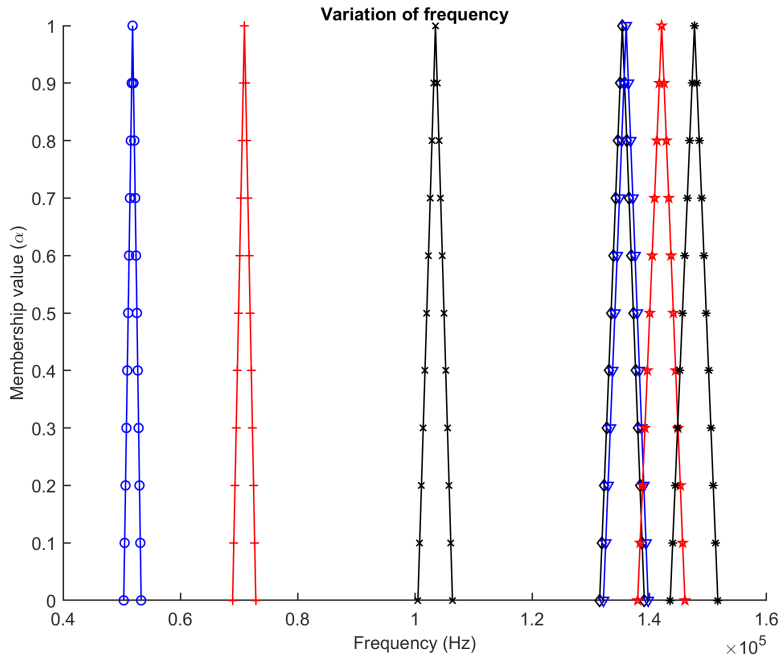

(a) Fuzzy frequency bound in x-direction at π

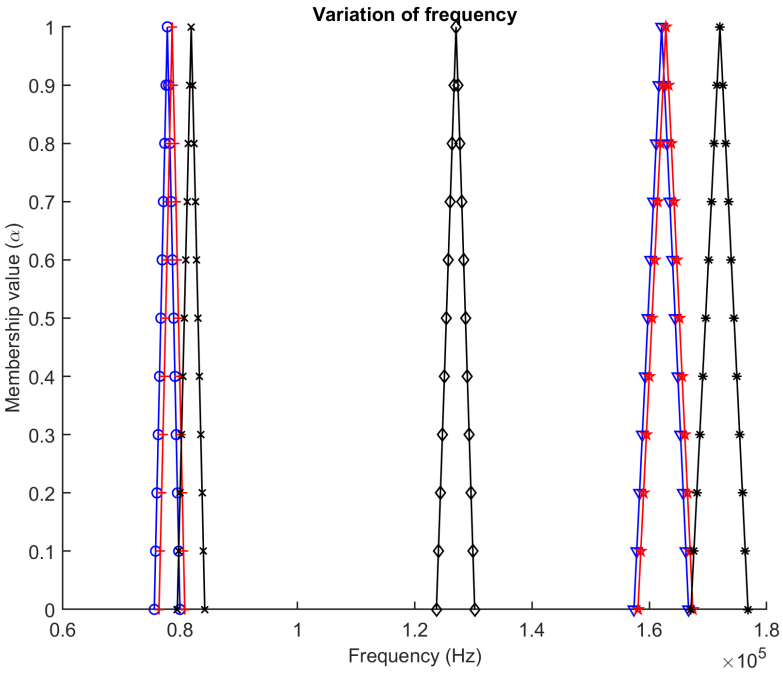

(b) Fuzzy frequency bound in y-direction at π

Figure 5.47: Variation of the frequency at given wavevector with 10% uncertainty. Variation of first eigen frequency (blue circle), second eigen frequency (red crosses), third eigen frequency (black stars), fouth eigen frequency (black diamonds), fifth eigen frequency (blue downward pointing triangles), sixth eigen frequency (red stars), and seventh eigen frequency (black asterisks).

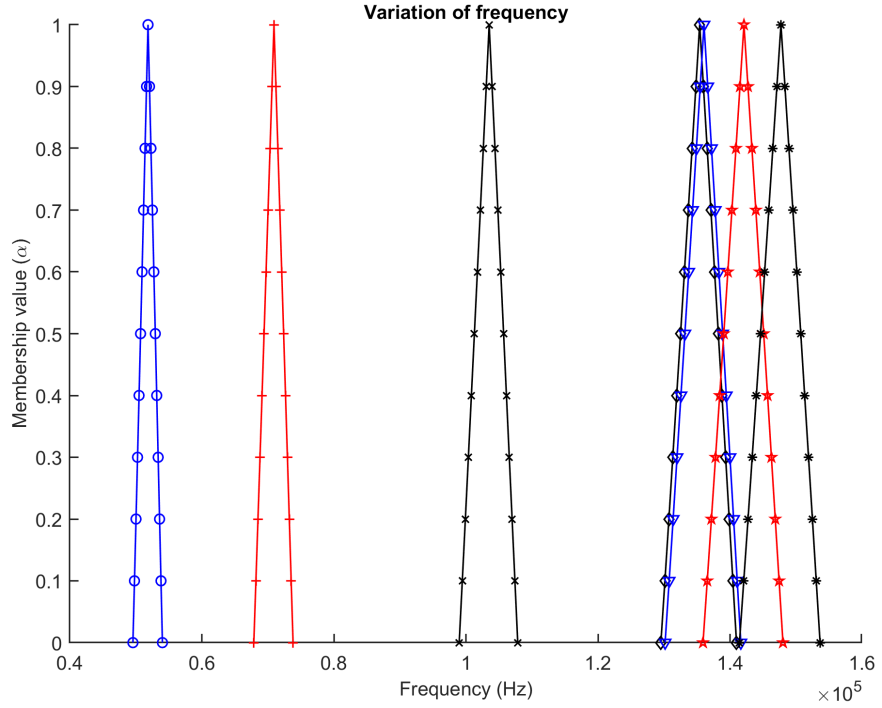

(a) Fuzzy frequency bound in x-direction at π

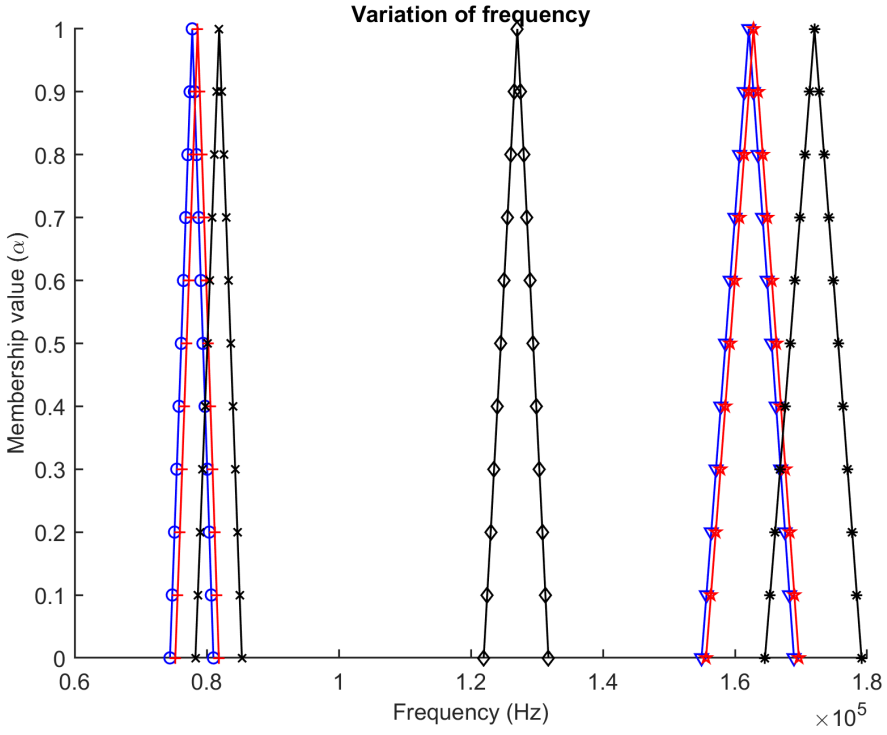

(b) Fuzzy frequency bound in y-direction at π

Figure 5.48: Variation of the frequency at given wavevector with 15% uncertainty. Variation of first eigen frequency (blue circles), second eigen frequency (red crosses), third eigen frequency (black stars), fouth eigen frequency (black diamonds), fifth eigen frequency (blue downward pointing triangles), sixth eigen frequency (red stars), and seventh eigen frequency (black asterisks).

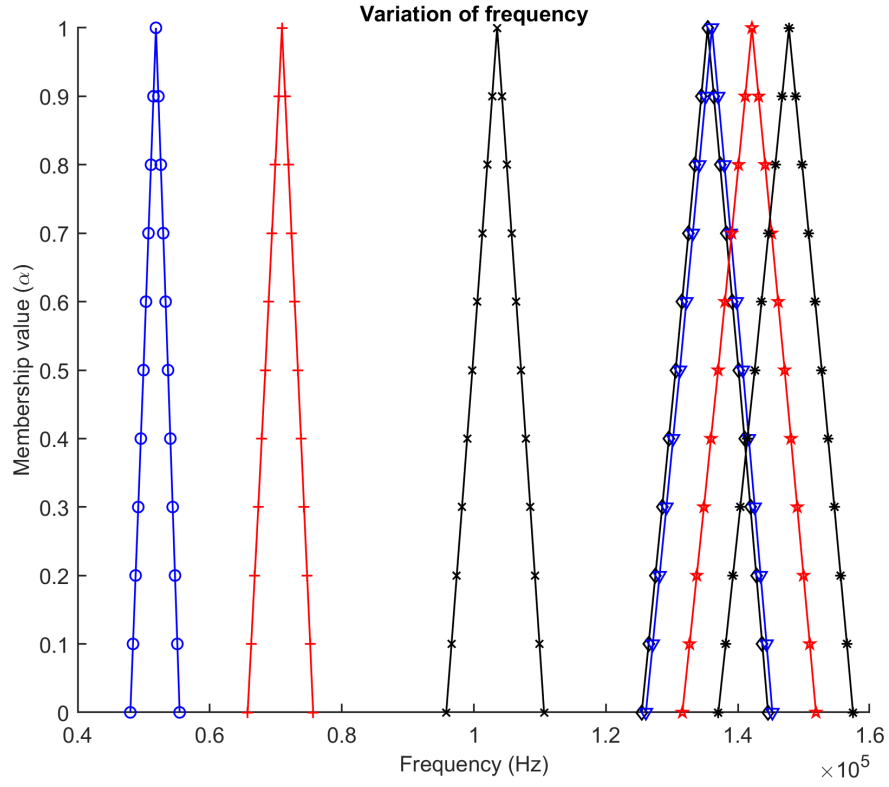

(a) Fuzzy frequency bound in x-direction at π

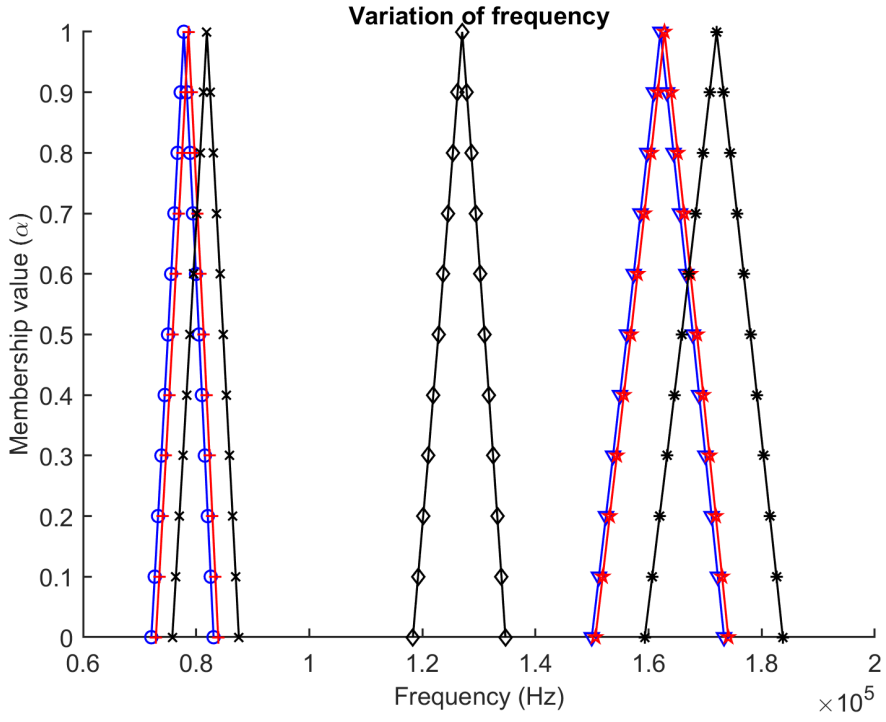

(b) Fuzzy frequency bound in y-direction at π

Figure 5.49: Variation of the frequency at given wavevector with 25% uncertainty. Variation of first eigen frequency (blue cirles), second eigen frequency (red crosses), third eigen frequency (black stars), fouth eigen frequency (black diamonds), fifth eigen frequency (blue downward pointing triangles), sixth eigen frequency (red stars), and seventh eigen frequency (black asterisks).

Chapter 6

Conclusions and future work

6.1 Conclusions

The design of periodic media is generally based on deterministic models without considering the effect of inherent uncertainties existing in these media. In general, the design is aimed at controlling the mechanical waves as much as possible; however, inherent uncertainties may affect the material characteristics. The uncertainties, in terms of material properties and geometrical parameters, are mostly exhibited in both manufacturing and assembly processes. To address this unavoidable actuality, the effects of parameter uncertainties is considered when analyzing frequency band structures (pass and stop bands) and frequency responses.

6.2 Summary of thesis achievements

In periodic structures, the wave dispersion can be obtained by applying the Floquet–Bloch theorem. Herein, we presented stochastic and fuzzy approach for the uncertainty quantification in periodic structures. The SWFEM TM formulation based on use of the state space, which uses the symplectic matrix for the classification of different modes of propagation, is extended to the periodic media in 1D cases. The formulation is detailed for free wave propagation and FRF. Various numerical cases are presented and validated with MCS, for free wave propagation in a periodic rod and periodic beam. In the FRF cases,

the periodic rod, metamaterial rod, geometrically varying beam, and metamaterial beam results validated the use of SWFEM. In the context of uncertainty quantification in periodic media, an elapsed computational time comparison is presented. The result of the simulation shows the computation advantage of the SWFEM over the MCS.

In the deterministic case, the dispersion curve is extracted by spectral analysis. The use of a state-space representation is an interesting alternative to spectral analysis. However, when using the TM method, numerical ill-conditioning may occur when a large number of the unit cells are involved in the periodic system model. To overcome this shortcoming for stochastic modelling, a stochastic spectral approach with a quadratic formulation is presented for 1D and 2D periodic media. The formulation proposes a straightforward approach for the stochastic wave modelling in the periodic structure. The main advantage of the formulation is that commercial FE packages and FE routines can be used for meshing capabilities during the modelling of the real structure. The choice of spectral problem is motivated by the fact that it offers a dynamic condensation of the inner element DOF to reduce computational DOFs, provides information about the imaginary part of the propagative wave that enables computation of forced response from a wave-based method, and it allows computation of group velocity for finding wave directivity. In addition, the formulation is adopted for the metamaterial structure.

In 1D cases, the proposed formulation is applied to a periodic rod and metamaterial rod. In 2D cases, homogeneous and periodic plates are validated. The effect of the parameter uncertainties on the longitudinal wavenumber dispersion is investigated considering stochasticity indicator and COV study. The effect on variation of longitudinal wavenumber is higher with elastic stochasticity than with stochastic density. It is noteworthy that in the metamaterial rod system, the developed formulation can handle a higher level of uncertainties. In the 2D homogenous plate case, it is found that variation of out-of-plane flexural wavenumber is slightly higher with uncertain elasticity than with uncertain density. For the 2D periodic plate case, uncertainties affect the out-of-plane flexural wavenumber scattering, and maximum value of the variation of flexural wavenumber occurs at the band gap edge frequency. The COV study highlights the linear variation of flexural wavenumber in the low-frequency region and shifts to higher variation with increasing frequency. The developed formulation offers computational cost savings. The computational cost savings

are very interesting, especially for optimization and reliability studies of complex periodic structures with material property uncertainties, and for damage detection and sensitivity analysis. Furthermore, the formulation can be employed for layered media, laminated, fiber-reinforced and complicated cross-section geometries, for determining the variation of dispersion properties, wavemodes, and group and phase velocities.

When information about the uncertainty variable is available, the probabilistic models are applicable. However, the application of a probabilistic approach faces two difficulties: (i) when little information is available, how to describe uncertain inputs; and (ii) how to efficiently compute the uncertainty in the response. There are non-probabilistic models, that can be introduced for the uncertainty propagation to overcome the difficulties. Due to imprecision and non-availability of the information about the uncertain variables, they are modelled as fuzzy variables. The FWFEM based on the state space formulation in conjunction with the fuzzy method is presented for 1D periodic media. The developed formulation is applied to the free wave propagation and FRF computation of a periodic rod and periodic beam. These numerical results are compared with WFEM MCS for validation purposes. The maximum fuzzy bounds of FRF is obtained at α=0, which decreases with increase in α-cuts. The elapsed time comparison is presented to determine the computation advantage of the FWFEM over the WFEM MCS.

A computationally inexpensive fuzzy spectral approach is formulated to study the effects of material property uncertainties in 2D periodic media. The free wave propagation problem can typically be solved by either the direct approach or inverse approach. In the direct approach, $\mu(\omega)$, imposes real ω (circular frequency), allowing description of the spatial wave attenuation; whereas the inverse approach, $\omega(\mu)$, imposes the real μ (propagation constant), that does not allow the wave attenuation, and can be applied to an undamped unit cell model. The formulation is derived for the FWFEM direct and inverse forms. The validation of the presented method is performed for free wave propagation for the homogeneous plate and periodic plate cases with the direct form, and with a bi-material square plate for the inverse form. In the homogenous plate case, it is found that variation of out-of-plane flexural wavenumber is slightly higher with uncertain elasticity. For the periodic plate case, uncertainties affect the out-of-plane flexural wavenumber and the maximum bounds of the flexural wavenumber occurs near the band gap edge frequency.

In the 2D inverse formulation case, the formulation is applied to the bi-material square lattice. The results obtained from the FWFEM inverse form are in excellent agreement with those from WFEM MCS. The uncertainty analysis suggests that the uncertainties have a significant impact on the band structures. It is highly desirable to include the uncertainties when designing and analyzing lattice and periodic structures. In terms of computation cost, the developed formulation offers substantial cost savings.

The main research achievements presented in this thesis are:

- The SWFEM based on a transfer matrix [Ichchou et al., 2011] is extended to 1D periodic media to obtain the band gap and FRF, for the weak level of uncertainties [Singh et al., 2018].
- The development of a spectral formulation based on a quadratic eigenvalue problem for the stochastic modelling of 1D and 2D periodic media for the weak level of uncertainties at reduced computation cost [Singh et al., 2020a].
- The development of new non-probabilistic uncertainty quantification method, which is effective when very little information about the uncertain parameter is available, or the available information is imprecise.
- The development of the FWFEM for 1D periodic media to obtain the band gap and FRF [Singh et al., 2018], and in 2D periodic media [Singh et al., 2020b] to obtain the dispersion curve through both direct and inverse formulation.

6.3 Suggestions for future work

The research and development of the probabilistic and non-probabilistic uncertainty propagation methods in periodic structures have inspired new ideas and questions that can be considered in future investigations.

- The choice of parameters in the stochastic and possibilistic modelling require considerable physical insight. The effect of different parameters on the performance of the uncertainty procedure can be investigated for structures with damping. The shift

shell operator method [Magliacano et al., 2019], [Collet et al., 2011] can be used for damped system modelling.

- The approach proposed in this thesis of SWFEM QEV was validated for the simplified unit cell, showing good precision and a much-reduced computational cost compared to that required by WFEM MCS. The SWFEM QEV can be considered for complex unit cell modelling and uncertainty propagation.

- In a metamaterial system, uncertainty can be introduced on the resonator parameters to assess the shift of the band gap size and location.

- The effects of uncertain parameters have been examined using first-order perturbation. The stochastic model could be further examined using second-order perturbation to include more uncertainty in the numerical simulations.

- Other membership functions, such as Gaussian and trapezoidal, should be explored for uncertain variable modelling in FWFEM investigations.

- In this thesis, the direct and inverse forms of the FWFEM are proposed. The computation cost of the FWFEM inverse form can be further lowered by combining the FWFEM with model order reduction strategies [Zhou et al., 2015b], [Zhou et al., 2015a], [Palermo and Marzani, 2016], [Boukadia et al., 2018].

- The effect of parameter uncertainties can be examined using the PCE. The stochastic model can be further applied to examine the geometrical uncertainty and forced uncertainty. The computational efficiency could be improved by combining the PCE with regression analysis to optimize the collocation points.

- In this thesis, the study has been limited to 1D and 2D periodic media, and this could be extended to 3D media in the future. Adding more dimensions will complicate the simulation process; however, it will provide more information as well.

- The hypothesis about uncertainties are to be periodic is considered to guarantees the assumed periodicity as in the deterministic WFEM, which comes from the Bloch theorem. The solution to relax the assumed hypothesis is supercells adaptation. The supercells offer the possibility to consider uncertainties arising within the periodic structure. The supercell in this form does not show symmetry, so the uncertainties

in one specimen inside the supercell can be estimated. Also applying Bloch theorem to the supercell and supercell is repeated infinitely as well.

- In the uncertainty analysis, in both probabilistic and non-probabilistic approach, only one global parameter is considered at a time. However, in the unit cell level uncertainties in more than one local parameter is considered. The approaches can be extended adapting all global parameters.

- Machine learning assisted methods can be attempted to lower the computation cost [Finol et al., 2019].

Bibliography

[Abdo et al., 2017] Abdo, H., Flaus, J. M., and Masse, F. (2017). Uncertainty quantification in risk assessment - Representation, propagation and treatment approaches: Application to atmospheric dispersion modeling. *Journal of Loss Prevention in the Process Industries*, 49:551–571.

[Arenas and Crocker, 2001] Arenas, J. P. and Crocker, M. J. (2001). A note on a WKB application to a duct of varying cross-section. *Applied Mathematics Letters*, 14(6):667–671.

[Ben Souf et al., 2015a] Ben Souf, M. A., Bareille, O., Ichchou, M., and Haddar, M. (2015a). The wave finite element method for uncertain systems with model uncertainty. In *Proceedings of the Institution of Mechanical Engineers, Part C: Journal of Mechanical Engineering Science*, volume 0, pages 1–12.

[Ben Souf et al., 2013a] Ben Souf, M. A., Bareille, O., Ichchou, M. N., Bouchoucha, F., and Haddar, M. (2013a). Waves and energy in random elastic guided media through the stochastic wave finite element method. *Physics Letters, Section A: General, Atomic and Solid State Physics*, 377(37):2255–2264.

[Ben Souf et al., 2013b] Ben Souf, M. A., Bareille, O., Ichchou, M. N., Troclet, B., and Haddar, M. (2013b). Variability of coupling loss factors through a wave finite element technique. *Journal of Sound and Vibration*, 332(9):2179–2190.

[Ben Souf et al., 2015b] Ben Souf, M. A., Chronopoulos, D., Ichchou, M., Bareille, O., and Haddar, M. (2015b). On the variability of the sound transmission loss of composite panels through a parametric probabilistic approach. *Journal of Computational Acoustics*, 23:1550018–1–23.

[Ben Souf et al., 2015c] Ben Souf, M. A., Ichchou, M., Bareille, O., Bouhaddi, N., and Haddar, M. (2015c). Dynamics of random coupled structures through the wave finite element method. *Engineering Computations*, 32(7):2020–2045.

[Bouchoucha et al., 2017] Bouchoucha, F., Ichchou, M. N., and Haddar, M. (2017). Stochastic wave finite element method in uncertain elastic media through the second order perturbation. *Journal of Applied Mechanics and Technical Physics*, 58(2):362–370.

[Boukadia et al., 2018] Boukadia, R. F., Droz, C., Ichchou, M. N., and Desmet, W. (2018). A Bloch wave reduction scheme for ultrafast band diagram and dynamic response computation in periodic structures. *Finite Elements in Analysis and Design*, 148(May):1–12.

[Brillouin, 1946] Brillouin, L. (1946). *Wave propogation in periodic structures: electric filters and crystal lattices*. McGraw-Hill Education, New York, first edition.

[Cai and Patil, 2007] Cai, L. W. and Patil, S. (2007). Effects of randomness on band gap formation in models of fiber-reinforced composite panels having quasirandom fiber arrangements. *Journal of Vibration and Acoustics*, 129(5):663–671.

[Chen and Rao, 1997] Chen, L. and Rao, S. (1997). Fuzzy finite-element approach for the vibration analysis of imprecisely-defined systems. *Finite Elements in Analysis and Design*, 27(1):69–83.

[Cheng et al., 2018] Cheng, Z. B., Shi, Z. F., and Mo, Y. L. (2018). Complex dispersion relations and evanescent waves in periodic beams via the extended differential quadrature method. *Composite Structures*, 187(January):122–136.

[Cicirello and Langley, 2014] Cicirello, A. and Langley, R. S. (2014). Efficient parametric uncertainty analysis within the hybrid Finite Element/Statistical Energy Analysis method. *Journal of Sound and Vibration*, 333(6):1698–1717.

[Collet et al., 2011] Collet, M., Ouisse, M., Ruzzene, M., and Ichchou, M. N. (2011). Floquet-Bloch decomposition for the computation of dispersion of two-dimensional periodic, damped mechanical systems. *International Journal of Solids and Structures*, 48(20):2837–2848.

[Comsol, 2017] Comsol (2017). LiveLink for MATLAB users guide.

[Daouk et al., 2015] Daouk, S., Louf, F., Dorival, O., Champaney, L., and Audebert, S. (2015). Uncertainties in structural dynamics: overview and comparative analysis of methods. *Mechanics & Industry*, 16(4):404.

[Droz et al., 2016] Droz, C., Zhou, C., Ichchou, M. N., and Lainé, J. P. (2016). A hybrid wave-mode formulation for the vibro-acoustic analysis of 2D periodic structures. *Journal of Sound and Vibration*, 363:285–302.

[DuBois and Prade, 1980] DuBois, D. and Prade, H. (1980). *Fuzzy sets and systems: theory and applications*. Academic Press.

[Fabro et al., 2019] Fabro, A., Ferguson, N., and Mace, B. (2019). Wave propagation in slowly varying waveguides using a finite element approach. *Journal of Sound and Vibration*, 442:308–329.

[Fabro et al., 2016] Fabro, A. T., Beli, D., Arruda, J. R. F., Ferguson, N., and Mace, B. R. (2016). Uncertainty analysis of band gaps for beams with periodically distributed resonators produced by additive manufacturing. In *Proceedings of ISMA2016*, pages 2031–2042.

[Fabro et al., 2015] Fabro, A. T., Ferguson, N. S., Jain, T., Halkyard, R., and Mace, B. R. (2015). Wave propagation in one-dimensional waveguides with slowly varying random spatially correlated variability. *Journal of Sound and Vibration*, 343:20–48.

[Faes and Moens, 2019] Faes, M. and Moens, D. (2019). Recent trends in the modeling and quantification of non-probabilistic uncertainty. *Archives of Computational Methods in Engineering*, pages 1–39.

[Faulkner and Hong, 1985] Faulkner, M. G. and Hong, D. P. (1985). Free vibrations of a mono-coupled periodic system. *Journal of Sound and Vibration*, 99(1):29–42.

[Finol et al., 2019] Finol, D., Lu, Y., Mahadevan, V., and Srivastava, A. (2019). Deep convolutional neural networks for eigenvalue problems in mechanics. *International Journal for Numerical Methods in Engineering*, 118(5):258–275.

[Ghanem and Spanos, 1990] Ghanem, R. and Spanos, P. D. (1990). Polynomial chaos in stochastic finite elements. *Journal of Applied Mechanics*, 57(1):197–202.

[Henneberg et al., 2020] Henneberg, J., Nieto, J. S. G., Sepahvand, K., Gerlach, A., Cebulla, H., and Marburg, S. (2020). Periodically arranged acoustic metamaterial in industrial applications : The need for uncertainty quantification. *Applied Acoustics*, 157:107026.

[Houillon et al., 2005] Houillon, L., Ichchou, M. N., and Jezequel, L. (2005). Wave motion in thin-walled structures. *Journal of Sound and Vibration*, 281(3-5):483–507.

[Hussein, 2009] Hussein, M. I. (2009). Reduced bloch mode expansion for periodic media band structure calculations. *Proceedings of the Royal Society A: Mathematical, Physical and Engineering Sciences*, 465(2109):2825–2848.

[Hussein et al., 2003] Hussein, M. I., Hulbert, G. M., and Scott, R. A. (2003). Band-gap engineering of elastic waveguides using periodic materials. In *ASME International Mechanical Engineering Congress*, pages 1–9.

[Ibrahim, 1987] Ibrahim, R. A. (1987). Structural dynamics with parameter uncertainties. *Applied Mechanics Reviews*, 40(3):309–328.

[Ichchou et al., 2011] Ichchou, M. N., Bouchoucha, F., Ben Souf, M. A., Dessombz, O., and Haddar, M. (2011). Stochastic wave finite element for random periodic media through first-order perturbation. *Computer Methods in Applied Mechanics and Engineering*, 200(41-44):2805–2813.

[Jensen and Sigmund, 2003] Jensen, S. J. and Sigmund, O. (2003). Systematic design of phononic band gap materials and structures by topology optimization. *Philosophical Transactions of the Royal Society: Mathematical, Physical and Engineering Sciences*, 361(3):1001–1019.

[Kiureghian and Ditlevsen, 2009] Kiureghian, A. D. and Ditlevsen, O. (2009). Aleatory or epistemic? Does it matter? *Structural Safety*, 31(2):105–112.

[Kleiber and Hien, 1992] Kleiber, M. and Hien, T. D. (1992). *The stochastic finite element method: basic perturbation technique and computer implementation.* Wiley.

[Kushwaha et al., 1994] Kushwaha, M. S., Halevi, P., Martínez, G., Dobrzynski, L., and Djafari-Rouhani, B. (1994). Theory of acoustic band structure of periodic elastic composites. *Physical Review B*, 49(4):2313–2322.

[Langley, 1995] Langley, R. (1995). Wave transmission through one-dimensional near periodic structures: optimum and to random disorder. *Journal of Sound and Vibration*, 188(5):717–743.

[Li et al., 2016] Li, G., Lu, Z., Li, L., and Ren, B. (2016). Aleatory and epistemic uncertainties analysis based on non-probabilistic reliability and its kriging solution. *Applied Mathematical Modelling*, 40(9):5703–5716.

[Li and Xu, 2017] Li, Y. and Xu, Y. (2017). Research on the effects of geometrical and material uncertainties on the band gap of the undulated beam. *AIP ADVANCES*, 095315:1–8.

[Liu and Rao, 2005] Liu, Q. and Rao, S. S. (2005). Fuzzy finite element approach for analysis of fiber reinforced laminated composite beams. *AIAA Journal*, 43(3):651–661.

[Ma and Li, 2018] Ma, X.-F. and Li, T.-J. (2018). Dynamic analysis of uncertain structures using an interval-wave approach. *International Journal of Applied Mechanics*, 10(2):1–19.

[Mace et al., 2005a] Mace, B. R., Duhamel, D., Brennan, M. J., Lars, H., Valle, M. L., Brennan, M. J., and Hinke, L. (2005a). Finite element prediction of wave motion in structural waveguides. *Journal of Acoustical Society of America*, 117(5):2835–2843.

[Mace and Manconi, 2008] Mace, B. R. and Manconi, E. (2008). Modelling wave propagation in two-dimensional structures using finite element analysis. *Journal of Sound and Vibration*, 318(4-5):884–902.

[Mace et al., 2005b] Mace, B. R., Worden, K., and Manson, G. (2005b). Uncertainty in structural dynamics. *Journal of Sound and Vibration*, 288:423–429.

[Magliacano et al., 2019] Magliacano, D., Ouisse, M., Khelif, A., De Rosa, S., Franco, F., Atalla, N., and Collet, M. (2019). Computation of dispersion diagrams for periodic porous materials modeled as equivalent fluids. *Mechanical Systems and Signal Processing*, 130(September):692–706.

[Manohar and Keane, 1993] Manohar, C. and Keane, A. (1993). Axial vibration of a stochastic rod. *Journal of Sound and Vibration*, 165(2):341–359.

[Massa et al., 2008] Massa, F., Ruffin, K., Tison, T., and Lallemand, B. (2008). A complete method for efficient fuzzy modal analysis. *Journal of Sound and Vibration*, 309(1-2):63–85.

[Mead, 1973] Mead, D. J. (1973). A general theory of harmonic wave propagation in linear periodic systems with multiple coupling. *Journal of Sound and Vibration*, 27(2):235–260.

[Mencik and Ichchou, 2005] Mencik, J. M. and Ichchou, M. N. (2005). Multi-mode propagation and diffusion in structures through finite elements. *European Journal of Mechanics, A/Solids*, 24(5):877–898.

[Mencik and Ichchou, 2007] Mencik, J. M. and Ichchou, M. N. (2007). Wave finite elements in guided elastodynamics with internal fluid. *International Journal of Solids and Structures*, 44(7-8):2148–2167.

[Mencik and Duhamel, 2016] Mencik, J.-M. M. and Duhamel, D. (2016). A wave finite element-based approach for the modeling of periodic structures with local perturbations. *Finite Elements in Analysis and Design*, 121(15):40–51.

[Mester and Benaroya, 1995] Mester, S. S. and Benaroya, H. (1995). Periodic and near-periodic structures. *Shock and Vibration*, 2(1):69–95.

[Miles, 1966] Miles, J. (1966). One-dimensional stress-wave propagation in a heterogeneous medium. *Journal of applied mech*, 33(4):11–12.

[Moens, 2012] Moens, D. (2012). Uncertainties in structural dynamics. *Mechanical Systems and Signal Processing*, 32:1–4.

[Moens and Hanss, 2011] Moens, D. and Hanss, M. (2011). Non-probabilistic finite element analysis for parametric uncertainty treatment in applied mechanics: Recent advances. *Finite Elements in Analysis and Design*, 47(1):4–16.

[Möller and Beer, 2008] Möller, B. and Beer, M. (2008). Engineering computation under uncertainty – Capabilities of non-traditional models. *Computers & Structures*, 86(10):1024–1041.

[Nakashima et al., 2008] Nakashima, K., Biwa, S., and Matsumoto, E. (2008). Elastic wave transmission and stop band characteristics in unidirectional composites. *Journal of Solid Mechanics and Materials Engineering*, 2(9):1195–1206.

[Nannapaneni and Mahadevan, 2016] Nannapaneni, S. and Mahadevan, S. (2016). Reliability analysis under epistemic uncertainty. *Reliability Engineering and System Safety*, 155:9–20.

[Nobrega et al., 2016] Nobrega, E. D., Gautier, F., Pelat, A., and Dos Santos, J. M. (2016). Vibration band gaps for elastic metamaterial rods using wave finite element method. *Mechanical Systems and Signal Processing*, 79:192–202.

[Palermo and Marzani, 2016] Palermo, A. and Marzani, A. (2016). Extended bloch mode synthesis: Ultrafast method for the computation of complex band structures in phononic media. *International Journal of Solids and Structures*, 100-101:29–40.

[Patle et al., 2018] Patle, B. K., Hirwani, C. K., Singh, R. P., and Panda, S. K. (2018). Eigenfrequency and deflection analysis of layered structure using uncertain elastic properties – a fuzzy finite element approach. *International Journal of Approximate Reasoning*, 98:163–176.

[Pawar et al., 2012] Pawar, P. M., Jung, S. N., and Ronge, B. P. (2012). Fuzzy approach for uncertainty analysis of thin walled composite beams. *Aircraft Engineering and Aerospace Technology*, 84(1):13–22.

[Psarobas et al., 2000] Psarobas, I., Stefanou, N., and Modinos, A. (2000). Scattering of elastic waves by periodic arrays of spherical bodies. *Physical Review B - Condensed Matter and Materials Physics*, 62(1):278–291.

[Quaranta, 2011] Quaranta, G. (2011). Finite element analysis with uncertain probabilities. *Computer Methods in Applied Mechanics and Engineering*, 200(1-4):114–129.

[Rao and Liu, 2004] Rao, S. S. and Liu, Q. (2004). Fuzzy approach to the mechanics of fiber-reinforced composite materials. *AIAA Journal*, 42(1):159–167.

[Roy and Oberkampf, 2011] Roy, C. J. and Oberkampf, W. L. (2011). A comprehensive framework for verification, validation, and uncertainty quantification in scientific com-

puting. *Computer Methods in Applied Mechanics and Engineering*, 200(25-28):2131–2144.

[Ruzzene and Tsopelas, 2003] Ruzzene, M. and Tsopelas, P. (2003). Control of wave propagation in sandwich plate rows with periodic honeycomb core. *Journal of Engineering Mechanics*, 129(9):975–986.

[Sarkar and Ghanem, 2002] Sarkar, A. and Ghanem, R. (2002). Mid-frequency structural dynamics with parameter uncertainty. *Computer Methods in Applied Mechanics and Engineering*, 191(47-48):5499–5513.

[Sigalas and Economou, 1992] Sigalas, M. and Economou, E. (1992). Elastic and acoustic wave band structure. *Journal of Sound and Vibration*, 158:377–382.

[Singh et al., 2017] Singh, R. P., De Rosa, S., Franco, F., Ichchou, M., and Bareille, O. (2017). A literature review for the analysis of structured and unstructured uncertainty effects on vibroacoustic. In *MEDYNA 2017: 2nd Euro-Mediterranean Conference on Structural Dynamics and Vibroacoustics*, pages 170–174.

[Singh et al., 2018] Singh, R. P., Droz, C., De Rosa, S., Franco, F., Bareille, O., and Ichchou, M. N. (2018). A study of structured uncertainties in wave characteristic of one-dimensional periodic structures. In *International Conference on Noise and Vibration Engineering (ISMA 2018)*, pages 4731–4740.

[Singh et al., 2020a] Singh, R. P., Droz, C., Ichchou, M. N., Franco, F., Bareille, O., and De Rosa, S. (2020a). Stochastic wave finite element quadratic formulation for periodic media: 1D and 2D. *Mechanical Systems and Signal Processing*, 136(106431):1–30.

[Singh et al., 2019] Singh, R. P., Ichchou, M., Bareille, O., Franco, F., and De Rosa, S. (2019). Uncertainties in wave characteristic of one-dimensional periodic media using the fuzzy wave finite element method. In *9th ECCOMAS Thematic Conference on Smart Structures and Materials (SMART 2019)*, pages 1169–1182.

[Singh et al., 2020b] Singh, R. P., Rosa, S. D., Franco, F., Bareille, O., Ichchou, M., and Petrone, G. (2020b). Uncertainties in wave characteristic of two-dimensional periodic media using the fuzzy wave finite element method. In *MEDYNA 2020: 3rd*

Euro-Mediterranean Conference on Structural Dynamics and Vibroacoustics, number February, pages 1–4.

[Soize, 2003] Soize, C. (2003). Random matrix theory and non-parametric model of random uncertainties in vibration analysis. *Journal of Sound and Vibration*, 263(4):893–916.

[Soize, 2005] Soize, C. (2005). A comprehensive overview of a non-parametric probabilistic approach of model uncertainties for predictive models in structural dynamics. *Journal of Sound and Vibration*, 288(3):623–652.

[Steele, 1976] Steele, C. R. (1976). Application of the WKB method in solid mechanics. In *Mechanics Today*, volume 3, chapter VI, pages 243–295. Pergamon Press.

[Stefanou, 2009] Stefanou, G. (2009). The stochastic finite element method: Past, present and future. *Computer Methods in Applied Mechanics and Engineering*, 198(9-12):1031–1051.

[Sun et al., 2017] Sun, X., Zhou, C., Ichchou, M., Lainé, J.-P., and Zine, A.-M. (2017). Multi-scale homogenization of transversal waves in periodic composite beams. *International Journal of Applied Mechanics*, 09(03):1750039.

[Syed and Bishay, 2018] Syed, M. and Bishay, P. L. (2018). Analysis and design of periodic beams for vibration attenuation. *Journal of Vibration and control*, 0(April):1–12.

[Tanaka et al., 2000] Tanaka, Y., Tomoyasu, Y., and Tamura, S. I. (2000). Band structure of acoustic waves in phononic lattices: Two-dimensional composites with large acoustic mismatch. *Physical Review B - Condensed Matter and Materials Physics*, 62(11):7387–7392.

[Tian et al., 2011] Tian, B., Tie, B., Aubry, D., and Su, X. (2011). Elastic wave propagation in periodic cellular structures. *Computer Modeling in Science and Engineering*, 76(4):217–233.

[Tomar et al., 2018] Tomar, S. S., Zafar, S., Talha, M., Gao, W., and Hui, D. (2018). State of the art of composite structures in non-deterministic framework: A review. *Thin-Walled Structures*, 132(July):700–716.

[Vasseur and Deymier, 1997] Vasseur, J. O. and Deymier, P. A. (1997). Propagation of acoustic waves in periodic and random two-dimensional composite media. *Journal of Materials Research*, 12(8):2207–2212.

[Waki et al., 2009] Waki, Y., Mace, B. R., and Brennan, M. J. (2009). Numerical issues concerning the wave and finite element method for free and forced vibrations of waveguides. *Journal of Sound and Vibration*, 327(1-2):92–108.

[Wang et al., 2017] Wang, P., Yi, Q., Zhao, C., Xing, M., and Tang, J. (2017). Wave propagation in periodic track structures: band-gap behaviours and formation mechanisms. *Archive of Applied Mechanics*, 87(3):503–519.

[Xia and Friswell, 2014] Xia, Y. and Friswell, M. I. (2014). Efficient solution of the fuzzy eigenvalue problem in structural dynamics. *Engineering Computations*, 31(5):864–878.

[Xiang and Shi, 2009] Xiang, H.-J. and Shi, Z.-F. (2009). Analysis of flexural vibration band gaps in periodic beams using differential quadrature method. *Computers & Structures*, 87(23-24):1559–1566.

[Xiao et al., 2012] Xiao, Y., Wen, J., and Wen, X. (2012). Longitudinal wave band gaps in metamaterial-based elastic rods containing multi-degree-of-freedom resonators. *New Journal of Physics*, 14(3):033042.

[Xie et al., 2017] Xie, L., Xia, B., Huang, G., Lei, J., and Liu, J. (2017). Topology optimization of phononic crystals with uncertainties. *Structural and Multidisciplinary Optimization*, 56(6):1319–1339.

[Xiu, 2009] Xiu, D. (2009). Fast numerical methods for stochastic computations: A review. *Communications in Computational Physics*, 5(2-4):242–272.

[Xiu and Em Karniadakis, 2002] Xiu, D. and Em Karniadakis, G. (2002). Modeling uncertainty in steady state diffusion problems via generalized polynomial chaos. *Computer Methods in Applied Mechanics and Engineering*, 191(43):4927–4948.

[Xu et al., 2014] Xu, M., Qiu, Z., and Wang, X. (2014). Uncertainty propagation in SEA for structural-acoustic coupled systems with non-deterministic parameters. *Journal of Sound and Vibration*, 333(17):3949–3965.

[Yu et al., 2008] Yu, D., Wen, J., Zhao, H., Liu, Y., and Wen, X. (2008). Vibration reduction by using the idea of phononic crystals in a pipe-conveying fluid. *Journal of Sound and Vibration*, 318(1-2):193–205.

[Zadeh, 1965] Zadeh, L. (1965). Fuzzy sets. *Information and Control*, 8(3):338–353.

[Zakian and Khaji, 2018] Zakian, P. and Khaji, N. (2018). A stochastic spectral finite element method for wave propagation analyses with medium uncertainties. *Applied Mathematical Modelling*, 63:84–108.

[Zhang et al., 2010] Zhang, H., Mullen, R. L., and Muhanna, R. L. (2010). Interval Monte Carlo methods for structural reliability. *Structural Safety*, 32(3):183–190.

[Zhang et al., 2015] Zhang, X., Qiu, Z., and Li, Q. (2015). Fuzzy variational principle for modal analysis of structures and its application. *Finite Elements in Analysis and Design*, 100:54–64.

[Zhao and Zhang, 2019] Zhao, Y. and Zhang, Y. (2019). Symplectic approach on the wave propagation problem for periodic structures with uncertainty. *Acta Mechanica Solida Sinica*, 32(3):2–87–297.

[Zhou et al., 2015a] Zhou, C. W., Lainé, J. P., Ichchou, M. N., and Zine, A. M. (2015a). Multi-scale modelling for two-dimensional periodic structures using a combined mode/wave based approach. *Computers and Structures*, 154:145–162.

[Zhou et al., 2015b] Zhou, C. W., Lainé, J. P., Ichchou, M. N., and Zine, a. M. (2015b). Wave finite element method based on reduced model for one-dimensional periodic structures. *International Journal of Applied Mechanics*, 07(02):1550018.

[Zhou et al., 2018] Zhou, C. W., Sun, X. K., Laine, J. P., Ichchou, M. N., Zine, A., Hans, S., and Boutin, C. (2018). Wave propagation feature in two-dimensional periodic beam lattices with local resonance by numerical method and analytical homogenization approach. *International Journal of Applied Mechanics*, 10(4):1850042.

[Zhu and Elis, 1993] Zhu, L. and Elis (1993). Hybrid probabilitic and convex modeling of excitation and response of periodic structures. *Mathematical Problems in Engineering*, 2:143–163.